VISCOELASTIC RESPONSE OF CELLS AND THE ROLE OF ACTIN CYTOSKELETAL REMODELLING

Priyanka Pravincumar

MEng – Medical Engineering (QMUL) 2009

2012

Queen Mary University of London

Mile End Road

E1 4NS

London

UK

This thesis is presented as part of the requirement for the degree
of Doctor of Philosophy

कर्मण्येवाधिकारस्ते मा फलेषु कदाचन |
मा कर्मफलहेतुर्भूर्मा ते सङ्गोऽस्त्वकर्मणि ||२-४७||

"Your right is to work only, but never to its fruits; let not the fruit-

of-action be your motive, nor let thy attachment be to inaction".

!! Shrimad Bhagavad Gita !!

ABSTRACT

The mechanical properties of living cells provide useful information on cellular structure and function. In the present study a micropipette aspiration technique was developed to investigate the viscoelastic parameters of isolated articular chondrocytes. The Standard Linear Solid (SLS) and the Boltzmann Standard Linear Solid (BSLS) models were used to compute the instantaneous and equilibrium moduli and viscosity based on the response to an aspiration pressure of 7 cm of water.

The modulus and viscosity of the chondrocytes increased with decreasing pressure rate. For example, the median equilibrium moduli obtained using the BSLS model increased from 0.19 kPa at 5.48 cmH_2O/s to 0.62 kPa at 0.35 cmH_2O/s. Cell deformation during micropipette aspiration was associated with an increase in cell volume and remodelling of the cortical actin visualised using GFP-actin. Interestingly, GFP-actin transfection inhibited the increase in cell moduli observed at the slower aspiration rate. Thus actin remodelling appears to be necessary for the pressure rate-dependent behaviour. A hypothesis is proposed explaining the role of actin remodelling and interaction with the membrane in regulating cell mechanics.

Further studies investigated a mechanical injury model of cartilage explants which resulted in significant increases in all three viscoelastic parameters. Treatment with IL-1β also increased the instantaneous moduli of cells treated in explants but there was no difference in equilibrium moduli or viscosity. IL-1β treatment in monolayer had no effect on cell mechanics suggesting that previously reported changes in actin associated with IL-1β may be lost during cell isolation or trypsinisation. Separate studies demonstrated increases in chondrocyte moduli and viscosity during passage indicating changes in cell structure-function associated with de-differentiation in monolayer.

In conclusion, this study has developed an optimised micropipette aspiration technique which was successfully used to quantify chondrocyte viscoelastic behaviour and to elucidate the underlying role of actin dynamics and response to pathological stimuli and in vitro culture.

This thesis is dedicated to

Dad – Pravincumar Bachu

Mum – Anita Pravincumar

Husband - Paras Makwana

Without you I wouldn't have achieved in my life what I have today.

ACKNOWLEDGEMENTS

TABLE OF CONTENTS

LIST OF FIGURES

18

19

LIST OF TABLES

LIST OF EQUATIONS

$$L(t_f) = \frac{\phi a}{\pi k_1}\left(1 - \frac{k_1}{k_1 + k_2}\right)P(t) + \frac{\phi a}{\pi k_1}\frac{k_1}{k_1 + k_2}\int_0^t \overline{\left[e^{-(t-t')/\tau}\,\overline{P(t')}\right]}dt' \quad$$

$$L(t) = \frac{\phi a}{\pi k_1}\left(1 - \frac{k_1}{k_1 + k_2}\right)P(t) + \frac{\phi a}{\pi k_1}\frac{k_1}{k_1 + k_2}Q\overline{\left[\tau - \tau^2 + \tau^2 e^{-t/\tau}\right]} \quad$$

$$L(t) = \frac{\phi a}{\pi k_1}\left(1 - \frac{k_1}{k_1 + k_2}\right)P(t) + \frac{\phi a}{\pi k_1}\frac{k_1}{k_1 + k_2}Q\overline{\left[e^{-(t-t_f)/\tau}(t_f\tau - \tau^2) + \tau^2(e^{-t/\tau})\pm\overline{\left[t_f - t_f\tau e^{-(t-t_f)/\tau}\right]}\right]}$$

Cell Surface Area during aspiration $$\left(\pi D_c^2\right) + \left(\pi D_p\left(L - \frac{D_p}{2}\right)\right) + \left(\frac{\pi D_p^2}{2}\right)$$

Cell Volume during aspiration $$\left(\frac{\pi D_c^3}{6}\right) + \left(\frac{\pi D_p^2\left(L - \frac{D_p}{2}\right)}{4}\right) + \left(\frac{\pi D_p^2}{12}\right)$$

Cell Surface Area = $$\left(D_1 + D_2\right)^2\pi + \pi D_p\left(L - L_A\right) + \left(\frac{\pi r_A^2}{2}\right)$$

Cell Volume = $$\frac{4\pi}{3}\left(\frac{D_1 + D_2}{3}\right)^3 + \frac{\pi D_p^2}{4}\left(L - L_A\right) + \frac{4}{6}\pi r_A^3$$

Chapter 1

ARTICULAR CARTILAGE

1.1 **GENERAL INTRODUCTION**

1.2 **EXTRACELLULAR MATRIX**

1.2.1 Collagen

1.2.2 Proteoglycan

1.2.3 Interstitial Water

1.2.4 Heterogeneity

1.3 **CARTILAGE BIOMECHANICS**

1.3.1 Cartilage Load Carriage

1.3.2 Zonal Variation in Mechanical Properties

1.4 **CHONDROCYTES**

1.4.1 Metabolism

1.4.2 Heterogeneity

1.4.3 Cytoskeleton Elements

1.4.4 Cytoskeletal Organisation in Chondrocytes

1.5 **MECHANOTRASDUCTION**

1.5.1 Invivo Evidence for Mechanotrasduction

1.5.2 Invitro Evidence for Mechanotrasduction

1.5.3 Signaling Pathways

1.6 **ARTICULAR CARTILAGE INJURY DISEASE AND REPAIR**

1.6.1 Acute Cartilage Injury

1.6.2 Osteoarthritis

1.6.3 Repair Techniques of Articular Cartilage

1. ARTICULAR CARTILAGE

1.1 GENERAL INTRODUCTION

Cartilage is an aneural, alymphatic, avascular soft connective tissue, which rapidly grows during skeletal development and mineralizes to form bone (Jerry, 2003). There are three different forms of cartilage found in the body, namely elastic cartilage, fibrocartilage and hyaline cartilage. Hyaline cartilage is found in articulating joints, nose, larynx, trachea and bronchi. Elastic cartilage is present in the external ear, epiglottis and small auditory tube. Fibrous cartilage serves as a transition between dense connective tissue (tendon) and hyaline cartilage which is found in menisci and intervertibral discs. Articular cartilage is a form of hyaline cartilage covering the bone ends within a diathrodial joint and represents the focus of the present thesis (Figure 1.1).
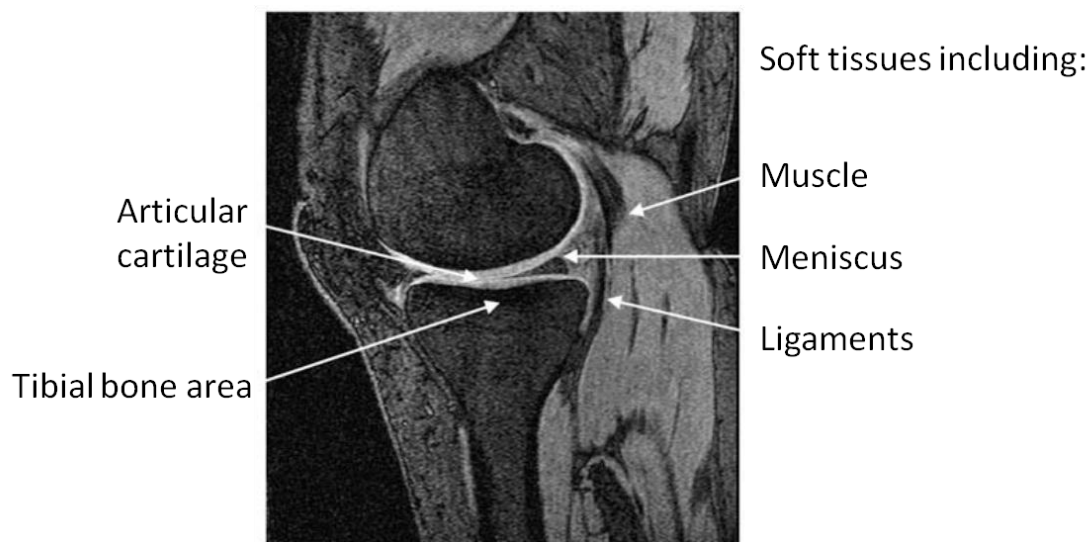
Figure 1.1. *Magnetic resonance imaging of sagittal section of knee joint. (Teichtahl   et al., 2008)*

Articular cartilage protects the subchondral bone from damage by deforming and therefore reducing contact stresses. It has the ability to distribute load during normal physical activities, thereby minimizing peak stresses on the subchondroral bone. Articular cartilage possesses great durability that in many cases, provides normal joint function for

80 years or longer. Additionally, its unique structure and composition provides low friction and a high lubrication joint surface with high wear resistance and stress absorption. However, cartilage has limited capacity to maintain and repair itself and thus these functions decrease with age. Accordingly the risk of progressive degeneration of articular cartilage increases with age, particularly in individuals over 40 years (Buckwalter et al., 2000). It is first important to understand the structure and composition of articular cartilage that provides it with its normal function.
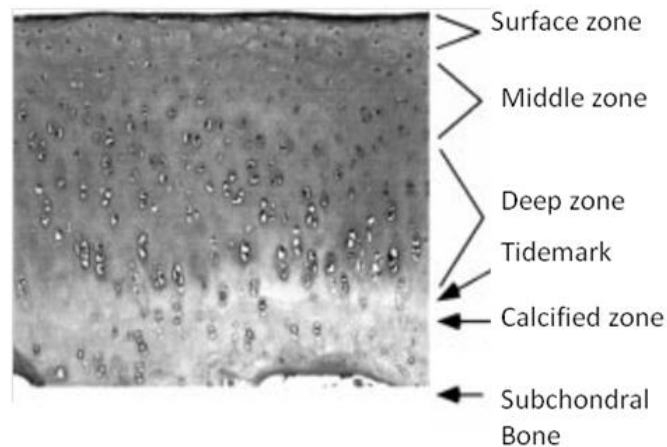
*Figure 1.2.*Histology of articular cartilage that can be classified into four zones based on structure, composition, and chondrocyte shape (Guilak, 2000).

Articular cartilage possesses a highly organised structure with complex interactions between extracellular matrix and its single cell type, the chondrocytes. A histological section through the tissue is illustrated in Figure 1.2. Articular cartilage is composed of 65-80% water by weight along with extracellular matrix components, collagen representing 15-20% of the wet weight, proteoglycans with 3-15% wet weight, noncollagenous proteins and glycoproteins contribute to 1% (Bader, 2000). By contrast, chondrocytes occupy between 1-10% of the tissue volume (Burstein et al., 2000). The organization and relative amounts of collagen and proteoglycan vary throughout the depth of articular cartilage reflecting the load distribution through the depth of tissue.

The extracellular matrix needs to support significant load applied respectively throughout the lifetime of an individual.

1.2 EXTRACELLULAR MATRIX

Extracellular matrix is divided into three distinct regions characterized by the distance from the individual cells, namely: the pericellular region, the territorial regions and the interterritorial region (Buckwalter et al., 2000). The pericellular and territorial regions of extracellular matrix provides cell with matrix macromolecules and protects the cell from damage during loading and deformation of the tissue. These regions may involve in mechanical signals transmission when the surrounding matrix is deformed during mechanical loading. The interterritorial region provides mechanical properties of the tissue.

PERICELLULAR MATRIX

The matrix forms a thin layer around cell membrane covering the surface of the cell. This region contains proteoglycan, non-collagenous proteins with little or no collagen fibrils.

TERRITORIAL MATRIX

The matrix surrounds pericellular region of the chondrocytes and in some location surrounds pairs or clusters of chondrocytes along with their pericellular matrices. The territorial surrounds stack of chondrocyte column in deep zone of the articular cartilage. In territorial region collagen fibrils form a fibrillar basket around the cells and at a distance from cell they intersect at different angle. The thin collagen fibrils from territorial matrix penetrate into pericellular matrix. As the distance from the cell increase, the diameter of the collagen fibrils increases and the organization changes to more parallel arrangement. This marks a boundary between territorial and interterritorial matrices. This region provides mechanical protection to chondrocytes

during loading (Guilak, 2000). The territorial and pericellular together form chondron (Stoklov et al., 2009).

INTERTERRITORIAL REGION

This is the largest of the all three regions and make up most of the volume of the mature cartilage. It is composed of large collagen fibrils and proteoglycan contributing to the material properties of the articular cartilage (Buckwalter and Mankin, 1998a). The collagen fibril does not surround the cell but are organized relative to the joint surface 90⁰ from the superficial zone to deep zone.
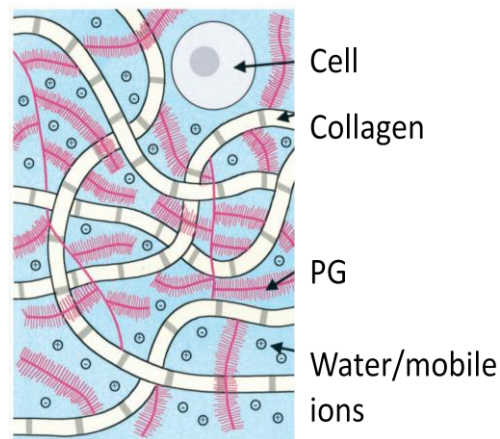
Figure 1.3. *Schematic of arrangement of collagen fibers proteoglycans and chondrocytes within articular cartilage (Ramage et al., 2009).*

The fluid phase of the extracellular matrix is composed of water, ionic and nonionic solutes. Collagen, chondrocytes, proteoglycan, lipids and minor amount of glycoproteins make up the solid phase of the tissue (Figure 1.3). In subsequent section components of solid phase and fluid phase of extracellular matrix are discussed.

1.2.1 COLLAGEN

Collagen provide tensile and shear strength to the articular cartilage (Lee, 2006). Collagen is a protein composed of approximately 1000 amino acids with a glycine at

every third amino acid. The type of collagen is determined by the precise arrangement of amino acids. The left-handed three alpha helices coil around into a right-handed helix to form a tropocollagen molecule (Figure 1.4). Collagen fibers are made up of tropocollagen molecules which are 300nm long and 1.5 nm wide (Jerry, 2003).
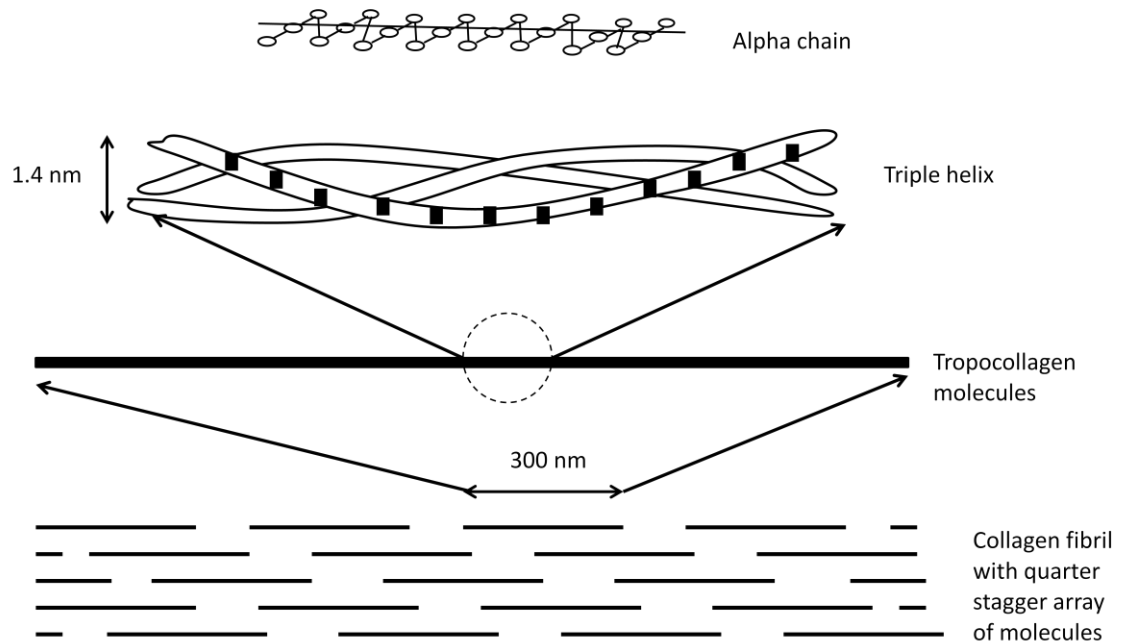
Figure 1.4. *Alpha chain is made up of amino acids, three of which is coiled into right handed configuration to form tropocollagen. The tropocollagen molecule is arranged in parallel fashion forming banded pattern of the collagen fibril. (Mow, 1980)*

The types of collagen found in articular cartilage can be divided into fibril forming; type II and type IX; and non-fibril forming types VI, IX and X. Type II comprising 90-95% of the total collagen in the matrix and is associated with Type IX to form collagen mesh. Type VI collagen is a microfibrilllar collagen preferentially located in the pericellular regions of the chondrocytes. Type IX acts as a bridge between aggrecan and collagen fibrils. Type IX covalently binds to type II collagen and form cross banded fibrils. The function of type IX and type XI is largely unknown (Buckwalter et al., 2005). However they are involved in stabilizing the collagen fibrils assembly predominately from Type II collagen. Type VI

collagen is found surrounding the chondrocytes and helps cells to attach to a matrix. Type X is involved in forming collagen network (Blaschke et al., 2000).

1.2.2 PROTEOGLYCANS

Proteoglycan is produced by chondrocytes and secreted into the extracellular matrix. Aggrecan consists of three globular regions (Figure 1.5) whereby G1 and G2 is separated by interglobular domain and the G2 and G3 regions are separated by glycosaminoglycans (GAG).
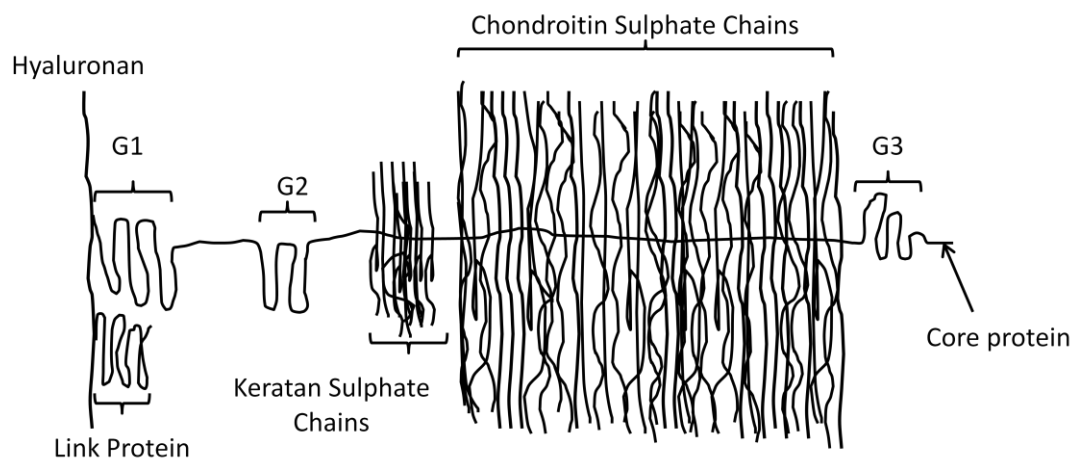
Figure 1.5. Schematic of aggrecan composed of keratan sulphate and chondroitin sulphate chains covalently bound to core protein. G1, G2 and G3 are globular protein regions. (Roughley, 2006)

A single GAG molecule is made up of unbranched repeating units of disaccharide which consist of keratan sulphate, chondroitin sulphate and dermatan sulphate. The negative charge of sulfate group effectively repels other and attract water and anions such Ca^{2+} and Na^{2+}. The negative charge of keratan sulphate and chondroitin sulphate repel with each other providing fully extended conformation and facilitate trapping of proteoglycans within the collagen framework.

Aggrecan is a modular proteoglycan, composed of about 90% polysaccharide and about 5% protein (Doege et al., 1991). A link protein is responsible for stabilising the binding

between hyaluronan and aggrecan core protein. In cartilage most of the proteoglycan exist in the form of aggrecan aggregates formed by the non-covalent bond between proteoglycan subunits and hyaluronan (Figure 1.6). More than 100 aggrecan monomers can bind to a single hyaluronan. The link protein binds to aggregate to stabilise the macromolecule complex (Roughley, 2006). Aggrecan has large number of keratin sulphate and chondroitin sulphate attached to a core protein. Although aggrecan is found throughout in extracellular matrix, it is concentrated in the pericellular and territorial regions (Poole et al., 1987).
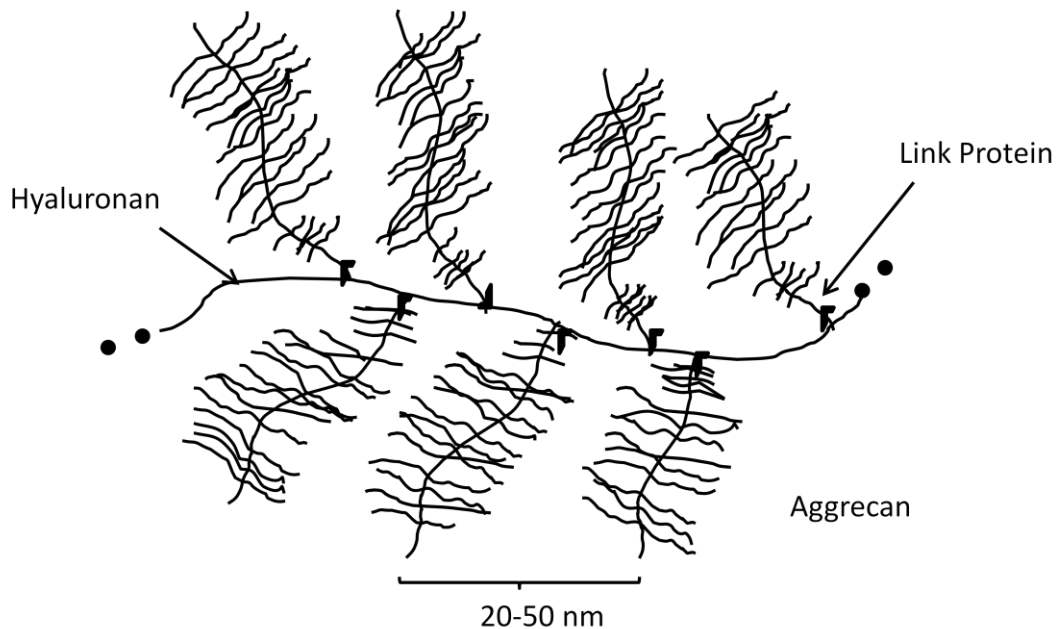
Figure 1.6. *Schematic of aggrecan, form aggregating proteoglycans. The proteoglycan monomers non-covalently bind to hyaluronan and link protein stabilises this binding region. (Roughley, 2006)*

The newly synthesised proteoglycan is capable of moving slowly within the tissue however when bonded to hyaluronan it forms the aggregate, hence immobilising the proteoglycan within the extracellular matrix. Proteoglycan and link protein are synthesised in the rough endoplasmic reticulum. Hyaluronan is synthesised at the plasma membrane therefore the proteoglycan and link protein can only interact with hyaluronan

once secreted by the chondrocytes. Articular cartilage consists of large aggregating molecules aggrecan, and other smaller proteoglycans such as decorin, biglycan and fibromodulin. Decorin has only one dermatan sulphate, biglycan has two dermatan sulphate and fibromodulin has several keratan sulphate, GAG chains attach to core protein (Roughley and Lee, 1994). Decorin is concentrated in pericellular region can bind to collagen types I, II and VI and regulate diameter of collagen type I fibrils (Cohen et al., 1998). Additionally, large nonaggregating proteoglycans is also present in articular cartilage that resemble as aggrecan in structure (Buckwalter et al., 1994). Aggrecan contribute about 90% of the proteoglycans mass in an extracellular matrix. Large nonaggregating proteoglycans contribute to 10% or less and small nonaggregating proteoglycans contribute to about 3%. Proteoglycan and noncollagenous proteins interact with collagenous meshwork, getting mechanically trapped inside and water is filled in the framework. The concentration of the proteoglycan changes with depth of articular cartilage, age, cartilage injury and disease.

The hyaluronan length varies from several hundred to more than 10000 nm (Buckwalter and Rosenberg, 1983). Large aggregates consist of more than 300 aggrecan molecules. The nonaggregating proteoglycans have shorter core protein. The small proteoglycan bind with other macromolecules such as decorin and fibromodulin bind with type II collagen and play a role in organising and stabilising the collagen network (Roughley and Lee, 1994). Biglycan interacts with type VI collagen and is present in the pericellular matrix (Roughley and Lee, 1994).

Among the noncollagenous proteins, few are attached to monosaccharides and oligosaccharides (Heinegard, 1992). Anchorin CII is a collagen-binding chondrocyte surface protein which help chondrocytes to anchor to matrix collagen fibrils (Heinegard, 1992).

1.2.3 INTERSTITIAL WATER

The interstitial water contains gases, small proteins, metabolites and cations. Its volume, concentration within the tissue is largely determined by aggregating proteoglycans that help to maintain fluid into the articular cartilage. The inorganic salts such as sodium, calcium, chloride and potassium are found to be dissolved in interstitial water. The large negative charges of the proteoglycans attract positively charged ions and repel negatively charged ions. Therefore the concentration of positive ions such as a sodium increases and negative charged ions such as chloride decreases. The collagenous networks entrap about 30% of the interstitial water and the rest is associated with proteoglycans that is freely exchangeable during joint loading and unloading. The flow of fluid across articular cartilage surface aids transport of nutrients to the chondrocytes (Jerry, 2003).

1.2.4 HETEROGENEITY

The organisation, composition and mechanical properties of the matrix, cell morphology and cellular functions changes with the depth from the surface of articular cartilage. On the basis of morphological changes of chondrocytes, matrix composition and organisation, the macrostructure of articular cartilage consist of four distinct zones: superficial, transitional, deep and calcified zone.
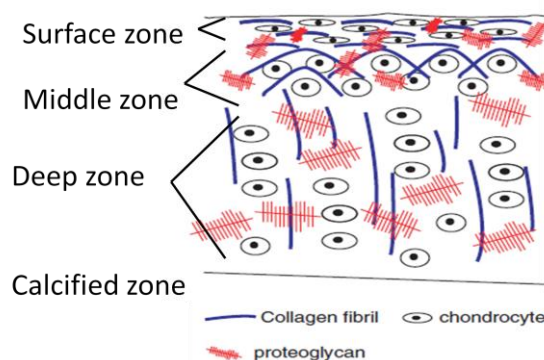
Figure 1.7. *Cartilage is composed of 75% electrolyte (water with mobile ions), 20% collagen, 5% of proteoglycans and chondrocytes make up less than 5% of tissue volume (Burstein et al., 2000)*

The different zones possess different alignment of collagen, variable appearance of chondrocytes (discussed in 1.4.2) as well as different concentration of proteoglycans and water content. The zonal variation of tissue is discussed in the light of ECM components such as collagen, proteoglycan and water.

Superficial Zone

The superficial zone is approximately 200 microns which is the thinnest of the four zones. It is covered by a fine layer of the collagen fibrils called the lamina splendens (Williams, 2007). The lamina splendens corresponds to clear film portion of the superficial zone with no cells (Mansour, 2009). Collagen is uniformly distributed throughout the depth of articular cartilage except in the superficial zone. The collagen fibrils are thin and run parallel to the articulating surface Figure 1.7. The alignment of collagen fibrils gives greater tensile strength compared to the deep zone. On removal of this zone, experimentally permeability of the tissue increases. The dense collagenous network provides a barrier to larger molecules such as antibodies or other proteins, isolating cartilage from immune system (Buckwalter et al., 2005). This zone contains the highest content of water about 80% of the wet weight and the lowest content of proteoglycans (Bobick et al., 2009). Therefore the disruption of superficial zone may not only alter the structure and mechanical properties of the articular cartilage but also release molecules responsible to stimulate an immune or inflammatory response.

Middle Zone

The middle zone is approximately 500-600 microns thick characterised by large diameters of collagen fibers that are poorly organized. The organisation and matrix composition of this zone is intermediate between the superficial zone and the deep zone. Collagen fibers intersect obliquely or randomly with each other Figure 1.7 (Clouet et al., 2009). The concentration of proteoglycan is higher with lower concentration of water and collagen compared to the superficial zone matrix. It occupies several times of volume compared to superficial zone.

DEEP ZONE

This zone is the largest zone of the all four zones containing the largest diameter collagen fibers. These fibers are well separated and orientated perpendicular to the articular surface Figure 1.7. The fibers from this zone extend to a tidemark, a basophilic line, indicating the beginning of calcified tissue with less refined composition. This zone contains the highest concentration of proteoglycan and the lowest concentration of water (Clouet et al., 2009).

CALCIFIED ZONE

This zone lies close to the bone and acts as a transition from soft tissue to the hard tissue. Type X collagen is found near chondrocytes of the calcified zone of the articular cartilage, suggesting that it has role in cartilage mineralisation. The calcification occurs on the collagen fibers that anchor the tissue on to the subchondral bone (Clouet et al., 2009). This zones blocks transport of nutrients from the underlying bone leaving chondrocytes to depend on synovial fluid for nutritional support (Arkill and Winlove, 2006).

1.3 CARTILAGE BIOMECHANICS

Cartilage is subjected to a range of types and magnitudes of mechanical stimuli, such as compression, shear strain, stress, hydrostatic pressure and fluid flow (Eckstein and Wirth, 2011). An average load of three times the body weight is experienced by the articular cartilage. The knee could be exposed to 10 times the body weight during running and 20 times body weight during jumping (Williams, 2007).

Together fluid and the solid phase of the tissue provides mechanical properties of stiffness and resilience (Ko et al., 2007). 95% of the applied load in healthy cartilage is supported by the interstitial fluid. In conjunction with a lubricant and synovial fluid, healthy cartilage exhibits a very low coefficient of friction, with a value of 0.005, during

normal joint articulation (Roemer et al., 2012). During compressive loading, cartilage and matrix deformation stimulates chondrocytes metabolism. When loading is removed, the nutrients from the synovial fluid return to the body of the cartilage. When the cartilage is subjected to tension, collagen fibers and aggrecan molecules stretch along the axis of loading (Wu et al., 2007). In addition cartilage distributes the joint loading, with a stiffness provided by pressurisation of water within the tissue, thus protecting the underlying bone.

The articular cartilage in the diarthrodoil joint is predominately loaded in compression. The contact stress in a human hip joint during static loading loading has been measured to be 1-4 MPa during walking and upto 20MPa while standing up from the chair or jumping (Urban, 1994). These peak stresses results over a short duration < 1 second leading to cartilage compressive stains of about 1% to 3%. On the other hand, static physiological stress of approximately 3.5 MPa subjected to knee joints for 3-30 minutes can results in 35% to 45% of compressive strains on articular cartilage.

During normal activities fluid flow is restricted to the superficial and transitional zones only. As fluid is exuded from the superficial layer, the chondrocytes experiences deformation. The compressive strain must be high due to water exudation that comprises of 70-80% of tissue. The porosity of solid matrix decreasing with fluid flow and so fluid is retained in the deep zone of the articular cartilage (Setton et al., 1998). The thickness of the superficial layer reduces during physical activity. Once the joint is unloaded fluid osmotic pressure is created in the articular cartilage which results in imbibition of water back into the cartilage thus restoring the thickness of the articular cartilage (Suh et al., 1995). The magnitude of cartilage thickness is relatively smaller as a result of fluid exudation during physical activity. The main load carrying capacity of the articular cartilage is attributed to the pressurisation of the interstitial fluid within the tissue in response to the mechanical loading. It can be said that collagen network resist tensile and shear stress and the interstitial fluid resist compression generated in the joint.

1.3.1 CARTILAGE LOAD CARRIAGE

Cartilage represents an anisotropic, viscoelastic and poroelastic material. There are two possible mechanisms responsible for the viscoelasticity of tissue: flow independent and flow dependent. The flow independent viscoelastic behavior is due to the internal friction of cartilage proteoglycan matrix and the flow dependent behavior is due to the frictional drag of interstitial fluid flow. The main source of viscoelastic behavior of an articular cartilage is drag from the interstitial fluid flow. Articular cartilage exhibits creep and stress relaxation (Buckwalter and Mankin, 1998b). The compressive characteristic of the cartilage is mainly dependent on the interactions between the osmotic swelling pressure of proteoglycan and tension within the collagen network (Raynauld et al., 2008). The physiochemical equilibrium in the articular cartilage is maintained by the balance between osmotic swelling pressure ($P_{swelling}$) of the proteoglycan and the hydrostatic pressure ($P_{collagen}$) generated within the collagen fiber network ,such that

$$P_{swelling} = P_{collagen} \hspace{3cm} \textit{Equation 1.1}$$

The solid phase of articular cartilage is porous and permeable which allows water to flow through the matrix when loads are applied (Hunter et al., 2007). When articular cartilage is subjected to one dimensional confined compression, tissue undergoes creep by exudation of interstitial fluid (Figure 1.8). The initial deformation is elastic and instantaneously recoverable (Armstrong et al., 1984). When load is applied the balance is altered by application of the hydrostatic pressure ($P_{applied}$) that produces a net pressure differential (ΔP) with fluid flow away from the compressed articular cartilage, which is given by

$$\Delta P = P_{applied} + P_{collagen} - P_{swelling} \hspace{2cm} \textit{Equation 1.2}$$

However fluid flow is inhibited by fluid permeability of the matrix and distance from the pressurized fluid (Maroudas and Bullough, 1968; Mow et al., 1984). GAG chains are brought into close proximity that increases resistance to further compression due to repulsion and water forced out of macromolecules. Initially the exudation of fluid is more rapid as seen from Figure 1.8 and rapid increase in rate the of deformation. The

osmolarity of the tissue increases due to an increase in inorganic ions creating the Donnan effect. The collagen resists Donnan osmotic pressure generated by the association of inorganic ions to proteoglycans (Buckwalter, 1992).
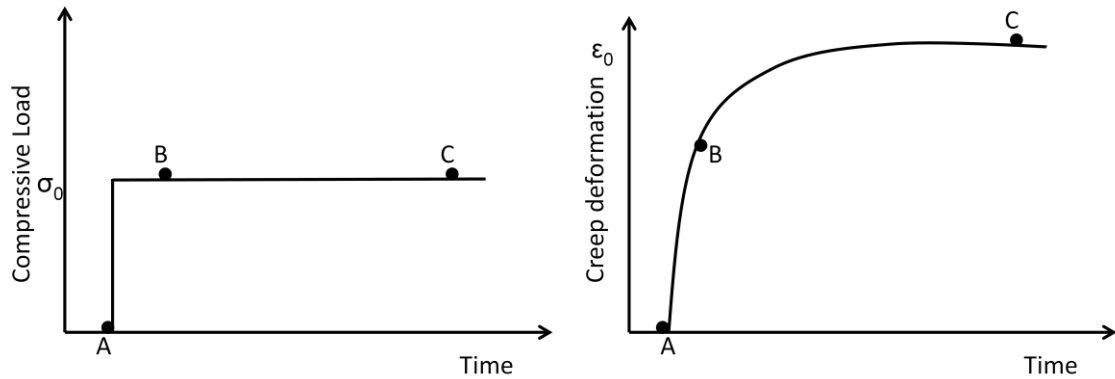
Figure 1.8. *When constant stress is applied to the sample of articular cartilage (A), the tissue deforms resulting in creep behaviour due to fluid exudation and it decreased from point A to B to C over time. At point C fluid flow cease and equilibrium is reached. (Mow, 1980)*

The external compressive load is balanced by the inner compressive stress generated within collagen-proteoglycan solid matrix due to frictional drag developed during exudation of interstitial fluid. When generated internal compressive stress is sufficient to balance the external compressive stress and at this point creep ceases and fluid exudation stops. At this point a new equilibrium state is achieved by the balance between the applied stress, tensile stress in the collagen fibers and increased swelling pressure.

$$P_{swelling} - P_{collagen} = P_{applied}$$

Equation 1.3

Figure 1.8 presents the creep behavior exhibited by the cartilage in response to the loading which are the characteristics of a time dependent viscoelastic material. Typically human and bovine articular cartilage with thickness of 2 to 4 mm takes 4 to 16 hours to reach creep equilibrium (Lu and Mow, 2008).
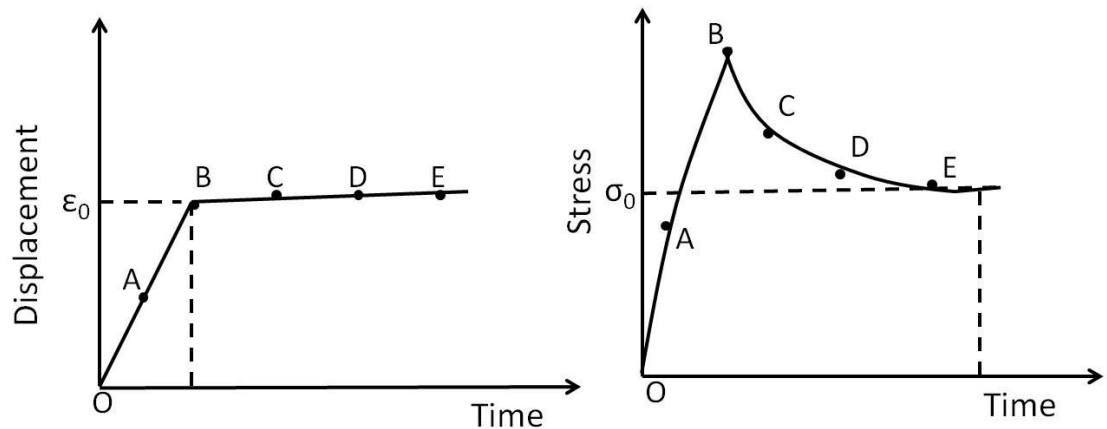
Figure 1.9 *A cartilage specimen is subjected to ramp displacement for maximum time of t_0 (bottom left) and resulting stress response (bottom right) under unaxial confined compression experiment. The specimen is loaded until maximum displacement of ε_0 is reached (point B) and load is held over time (B to E). The stress in the specimen increase to a peak stress at point B and then decreases from points B to D until equilibrium is reached (point E). The exudation of fluid gives rise to peak stress and fluid redistribution gives rise to stress relaxation. (Mow, 1980)*

Figure 1.9 shows the stress relaxation behavior of articular cartilage when subjected to one-dimensional unconfined compression test. In this test tissue is deformed until a given deformation is reached ε_0. The deformation is maintained beyond point B. The stress continuously increases until a given stress is achieved. The stress continuously decays (BCDE) during the relaxation phase, until an equilibrium is reached. The internal stress is generated due to fluid exudation and compaction of the solid matrix near the surface. The stress relaxation ceases when the compressive stress is balanced by the intrinsic compressive modulus of solid matrix (Mow et al., 1984).

Three independent variables are yielded by modeling articular cartilage with biphasic theory: the equilibrium compressive modulus, the Poisson's ratio, and the permeability. An aggregate modulus of human articular cartilage ranges from 0.53 to 1.34 MPa, Poisson's ratio ranges from 0 - 0.14 and permeability from $0.95 \times 10^{-15} m^4/Ns$ to $4.56 \times 10^{-15} m^4/Ns$ (Athanasiou et al., 1994; Athanasiou et al., 1995; Athanasiou et al., 1991).

1.3.2 ZONAL VARIATION IN MECHANICAL PROPERTIES

The structural and compositional heterogeneity of the articular cartilage is directly translated into mechanical properties (Baum et al., 2012). Variation in the collagen fibril orientation, density, diameter and collagen type along with variation in the amount of proteoglycan present with depth contribute to the variation of the mechanical properties over the depth of articular cartilage. The presence of lubricin and arrangement of collagen fibers on the surface provides an ideal structure for dispersing stresses (Raynauld et al., 2008). Performing compressive testing on the articular cartilage resulted in the compressive modulus 0.079 ± 0.039 MPa in the superficial zone to 2.10 ± 2.69 MPa in the deepest zone (Schinagl et al., 1997). Additionally tensile strength varies with depth from 25 MPa in the superficial zone and reduced to 15 MPa in the deep zone (Kempson et al., 1976). The permeability is higher in the middle zone compare to the superficial zone (Maroudas and Bullough, 1968).

1.4 CHONDROCYTES

Chondrocytes differentiate from mesenchymal stem cells of the bone marrow (Zhang and Chen, 2009). The diameter of chondrocytes varies in size from 7 to 30 µm. They are responsible for matrix remodeling, secret matrix components and enzymes that degrade matrix. Chondrocytes rarely divide once skeletal development is completed. Chondrocytes are surrounded with extracellular matrix and they do not make cell-to-cell contacts. Although chondrocytes do not provide direct resistance to the loading, their cellular shapes and chemical environment are directly influenced by the deformation of extracellular matrix and local fluid pressure and flow (Eckstein and Wirth, 2011).

1.4.1 METABOLISM

Cartilage experiences low oxygen tension ranging from 1-7%. Chondrocytes are able to survive in such hypoxic conditions by metabolising via the anaerobic pathway, glycolysis. Chondrocytes obtain nutrients through diffusion. Although chondrocytes from different zones differ in size and shape, they all contain matrix synthesis organelles such as Golgi membrane and endoplasmic reticulum. The matrix components such as proteins and GAG chains are produced by chondrocytes and secreted in the extracellular matrix. To maintain the articular cartilage, degraded matrix macromolecules must be replaced and new matrix macromolecular framework be generated in response to joint use. In order to facilitate these events, the cell must sense changes in the extracellular matrix and mechanical demands imposed on the tissue, then respond by synthesising required amounts of appropriate macromolecules.

The remodeling of extracellular matrix takes place through degrading enzyme secreted by chondrocytes therefore chondrocytes maintain a normal extracellular matrix by balancing synthesis of matrix components with its catabolism and release. The chondrocytes are metabolically active and respond to the soluble mediators such as growth factors and interleukins (Flik, 2007).The chondrocyte's ability to respond to anabolic stimuli such as growth factors and synthesis of proteoglcyans changes with aging (Buckwalter et al., 1993). This imposes limit on chondrocytes ability to maintain and restore the tissue (Martin and Buckwalter, 2002)

1.4.2 HETEROGENEITY

The morphology, size and shape of chondrocytes changes with depth of the articular cartilage. Additionally their metabolic activity differ with different zones of the cartilage .

SUPERFICIAL ZONE

 The chondrocytes are elongated and oriented in direction of shear stress. Chondrocytes possesses few organelles and synthesise specific proteoglycan. They secrete zone-

specific protein to provide lubrication properties (Clouet et al., 2009). Chondrocytes attach to the tissue culture surface more slowly compared to deep zones cells (Siczkowski and Watt, 1990).

MIDDLE ZONE

The cells are ellipsoidal and randomly oriented. The chondrocytes have a higher concentration of matrix synthesis organelles such as endoplasmic reticulum and Golgi membrane than superficial zone chondrocytes (Buckwalter et al., 2005).

DEEP ZONE

The chondrocytes are ellipsoidal or rounded and form stack of columns perpendicular to the articulating surface. The chondrocytes present in the transitional and the deep zone posses large cytoplasmic volume containing endoplasmic reticulum and golgi complexes (Bader, 2000). Chondrocytes in this zone are more synthetically active than in the rest of the tissue (Wong et al., 1996).

CALCIFIED ZONE

In this zone hypertrophic chondrocytes are present. The chondrocytes are surrounded by calcified cartilage. The volume of cell in this zone is smaller than the cells of the middle zone. The chondrocytes contains small amounts of Golgi membrane and endoplasmic reticulum reflecting the low level of metabolic activity (Buckwalter et al., 2005).

1.4.3 CYTOSKELETON ELEMENTS

The cytoskeleton is dynamic in nature and provides a structural scaffold within the cell. It remodels in response to external stimuli and enables contraction of the cell. The cytoskeleton is regarded as a crucial component for the anchorage-dependent cells since it contribute to the mechanical properties of the cell. The cytoskeleton comprises of three main components: actin microfilaments, tubulin microtubules and vimentin

intermediate filaments. These structures are seen in cells cultured in the monolayer as shown in Figure 1.10.
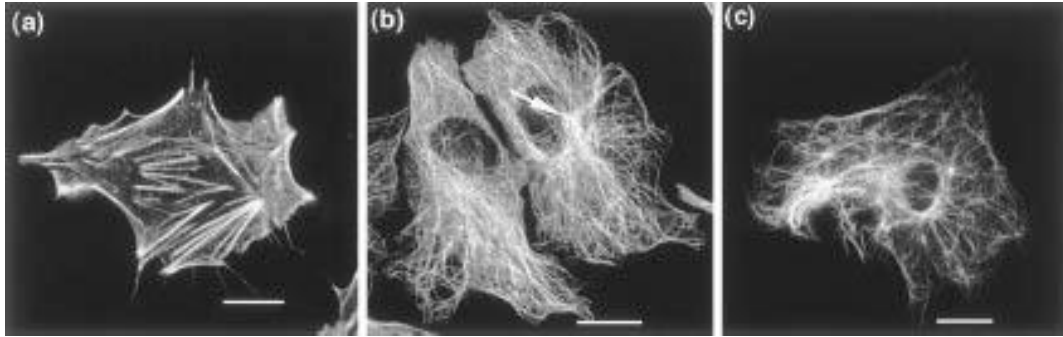
Figure 1.10. *Structure of microfilaments (a), microtubules (b) and vimentin intermediate filaments (c) in chondrocytes cultured in monolayer for 7 days. Scale bar 5 µm. (Idowu et al., 2000).*

MICROFILAMENTS

Microfilaments, also known as actin filaments are double-stranded helical polymer chains that make up to 5% of the cell protein content. The diameter of each microfilament is 5-9 nm and interacts with other filaments to form a network (Athanasiou and Shieh, 2002). Although actin filaments are found throughout the cytoplasm, they are more concentrated in the cell cortex.

Actin filaments are necessary in cell motility, contractility and adhesion. In response to cell adhesion, actin filaments form a bundle of the microfilaments called stress fibres that connect via intergrin in the plasma membrane to form focal adhesion as indicated in Figure 1.10. The focal adhesion forms a direct connection between the extracellular matrix and intracellular filaments allowing transmission of the forces from outside to inside (Burrige et al., 1996). Actin can bind with myosin to exert contractile forces on its surroundings. This contractile force allows a cell to maintain its morphology.

Cytoplasmic actin exists in two forms, globular G-actin and filamentous F-actin. G-actin assemble into highly organised filaments (Figure 1.11A). The mechanical behaviour of the actin filaments is dependent on the molecular structure of G-actin and on the intermolecular interactions forming a network. F-actin possesses "barbed" ends where association of G-actin monomer takes place and "pointed" ends where dissociation of microfilaments takes place. This process is termed as treadmilling that is regulated by association of regulatory proteins with cytoplasm such as thymosin β_4 and β_{10}, profiling and cofilin (Blain, 2009).

Mg^{2+}-ATP-bound G-actin integrates into growing filaments at the barded end (Ono, 2007). ADP-actin filaments is disassembled through loss of ADP-actin monomer, in turn ADP- monomer undergo nucleotide exchange to generate ATP-actin monomer. Furthermore actin assembly and disassembly is regulated by actin binding proteins. There are four kinds of actin binding proteins, 1) actin filament promoting protein such as the Arp2/3 complex and profiling (M.D., 2006) 2) actin filament depolarising such as ADF/cofilin family Ono, 2007) 3) protein associated with G-actin such as thymosin β_4 (Yarmola and Bubb, 2004) and 4) protein such as gelsolin cap the filament ends. Certain actin binding proteins severe filaments ends allowing formation of nucleation site for actin polymerisation (Witke et el., 1995). F-actin bundle up by actin binding proteins to form a thick cables known as stress fibers (Matsidaira, 1994).

The capping of the barbed end of the actin filaments results in an increase in critical concentration with monomer-polymer interaction restricted to the point ends of the filament. Actin binding proteins can also decrease the critical concentration by binding to F-actin over G-actin. The polymerization of actin in response to the changes in the environment requires a pool of monomeric G-actin. The size of monomeric G-actin depends on the value of critical concentration because the impound actin is at equilibrium with free G-actin. The depolymerising proteins such as cofilin possesses ability to severe actin filaments and sequester actin monomers (Sun et al., 1995). Profilin

is an actin binding protein found in all cells of living organism that increases the rate of filament elongation at low concentration of free G-actin.

Stable actin filaments enables force generation, stress fibers formation and intracellular transport. Crosslinked actin filaments form actin meshwork that supports the cell membrane providing structural integrity to the cell. Stable proteins are sometimes capped on both ends to prevent actin filaments elongation and depolymerisation. Alternatively formation of lamellipodia, filopodia during cell motility depends on dynamics of actin monomer-polymer interactions. In response to increase and decrease of actin monomer, actin filaments assemble or dissemble.

The polymerisation an depolymerisation is modulated by actin binding proteins which in turn regulated by upstream signals transmitted through mechanotransduction. Actin remodeling regulates intracellular membrane fusion, endocytosis and exocytosis (Eitzen, 2003). Following injury actin remodeling initiates repair of the injury site by increasing plasma membrane fluidity and intracellular transport (Godin et al., 2011). Furthermore actin remodeling is shown to be dependent on the calcium signaling (Erickson et al., 2003).
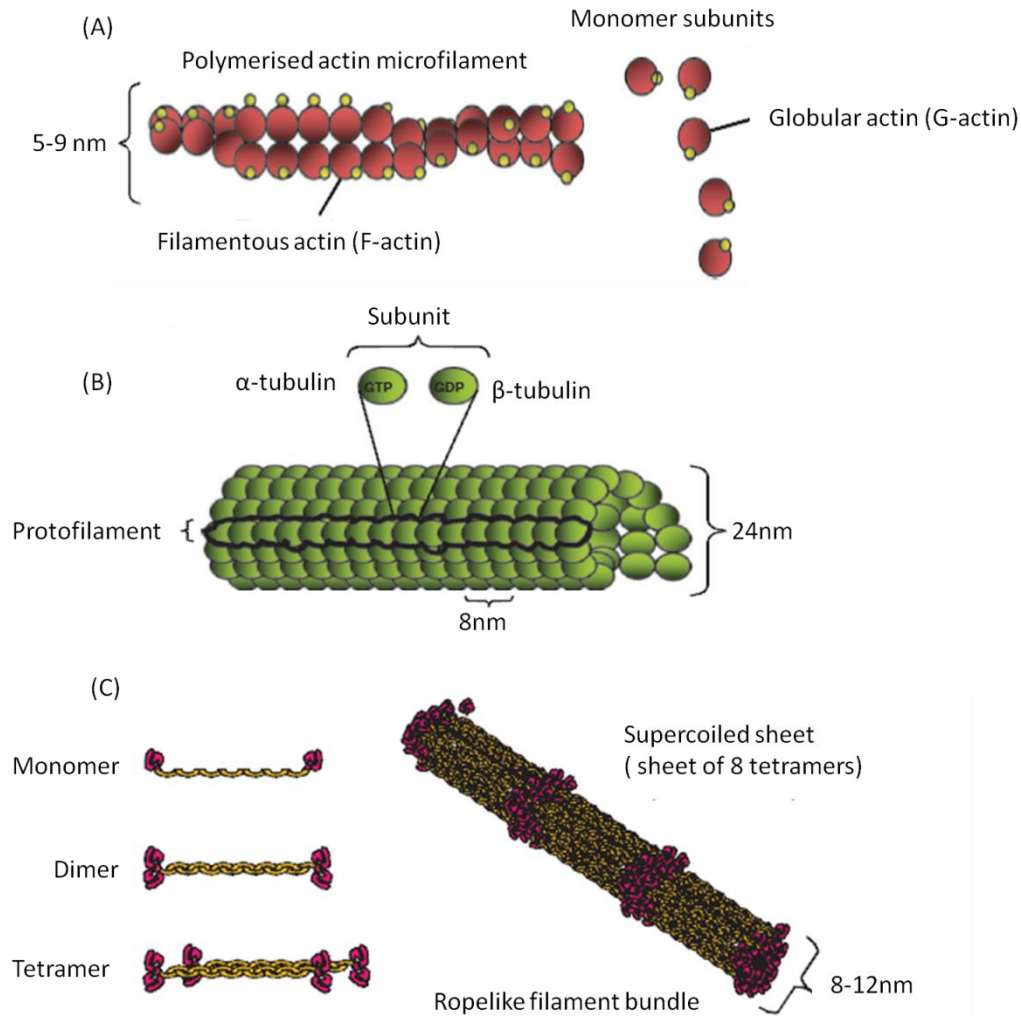
Figure 1.11. *Illustration of cytoskeletal components of cells: (A) actin microfilaments, (B) tubulin microtubules and (C) vimentin intermediate filaments. (Blain, 2009).*

TUBULIN MICROTUBULES

Tubulin plays a crucial role in cell division, organelle transport, cell morphogenesis and organisation. α-tubulins and β-tubulins are protein monomers with approximately 450 amino acids (Valiron et al., 2001). The dimeric proteins self-assemble to form microtubular configuration. Microtubules arrange linearly to form protofilament which in turn arrange laterally to form cylindrical structure as indicated in Figure 1.11B. A GTP

molecule binds to α-tubulin that is non-exchangeable and β-tubulin that is exchangeable (Sheih and Athansiou, 2000).

Microtubules continuously undergo polymerisation and depolymerisation of tubulin. It has been reported that the assembly of the microtubule is regulated by the mechanical forces (Putnam et al. 1998; Putnam et al. 2001). Microtubules, with a diameter of 25nm, are more rigid than microfilaments particularly loaded in bending and compression (Kurachi et al., 1995). The microtubules originated from the centrosome in the cell, as indicated in Figure 1.10, play a crucial role in mitosis and intracellular transportation (Kurachi et al., 1995). It is believed that the microtubule elements contribute to the viscous properties of the cytosol and are important in resisting compressive loading. The toxins such as colchicines, colcemid and nocodazole are used to examine the role of the microtubules in the overall material properties of the cell. They inhibit polymerisation by binding to free tubulin and subsequently affect mitosis (Sheih and Athansiou, 2000).

VIMENTIN INTERMEDIATE FILAMENTS

Vimentin filaments facilitate intracellular transport, maintaining mechanical integrity important for signal transduction. They are highly organised fibrous protein structures connecting the cell periphery with the nucleus which are produced from several subunits. Intermediate filaments fall in between microfilaments and microtubules in terms of size, with diameter approximately 10nm. Intermediate filaments possesses α-helical rod with non- α-helical head at both ends; N-(head) and C-terminal (tail) domains Figure 1.11C. These non- α-helical terminals differ in size and sequence. The monomeric vimentin subunits arrange in parallel fashion to form homodimers which inturn associates in anti-parallel fashion into tetramers. Eight of these tetramers interact laterally forming ropelike filament (Sokolova et al., 2006). The assembly and disassembly of intermediate filament is regulated by phosphorylation and dephosphorylation.

However, the definite function of the intermediate filaments is not clear. Nonetheless they can withstand considerable tensile stresses without rupturing, suggesting their

importance in mechanical functions of the cells. They directly link to the nucleus, hence provide means of direct force transmission from the cytoskeleton to the nucleus (Goldman et al., 1986).

1.4.4 CYTOSKELETAL ORGANISATION IN CHONDROCYTES

The cytoskeleton acts as a physical interface between the extracellular matrix and chondrocytes in sensing the mechanical stimulus and initiating biosynthetic activity within the chondrocytes. Typical architecture of actin microfilaments, tubulin microtubules and vimentin intermediate filaments in primary chondrocytes are presented in the Figure 1.12. The structure of the cytoskeletal network has been characterised in articular catilage explants (Durrant et al., 1999) in primary chondrocytes cultured in agarose and in monolayers (Idowu et al., 2000).

The heterogeneity exists in terms of the extracellular matrix, morphology of chondrocytes and variation also exist in cytoskeleton structure with depth. The microtubules and intermediate filaments are predominantly found in the middle and deep zones. Microfilaments are evenly distributed through the depth of the cartilage (Durrant et al., 1999) (Figure 1.12 A-I). F-actin is primarily localised at the cortex and distributed within the periphery of the chondrocytes. By contrast, the tubulin microtubules are uniformly distributed throughout the chondrocyte cytoplasm (Blain et al., 2006). Vimentin intermediate filaments form a highly organised structure, which is distributed throughout the cytoplasm of chondrocytes from the periphery to the nuclear membrane. The chondrocytes in healthy adult cartilage do not divide and migrate even in response to growth factors. This means, the roles of microfilaments in chondrocytes are in cell signalling, cell-matrix interaction, differentiation, intracellular transport, cell shape and control of secretion/endocytosis (Martin et al., 1999).

The phenotype of chondrocytes is controlled by microfilaments. Stress fibril, focal adhesions, lamellipodia and filopodia are prominent actin features in the monolyar as seen in Figure 1.10. These features are not seen, when chondrocytes are cultured in 3D

environment. Chondrocyte in the monolayer represents the fibroblastic phenotype and increase in type I collagen synthesis (Haudenschild et al., 2009).
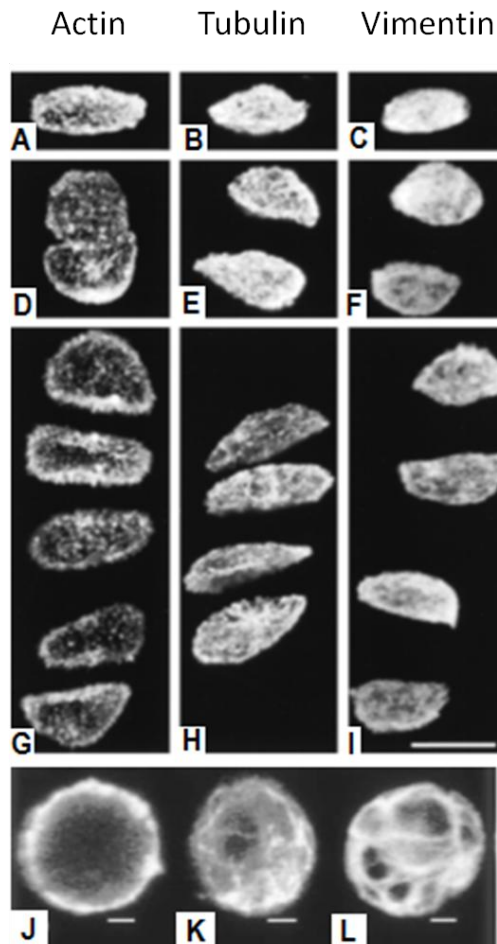
Figure 1.12. *Three-dimensional reconstructions of cartilage sections cartilage sections labeled for actin microfilaments (A,D,G),β-tubulin (B,E,H), and vimentin (C,F,I) using confocal laser scanning microscopy from different zones: tangential (A–C), transitional (D–F), and radial (G–I) (Bar 10 μm) (Durrant et al., 1999). Chondrocytes stained for actin microfilaments (J), microtubules (K) or vimentin intermediate filaments (L) within agarose constructs. Scale bar 2 μm. (Idowu et al., 2000)*

1.5 MECHANOTRANSDUCTION

Chondrocytes in the human body are subjected to stresses and strains arising from both the external environment and internal physiological conditions. Cells respond to these

stimuli depending on the magnitude, direction, distribution and nature of the mechanical stimuli. For example it has been long established that the mechanical compression modulates proteoglycan synthesis in chondroycte (Bachrach et al., 1995; Buschmann et al., 1995). The mechanical loading can alter the behavior of the cell in the process known as mechanotransduction (Bader and Knight 2008). The applied force results in cell deformation and induced variety of cell process such as growth, differentiation, adaptation and cellular breakdown. Therefore understanding the cell response to mechanical loading is the first step towards investigating the transmission and distribution of the mechanical signals that are converted into biochemical responses in the cell (Wang et al., 1993; Ingber, 2003). Additionally understanding the deformation experienced by cells will elucidate these mechanotransduction processes which play a crucial role in many aspects of tissue health, damage and diseases. Tissue can undergo atrophy without mechanical stimulation.

1.5.1 Iɴ ᴠɪᴠᴏ Eᴠɪᴅᴇɴᴄᴇ ꜰᴏʀ Mᴇᴄʜᴀɴᴏᴛʀᴀɴꜱᴅᴜᴄᴛɪᴏɴ

It has been demonstrated that when knee joint is unloaded, the GAG content of articular cartilage decreases particularly in the periphery region on the joint (Kiviranta et al., 1987). This suggests that even the contact forces in the central region of the joint are sufficient for maintaining tissue. On other hand the joint exposed to increased weight bearing results in increase in the GAG content of the tissue. The increase of GAG content is seen in all zones except in the superficial zone. This is due to the local depletion of the GAG content. The studies performed on the animal joints have shown that immobilising or reduce loading on the joint results in a decrease in matrix synthesis and contents leading to softening of the tissue (Behrens et al., 1989). On other hand, dynamic loading or remobilisation of a joint increases the concentration of aggrecan. However severe impact or strenuous exercise can result in cartilage degeneration.

1.5.2 IN VITRO EVIDENCE FOR MECHANOTRANSDUCTION

Application of compression on the cartilage, results in deformation of cells and extracellular matrix (Grodzinsky et al., 2000). Static compression also results in physiochemical changes within the matrix such as changes in the matrix water content, fixed charge density, ion concentration and osmotic pressure. It has been demonstrated that static compression of cartilage in vitro within a physiological range can be reversible and inhibit production of matrix components (Urban, 2000). Therefore static compression down regulates the synthesis of type II collagen, aggrecan core protein and link protein. By contrast, cyclic compressive strain or hydrostatic pressure can stimulate synthesis of aggrecan core protein. Mechanical forces in the surrounding of the chondrocytes significantly affect the production and degradation of matrix macromolecules.

The compressive loading of cartilage explants have been shown to modulate chondrocyte viability (Steinmeyer et al., 1997), gene expression (Fitzgerald et al., 2004) and synthesis of extracellular matrix macromolecules. Furthermore it has been shown that at physiological level of strain (2 - 10%) (Fitzgerald et al., 2004) or stress $0.5 - 1.0$ MPa (Steinmeyer et al., 1997) and 0.01 - 1.0 Hz frequencies can induce the synthesis of proteoglycan (Loeser, 2000).

It has been demonstrated using cell/agarose constructs that dynamic loading of 3% strain with $0.01 - 1$ Hz frequency over 10 hours raises proteoglycan synthesis by 6 - 25% (Buschmann et al., 1995). Additionally Lee et al have shown that dynamic compression at 15% strain, 1 Hz increases 50% of glycosaminoglycan synthesis by chondrocytes from deep (Lee et al., 2000b) and proliferation of the superficial zone chondrocytes increases by 40% (Shelton et al., 2003). Loening et al (2000), reported that compression of the bovine explants at a stain of 30 - 50% for period of 5 minutes results in peak stress between 4 and 25 MPa (Loening et al., 2000).

Ragan et al. (1999) had loaded the bovine explants with various compressive loading regimens to investigate the changes in Type II collagen, protein synthesis and aggrecan They observed that sulphate, aggrecan mRNA incorporation decreases in a dose and time dependent manner due to static loading (Ragan et al., 1999).

1.5.3 Signaling Pathways

Compressive loading is an array of events including the deformation of cells and matrix, the presence of hydrostatic pressure gradient, fluid flow, and altered water content, osmotic pressure and the development of streaming potential due to the movement of cations (Urban, 1994). In order to better understand which load induces physiochemical changes, various cellular pathways have been suggested that are responsible for generating biosynthetic response.

 The foremost pathway is the deformation of the cell, whereby cell is deformed by application of mechanical force in situ or in vitro. The estimated equilibrium modulus of chondrocytes is 1000 fold lower than the cartilage reflecting that chondrocytes deforms when tissue is deformed (Guilak et al., 1999). Cell shape is changed when deformed by mechanical loading (Kim et al., 1994).

Secondly, integrins are located in such a way that form bridges between extracellular matrix and chondrocytes, this suggests that it plays a role as mediators in the mechanotransduction pathway (Ingber et al., 1994). It has been suggested that upregulation of GAG synthesis and proliferation in response to dynamic loading is attributed by α5β1 through TGF-β3 dependent pathway (Chowdhury et al., 2004). Growth factors and cytokines modulate integrin mechano receptor expression and integrin-matrix affinity. This leads to changes in integrin signaling following changes in the matrix protein production (Kalichman et al., 2007), stimulation of MMPs and aggrecanases (Bamac et al., 2006).

Mechanical stimuli can be transferred by cell membrane ion channels and transporters (Hill et al., 2007). Ca^{2+} is a second messenger in various signaling pathways after

subsequent cell deformation (Yellowley et al., 1997). It has been shown with calcium channel blocker suppresses stretch-induced proliferation and maturation of chondrocytes (Wu and Chen, 2000). Apart of calcium ion channels there are other channels that may be involved in mechanotransduction pathways.

As a result of activation of integrins and ions channels a complex chain of events is initiated by release of various autocrine/paracrine molecules or activation of other pathways. This chain of reactions is known as downstream signaling. It has been reported that adenosine tri-phosphate is released in response to mechanical loading of cells which act as an autocrine/paracrine molecules and affect membrane hyperpolarization (Millward-Sadler, 2004).

Chondrocytes derived from both normal and abnormal cartilage respond to mechanical stimuli by integrin recognition of stimulus (Conaghan et al., 2006). A number of differences exist in the signaling cascades associated with normal and diseased chondrocytes. Initial events are similar such as α5 β1 integrin, followed by rapid tyrosin phosphorylation of FAK, paxillin and β-catenin (Lee et al., 2000a). However, actin is involved in integrin mediated signaling mechanism in normal chondrocytes (Issa et al., 2007).

1.6 Articular Cartilage Injury, Diseases and Repair

It is believed that mechanical forces either acting upon a structurally abnormal joint or abnormal forces acting upon normal joints are involved in pathophysiological process then eventually leading to osteoarthritis (Kornaat et al., 2006). Mechanical injury can directly induce damage in articular cartilage by mediating chondrocytes matrix degrading enzyme thereby reducing synthesis of matrix macromolecules (Kurz et al., 2005). The degeneration of articular cartilage and progressive loss of the normal cartilage structure and function leads to osteoarthritis (Buckwalter et al., 2000). Osteoarthritis (OA) is a condition of jointpain and dysfunction caused by the joint degradation which could be

due to the injury or age related factors, genetic and developmental abnormalities. Mechanical over load due to trauma or abnormalities in joint due to obesity (Gelber et al., 2000), altered joint geometries (Murphy et al., 1995) have been recognised as risk factors for secondary osteoarthritis.

1.6.1 ACUTE CARTILAGE INJURY

Cartilage possesses limited healing capacity after injury due to relatively low cell density, lack of vascularity and lack of progenitor cells. The two main criteria that need to be addressed for articular cartilage tissue repair are to fill the defect with the tissue possessing similar mechanical properties to the native tissue and promote successful integration between the native and repair tissue.

PARTIAL THICKNESS DEFECTS

This defect is similar to cleft and fissures observed during the initial phases of osteoarthritis. It is thought that this defect fails to heal due to the fact that it does not penetrate the subchondral bone and therefore is unable to access the progenitor cells of the bone marrow space as indicated in Figure 1.13.

FULL THICKNESS DEFECTS

Full thickness defect penetrates the subchondral bone through the calcified zone of the articular cartilage thereby gaining access to the bone marrow stem cells as indicate in Figure 1.13. As a result, a repair process is initiated with formation of a fibrocartilaginous tissue in the defect void. However this repair tissue has poor mechanical properties compared to the native articular cartilage and with time repair tissue degenerates (Redman et al., 2005).

A: partial thickness defect

articular
cartilage

subchondral
bone

B: full thickness defect
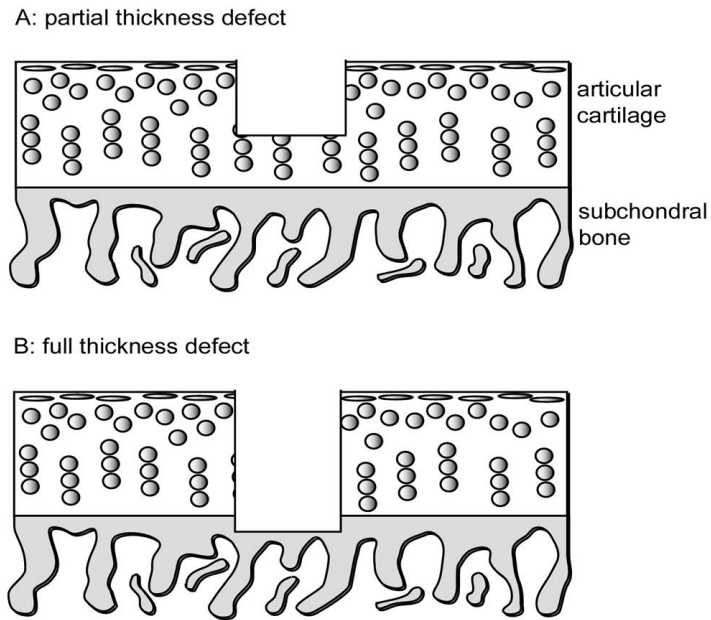
Figure 1.13: *Schematic illustrating the a partial thickness defect in articular cartilage (A) and a full thickness defect that penetrates to the subchondral bone (B). (Redman et al., 2005)*

1.6.2 OSTEOARTHRITIS

The osteoarthritic cartilage has a rough surface compared to the normal cartilage (Aigner et al., 2006). Chondrocytes in the osteoarthtic tissue divide and form cluster. During the early stage of the degeneration the level of the proteoglycan and collagen fibres increases as chondrocytes tries to compensate for the unregulated catabolism (Lippiello et al., 1977). Hence this could contribute to the late mechanism of cartilage degeneration (Kim and Blanco, 2007). A multiples-step signaling mechanism is initiated with upstream of activators such as interlukin 1 (IL-1) and nitric oxide. In future inhibition of chondrocytes apoptosis through the signaling cascade can provide therapeutic target for the OA (Clouet et al., 2009).

The loss of the aggrecan causes largely alteration of extracellular matrix, destructing cartilage. Despite the compensating activity of the chondrocytes the imbalance between catabolic and anabolic metabolism occurs. The anabolic factors such as insulin growth factors (IGF-I), transforming growth factors-beta (TGF-β), Bone morphogenetic protein

and fibroblast growth factors are found to decrease with age and advanced OA (Clouet et al., 2009).

Matrix metalloproteinases are the enzymes responsible for the ECM degradation (Clutterbuck et al., 2009). Additionally, synovitis leads to overexpression of the cytokines such as IL-1β, TNF-α and –β which subsequently contribute to the catabolic degenerative processes of the cartilage (Benito et al., 2005). Consequently the production of nitric oxide is stimulated by the upregulation of iNOS (inducible Nitric Oxide Synthase) and other pro-inflammatory cytokines and chemokines (Goldring and Goldring, 2004).

Various in vitro injury models have been developed to over load or injure cartilage explants see review (Kurz et al., 2005). Although there are many variations in protocols and specimen preparation, similar trends exist in the pathomechanism of cartilage overload and injury. The cartilage injury results in cell death, release of matrix macromolecules such as proteoglycans, water content of tissue and swelling increases, decrease in the mechanical integrity and function, and impair response to further mechanical loading (Kurz et al., 2005).

Chondrocytes obtained from diseased tissue have different cellular response to mechanical stimulation when compared to cells from healthy tissue. The production of cytokines, such as IL-1 β and IL-6, increases with an associated decrease in aggrecan mRNA following mechanical stimulation (Conaghan et al., 2006; Eckstein et al., 2006). It has been proposed that chondrocytes derived from a diseased tissue, activates different signaling mechanism in response to mechanical stimuli as a result of altered mechanotransduction.

In case of the OA, catabolic events are upregulated compared to synthesis of macromolecule leading to the loss of extracellular matrix. OA is characterised by altered chondrocyte gene expression (Reginato and Olsen, 2002) and reduction in proteoglycan and collagen type II synthesis with associated secretion of pro-inflammatory cytokines and proteases (Goldring, 2000).

1.6.3 REPAIR TECHNIQUES OF ARTICULAR CARTILAGE

ARTHROSCOPIC REPAIR PROCEDURE

This technique includes repair procedure such as abrasion arthroplasty, Pridie drilling and microfracture. Abrasion arthroplasty involve using automated burr to access the vasculature in conjuction with debridement (Singh et al., 1991). In Pridie drilling, the subchondral bone is drilled to stimulate bleeding (Beiser and Kanat, 1990). Microfracture procedure involves the debridement of damaged cartilage down to subchondral bone and to induce bleeding it is perforated by small holes approximately of 2-3mm in size apart (Sledge, 2001). These techniques are solely dependent on the formation of the blood clot leading to formation of fibrous tissue.

OSTEOCHONDRAL TRANSFER TECHNIQUES

This technique is used to treat predominately large osteochondral defects. A cartilage osteochondral graft from a limited weight bearing chondral surface is harvested and transferred into defect area, using a press fit technique (Hangody et al., 1997) as indicated in Figure 1.14. The disadvantage are donor site morbidity, short-term fixation, and peripheral death of chondrocyte due to harvesting and grafting and difficulty in restoring concave and convex shape (Clair et al., 2009). Osteochondral allograft transplantation involves the usage of the graft harvested and maintained in the tissue bank, and used within 28 days of the harvest from the individual (Williams et al., 2004). The implantation technique is similar to osteochondral autograft transplantation. However the one advantage of this technique is that it avoids the donor site morbidity.
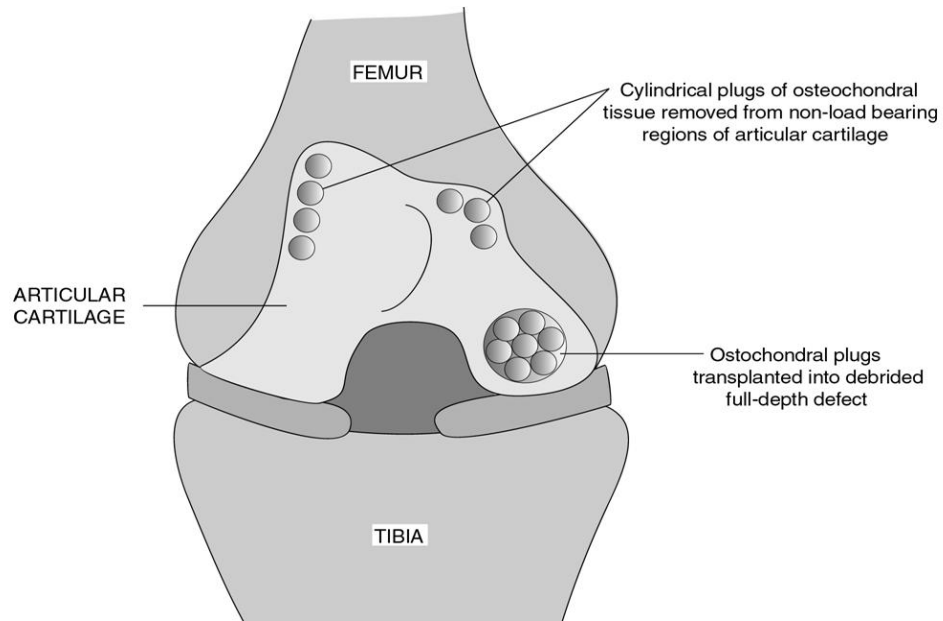
Figure 1.14. *Schematic depicting the procedure involved in osteochondral transfer. (Redman et al., 2005).*

OSTEOCHONDRAL GRAFT SUBSTITUTES/SCAFFOLDS

Bioreabsorbable scaffold is designed to be osteoconductive, chondroconductive or both. They are developed to treat focal chondral and osteochondral lesions (Clair et al., 2009). The scaffolds are designed to be integrated with the adjacent cartilage layer and subchondral bone to initiate ingrowth of osteous and cartilaginous cells into the scaffold, as a result a new matrix is generated. Additionally this scaffold can be used to fill the defect at the donor site. This strategy has the advantage of being both cost effective and time efficient and represents a single stage procedure thus avoiding donor site morbidity. However it has been shown in animal models that the frictional forces and debris between implants and interface leads to periprosthetic inflammation and osteolysis (Nizegorodcew et al., 1997).

AUTOLOGOUS CHONDROCYTE IMPLANTATION

Autologous chondrocyte implantation (ACI) was first reported by (Brittberg et al., 1994). The procedure involves excision of the healthy biopsy from minimal weight bearing sites of the articular cartilage. The chondrocytes are isolated by enzymatic digestion. The extracted chondrocytes are cultured in monolayer to permit expansion in vitro. The second stage of the implantation involves injecting the cells into the defected area which is then covered with a periosteal flap taken from the proximal medial tibia as indicated in Figure 1.15. There is a possibility of periosteal hypertrophy resulting in the disintegration of the graft, hence failure of the procedure (Brittberg et al., 1994). Furthermore limited activity is recommend to the patient for up to 6-8 weeks and full return to activity for up to 12 months.

Matrix-Induced autologous chondrocyte Implantation represents a second generation of autologous implantation. This procedure involves cultivation of the chondrocytes on a scaffold inducing chondrocyte growth. These scaffolds are biodegradable and provide temporary support for the cells to grow until they generate a new matrix (Bartlett et al., 2005). Mesenchymal stem cells are capable of the differentiating into articular cartilage. Therefore instead of the autologous chondrocytes, stem cells can be used to implant in the defect. It has been reported that the result of the mesechymal cells and autologous chondrocyte is comparable (Hui et al., 2004).
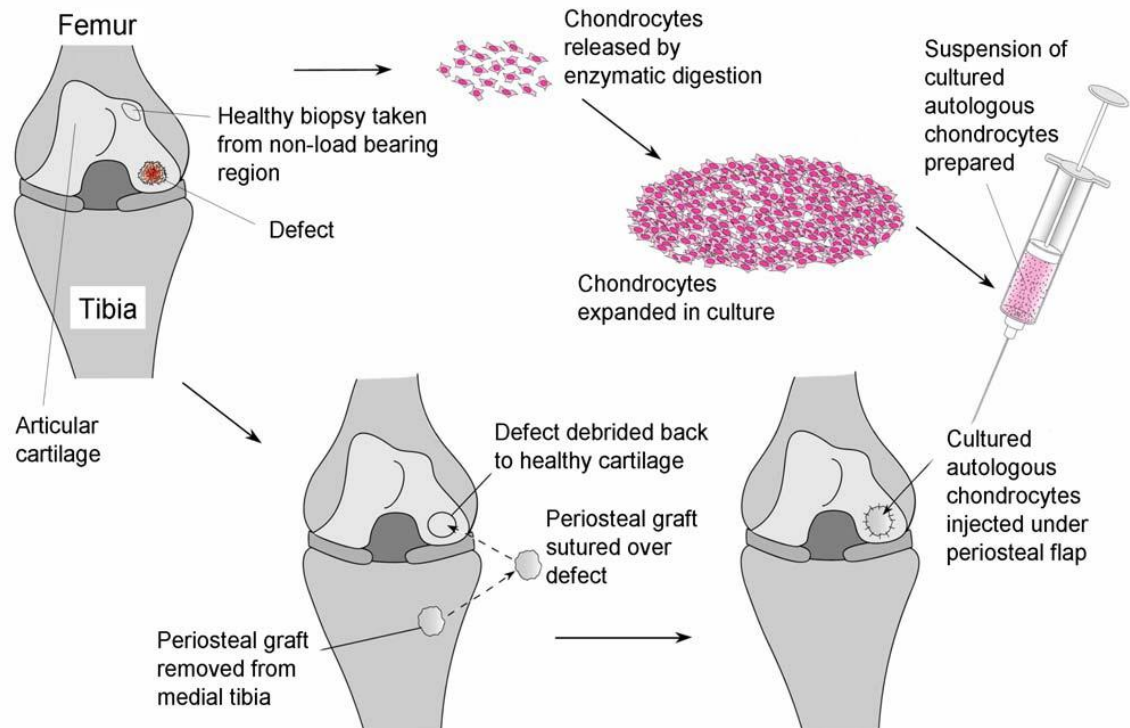
Figure 1.15: *Schematic illustrating the steps involved in the autologous chondrocyte implantation. (Redman et al., 2005)*

Chapter 2

MEASUREMENTS OF CHONDROCYTES MECHANICS

2.1   **INTRODUCTION**

2.2   **EXPERIMENTAL TECHNIQUES**

2.2.1   Atomic Force Microscopy

2.2.2   Cytoindentation

2.2.3   Cytocompression

2.2.4   Optical Tweezers

2.2.5   Magnetic Tweezers

2.2.6   Compression of Cells within 3D Scaffold

2.2.7   Micropipette Aspiration

2.2.8   Selection of Experimental Technique

2.3 MICROPIPETTE ASPIRATION

2.3.1   Liquid Drop Model

2.3.2   Elastic Solid Model

2.3.3   Viscoelastic Solid Model

2.4   **MECHANICAL PROPERTIES OF CHONDROCYTES**

2.4.1   The Influence of Age on Chondrocytes Mechanics

2.4.2   The Influence of Zonal Variation on Chondrocytes Mechanics

2.4.3   The Influence of Disease on Chondrocytes Mechanics

2.5   **THE ROLE OF ACTIN IN CELL MECHANICS**

2.5.1   Actin Bleb Formation

2.5.2   Mechanical Behavior of Isolated/Purified Actin   .

2.5.3   Influence of Actin on Cell Mechanics

2.5.4   Effect of Chemical Agents on Actin Dynamics

2.5.5   Critical Summary of the Literature

2.6   **AIMS AND OBJECTIVES**

2. MEASUREMENTS OF CHONDROCYTES MECHANICS

2.1 INTRODUCTION

This chapter begins with the description of the different experimental techniques used to measure the mechanical properties of the cells. Amongst these techniques micropipette aspiration technique has been selected for the experimental work performed in this thesis. The experimental outcome of this technique is examined by using the analytical models, particularly viscoelastic models. This is followed by the description of the different factors such as age, zonal variation and disease on the cell mechanics. Furthermore role of actin is discussed in the light of the cell mechanics. This chapter ends with the aims and objectives of the present thesis.

2.2 EXPERIMENTAL TECHNIQUES
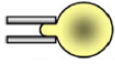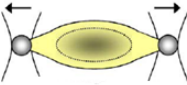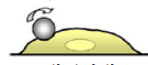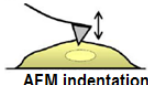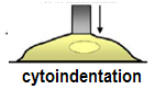
In the last decades, there has been an emergence of range of techniques (Table 2.1) which have been used to measure forces in vitro ranging from nanonewtons (nN) to piconewtons (pN). They have been employed to investigate the biomechanical properties of a range of cell types. The experimental techniques can be conveniently classified into three types:

Type A – involves application of the mechanical force such as atomic force microscopy (AFM), micropipette aspiration (MA) and cytoindentation or cytocompression.

Type B – involves application of field gradients traps such optical tweezers (OT), magnetic tweezers (MT) and dielectrophoretic traps (DEP).

Type C – involves loading of the population of the cell by application of the mechanical loading. This type includes loading of the cell in agarose construct or tissue explants.

Table 2.1*. Mechanical models developed for different techniques (Lim et al., 2006)*

These diverse experimental techniques have been used at a range of loading rates and magnitude of pressure. A number of distinct mechanical models have been used to estimate parameters and characteristics of cellular behaviour (Table 2.1).

2.2.1 ATOMIC FORCE MICROSCOPY

Binning et al., (1986), first developed the atomic force microscopy (AFM) describing it as a powerful tool that can provide 3-D images of the surface topography of biological samples in both liquid and gaseous surroundings. They also noted that the AFM may be used to determine the mechanical properties of material surfaces including biological material and manipulating mechanical properties of biological materials (Binnig et al., 1986). The AFM comprises of a microfabricated cantilever tip (Figure 2.1A) from silicon and silicon nitride of 100-500 μm in length and 0.5-5 μm in thickness (Alonso and Goldmann, 2003). The tip of the cantilever can take number of geometrical shapes. Most commonly, a pyramidal shape cantilever tip is used due to its lower mechanical resistance to vertical deflection and high resistance to lateral torsion. This tip typically has a radius of curvature of less than 20 nm with height of 0.6 μm and diagonal base length of 4 μm. When the probe is brought into proximity of the specimen surface, force

between the probe and the sample results into a deflection of the cantilever (Figure 2.1B). This is measured by the reflected laser spot from the back of the cantilever beam and collected in the photodiode. The generated elastic and viscoelastic responses of the cell can be analysed using respective models.

A)   B)
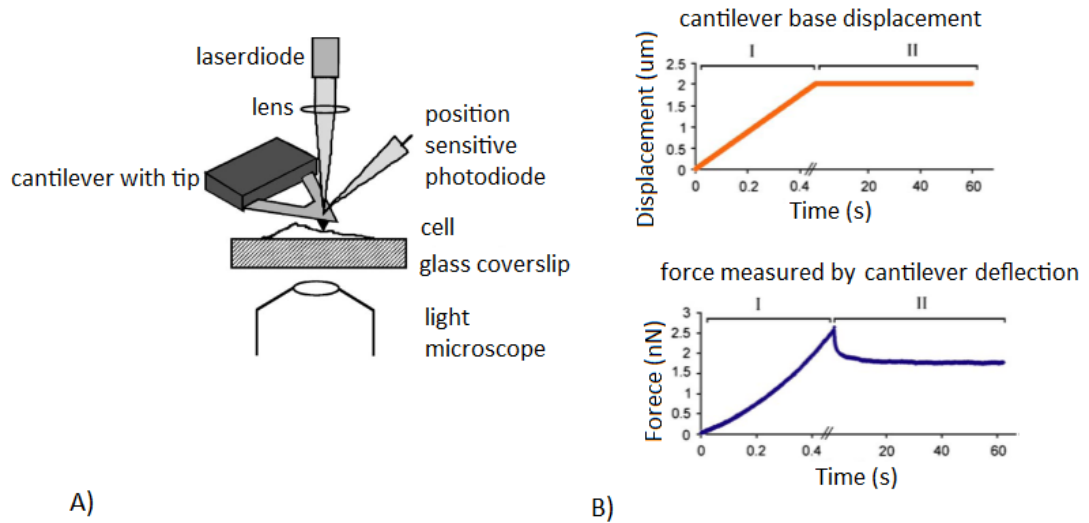
Figure 2.1. A) Diagrammatic representation of an AFM. The tip is mounted on the cantilever and the displacement of the cantilever is detected by the photo sensitive diode using a laser beam. The light microscope is used to positioned and visualise the sample (Alonso and Goldmann, 2003).B) Plots of the cantilever displacement and force with time, respectively. Phase I and II represents the elastic and viscoelastic responses of the cell (Darling et al., 2006a).

The stiffness of living a cell can be estimated from AFM derived force-indentation curves in conjuction with theoretical models (Figure 2.1B). AFM has been widely used to measure the mechanical properties of different cells (Sen and Kumar, 2010). However, the results are dependent on the geometry of the indenter tip and the associated analytical models. In addition this technique produces measurements with a high spatial resolution. Therefore in the case of cell mechanics, modulus values are heavily influenced by underlying structure such as individual actin stress fibers (Lu et al., 2008).

Finally, although AFM has been used to obtained the mechanical properties of cells in suspension, it is best suited to localised measurement of adherent cells in monolayer.

2.2.2 CYTOINDENTATION

Athanasiou and co-workers have developed a cytoindentation system to determine the viscoelastic creep properties of isolated chondrocytes (Koay et al., 2003)
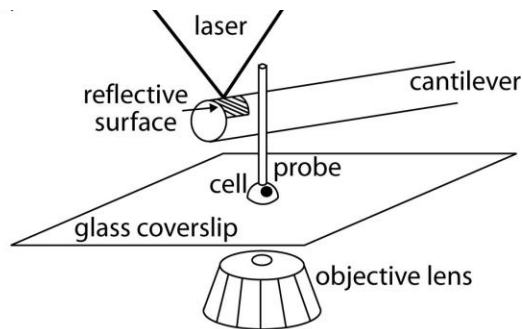
Figure 2.2. *Schematic of creep cytoindentation apparatus consisting of closed loop control algorithm to apply constant stress to the surface of adherent cells by way of a .glass probe fixed to the end of a cantilever beam which may be detached using a laser (Koay et al., 2003).*

Figure 2.2 indicates the schematic of cytoindentation system. This system is designed to apply a constant compressive stress on individual adherent cells. The resulting deformation is measured using closed loop control algorithm for which apparatus used are a force transducer (cantilever), sensor (laser micrometer), a motor (piezoelectric translator) and controller (PC running LabView). The cantilever is made from borosilicate (Koay et al., 2003). A indenting probe is fixed at the end of glass cantilever beam. The probe dimension is selected depending on the assumptions made for mathematical models required to compute mechanical properties.

The 1 mm extension of the free end of cantilever beam is coated with chrome paint to facilitate the measurement of deflection of the beam by a laser micrometer. The laser

micrometer record the position of the end of the cantilever beam while a piezoelectric translator records the position of the base. The difference between displacement of the end of the cantilever beam and movement of piezoelectric translator controlled by computer provides net deflection of the cantilever beam which is further use to compute applied force and subsequently Young's modulus using continuum mechanics modelling.

2.2.3 CYTOCOMPRESSION

This technique is used to apply unconfined compression to isolated cells in suspension or monolayer culture (Leipzig and Athanasiou, 2005; Shieh and Athanasiou, 2006). A piezoelectric actuator is used to apply compressive forces directly to a single cell via a 50 µm diameter compression probe. The cell deformation is quantified from the displacement of the probe which is measured using a laser meter as shown schematically in Figure 2.3. Typical experiments involve application of a static load and measurement of the resulting cell deformation which exhibits characteristic viscoelastic creep. The temporal change in cellular deformation may be fitted using analytical models to estimate the modulus and viscosity of the cell.
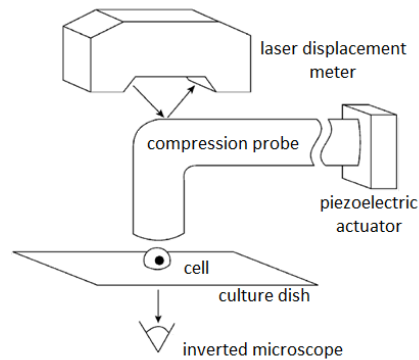
Figure 2.3. Schematic of the cytocompression system in which direct compression is applied to a single cell using a cantilevered tungsten rod. A laser displacement meter measures the position of the cantilever free end and hence the degree of cell deformation. (Shieh and Athanasiou, 2006)

2.2.4   Optical Tweezers

Optical tweezers, also known as laser tweezers or laser traps may be used to measure cell mechanics and work on the principle of radiation pressure. In this technique a laser is focused through a microscope objective lens and traps/attracts a bead of high refractive index. Beads are either coated with ECM proteins or cell-adhesive peptides (Lele et al., 2007) that are distributed on the surface of the cells. This bead is attached to the cell surface such that displacement of the laser beam moves the bead exerting a force and corresponding deformation on the cell. One approach used in cell mechanics involves bringing the bead into close proximity of the cell allowing it to adhere to the surface. The bead is then attached with optical tweezers, pulling the plasma membrane tether as indicated in Figure 2.4. The velocity of tether elongation in relation to the applied force may be used to characterise local mechanical properties of the cell.
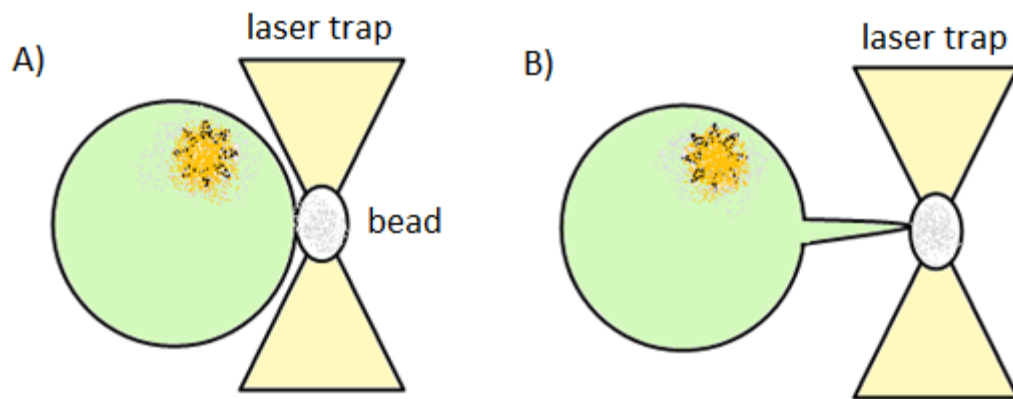
Figure 2.4. *Application of laser tweezers for the study of cell mechanics. (A) An RGD coated bead is brought into proximity of the cell. (B) The bead is then pulled away resulting in extension of the cell. (Huang et al., 2003)*

The laser output controls the force generated by the optical tweezers, which is typically in the pN range, and should be small enough to minimise damage to the cells. Alternatively a bead-free approach may be used where the refractive index mismatch

between the cell and the media is sufficient to generate a force to deform the cells (Chalut et al., 2012). This technique has been used to investigate the chondrocytes plasma membrane tether formation with time. This quantifies the force required to separate the plasma membrane from cytoskeleton. The force required to separate the membrane increasing the culture time (Huang et al., 2003).

2.2.5   Magnetic Tweezers

Magnetic tweezers operate in similar way to optical tweezers but in this case a magnetic field is applied to manipulate paramagnetic or ferromagnetic beads bound to the cell surface sample Figure 2.3. The magnetic field may be used to displace the bead(s) (Figure 2.3), or alternatively the beads may be rotated through a technique known as magnetic twist cytometry.

In this technique, a strong magnetic field is applied for a very short period to induce the magnetic dipoles of the bead to align along the horizontal direction. Subsequently a weaker magnetic field is applied perpendicular to the original field causing the beads to re-align in the new direction. This second weaker field is insufficient to realign the moments of the beads therefore instead causing the beads to twist. The magnetic twisting effectively applies angular strain to the cell receptors the shear stiffness is computed by measuring rotation or angular bead strain (Bausch et al., 1999).
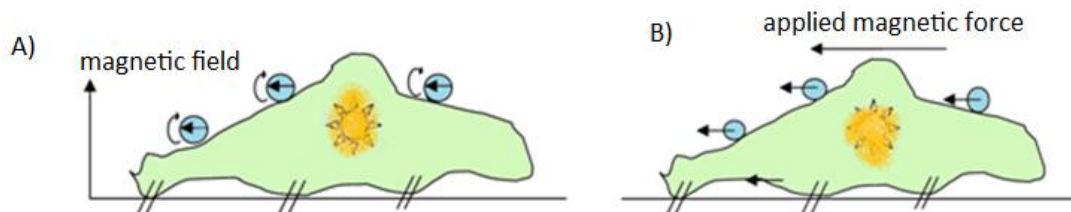
Figure 2.5. Schematic showing one approaches for the use of magnetic tweezer in the study of cell mechanics. (A) Magnetic beads are noncovalently attached to the cells and poles of beads aligned due to magnetic field. (B) Drag force is applied to bead via a magnetic field. (Athanasiou and Shieh, 2002; Bausch et al., 1999).

2.2.6 COMPRESSION OF CELLS WITHIN 3D SCAFFOLD

Cellular mechanics has also been examined by applying compression to isolated chondrocytes seeded within 3D hydrogel scaffolds, such as agarose and alginate, and simultaneously measuring the resulting cell deformation (Figure 2.6) (Knight et al., 2006). With knowledge of the gross mechanical properties of the scaffold it is possible to estimate the cell modulus. Static compression of cell seeded alginate gels results in viscoelastic stress relaxation. This produces a temporal reduction in cell deformation from an oblate ellipsoid to a more spherical morphology (Knight et al., 2002). Previous studies have therefore used the instantaneous modulus of the gel and the corresponding instantaneous cell strain to estimate the chondrocyte modulus at a value of 3 kPa (Knight et al., 2002). Similarly in 1% (w/v) agarose, gross 20% compression results in a cell strain of approximately 13.8% at an equilibrium gross stress 0.38 kPa. Thus the modulus of the cell has been estimated at 2.7 kPa (Bader et al., 2002).
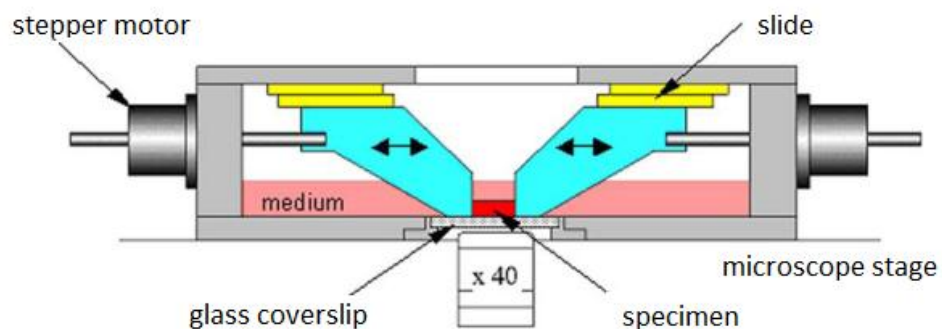
Figure 2.6. *Schematic cross-section of a loading rig for the application of compressive strain to cell-seeded hydrogels. Compression is applied using one or two sliding platens connected to stepping linear actuators controlled via a PC. The specimen is placed on a coverslip hydrated in medium and the whole rig mounted upon an inverted microscope stage to enable visualization and quantification of cell deformation during gross compression. (Bader and Knight, 2008)*

For stiffer gels, the level of cell strain is typically approximately equal to the applied gross strain given the very low cellular volume fraction. This makes it difficult to estimate the modulus of the cells. However, more sophisticated linear elastic and viscoelastic models

based on finite element analysis may be used to provide more accurate estimates of cell moduli for a variety of gels. This approach of quantifying cell mechanics from cell deformation in 3D scaffolds has the advantage of enabling the mechanical properties of articular chondrocytes to be derived from physiological levels of gross cell strain rather than localised membrane distortion as is often the case with other techniques. The same agarose and alginate model systems have also been widely used to investigate mechanotransduction and the specific role of cell deformation in isolation from factors associated with compression of the charged extracellular matrix (Chowdhury and Knight, 2006). Indeed these model systems maintain chondrocytic phenotype as shown by the production of type II collagen and aggrecan. This represents a further advantage of the technique for measurement of chondrocyte mechanics.

2.2.7   Micropipette Aspiration

The micropipette aspiration technique for the measurement of cellular biomechanics involves the application of a gentle suction pressure, typically less than 10 cm of water, to the surface of the cell by way of a micropipette. The suction pressure is usually generated by reducing the height of fluid within a reservoir connected to the micropipette. In the past, this has simply been achieved by moving the reservoir flask vertically by way of a jack as shown in Figure 2.7.

The micropipette is mounted on the stage of an inverted microscope enabling measurements of cell deformation to be made as the cell is aspirated into the micropipette. The deformation and pipette geometry, together with applied pressure, is then used in combination with theoretical models to establish intrinsic mechanical properties of the cell. Cells are typically partially or completely aspirated whilst in suspension, but the technique may also be used for adherent cells as shown schematically in Figure 2.8. When used with spherical cells the partial aspiration technique may be used to study the elastic or viscoelastic properties of the cell. The two approaches require slightly different experimental protocols as discussed in section 2.3.
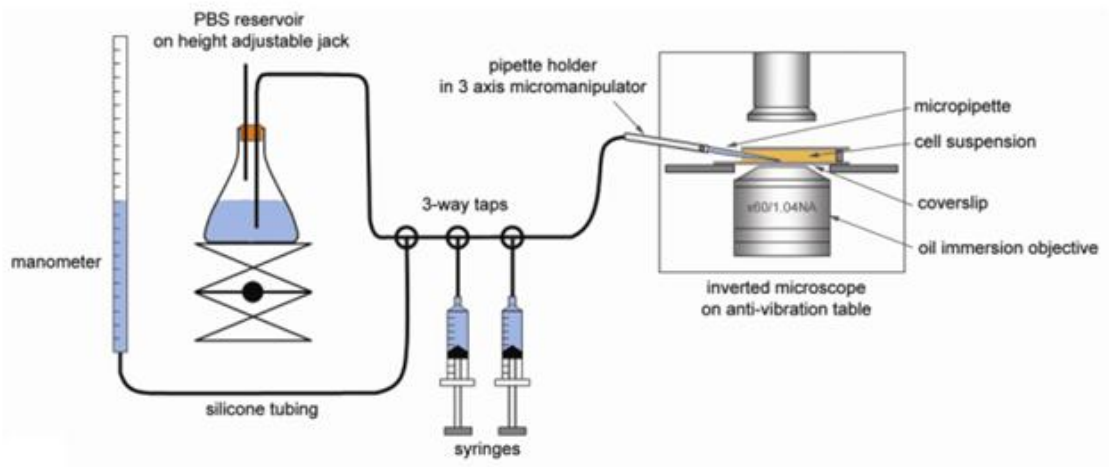
Figure 2.7. *Diagrammatic representation of the micropipette aspiration system in which suction pressure is produced by downward movement of the reservoir located on an adjustable jack. A manometer is used to measure the applied pressure. Two syringes are connected via 3 way taps to allow filling of the tubing and rapid ejection of any aspirated cells.*
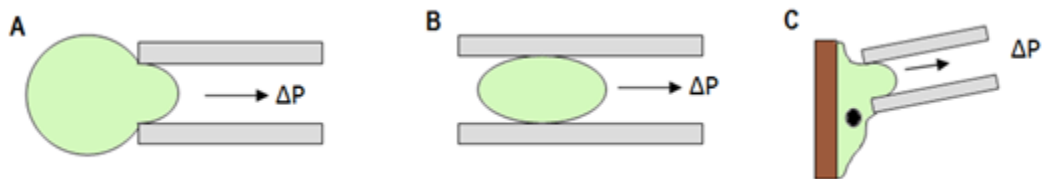
Figure 2.8. *A spherical cell being partially (A) and completely (B) aspirated into micropipette on application of suction pressure ΔP (C) An attached cell being aspirated. (Hochmuth, 2000)*

2.2.8 SELECTION OF EXPERIMENTAL TECHNIQUE

For the purpose of the chondrocytes mechanics studies described within this thesis the micropipette aspiration technique was adopted. This has the advantage over AFM laser and magnetic tweezers in that it can be used to provide more global measurement of cell mechanics less influenced by spatial location and underlying spatial heterogeneity. Whilst the variation of cellular mechanical properties from measurements of

deformation in 3D scaffold has greater physiological relevance, the required analytical models have not been developed. Furthermore the experimental setup for micropipette aspiration is relatively simple and was available in house at Queen Mary University of London. The technique is also ideally suited for the study of chondrocytes which need to be maintained in a rounded morphology for maintenance of chondrocyte phenotype and cytoskeletal organisation. Finally, numerous previous studies have used micropipette aspiration for investigating the biomechanics of isolated chondrocytes allowing useful comparison with also data obtained in the present study.

2.3 MICROPIPETTE ASPIRATION

When a cell is aspirated, initially a hemispherical projection is formed inside the pipette. Further decrease in pressure, beyond this critical pressure, causes a liquid-like cell with a constant cortical tension to aspirate completely into the micropipette (Evans and Yeung, 1989).

2.3.1 LIQUID DROP MODEL

This behaviour is typically exhibited by white blood cells enabling calculation of cortical tension and viscosity using the liquid drop model (Lim et al., 2006). According to the law of Laplace, when suction pressure is applied to the cell through the micropipette, where pressure is given as follows:

$$\Delta P = 2T_c \left(\frac{1}{R_p} - \frac{1}{R_c} \right)$$

Equation 2.1

$\Delta P = \Delta P_c$ when $\dfrac{L_p}{R_p} = 1$

where T_c is the cortical tension, R_c is the radius of the cell outside the pipette, R_p is the radius of the micropipette, L_p is the aspiration length of the cell into the micropipette and P_c is the critical pressure when $\dfrac{L_p}{R_p} = 1$.

The cell will deform at the constant rate as the suction pressure is small relative to the osmotic pressure of isotonic saline. If the suction pressure is increased further than critical value, the radius of the cell outside the pipette will decrease. The pressure remains almost constant beyond the point, where $\dfrac{L_p}{R_p} = 1$ for small diameter pipettes, because the radius of the cell outside the micropipette hardly decreases as the cell is further drawn into the pipette (Hochmuth, 2000). However articular chondrocytes do not exhibit this behaviour and therefore be modelled as either an elastic or viscoelastic solid.

2.3.2 ELASTIC SOLID MODEL

The solid model assumes the cell to be homogeneous without any distinction of the cortical layer. The material is considered as either an incompressible elastic solid or an incompressible viscoelastic solid. The basic principle on which solid models are based is that equilibrium partial aspiration can be achieved. It has been shown by both modeling (Theret et al., 1988) and experimental (Jones et al.,1999b), that after application of step pressure the cell eventually ceases to deform and hence attains equilibrium in agreement with the solid model prediction.

Elastic models are inadequate to explain the cell mechanics as the elasticity of the viscoelastic material is influenced by loading rate and loading history. Elastic solids models can be generated in context to different experimental settings for e.g. AFM, MTC. The discussion of the models for different experimental settings is beyond the scope of this study (Lim et al., 2006). In the present study the model used to compute the mechanical properties of the cells from the raw data obtained using micropipette aspiration will be discussed.

Theret et al. (1988), has developed elastic model in regard to micropipette aspiration settings. The model approximates cells as an incompressible elastic half-space because the radius of the pipette is very small compared to the radius of the cells (Theret et al., 1988). Cells behaves like an elastic solid for the cases where $\frac{L_p}{R_p} < 1$. The aspirated length is directly proportional to the aspiration pressure and inversely proportional to the elastic modulus as

$$L = \frac{3\Delta P R_p \phi(\eta)}{2\pi E}$$ Equation 2.2

Where E is the Young's modulus, ΔP is the suction pressure, φ is the wall parameter, L is the aspirated length and R_P is pipette radius. The wall parameter (φ) is based on that for the punch model in which the displacement in the perpendicular or normal direction is assumed to be zero (Theret et al., 1988). The entire half space is also assumed to be free of tangential traction and as a consequence it is assumed that there is no friction between the cell and the micropipette. ϕ is dependent on the η which is the ratio of inner (a) and outer (b) radii of the micropipette, $\eta = \frac{(b-a)}{a}$ (Sato et al., 1990). Thus for the typical micropipettes used in the majority of studies, including this one, the value of the wall parameter is 2.1 (Theret et al., 1988)
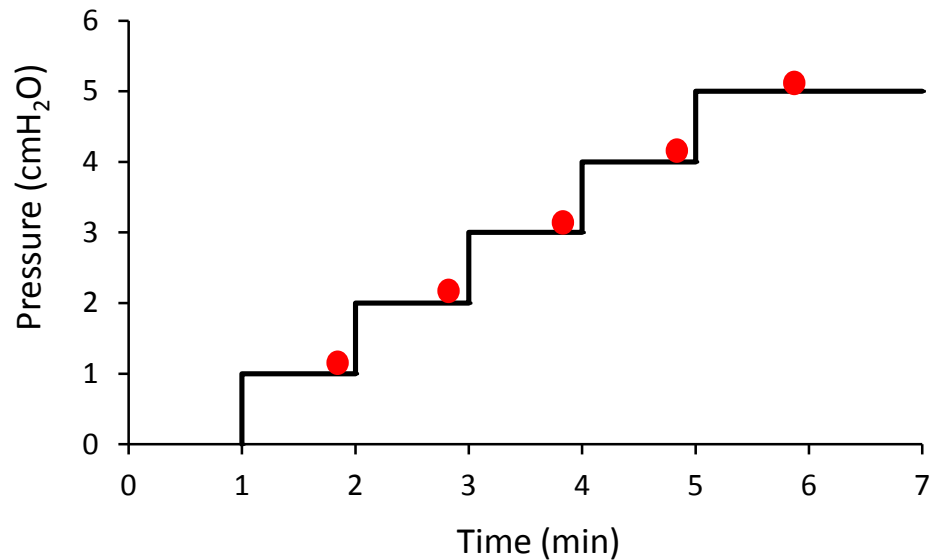
Figure 2.9. *Schematic of the micropipette aspiration protocol for estimating the elastic properties of the cells.*

The images are collected during micropipette aspiration at corresponding to the red dots. In order to use the solid elastic model to derive the cellular Young's modulus, the cell is subjected to a step aspiration protocol where by pressure is applied in a series of increments (Figure 2.9), typically of 1 cmH_2O, up to a total pressure of 7-10 cmH_2O. The equilibrium aspiration length is recorded at each pressure increment and plotted against pressure such that the gradient , ΔP/L is calculated and used in equation to derive the modulus. However this model is not used in the present study.

2.3.3 VISCOELASTIC SOLID MODEL

An alternate to the solid elastic model is the viscoelastic solid which provides a more accuate model of chondrocyte behaviour. The theoretical representation of the micropipette and the aspirated cell is shown in Figure 2.10. The analysis of this model yields three different parameters which are k_1, k_2, μ. These are solved subsequently to obtain the elastic instantaneous and equilibrium moduli and apparent viscosity.
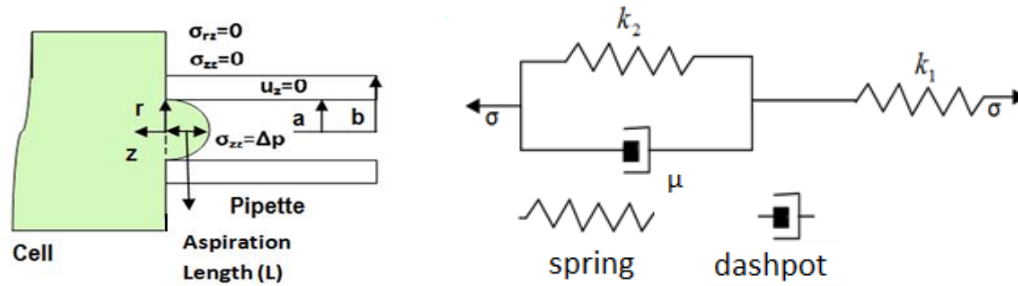
Figure 2.10. *A theoretical representation of micropipette aspiration of the cell in that cell is represented as a homogneous half-space. The stresses outside the pipette and, the shear stress on the suface are assumed to be zero. The standard linear solid (SLS) model was used to represent the viscoelastic properties of chondrocytes. (Theret et al., 1988)*

The creep compliance of the standard linear solid (SLS) model is given as follows:

$$J(t) = \frac{1}{k_1}\left[1 + \left(\frac{k_1}{k_1 + k_2} - 1\right)e^{-(t-t')/\tau}\right]H(t) \qquad\qquad \text{Equation 2.3}$$

where H(t) is the Heaviside function. This implies that the model is only valid for step loading. Consequently the governing equation for micropipette aspiration of this SLS viscoelastic half-space can be obtained from the analogous elastic solution in combination with SLS model:

$$L(t) = \frac{\phi_p(\eta)\Delta P R_p}{2\pi k_1}\left[1 + \left(\frac{k_1}{k_1 + k_2} - 1\right)e^{-(t-t')/\tau}\right]H(t) \qquad\qquad \text{Equation 2.4}$$

where t is the time.

The elastic parameters k_1 and k_2 are related to the standard elasticity by following relationships:

$$E_{in} = \frac{3}{2}(k_1 + k_2) \qquad\qquad \textit{Equation 2.5}$$

$$E_{eq} = \frac{3}{2}k_1 \qquad\qquad\qquad \textit{Equation 2.6}$$

$$\mu = \tau\left(\frac{k_1 k_2}{k_1 + k_2}\right) \qquad\qquad \textit{Equation 2.7}$$

where is E apparent Young's modulus, E_{in} is the instantaneous modulus, E_{eq} is the equilibrium modulus and µ is apparent viscosity. In order to derive the viscoelastic parameters of the cell, the cell is subjected to a step pressure typically of 4-10 cmH$_2$O/s (Jones et al., 1999) followed by holding of the constant pressure as shown in Figure 2.11.
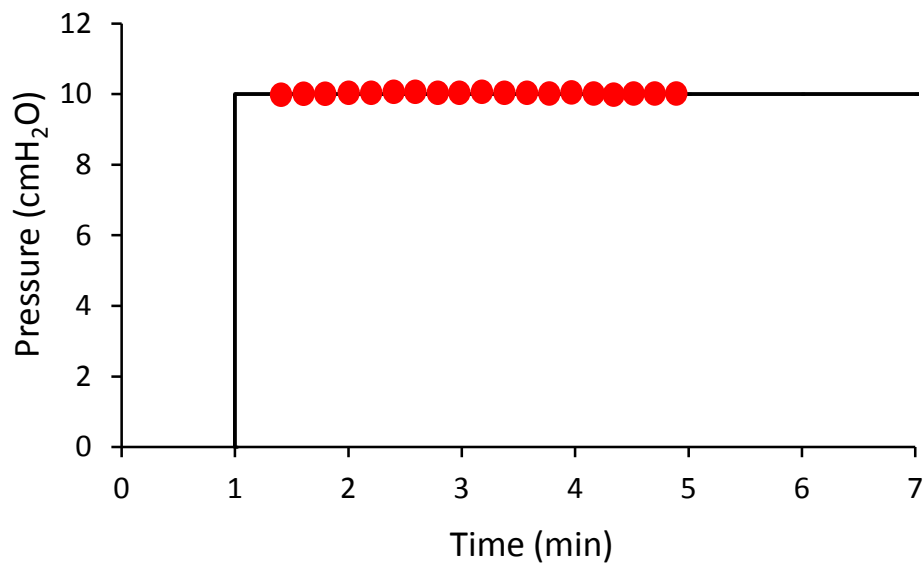
Figure 2.11. *Schematic of the micropipette aspiration protocol for estimating the viscoelastic properties of the cells. The images are collected during micropipette aspiration at corresponding to the red dots.*

When pressure is applied to chondrocyte, an initial deformation occurs followed by a slow asymptotic entry into micropipette up to two times its radius Figure 2.12. The experimental plot of the change in aspiration length versus time for given pressure is solved using non-linear regression to determine $k_1, k_2, \mu,\ k_1 + k_2$ and time constant.
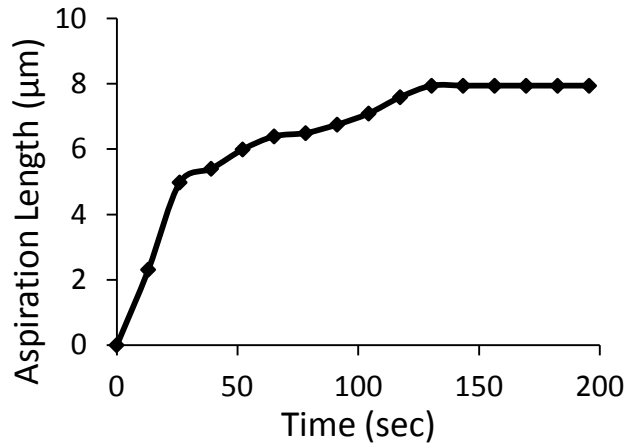
Figure 2.12: *Temporal changes in the aspiration length showing the viscoelastic behaviour of the cell.*

The SLS model assumes the loading to be step change. However the time factor is associated with the loading which is not considered in this model. For this the Boltzmann superposition principle is applied to SLS model to incorporate the loading time that gave rise to Boltzmann standard linear solid model (BSLS). Both the models are discussed further in section 3.5.

2.4 MECHANICAL PROPERTIES OF CHONDROCYTES

Numerous studies have attempted to determine the mechanical properties of articular chondrocytes using a variety of different experimental and computational techniques. Such studies provide information pertaining to the levels of cell deformation in vivo and hence the possible mechanotransduction. Other studies have examined the biomechanics of intracellular structure such as the actin cytoskeleton and the nucleus, and their contribution to gross cell mechanics. The studies also aim to identify the influence of factors such as age, diseases, location in the joint and loading conditions and the mechanism involved. The mechanical properties measured by the different techniques are given in the Appendix A.

2.4.1 THE INFLUENCE OF AGE ON CHONDROCYTES MECHANICS

The mechanical properties of the chondrocytes changes with ageing of the individual (Starodubtseva, 2011). These ages related change in the mechanical properties is due to the changes in the intracellular structures. Steklov et al., 2000 demonstrated that the mechanical properties of the cell changes with the age. They have shown the significant difference in the viscoelastic properties of chondrocytes obtain from human age 55+ and age group between 18-35 (Steklov et al., 2009). These changes were again attributed to the changes in the cytoskeletal components of the cell. The stiffness of the cell may have influence on the mechanotransduction of the cell hence altering the cell function.

2.4.2 THE INFLUENCE OF ZONAL VARIATION ON CHONDROCYTES MECHANICS

Articular cartilage is a heterogenous tissue with depth dependent variation in cell morphology, intracellular organisation and metabolism as well as variation in extracellular composition and mechanics (see section 1.3.2). Previous studies using cytocompession have reported that chondrocytes isolated from the superficial zone are stiffer than those from the deep zone (Shieh and Athanasiou, 2006). This was characterised by statistically significant differences in instantaneous modulus with mean values of 1.20 kPa for superficial cells and 0.78 kPa for deep zone cells. Similarly Shieh and Athanasiou (2006) also reported significant difference in equilibrium modulus with mean values of 0.80 kPa and 0.64 kPa for superficial and deep zone cells respectively. Further studies using AFM also reported that superficial cells are stiffer than deeper zone cells with alterations in elastic and viscoelastic properties (Darling et al., 2006a). In particular they reported a significant difference in the equilibrium moduli with values of 0.46 for isolated superficial zone cells and 0.26 kPa for deep zone cells. This variation in the mechanical properties is attributed to the F-actin organization in the superficial and deep zone chondrocytes such that superficial zone cells have been shown to exhibit increases F-actin organisation both in situ (Langelier et al., 2000) and in isolated chondrocytes (Lee et al., 2000a).

2.4.3 THE INFLUENCE OF DISEASE ON CHONDROCYTES MECHANICS

Jones et al. (1999) have characterised the mechanical properties of the primary chondrocytes using the solid elastic protocol (section 2.3.2). They have observed no significant difference between the Young's moduli of normal (0.65 ± 0.63 kPa, n = 44) and osteoarthritic chondrocytes (0.67 ± 0.86 kPa, n = 69). However significant difference was reported in cell volume between normal and osteoarthritic chondrocytes suggesting the alteration in volume regulation capabilities in regard to mechanical loading (Jones et al., 1999).The same research group performed a further study on the normal and osteoarthritic human chondroyctes investigating the viscoelastic properties of the cell. Interestingly, they reported significant differences in both the instantaneous and equilibrium moduli with osteoarthritic chondrocytes properties being stiffer than normal chondrocytes (Trickey et al., 2000). This difference in properties was attributed to the cytoskeleton of the cell. However osteoarthritic chondrocytes showed higher recovery time compare to the normal suggesting that chondrocytes are compressible. This is due to the Poisson's ratio of the chondrocytes obtained from non-osteoarthritic cartilage and osteoarthritic cartilage was reported to be 0.38 and 0.36 respectively (Trickey et al., 2006).

2.5 THE ROLE OF ACTIN IN CELL MECHANICS

With increasing knowledge of actin cytoskeleton involvement in all aspects of cellular behaviour in health and disease (Bao and Suresh, 2003), it has become important to understand actin mechanics and the contribution of actin to cell mechanics. There have been two approaches to understand cytoskeletal mechanics One approach is based on testing of purified actin proteins ex vivo (Xu et al., 2000) and the alternate approach involves testing the mechanics of whole cells with and without cytoskeletal manipulation and/or visualization (Trickey et al., 2004). This experimental approach is frequently combined with computational models such as the tensgrity model (Ingber et al., 1994) or cortical actin shell model (Lim et al., 2006).

2.5.1 ACTIN BLEB FORMATION

Blebs are defined as protrusion at the cell surface and are mostly hemispherical in shape. Different types of the bleb formation are observed in cells from same culture (Keller et al., 2002). In response to different types of the bleb formation different mechanism is suggested for the formation of bleb. Three types of blebs formation have been identified: Type 1 - plasma membrane dissociates from the cortical actin Type 2 – impaired cortical layer results in reduction of resistance to deformation and Type 3 – local rupture of the cortical actin.

Once the bleb is initiated by local rupture of cortex or dissociation of the cortex from plasma membrane it is followed by rapid extension of the membrane tongue into the micropipette. During membrane extension into the micropipette, polymerisation of new actin cortex takes place which occurs predominantly at the plasma membrane while depolymerisation occurs throughout the cortex leading to constant flow of actin away from membrane – treadmilling. The cortex-membrane stability is affected by the loading rate predicted from the theoretical remodelling. In some instances the membrane stops and is retracted back to the cell body. The bleb formation during micropipette aspiration is combined with theoretical modelling (Brugues et al., 2010).

2.5.2 MECHANICAL BEHAVIOR OF ISOLATED/PURIFIED ACTIN

A homogeneous network of F-actin is formed in vitro from polymerisation of purified actin and crosslinking proteins. This network is observed to undergo "sol-gel" transition by altering the concentration of crosslinking proteins and F-actin (Janson et al., 1991). F-actin in vitro demonstrates diversity in mechanical behavior. Even though the structure of F-actin network is different from those found in the cells it provides the basic model system to study F-actin mechanics in response to mechanical stimuli.

However physiologically, most of the cross-linkers are dynamics and have finite binding affinity to F-actin (Lieleg et al., 2008). The unbinding of the cross-linkers allows for the rearrangements that play an important role in viscous response of the actin. On the

other hand viscous response of the actin is eliminated with the permanent crosslinking due to restriction in unbinding from actin filaments over time (Tharmann et al., 2007). The mechanical response of the F-actin network is dependent on the magnitude of applied stress or strains (Xu et al., 2000). In the presence of low concentration of the cross linkers F-actin network softens as large strains (Gardel et al., 2004; Head et al., 2003a; Head et al., 2003b). While at higher concentration F-actin network stiffens at intermediate strains and softens as large strain. It has been suggested that small stress can be supported by dynamic cross-links resulting into strain hardening and larger stress can lead to unbinding of cross-links resulting into fluidisation (Humphrey et al., 2002; Liverpool et al., 2001).

2.5.3 INFLUENCE OF ACTIN ON CELL MECHANICS

Mechanical stimuli influence the actin organisation in the cells. It has been reported that the actin polymerisation in response to mechanical stimulus is dependent on the amount and the time of loading (Pender and Mcculloch, 1991). The gene expression for actin depolymerising proteins such as cofilin and destrin are upregulated in response to cyclic compression (Campbell et al., 2007). This suggests that cortical actin dynamics is altered in response to loading the providing mechanism to adapt mechanical properties to local mechanical environment. It has been shown that localised mechanical stress induces the actin remodeling and stiffening of cultured airway smooth muscles cells (Deng et al., 2004). Furthermore studies are performed to understand the mechanism by which actin bundles in the form of stress fibers response to loading. Actin stress fibers are shown to be dynamically active in mechanical stimulus (Colombelli et al., 2009; Kumar et al., 2006). Actin remodeling has been shown to dependent on the magnitude and frequency of the mechanical loading (Dipaolo et al., 2010).

2.5.4 EFFECT OF CHEMICAL AGENTS ON ACTIN DYNAMICS

To study a relationship between the actin organisation, dynamics and functions, different pharmacological agents are used to perturb actin structures. The anti-actin drugs have

been shown to influence the mechanical properties of the cell (Wakatsuki et al., 2001). Cytochalasins are used to investigate the involvement of actin in maintenance of cell shape, cell division, cell locomotion and signal transduction. Cytochalasins binds to the barbed end of the actin filament, sever actin filament, sequester actin monomer and dimer, promote nucleation and stimulate ATPase activity of G-actin (Cooper, 1987) preventing association and dissociation of actin monomers at that end.

Cytochalasin has been shown to disrupt actin organisation with diverse effect, inducing actin polymerisation and depolymerisation of F-actin or redistribution of F-actin without interfering with actin-polymerisation state. Ballestrem et al. (1998) have shown that on treatment of cell in monolayer with cytochalasin B, fragmentation of the large actin stress fibers takes place within the seconds of addition. The severing of actin filaments was followed by depolymerisation of the fragments. Within 10 minutes most of the actin was depolymerised. In stationary cells, stress fibers at the peripheral region depolymerised rapidly compare to stress fibers in the centre of the cell (Ballestrem et al., 1998). Furthermore Cytochalasin D has been shown to reduce the stiffness of the chondrocytes (Trickey et al., 2004). Phalloidin is a another anti-actin drug widely used that promotes actin polymerization (Cooper, 1987). This pallotoxin does not enter in live cell therefore is used as fluorescent derivatives to visualize actin structure in fixed cells.

Other agents are being used such as Latrunculin as a research tools to understand actin structure organization and functions. The Latrunculin A and Latrunculin B disrupt actin organisation (Rotsch and Radmacher, 2000). They mimic the mechanism action of β-thymosins by sequestering action monomers. They inhibit G-actin polymerisation and induce actin depolymerisation. Moreover Jasplakinolides induces actin polymerisation in vivo and in vitro (Bubb et al., 2000) (Rotsch and Radmacher, 2000). There are other anti-actin drugs such as Swinholide A, Halichondramides etc used to study actin dynamics (Spector et al., 1999).

2.5.5 CRITICAL SUMMARY OF THE LITERATURE

THE INFLUENCE OF ASPIRATION PRESSURE RATE

Numerous previous studies have used a variety of different techniques to investigate the influence of age, zonal variation and diseases on chondrocyte mechanics as reviewed in section 2.4. Many of these studies have utilised micropipette aspiration which, in conjunction with analytical models such as the SLS and BSLS model, provides an estimate of the viscoelastic parameters; instantaneous modulus, equilibrium modulus and viscosity. The rate at which mechanical loading is applied is known to regulate the viscoelastic response. However the previous micropipette aspiration systems have not provided precise control over the rate at which pressure is applied to the cell (Jones et al., 1999). Consequently the influence of pressure rate on cell mechanics is completely unknown.

THE ROLE OF ACTIN REMODELLING IN VISCOELASTIC BEHAVIOR

Previous studies have shown that the cytoskeleton and particularly the actin microfilaments are important in providing the cell with its mechanics properties. However these studies have frequently used cytoskeletal disruptive agents, such as cytochalasin D, which completely destroys the integrity of the cytoskeletal networks resulting in softening of the cell (Trickey et al., 2004). Although with the use of disrupting agents provide information on the importance of the cytoskeletal elements in cell mechanics, it is relatively crude and does not reveal the role of cytoskeletal dynamics and remodelling. Previous studies have shown that actin remodelling occurs in response to mechanical stimuli, and is fundamental to many cellular processes (Chen et al., 2010). However no studies have visualised actin dynamics during micropipette aspiration nor investigated the importance of remodelling in viscoelastic behaviour.

PATHOLOGICAL CHANGES IN CHONDROCYTE MECHANICS

Previous studies have shown the effect of osteoarthritis on the viscoelastic properties of the chondrocyte (Trickey et al., 2000). However the underlying governing mechanism and the role of the pathological microenvironment remains unclear.

THE INFLUENCE OF PASSAGE ON CHONDROCYTE MECHANICS

The expansion of chondrocytes in monolayer is carried out to increase the cell number for the autologous chondrocytes transplantation and other possible cartilage repair strategies. However, it has been shown that phenotypic expression of the chondrocytes changes when cultured in monolayer and that this is associated with changes in the actin cytoskeleton (Darling and Athanasiou, 2005). Such changes may well be associated with alterations in cell mechanics as suggested by previous studies using AFM (Darling et al., 2009). However, no published studies have examined the viscoelastic properties of chondrocytes during cell passage and dedifferentiation.

2.6 AIMS AND OBJECTIVES

AIMS

In order to examine how mechanical forces control cellular function it is important to understand how cells respond to the mechanical force and the structure-function relationships which govern cell behaviour. The aim of the current study was therefore to investigate the viscoelastic properties of articular chondrocytes and the role of actin cytoskeletal dynamics and remodelling. In particular the study set out to examine the influence of aspiration pressure rate, mechanical injury, cytokine exposure and cell passage in monolayer.

OBJECTIVES

1. Develop a micropipette aspiration system capable of determining the influence of aspiration pressure rate on the viscoelastic properties of chondrocytes.

2. Develop protocols for measuring the deformation and morphology of chondrocytes during micropipette aspiration.

3. Quantify the effect of aspiration pressure rate on chondrocyte mechanics.

4. Establish protocol to visualize and quantify actin dynamics during micropipette aspiration system.

5. Determine the role of actin deformation and remodeling in chondrocyte mechanics and response to different aspiration rates.

6. Examine changes in cell mechanics associated with an established cartilage explant injury model.

7. Determine the influence of IL-1β on the mechanics of isolated chondrocytes.

8. Determine influence of passage on chondrocyte mechanics.

Chapter 3

DEVELOPMENT OF MICROPIPETTE ASPIRATION EXPERIMENTS

3.1 **INTRODUCTION**

3.2 **MICROPIPETTE FABRICATION**

3.3 **PUMP SYSTEM FOR THE CONTROL OF ASPIRATION PRESSURE**

3.3.1 System Design

3.3.2 Pump Calibration

3.3.3 LabView Interface

3.4 **IMAGING**

3.4.1 Confocal Microscopy

3.4.2 Bright field Imaging

3.4.3 Microscope Settings

3.5 **MODELING OF THE CELL BEHAVIOUR**

3.5.1 Standard Linear Solid Model

3.5.2 Boltzmann Standard Linear Solid Model

3.6 **MATERIALS AND METHODS**

3.6.1 Preparation of the Culture Media

3.6.2 Isolation of the Chondrocytes

3.6.3 Micropipette Aspiration of the Cell

3.6.4 Calculation of the Cell Morphological Properties

3.6.5 Statistical Analysis

3.7 **RESULTS**

3.7.1 Mechanical Properties of the Cells

3.8 **DISCUSSION**

    3.8.1   Influence of the Pipette Diameter on Cell Micropipette Aspiration

    3.8.2   Viscoelastic Properties of the Chondrocytes

3.9 **STANDARD OPERATING PROCEDURE**

    3.9.1   Micropipette Aspiration of the Cells

    3.9.2   Analysis of the Viscoelastic Properties of the Cells

3. DEVELOPMENT OF MICROPIPETTE ASPIRATION EXPERIMENTS

3.1 INTRODUCTION

This chapter starts with describing the fabrication of the micropipettes from the raw capillaries. This is followed by the development of the micropipette aspiration system used in the experimental work throughout this thesis. Confocal microscopy is used in conjunction with a micropipette aspiration system to collect the experimental data. The images acquired during the micropipette aspiration of the cells are processed to measure the temporal changes in the cell dimensions required for the subsequent data analysis. Two different models, namely Standard Linear Solid (SLS) model and Boltzmann Standard Linear Solid (BSLS) model are used to compute the mechanical properties of the cells. Additionally, the formulation of the BSLS model is detailed in this chapter. Thereafter a section follows that details the materials and methods used throughout the experimental work, including the isolation of the bovine articular chondrocytes. This in turn, highlights the micropipette aspiration of the chondrocytes and calculation of the geometrical parameters from the measured data. Analysis of the micropipette aspiration of the chondrocytes results in the generation of three distinct viscoelastic parameters of the cells that also described. This chapter is completed with a summary of the standard operating procedures, which are adopted throughout the subsequent experiment chapters.

3.2 MICROPIPETTE FABRICATION

Micropipette fabrication consists of three stages involving pulling, polishing and coating. These are detailed in Appendix B. The puller is used to produce the raw micropipettes from the capillaries. The micropipettes are fractured to prescribed diameter, using the microforge. Subsequently the inner region of each micropipette was coated with the

Sigma coating to prevent cell adhesion, a process which has been employed in other micropipette aspiration studies (Jones et al., 1999; Trickey et al., 2000).

3.3 PUMP SYSTEM FOR THE CONTROL OF ASPIRATION PRESSURE

3.3.1 SYSTEM DESIGN

As detailed in section 2.2.7 the micropipette aspiration protocol involves reducing the height of the fluid filled reservoir, connected to the micropipette and thereby generating a suction pressure at the opening of the micropipette. This stage has typically been achieved by moving a reservoir flask vertically by means of a mechanical jack. However, with this test mechanism, it is difficult to apply precise temporal regulation of the applied pressure. This is particularly important when modeling cell behaviour using either the SLS model, where a step pressure has to be applied within a finite time, or the BSLS model, for which the effect of applied pressure rates are examined.

Accordingly, in order to ensure precise temporal control of the aspiration pressure, a control pump system was developed. A peristaltic pump (MCP Standard, ISMATEC), controlled by custom-written LabView software, enabled accurate temporal control of the fluid height in the reservoir and hence the suction pressure. The pump control system was developed to allow suction pressure to be applied to a cell in two different regimes, in order to derive either elastic or viscoelastic parameters as described in sections 2.3.2 & 2.3.3. For derivation of simple elastic parameters, the pump delivers a stepwise incremental pressure with control of the pressure increment (Figure 2.9), such that each pressure level is maintained for a prescribed period. By contrast, for derivation of the viscoelastic parameters, a single step pressure (Figure 2.11) is applied and maintained for a prescribed period during which temporal changes in aspiration length are measured from the continuous images. In both cases, the rate of pressure change can also be controlled.

(A)

(B)
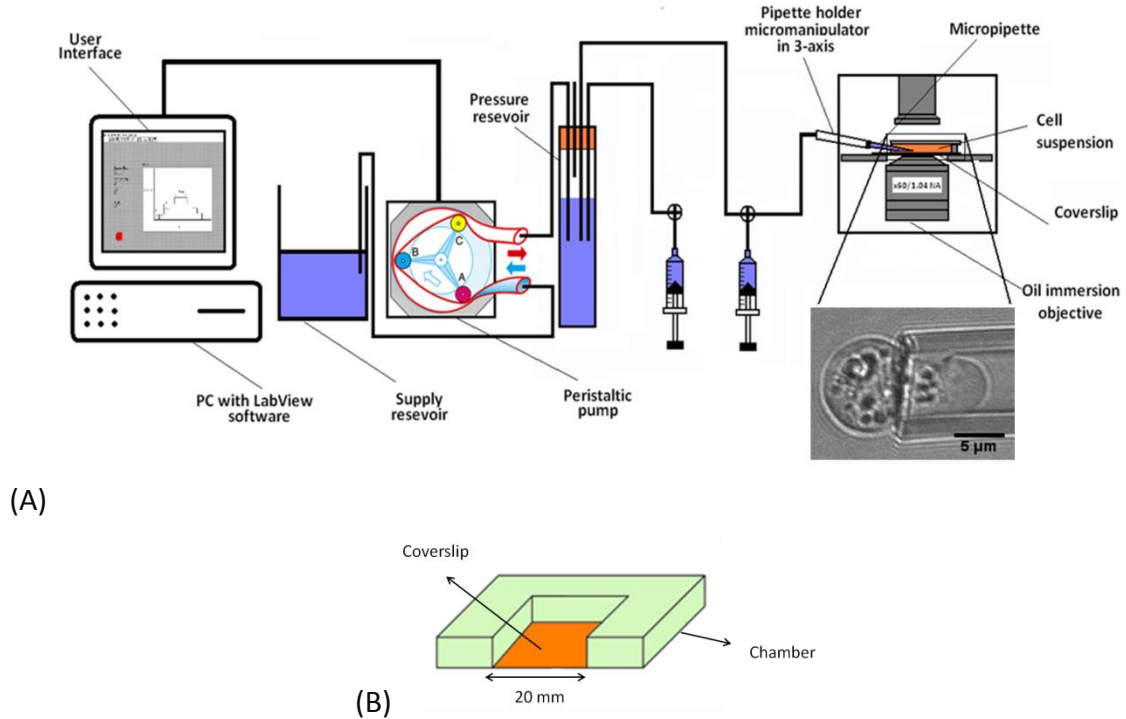
Figure 3.1. *A) Diagrammatic representation of the modified micropipette aspiration set-up incorporating a peristaltic pump with LabView controller to adjust the height of fluid in the reservoir. B) Schematic diagram showing the custom made chamber used to contain cell suspension on the stage of an inverted microscope.*

The modified set-up for micropipette aspiration is shown in Figure 3.1A. Syringes are used to manually change the level of fluid in the pressure reservoir, to either increase or decrease the pressure at the micropipette tip. This arrangement is also used to apply positive pressure, which is necessary to expel the cell from the tip of the micropipette after the aspiration protocol. A custom built chamber was also designed to hold approximately 1 mL of cell suspension and permit entry of the micropipette from the side as shown in Figure 3.1B. The test protocol demands that the micropipette remains in a horizontal plane to minimise inaccuracies in measuring the aspiration length from the projected transmitted light images.

3.3.2   PUMP CALIBRATION

In order to generate precise temporal control of the aspiration pressure, a program written in LabView provides direct regulation of the pump flow rate and/or the time for which the pump is operational. The SLS model for determining cellular viscoelastic properties required a single step aspiration pressure, typically of magnitude between 7-10 cm of water, to be delivered in less then 2 s (Zhao et al., 2009). The pump system was required to deliver a pressure change rate of at least 3.5 cm/s, which was itself dependent on the flow rate and the cross-sectional area of the pressure regulating resevoir. The flow rate is directly proportional to the cross-sectional area of the peristaltic tubing and speed of the rollers, which is determined by the input voltage. Accordingly it was necessary to calibrate the system by determining the relationship between the pump speed and the rate of change of height of the pressure resevoir (Figure 3.1A).

The calibration involved measuring the time taken to pump 185 mL of water, at pump speeds ranging from 20 rpm to a maximum of 240 rpm. The procedure was performed using 3 different tubings with inner diameter (I.D.) of 4.8 mm, 6.4 mm and 9.5 mm. The initial configuration of the pump system involved a pressure regulating reservoir (Figure 3.1A) with a cross-sectional area of 17.93 cm^2. The results of the pump speed versus the rate of pressure change in cmH$_2$O/s for the largest diameter tubing (9.5 mm I.D.) is shown in Figure 3.2. Using the two smaller diameter tubes (4.8 and 6.4 mm I.D.) resulted in a rate of pressure change of less than 0.5 cmH$_2$O/s, wherase the 9.5 mm I.D. tube predicted a pressure change rate of more than 2.5 cmH$_2$O/s (Figure 3.2). The data indicates a linear relationship between both parameters up to the maximum speed of 240 rpm. By contrast, when using the two smaller diameter (4.8 mm and 6.4 mm I.D.) the relationship between the speed and rate of pressure change is only linear up to a pump speed of 80 rpm. Above which the flowrate decreases as the pump loses its efficiency. These findings strongly suggest that for tubing with smaller diameters, 80rpm is the

effective maximum speed. However, for the larger tube of 9.5 mm I.D., the pump can operate at its maximum pump speed of 240 rpm.
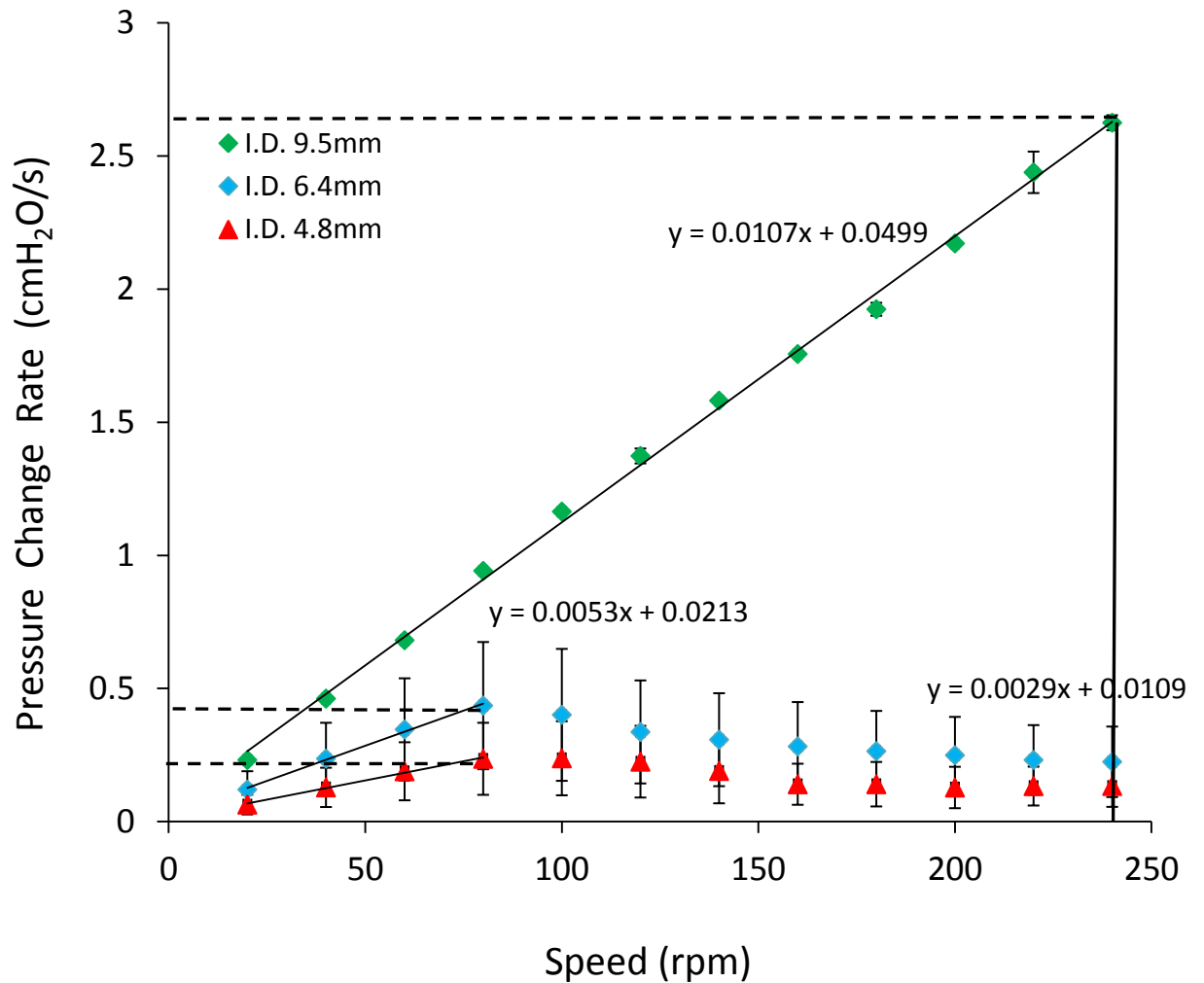
Figure 3.2. *The relationship between changes in the height per second versus pump speed for each of three tube diameter (I.D). Dotted lines represent the maximum rate of the pressure change that can be obtained for each tubing, based on the three linear models whose equations are indicated.*

Thus the maximum rate of pressure change for three different tubings with a diameter 9.5, 6.4, 4.8 mm is 0.23, 0.42 and 2.6 cmH_2O/s, respectively (Figure 3.2). All values fall short of the required rate of 3.5 cmH_2O/s, when used in conjunction with the existing

reservoir. Additionally, it was not possible to increase the pressure change rate by increasing the I.D. of the tubing above 9.5 mm. Therefore the only variable that could be changed was the cross-sectional area of the reservoir. Figure 3.3 indicates that by reducing the cross-sectional area, the rate of maximum pressure change can be increased for each of the three tube diameters. Indeed values of greater than 5 cmH$_2$O/s, could be achieved if the cross-sectional area was reduced by 50% or greater. However, to achieve the prescribed rate of 3.5 cmH$_2$O/s, the cross section of the reservoir needed to be reduced by 25% for the maximum I.D. tubing of 9.5 mm.
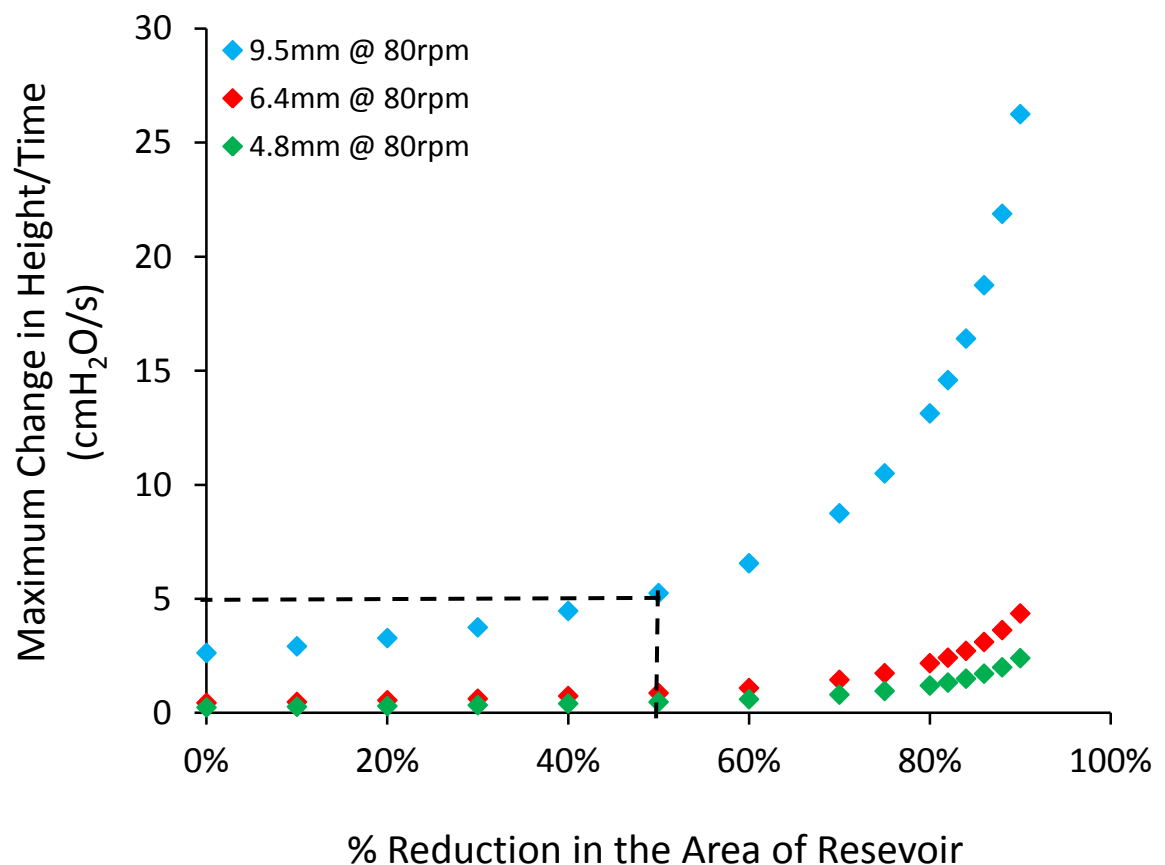
Figure 3.3. *The effect of reduced area of reservoir on the maximum pressure change rate at a pump speed of 80 rpm for each of the three tube diameters.*

Subsequently a smaller diameter reservoir was utilised with a cross sectional area of 8.6 cm^2 equivalent to a reduction of 50%. Using the new reservoir and the 9.5 mm (I.D) tubing, the pressure changes were measured at a variety of pump speeds ranging from 20-240 rpm. The results as indicated in Figure 3.4, revealed a linear relationship. The linear model was fitted through the data points to obtain a gradient which represents a numerical factor, designated C, that needed to be inserted into the designed LabView program.
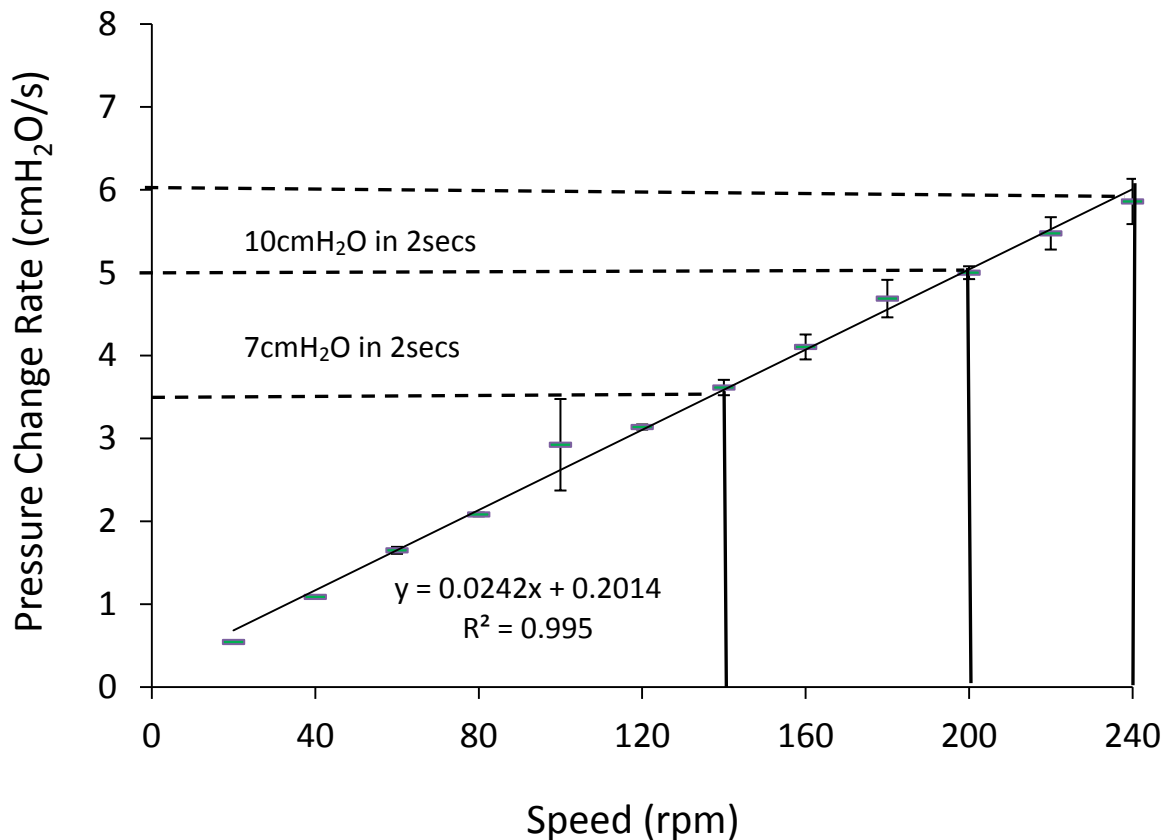
Figure 3.4. *The effect of peristaltic pump speed on the maximum pressure change rate for 185 mL.*

It was necessary to calculate the required pump speed (V) in rpm for a given pressure change (ΔP) in a time (T) as indicated in the equation.

$$V = \frac{\Delta P \times A_E \times C}{T}$$

Equation 3.1

A_E = Effective area of the reservoir such that:

$A_E = A_c - (A_1 + A_2 + A_3)$

Equation 3.2

where A_c is the area of cylinder, A_1, A_2 and A_3 are the cross sectional area of the rods as shown in Figure 3.5.
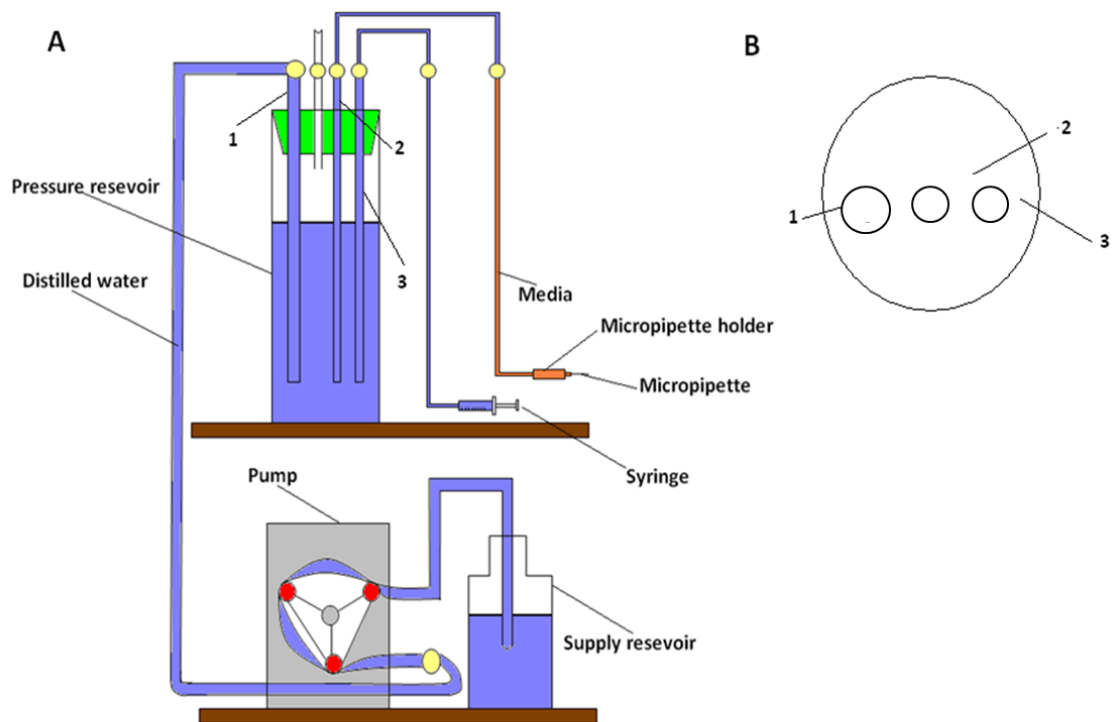
Figure 3.5. *A) Diagrammatic representation of the pump system showing the detail arrangement of the reservoirs and peristaltic pump. B) Cross-sectional area of pressure reservoir. Rigid silicone tubing (inside diameter 6.4 mm) is used throughout except for the section of norprene tubing within the pump head.*

3.3.3 LABVIEW INTERFACE

A LabView program was developed to control the pump speed and pump time in order to regulate the following parameters:

- aspiration pressure

- rate of change of aspiration pressure

- time interval between successive pressure increments.

 In addition, the system was developed to enable application of a tare pressure (P_T) and a delay before the 1st step change pressure (T_0). The tare pressure is used to apply an initial negative pressure sufficient to maintain the cell in contact with the micropipette tip before aspiration. The delay time enables initial images to be acquired after the application of the tare pressure but prior to the application of incremental aspiration pressures. The user interface is shown in Figure 3.6. The same interface could also be used to apply multiple pressure increments, as required for the calculation of the elastic properties.
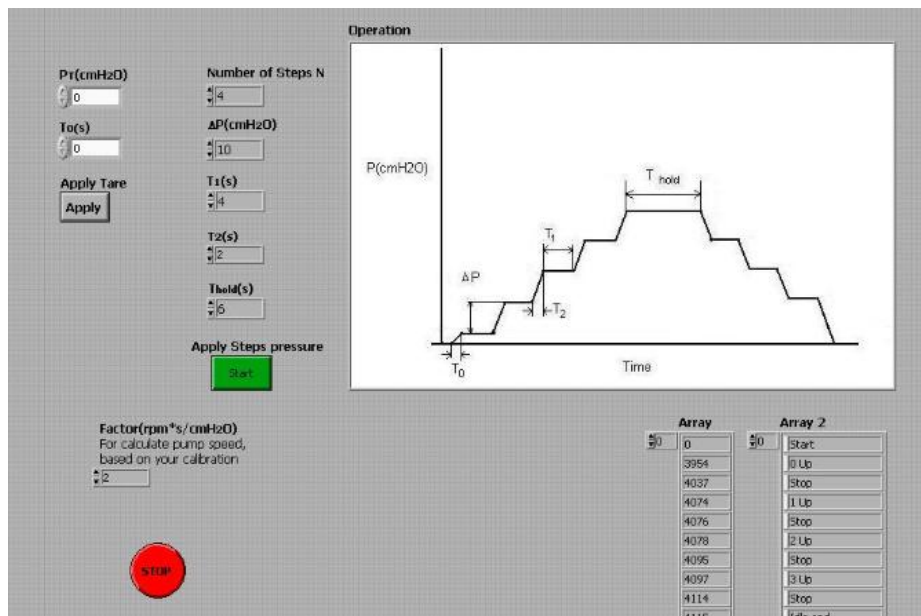
Figure 3.6. *User interface of the LabView software used to execute the program for the micropipette aspiration. The input parameters are no of steps: (N), step pressure: (ΔP), dwell time at each step (T_1), ramp time for each step (T_2) and hold time at maximum pressure (T_{hold}).*

3.4 IMAGING

3.4.1 CONFOCAL MICROSCOPY

Confocal microscopy has several advantages over conventional wide field microscopy including, the ability to control depth of the field, eliminate or reduce light away from the focal plane and collect optical sections from the thick specimens. Indeed, the critical feature of the confocality is the removal of out-of-focus light, such that image clarity is improved. This is achieved by the arrangement of mirrors, filters and aperture, as indicated in diagrammatic representation of a epi-flourescence laser scanning microscope in Figure 3.7.

The principle involves emitted light from the laser excitation source passing through an excitation pinhole, which ensures that only the focal plane is illuminated. The laser light is reflected by the dichromatic mirror onto the specimen, but secondary fluorescence emitted from the specimen, passes back through the dichromatic mirror due to its longer wavelength. The resulting fluorescent emission then passes through a second pinhole placed in front of the photomultiplier tube (PMT) detector to remove any light from above or below the focal plane, as indicated in Figure 3.7. For optical imaging, the Raleigh criterion states that the pixel size should be equivalent to one quarter of the resolution limit. The spatial resolution is governed by the numerical aperture (N.A) of the optical components and by the wavelength (λ). The most common axial resolution (R) for the confocal configuration is given by:

$R = 0.4\lambda/N.A$ *Equation 3.3*
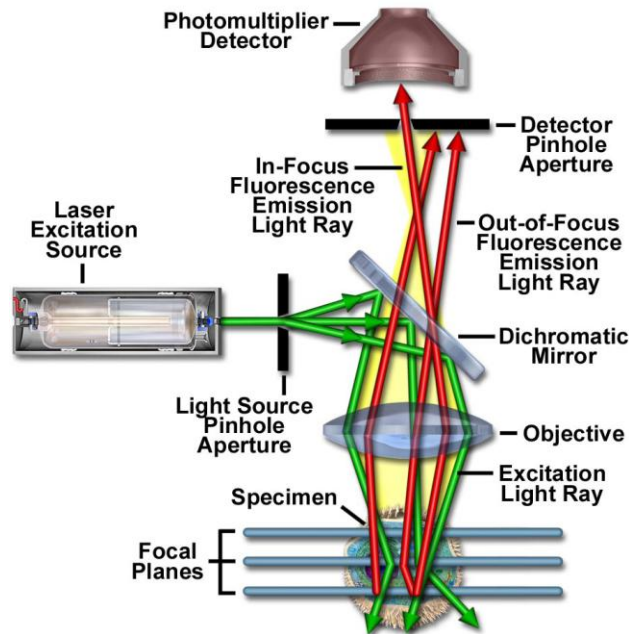
Figure 3.7. *Schematic diagram of laser scanning confocal microscope. (Claxton et al., 2000)*

3.4.2 BRIGHT FIELD IMAGING

The confocal microscope (SP2, Leica) used in the present study allows for simultaneous imaging of both confocal fluorescence and brightfield. Bright-field optical microscopy is the conventional technique that was used to image cells during the process of aspiration, whereas confocal will be used in later chapters for visualisation of actin cytoskeleton labelled with GFP. The software associated with the confocal microscope was used to measure the cell aspiration length inside the micropipette from the brightfield images. In the present work, a 488 nm excitation was employed with a x63/1.4 NA objective. According a pixel size of 0.11 μm was adopted, which according to equation 3.3 yielded an axial resolution of 0.139 μm.

3.4.3 MICROSCOPE SETTINGS

Image acquisition is controlled by the power of the laser, and its offset and gain. The values of different settings are presented in Table 3.1. These values are used throughout the work unless otherwise stated.

Table 3.1. *Microscope setting parameters.*

	Brightfield	Fluorescent
Line averaging	2	4
Zoom	4	4
Speed	400 Hz	400 Hz
Format	512x512	512x512
UV	3mW	
488 nm		25%

3.5 MODELING OF THE CELL BEHAVIOR

3.5.1 STANDARD LINEAR SOLID MODEL

Generally a standard linear solid (SLS) model has been traditionally used to model the behaviour of viscoelastic materials (Ferry, 1970). The SLS model involves a linear combination of springs and a dashpot to represent elastic and viscous component, respectively (section 2.3). The SLS model is able to predict both stress relaxation and creep characteristics. This model has been previously used to model viscoelastic behaviour of the cell generated from micropipette aspiration experimental (Jones et al., 1999; Trickey et al., 2000).

In this model the cell is assumed to be a homogenous viscoelastic half-space with the micropipette applying uniform pressure to the cell. The governing equation of the SLS model is shown in the equations below.

$$L(t) = \frac{\phi a \Delta P}{\pi k_1}\left[1 - \left(\frac{k_1}{k_1 + k_2} - 1\right)e^{-t/\tau}\right]$$

$$E_{in} = \frac{3}{2}\left(k_1 + k_2\right)$$

$$E_{eq} = \frac{3}{2}k_1$$

$$\mu = \tau\left(\frac{k_1 k_2}{k_1 + k_2}\right)$$

where L(t) is the aspiration length of the cell at time t, E_{in} and E_{eq} represents the instantaneous and equilibrium moduli, respectively, and τ is the time constant. μ is the apparent viscosity and k_1 and k_2 are viscoelastic parameters that can be determined from a non-linear regression of the experimental data of aspiration length versus time following application of aspiration pressure.

3.5.2 BOLTZMANN STANDARD LINEAR SOLID MODEL

The SLS model assumes that the loading occurs instantaneously with a step change in pressure. It was recently suggested that the Boltzmann superposition principle could be applied to the SLS model to incorporate a ramp loading protocol (Merryman et al., 2009). Using this principal the final governing equation 3.4 may be solved analytically in MatLab.

$$L(t) = \int_0^t \frac{\phi a}{\pi k_1}\left[1 - \left(\frac{k_1}{k_1 + k_2} - 1\right)e^{-(t-t')/\tau}\right]\frac{dP}{dt'}dt' \qquad \text{\textit{Equation 3.4}}$$

The experimental procedure includes both the loading phase during which pressure is applied and the holding phase at constant pressure. Hence the governing equation has to be solved for two different conditions.

$$P(t) = \begin{cases} Qt' & 0 \leq t \leq t_f \\ Qt_f & t \geq t_f \end{cases}$$

Equation 3.5

where Q is the rate of pressure change (cmH$_2$O/s), t is the time and t$_f$ is the time taken to reach maximum set pressure.

For $0 \leq t \leq t_f$

$$L(t_f) = \frac{\phi a}{\pi k_1}\left(1 - \frac{k_1}{k_1 + k_2}\right)P(t) + \frac{\phi a}{\pi k_1}\frac{k_1}{k_1 + k_2}\int_0^t \left[e^{-(t-t')/\tau}\right]\underline{P}(t')dt'$$

Equation 3.6

$$L(t) = \frac{\phi a}{\pi k_1}\left(1 - \frac{k_1}{k_1 + k_2}\right)P(t) + \frac{\phi a}{\pi k_1}\frac{k_1}{k_1 + k_2}Q\left[t\tau - \tau^2 + \tau^2 e^{-t/\tau}\right]$$

Equation 3.7

For $t \geq t_f$

$$L(t) = \frac{\phi a}{\pi k_1}\left(1 - \frac{k_1}{k_1 + k_2}\right)P(t) + \frac{\phi a}{\pi k_1}\frac{k_1}{k_1 + k_2}\left(\int_0^{t_f}\left[e^{-(t-t')/\tau}\right]\underline{P}(t')dt' + \int_{t_f}^t\left[e^{-(t-t')/\tau}\right]\underline{P}(t')dt'\right)$$

Equation 3.8

$$L(t) = \frac{\phi a}{\pi k_1}\left(1 - \frac{k_1}{k_1 + k_2}\right)P(t) + \frac{\phi a}{\pi k_1}\frac{k_1}{k_1 + k_2}Q\left[e^{-(t-t_f)/\tau}(t_f\tau - \tau^2) + \tau^2(e^{-t/\tau}) + t_f - t_f\tau e^{-(t-t_f)/\tau}\right]$$

Equation 3.9

The initial parameters were assigned as follows k$_1$ = 100 kPa, k$_2$ = 100 kPa and μ = 100 kPa.s. The non linear least square method was then used to determined the actual parameter values by fitting each L(t) experimental response, for both models BSLS and SLS.

3.6 MATERIALS AND METHODS

3.6.1 PREPARATION OF THE CULTURE MEDIA

In this section, the preparation of the standard culture medium used thought out the cell culture work described in this thesis. Dulbeccos Minimal Essential Medium (DMEM) supplemented with 10% (v/v) Foetal Calf Serum (FCS) was employed for the culture medium. Unless otherwise stated, all reagents were obtained from Sigma (Poole, UK). For preparation of the culture medium using 500 mL of D5921 DMEM, 100 mL of FCS, 10mL of hepes buffer, 5 mL of L-glutamine (200 mM), 5 mL penicillin/streptomycin and 0.075 g of L-ascorbic were mixed in the DMEM bottle. The media was sterilised by filtering the culture medium using a 0.22 μm pore sterile filter prior to use. 100 mL of the culture medium was frozen in aliquots until needed. The osmolality of the media was measured at 320 mOsmol/kg.

3.6.2 ISOLATION OF THE CHONDROCYTES

The technique used to isolate the bovine articular cartilage chondrocytes was similar to that reported in previous studies in the host laboratory (Lee et al., 1998). To review briefly, front feet of adult steers were obtained within 2 h of collection from a local abattoir. The feet were scrubbed and soaked in virkon for 20 minutes followed by 70% (methyl) alcohol for 15 minutes. Bovine full depth cartilage was sliced from the proximal articular surfaces of the metacarpalphalangeal joints. The cartilage explants were immersed in culture medium (DMEM + 10%FCS). The slices from at least 2 different joints were pooled for each experiment. Pronase and collagenase were prepared in DMEM (Gibco Ltd, Paisley, UK) with 10% (v/v) FCS and sterilised by passing through a 0.22 μm pore filter. The explants were finely diced and transferred to a 50 mL falcon conical tube along with addition of 10mL pronase followed by 1 h on the rolamixer in the 37 °C oven. The pronase solution was then replaced with 15 mL of collagenase and the samples were incubated on the rolamixer at 37 °C for 16 h. A cell suspension was obtained by filtering the digest through a 7 μm sterile cell sieve (Falcon Ltd, Oxford UK.). The cell suspension

was washed thrice in fresh DMEM + 10% FCS. Chondrocytes were resuspended in the culture media at a density of 0.5 x 10^6 cells/mL, ready for subsequent micropipette aspiration.

A viability assay was performed using trypan blue (Sigma Chemical Co., Poole, UK.) which stains non-viable cells blue. The cell count was performed using a haemocytometer (Sigma Chemical Co., Poole, UK.) to give the total yield of viable cells and a percentage of cell viability. A cell viability in excess of 95% was obtained in all cases.

3.6.3 MICROPIPETTE ASPIRATION OF THE CELL

Micropipette aspiration was performed, using a technical protocol similar to those described previously (Jones et al., 1999; Sato et al., 1990; Theret et al., 1988), although some specific modifications to the control system were included in the present study. Micropipettes made from drawing capillary tubes with a pipette puller were fractured on the microforge (MF-900, Narishige) to an inner diameter ranging between 3-7 µm. The inner region of the micropipette was coated with silicon coating to prevent cell adhesion.

Approximately 1 mL of the cell suspension at a density of 0.5 x 10^6 cell/mL was placed in the chamber designed to allow entry of the micropipette from the side (Figure 3.1B). All experiments were performed at room temperature. The experimental protocol was initiated by applying a tare pressure of approximately 1 cmH$_2$O to ensure each cell made contact with the tip of the micropipette. The cell surface was subjected to a negative pressure of 7 cmH$_2$O generated from the custom-built pump control water reservoir over a period 1.3 s. Further parameters are detailed in Table 3.2. The deformation of the cell was imaged using brightfield microscopy for 180 s at an imaging frequency of 0.6 Hz. Brightfield microscopy indicated no visible pericellular matrix surrounding the chondrocytes in suspension from any of the different treatment groups used throughout this thesis. Therefore the mechanical contribution of any pericellular matrix has been ignored. This is supported by previous immunohistochemical studies that show minimal

levels of type VI collagen and chondroitin sulphate surrounding freshly isolated chondrocytes (Knight et al., 2001).

The length of the cell projected into the micropipette, were measured using a commercial software program for subsequent data analysis (Leica LCS Lite). The measured data of the cell were executed into MatLab using a curve fit for both SLS and BSLS models. This enabled the estimation of a number of mechanical parameters, including the instantaneous modulus (E_{in}), equilibrium modulus (E_{eq}) and apparent viscosity µ, using equation 2.5-2.7 respectively. The Matlab program was designed to calculate the best fit to the temporal aspiration length data based on an optimisation of all three parameters (k1, k2, µ). An alternative approach of fitting each parameter separately could be adopted but that this was rejected since it would not provide a single temporal profile for the viscoelastic response.

Table 3.2. *Parametric values employed to estimate viscoelastic parameters of the cell during micropipette aspiration.*

Parameters	Values
Tare Pressure : P_T (cmH$_2$O)	1
Initial Time: T_0 (secs)	2
Step pressure: ΔP (cmH$_2$O)	7
No of steps:	1
Time interval: T_1 (secs)	0
Step time : T_2	1.3
Hold time: T_{hold} (secs)	180

3.6.4 CALCULATION OF THE CELL MORPHOLOGICAL PROPERTIES

For the calculation of the approximate cell surface area and cell volume, regions of the cell was divided into symmetrical shapes as indicated in Figure 3.8.
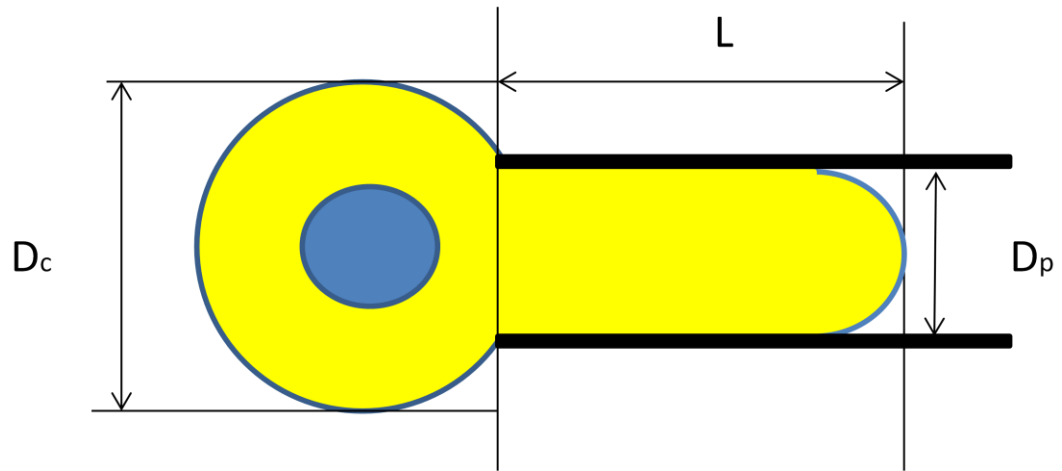
Figure 3.8. *Schematic of cell being aspirated into the micropipette.*

The following equations were derived for the calculations of the cell surface area and volume assuming a symmetrical geometry of the cell (Figure 3.8):

Cell Surface Area during aspiration

$$\left(\pi D_c^2\right) + \left(\pi D_p\left(L - \frac{D_p}{2}\right)\right) + \left(\frac{\pi D_p^2}{2}\right) \qquad \textit{Equation 3.10}$$

Cell Volume during aspiration

$$\left(\frac{\pi D_c^3}{6}\right) + \left(\frac{\pi D_p^2\left(L - \frac{D_p}{2}\right)}{4}\right) + \left(\frac{\pi D_p^2}{12}\right) \qquad \textit{Equation 3.11}$$

where D_c is the diameter of the cell region outside micropipette which is assumed to be spherical, D_p is the pipette diameter, L is the aspiration length of the cell into the micropipette as indicated in Figure 3.8. The leading edge of the aspirated cell was assumed to be hemispherical with diameter equivalent to that of the micropipette. The percent change in the cell surface area and volume were computed from the pre-aspiration state considering the cell to be initially spherical with a diameter (D_c).

The above approach ignores the inherent ruffled state of the chondrocyte membrane as shown in previous published studies (Lee et al., 2000a). This is likely to have most effect on the surface area calculation which will be an underestimate of the true cell surface area. However the adopted surface area measurement is still useful for estimating the possible global distortion of the cortical actin. An alternative approach would be to use confocal 3D reconstruction to estimate volume and surface area. However such an approach would not account for the membrane ruffles unless a specific membrane fluorescent dye was used which might influence cell and membrane mechanics. Furthermore the confocal 3D reconstruction approach is also likely to be inaccurate due to the poor axial resolution and axial distortion of the confocal microscope.

3.6.5 STATISTICAL ANALYSIS

In the present study, the sample population was assumed to be non-Gaussian in nature, and therefore non-parametric statistics were employed. The data throughout the thesis was presented in standard box plots, and sample populations were described in terms of median values and inter quartile ranges. The significant difference between the sample population of the cell was obtained using the Mann Whitney U-test for non-paired data. A value of 5% was considered to be statically significant ($p < 0.05$).

3.7 RESULTS

The median value of the diameter of the primary chondrocytes before the micropipette aspiration was found to be 12.9 µm. The surface area and the volume of chondrocytes were computed using the equations 3.10 and 3.11 respectively. The percentage change in the surface area and volume of the chondrocytes after aspiration was found approximately to be 15% and 4% respectively. The surface area ($p < 0.001$) and volume ($p < 0.05$) of the chondrocytes significantly changed after the micropipette aspiration, with greater changes found in the case of the chondrocyte surface area

3.7.1 MECHANICAL PROPERTIES OF THE CELLS

Chondrocytes when subjected to negative pressure through the micropipette, reveal four distinct responses, which are clearly indicated in the Figure 3.9. They may be catagorised into four modes of the chondrocyte aspirations:

I: Membrane rupture and detachment of sections of the cell as indicated by arrows in Figure 3.9.

II: Minimal aspiration - Aspiration length < 10% of the mean aspiration length for that sample.

III: Uneven Aspiration – Cell appeared twisted during the aspiration process.

IV: Uniform Aspiration – A hemispherical projection of the cell is formed into the micropipette.

The percentage of cells in each category was recorded on sample population of 21 chondrocytes, as presented in Table 3.3. As indicated, the majority of cells exhibited aspiration behaviour characterised by modes III and IV with 67% in the latter case. An example of representative images of the cell indicating uniform aspiration is presented in Figure 3.10, both in the brightfield mode and fluorescent staining with Calcein AM. It is very evident that the membrane remains intact when 7 cmH_2O is applied in 1.3 s, as the dye does not leaked from the hemispherical projection of the aspirated cell.

Table 3.3. *Summary of the percentage of cells experiencing different mode of the aspiration.*

Pressure Rate (cmH_2O/s)	Total No. of Cells Tested	Cell Aspiration	I	II	III	IV
5.48	22	18 (90%)	2(9%)	4(22%)	2(11%)	12(67%)

I – Membrane rupture; II – Minimal aspiration; III – Uneven aspiration;

IV – Even aspiration.
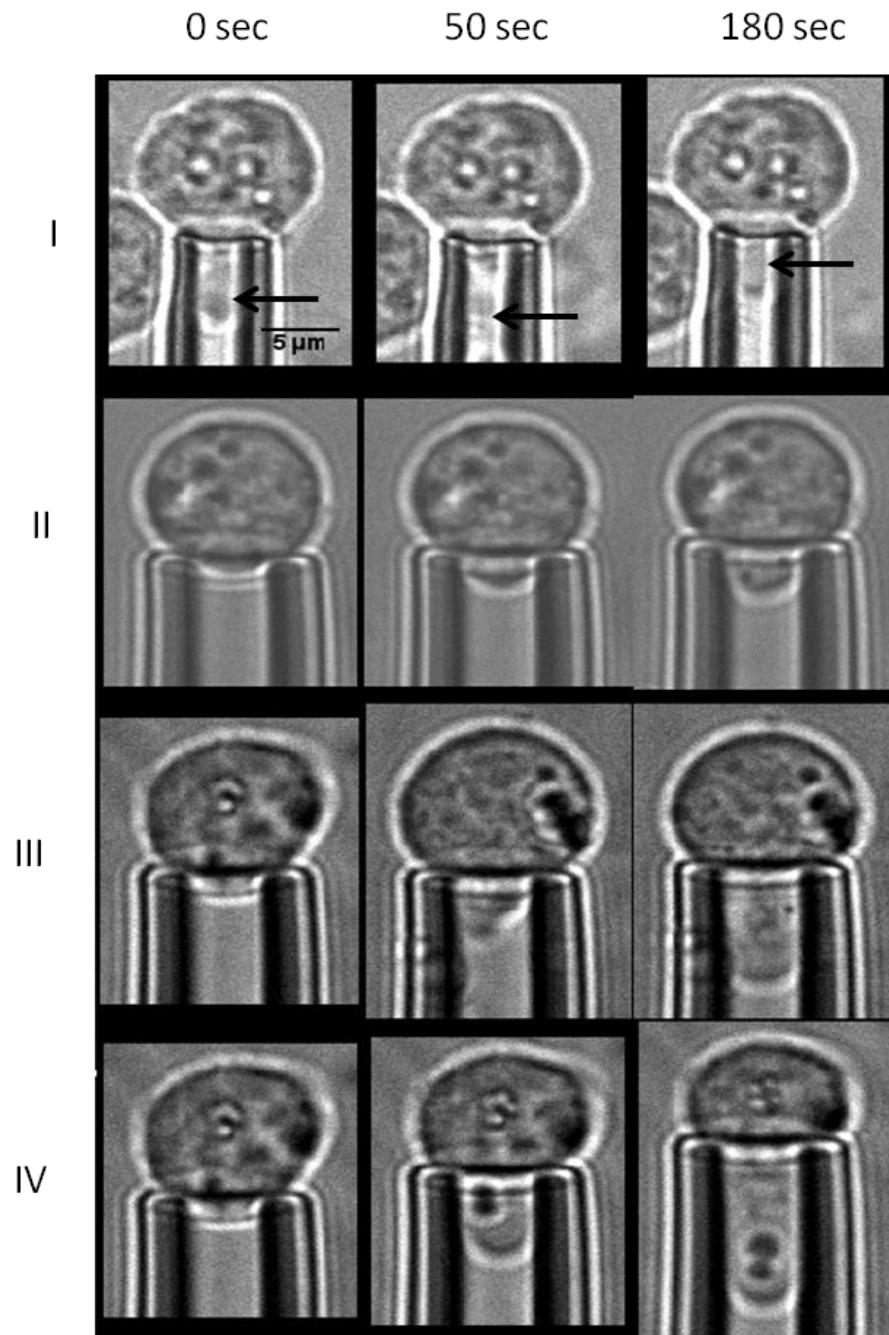
Figure 3.9. *Four distinct modes of chondrocytes respect to modes of micropipette aspiration. I – Membrane rupture (arrow indicated detached portion of the cell): II - Minimal aspiration: III - Uneven aspiration, IV- Uniform aspiration. Scale bar 5 μm.*

116

The temporal profile of the aspiration length following an aspiration pressure of 7 cmH$_2$O is presented in Figure 3.11. It is very clear that the chondrocytes exhibit viscoelastic creep behaviour in response to an increment pressure change followed by a constant pressure. This is characterised by an initial displacement of the chondrocytes into the micropipette, followed by a decreasing rate of the deformation until an equilibrium length is reached. To determine the viscoelastic properties of the chondrocytes, the progress of the aspiration length of the chondrocytes with time was executed in MatLab for a curve fit analysis using SLS and BSLS models. Only the cells from the mode II, III and IV were used for the calculation of the cell mechanical properties and cell obtained from the mode I were rejected.
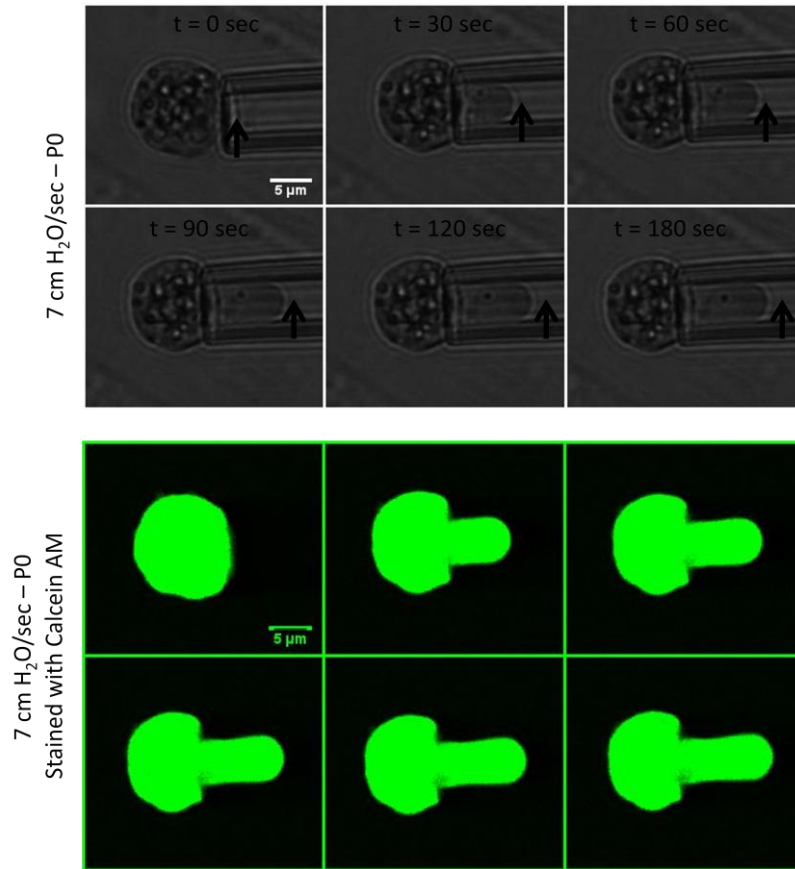
Figure 3.10. *Representative sequential images of the freshly isolated chondrocytes (P0) (Above panel), P0 stained with Calcein AM (Below panel). Scale bar 5µm.*
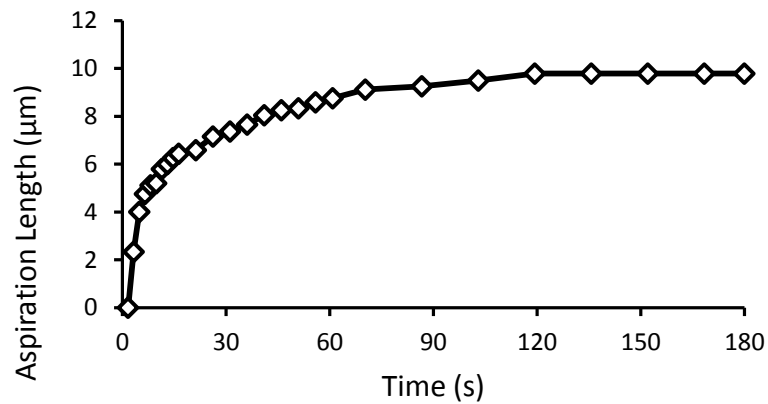
Figure 3.11. *Temporal changes in the aspiration length of the chondrocytes into the micropipette when aspirated at 7 cmH$_2$O.*

The curve fitting for three typical chondrocytes using both SLS and BSLS model for three different modes of aspiration is shown in Figure 3.12. Cells that were successfully aspirated were included in the analyses of cell morphology. However, cells were rejected (Table 3.4) from the cell mechanics analyses if:

- the cells did not aspirate

- the analytical model did not converge or produce an accurate fit (R < 0.95)

- the estimated constants reached the pre-set limit ($k_2 > 100$)

Table 3.4. *Shows the number of cells rejected under each of the above criteria and hence the total number successfully analysed for each condition.*

Pressure Rate (cmH_2O/s)	Total No. of Cells Tested	Cell Aspiration	Convergence		R ≥ 0.95		Cells Excluded $k_2 < 100$	
5.48	20	16	SLS	BSLS	SLS	BSLS	SLS	BSLS
			14 (88%)	14 (88%)	14 (100%)	14 (100%)	14 (100%)	14 (100%)

The curve fitting of the experimental data with SLS and BSLS model generated k_1, k_2 and μ values. These parameters were used in equations 2.5-2.7 to compute the mechanical parameters namely instantaneous modulus, equivalent modulus and apparent viscosity, the values of which are presented in Figures 3.13A-C, respectively. No significant difference exists between the two models for any of the three parameters (p > 0.05). It is also noteworthy that the parameters values were similar in magnitude to those previously reported for both normal and osteoarthritic (OA) chondrocytes (Trickey et al., 2000)

A)

B)
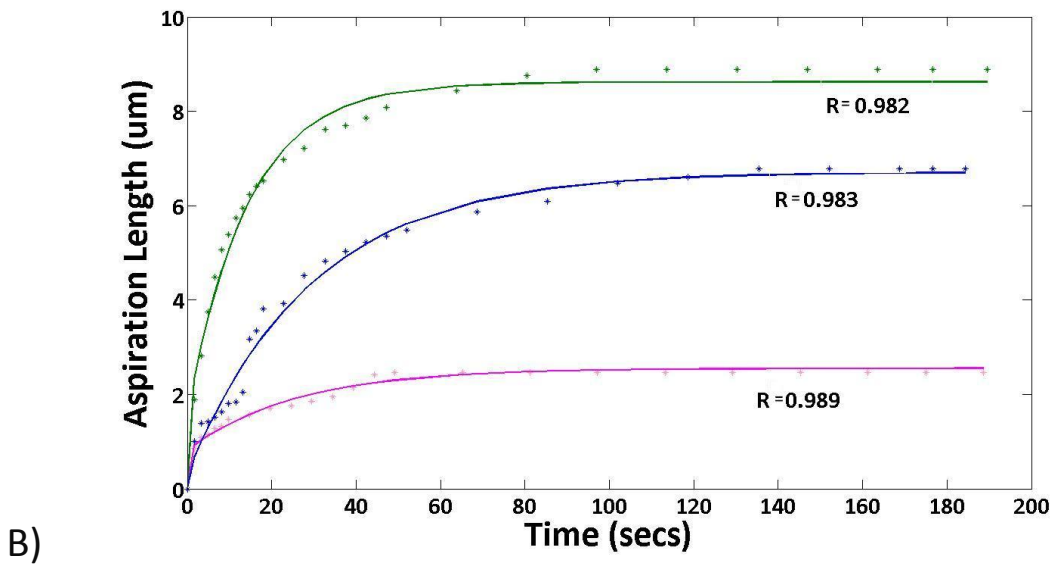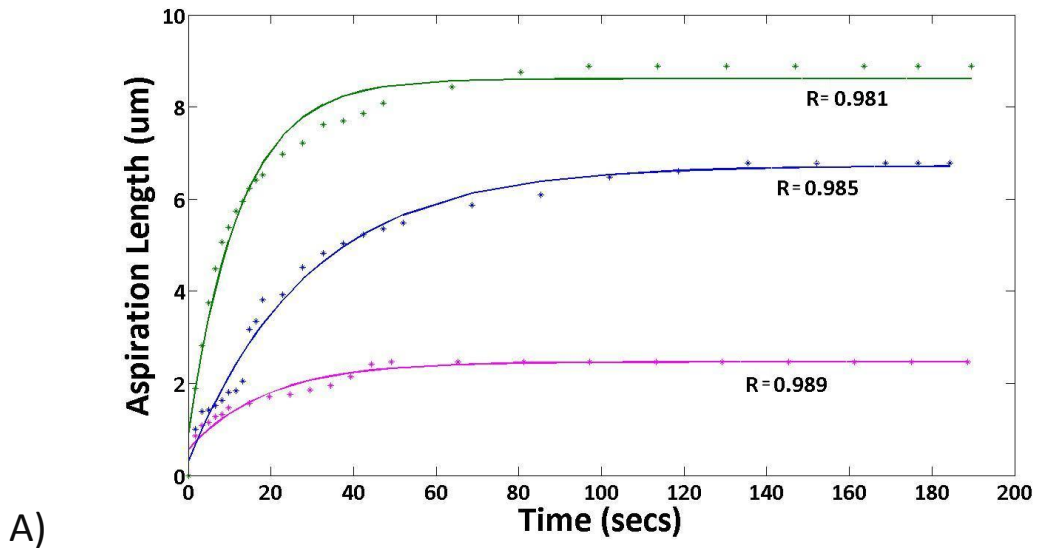
Figure 3.12. *Aspiration data for three chondrocytes showing aspiration modes II (pink), III (blue) and (IV) green. Temporal changes in aspiration length have been fitted using the non linear least square method executed in MatLab. Curve fitting for different aspiration mode using A) SLS and B) BSLS models. Chondrocytes were aspirated at 7 cmH$_2$O/s.*
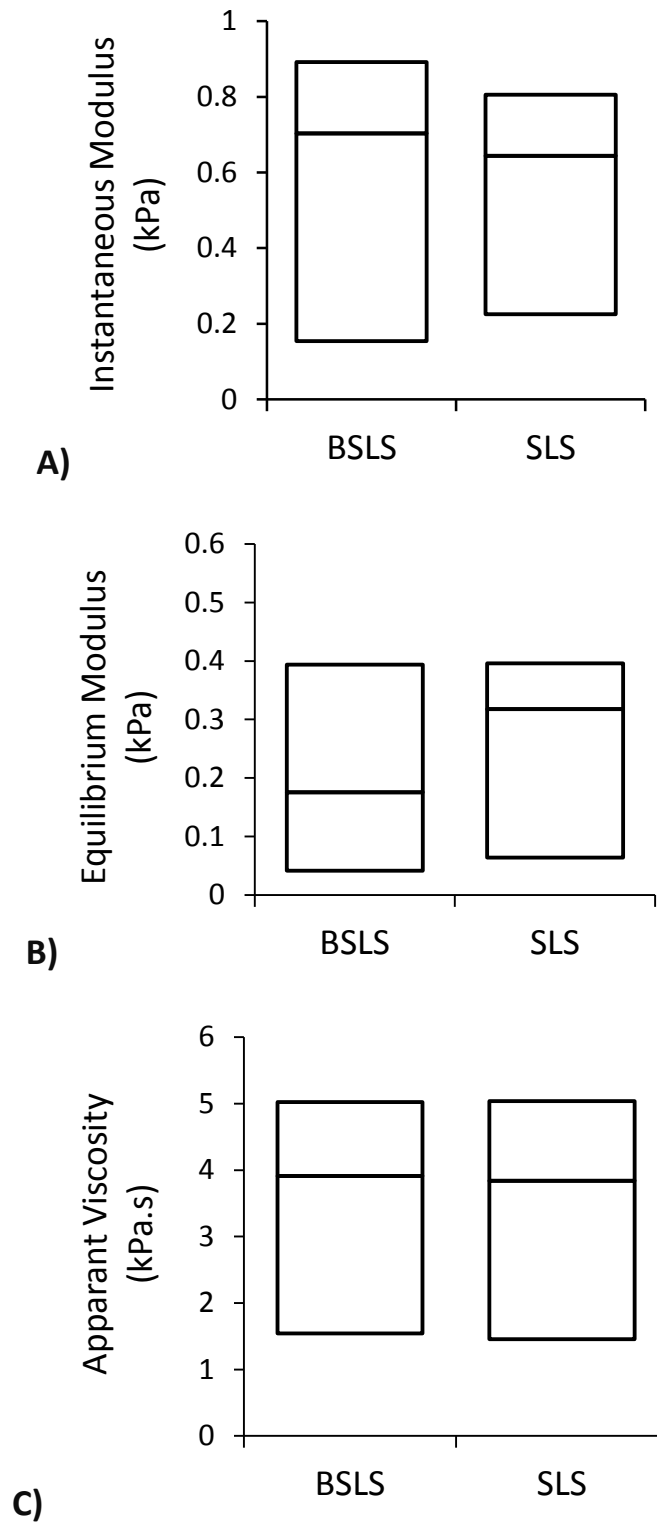
Figure 3.13. *The three viscoelastic parameters of the primary chondrocytes generated from the data analysis using SLS and BSLS model.*

3.8 DISCUSSION

The micropipette aspiration technique has been widely used to determine the mechanical properties of many cells, including articular chondrocytes. In the present study, micropipette aspiration system has been successfully developed to allow temporal control of the aspiration pressure applied to articular chondrocytes of bovine source. The chondrocytes exhibited viscoelastic creep behaviour following the micropipette aspiration as seen from the Figure 3.11 and this is consistent with the previous studies (Jones et al., 1999; Trickey et al., 2000).

3.8.1 INFLUENCE OF THE PIPETTE DIAMETER ON CELL MICROPIPETTE ASPIRATION

The micropipette aspiration was performed on the chondrocytes using micropipettes of different diameters, ranging from 3-7 µm. It can be seen from Figure 3.14 that the percentage of cells which exhibited mode IV aspiration increased with pipette diameter. Accordingly over 80% of cells were successfully aspirated using pipettes of diameters between 6 and 7 µm. In a previous study authors have suggested that if the ratio of cell diameter to pipette diameter is greater than 3, the solution of both SLS and BSLS models becomes inaccurate (Baaijens et al., 2005). This implies that small diameter micropipettes should be used, although there are inevitable caveats associated with using small diameter micropipettes. However smaller diameter micropipettes have a tendency to rupture the cell membrane due to the boundary conditions at the inner wall of the micropipettes. Furthermore in the present study a high percentage of the cells were either not aspirated or were minimally aspirated using smaller diameter micropipettes (Figure 3.14). The ratio of cell diameter to pipette diameter in present study was 2.01 ± 0.23, which equivalent to that used in previous study (Table 3.5).
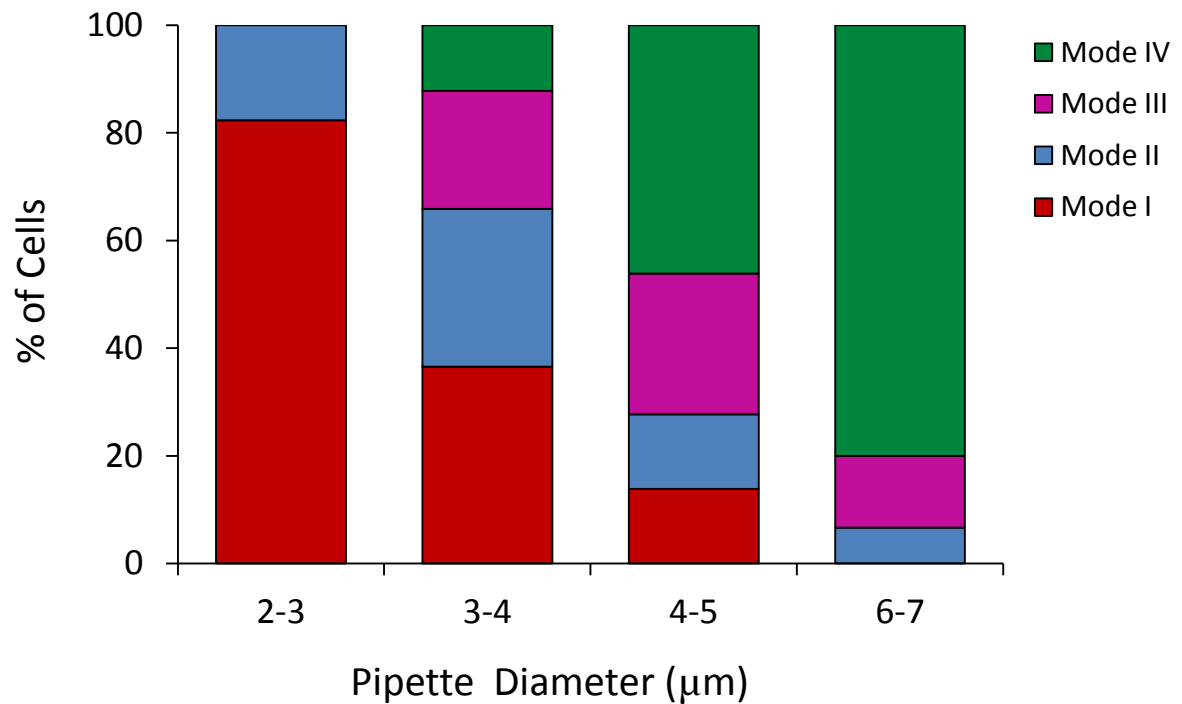
Figure 3.14. *Effect of the pipette diameter on the response of the cell aspiration. Uniform and uneven aspiration is referred to as mode IV and III respectively as indicated in Figure 3.11.*

Table 3.5. *Parameters used for micropipette aspiration technique. Cell diameter (C.D) and pipette diameter (P.D).*

References	Cell Source	Pressure (kPa)	C.D (µm)	P.D. (µm)	C.D/P.D (µm)
(Trickey et al., 2000)	Human knee and hip	0.4-0.7	13.1±1.5 (Non OA)	6	2.2
			15 ± 2 (OA)		2.5
(Zhang and Chen, 2009)	Rabbit knee	0.3	-	5.5	
(Steklov et al., 2009)	Human knee	0.7	13.8±1.5 (18-35 old)	5.5	2.5
			14.75±2.3 (55+ Normal)		2.7
			15.45±1.02 (55+OA)		2.8

3.8.2 VISCOELASTIC PROPERTIES OF THE CHONDROCYTES

The optimised micropipette aspiration system provides a versatile tool to investigate both elastic (demonstrated in Appendix C) and viscoelastic properties of the cells. This can be achieved by modifying the protocol of the micropipette aspiration according to the requirement of the experiment. Four different modes of aspiration were observed in the present study (Figure 3.9). Given the damaging nature of mode I, this was excluded from all subsequent analyses of the viscoelastic properties of the cells throughout the thesis. The membrane rupturing and detachment of the chondrocyte section observed in mode I could be due to the extensive tension on the cell membrane. Cells exhibiting minimal aspiration may not have developed an adequate seal with the opening tip of the micropipette. Furthermore the cells exhibiting the uneven and uniform mode of the aspiration may have experience variation in suction pressure.

To compute the mechanical parameters, SLS and BSLS models have been utilised. It has been reported that, if the ramp time is greater than 2 s then the SLS model becomes inaccurate for the computation of the mechanical properties (Zhao et al., 2009). This criteria was successfully fulfilled during the optimisation of the system, whereby 7 cmH$_2$O pressure can be applied within 1.3 s. The curve fitting performed using MatLab was observed to accommodate the majority of the experimental data with values of R in the range of 0.95 - 0.99 (Figure 3.12), irrespective of the model used. No significant difference was observed in the viscoelastic parameters computed using SLS and BSLS. This could be due to the less than 2 s ramp time used in the present study. The results of present study are in agreement with a previous study performed on chondrocytes (Table 3.6).

Table 3.6. *Median and mean* values of the viscoelastic parameters estimated from micropipette aspiration of both healthy (non-OA) and osteoarthritic (OA) chondrocytes in suspension culture.*

Mechanical Properties	BSLS	SLS	SLS (non-OA)*	SLS (OA)*
Instantaneous Modulus (kPa)	0.69	0.67	0.41	0.63
Equilibrium Modulus (kPa)	0.25	0.30	0.24	0.33
Apparent Viscosity (kPa·s)	3.44	3.47	3.0	5.8

*Adapted from Trickey et al., (2000)

3.9 STANDARD OPERATING PROCEDURE

3.9.1 MICROPIPETTE ASPIRATION OF THE CELLS

- Micropipettes were made by drawing capillary tubes (G -1, Narishige, Tokyo, Japan) with a micropipette puller (P-97, Sutter Instruments, Novato, California, USA) and fractured using a microphorge (MF-90, Narishige, Tokyo, Japan) to an inner diameter 6.5-7.5 μm (see Appendix B).

- The micropipettes were coated with silicone solution (Sigmacote, Sigma, MO, USA) to minimise cell adhesion.

- Prior to testing, approximately 1 mL of cell suspension (0.5×10^6 cells.mL^{-1}) was placed in a custom-built cell chamber, which is designed to allow the micropipette to enter in a horizontal plane (Figure 3.1).

- The micropipette must be filled with DMEM + 10% FBS, as using distilled water affects the osmolarity and could lead to crystal formation.

- The micropipette holder was placed on the stage and connected to a micro-manipulator (MO-203, Narishige, Tokyo, Japan) that was then used to position the micropipette in the proximity of a selected cell surface.

- Before the start of the experiment, a tare pressure is apply which allows to ensure a seal formation between the pipette and cell membrane necessary for

the cell to be successfully aspirated. A tare pressure of 1 cmH$_2$O was applied to the surface of the chondrocytes, using the custom built pressure control system.

- The aspiration pump system was set to operate according to the parameters in Table 3.2, unless otherwise stated.

- Micropipette aspiration was performed on the stage of a confocal microscope system (TCS SP2, Leica Microsystems, and Germany). The precise imaging protocol (Table 3.1) depended on the type of the experiment.

- The micropipette should be completely free of air bubbles. This is to avoid a non-zero pressure datum point at the micropipette tip. This would occur, for example, when the level of the fluid in the pipette and reservoir is the same.

- The angle at which the micropipette is inclined relative to the horizontal axis of the micropipette is very important. It will determine whether the cell could be aspirated or not, dependent on the quality of contact between the membrane of the cell and the tip of the micropipette.

- Coating of the micropipette should be thoroughly dried to avoid difficulty associated with removing the debris from the pipette.

3.9.2 ANALYSIS OF THE VISCOELASTIC PROPERTIES OF THE CELLS

- Brightfield and fluorescent images were taken using x63/0.95 NA oil immersion objective lens at time interval of 1.6 s for 180 s. A 512 x 512 pixel image format was used which yields a voxel size of 0.11µm x 0.11µm. Additionally UV light was used to obtain bright field images with clarity.

- Images were analysed using software Leica LCS lite to measure temporal changes in the aspiration length of the cell into the micropipette.

- The experimental data (aspiration length versus time) were modelled in MatLab by using non-linear least square method with either the SLS or BSLS model to yield the parameters: instantaneous modulus, equilibrium modulus and apparent viscosity.

CHAPTER 4

EFFECTS OF ASPIRATION PRESSURE CHANGE RATE ON THE MECHANICS OF CHONDROCYTES

4.1 INTRODUCTION

4.2 METHODOLOGY

    4.2.1   Micropipette Aspiration

    4.2.2   Statistical Analysis

4.3 RESULTS

    4.3.1   Effects of Applied Pressure Change Rate

    4.3.2   Effects of Repeat Aspiration

4.4 DISCUSSION

    4.4.1   Effects of Applied Pressure Change Rate

4. EFFECTS OF ASPIRATION PRESSURE CHANGE RATE ON THE MECHANICS OF CHONDROCYTES

4.1 INTRODUCTION

This chapter describes a series of experiments involving the micropipette aspiration technique for measuring the biomechanics of isolated chondrocytes at three different pressure rates, i.e. 0.35, 0.70 and 5.48 cmH$_2$O/s. In addition, repeat aspiration of the chondrocytes was performed using the slow and fast pressure rates of 0.35 cmH$_2$O/s and 5.48 cmH$_2$O/s, respectively. The temporal changes in the aspiration lengths of the chondrocytes in response to different pressure rates provided inputs to both the solid linear standard (SLS) and Boltzmann SLS (BSLS) models. Further, MatLab was used to compute the viscoelastic parameters of the cells, i.e. instantaneous modulus, equilibrium modulus and apparent viscosity.

4.2 METHODOLOGY

Bovine articular chondrocytes were isolated from full-depth adult cartilage from the metacarpo-phalangeal joints, as described in section 3.6.2. The cells were subjected to micropipette aspiration immediately following the isolation procedure.

4.2.1 MICROPIPETTE ASPIRATION

The micropipette aspiration techniques described in section 3.6.3 were used to determine the viscoelastic properties of individual chondrocytes. The cell suspension was placed in a custom-built chamber on the stage of an inverted microscope with a confocal system. Each experiment was initiated by applying a tare pressure of approximately 1 cmH$_2$O to attach an individual cell to tip of the micropipette. Subsequently, a step pressure of 7 cmH$_2$O was applied by changing the height of the water in a reservoir connected to the micropipette. During the micropipette aspiration, bright-field images of

the chondrocytes were recorded at 1 frame/1.63 s for 180 s using a ×63/1.4 NA oil immersion objective. For each experiment, three different pressure rates were used, namely, 0.35, 0.70 and 5.48 cmH$_2$O/s, as indicated in (Figure 4.1A). After 180 s, the applied pressure was removed and the cell was imaged for a further 180 s, which was termed the recovery phase (Figure 4.1B).
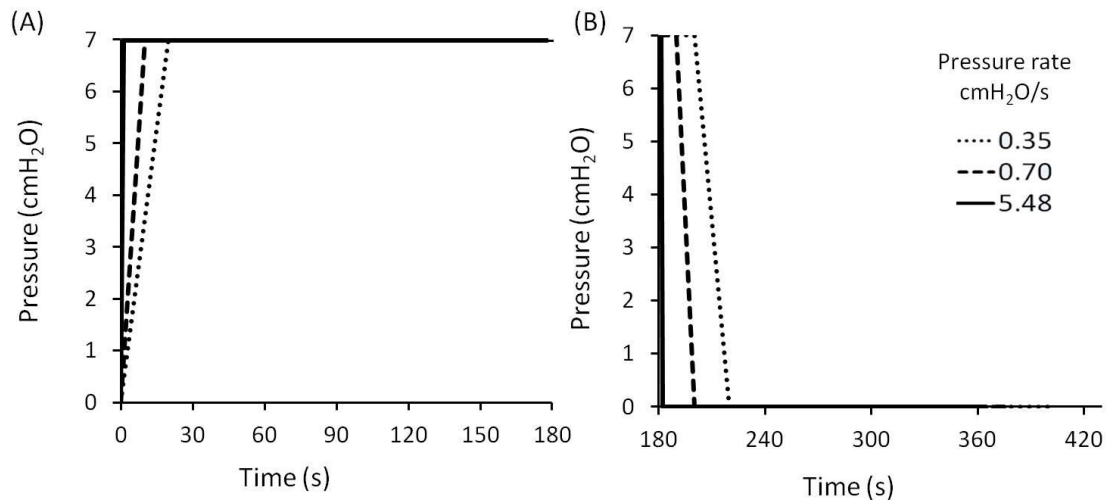
Figure 4.1. *The micropipette aspiration protocol showing the temporal change in aspiration pressure during the aspiration phase (A) and subsequent recovery phase (B) for three different pressure rates 0.35, 0.70 and 5.48 cmH$_2$O/s.*

Furthermore, a separate group of chondrocytes were subjected to repeat aspiration. The cells were pre-conditioned with an initial aspiration using an pressure rate of 0.35 cmH$_2$O/s. After a 180 s recovery phase, the same individual cells then underwent a second aspiration which was applied at either 0.35 cmH$_2$O/s or 5.48 cmH$_2$O/s (Figure 4.2).

129
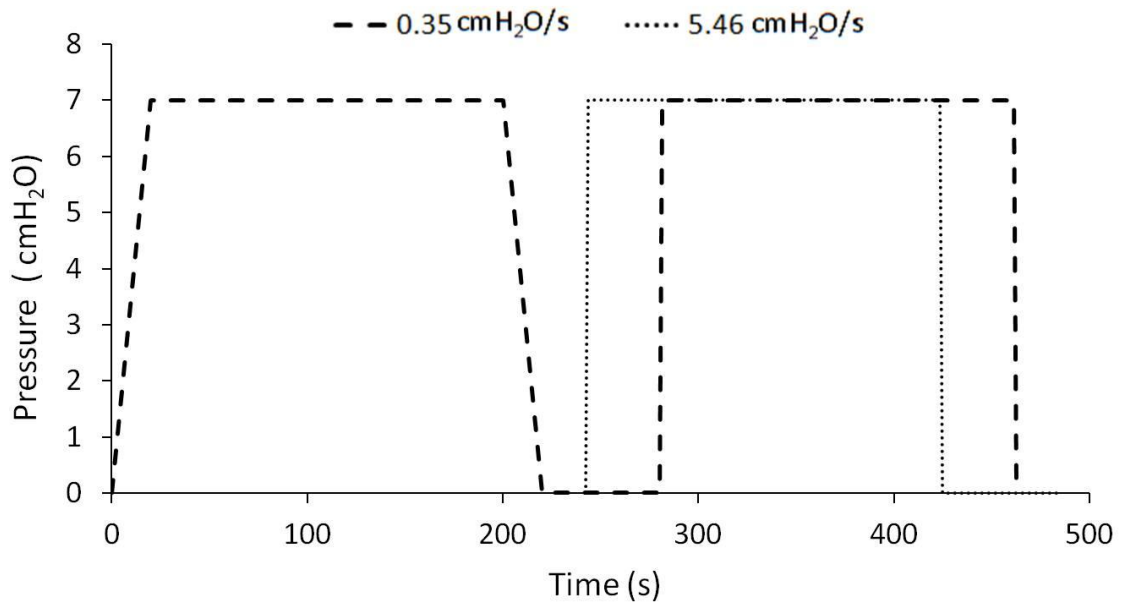
Figure 4.2. *Protocol for the repeat aspiration experiment showing the temporal change in aspiration pressure using two different pressure rates for the second aspiration 0.35 cmH₂O/s and 5.48 cmH₂O/s.*

The aspiration length (L) of the cell within the micropipette was measured from the bright-field images for each pressure rate ($\Delta P/t$). The surface area and volume of the cells were computed using equations 3.10 and 3.11 respectively. Additionally the viscoelastic parameters were calculated using two previously reported models, the SLS model and (Sato et al., 1990) the BSLS model (Merryman et al., 2009). The viscoelastic parameters namely instantaneous modulus, equilibrium modulus and apparent viscosity were determined by fitting equation 2.4 and 3.4 using non-linear regression analysis for SLS and BSLS model respectively (see section 3.5 for detailed information).

4.2.2 STATISTICAL ANALYSIS

The surface area and volume data of the cell was assumed to be normal distribution and values of mean and standard deviation was estimated. The paired Student's t-test was used to determine the significant difference before and after aspiration and unpaired Student's t-test was used to determine the significant difference between the pressure rates.

The cell diameter, aspiration length of cell and mechanical property data of the cell was assumed to be non-normal distribution and was presented in terms of the median and interquartile range. Accordingly Mann-Whitney U tests (2-tailed) were used to determine the statistical significance of the differences in each of the three viscoelastic mechanical parameters. The level of statistical significance both the parametric and non-parametric analysis of the data was set at $p < 0.05$, unless otherwise mentioned

4.3 RESULTS

The effects of the loading rate on the mechanics of the chondrocytes were examined using the micropipette aspiration technique with different pressure rates. Cells were rejected from analysis depending on the three conditional phases:

- the cells did not aspirate
- the analytical model did not converge or produce an accurate fit ($R < 0.95$)
- the estimated constants reached the preset limit ($k_2 > 100$)

Table 4.1 shows the number of cells rejected under each of these conditions and the total number of successfully analysed cells using both the SLS and BSLS models. It can be seen that between 62% and 88% of the cells progress to analysis, with higher percentages generally associated with the BSLS model. Furthermore it can be noted that at slower pressure rate 0.35 cmH$_2$O/s, the higher percentage of the cells analysed using BSLS model reached the preset limit compared to the SLS model.

Table 4.1. *The number of cells accepted for each experimental conditions. Percentage values represent those cells of the total which were successively analysed using SLS and BSLS models.*

Pressure Rate (cmH$_2$O/s)	Total No. of Cells Tested	Cell Aspiration	Convergence		R ≥ 0.95		k$_2$ < 100	
			SLS	BSLS	SLS	BSLS	SLS	BSLS
5.48	26	23	23	23	22	23	21 (80%)	20 (77%)
0.70	16	16	16	16	14	15	12 (75%)	13 (82%)
0.35	16	16	16	16	15	16	10 (62%)	14 (88%)

4.3.1 EFFECTS OF APPLIED PRESSURE CHANGE RATE

At each pressure rate, chondrocytes initially aspirated rapidly into the micropipette. Subsequently, the rate of deformation into the micropipette decreased until an equilibrium aspiration length was reached. Figure 4.3 shows the brightfield images of individual representative cells aspirated at pressure rate of 0.35, 0.70 and 5.48 cmH$_2$O/s upto 7 cmH$_2$O for 180 s. The corresponding images during the recovery phase following aspiration are also indicated in Figure 4.3. The resulting temporal changes in the aspiration length of the chondrocytes are shown in Figure 4.4.
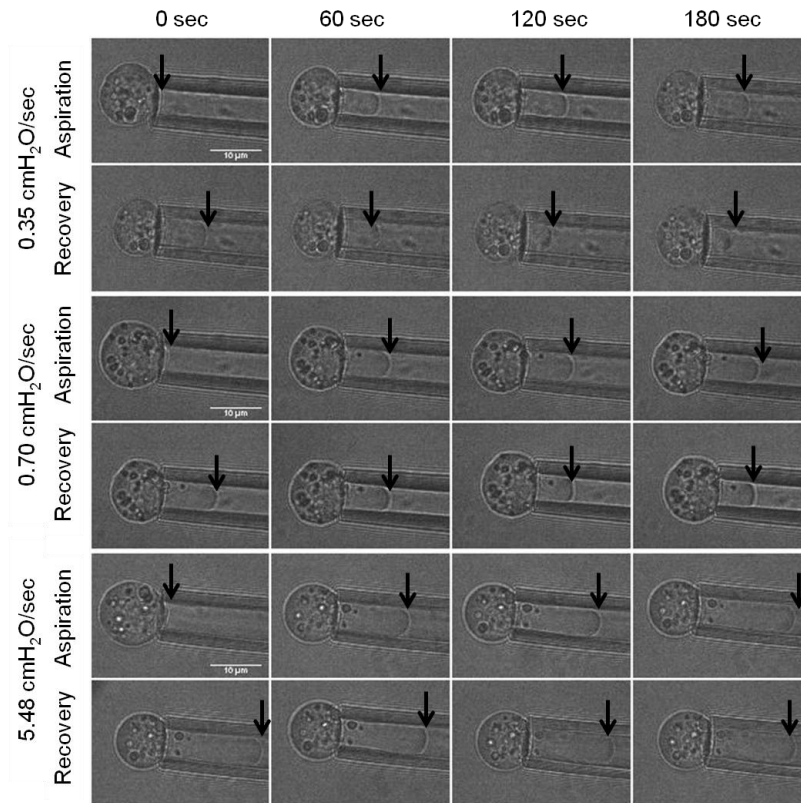
Figure 4.3. *Micropipette aspiration of the chondrocytes at pressure rates of 0.35, 0.70 and 5.48 cmH₂O/s, respectively, and their post-aspiration recovery phase. The arrows indicate the extent of the aspiration length into the micropipette. Scale bar 10 μm.*
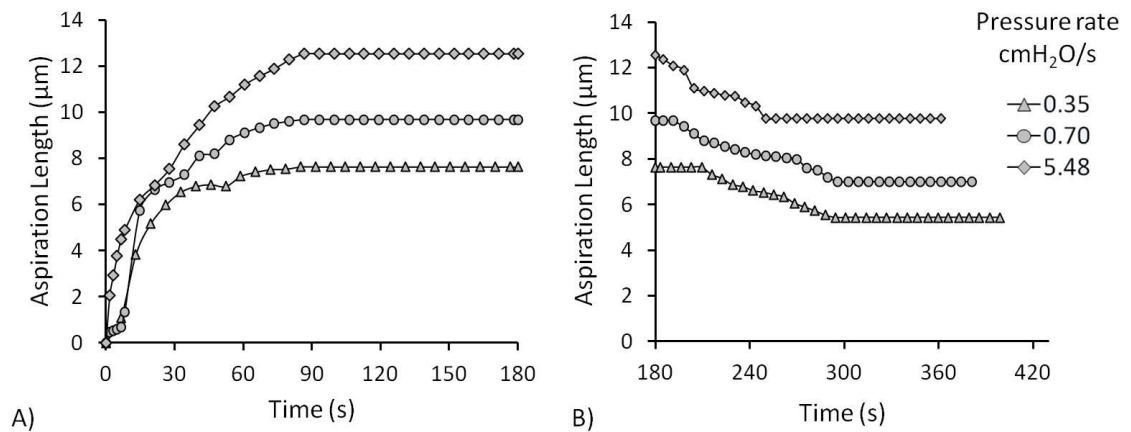
Figure 4.4. *A) Viscoelastic creep behaviour and B) post-aspiration recovery of the chondrocytes at three different pressure rates.*

After the aspiration pressure was removed, cells exhibited partial recovery, reaching equilibrium state with a recovery length of approximately 30% of the peak aspiration length (Figure 4.5). It is evident that the higher pressure rate was associated with an increase in maximum aspiration length and an increase in equilibrium recovery length measured 180 seconds after the onset and removal of pressure, respectively. The differences for the aspiration lengths between the three pressure rates were statistically significant (Figure 4.5). Further analysis of the data for individual cells revealed that the recovery length was proportional to the maximum aspiration length, as indicated in the linear model shown in Figure 4.6.
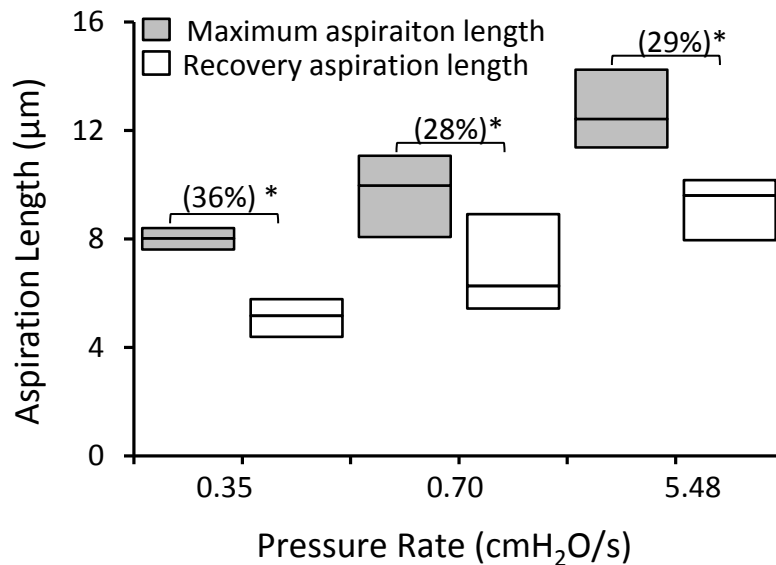
Figure 4.5. *Median and interquartile values for cells subjected to the aspiration pressure of 7 cmH₂O applied at 0.35, 0.70 and 5.48 cmH₂O/s. A statistically significant decrease in the aspiration length was observed for all the cells during the recovery period (*, p < 0.05). The median percentage recovery of the aspiration length is given in parentheses.*
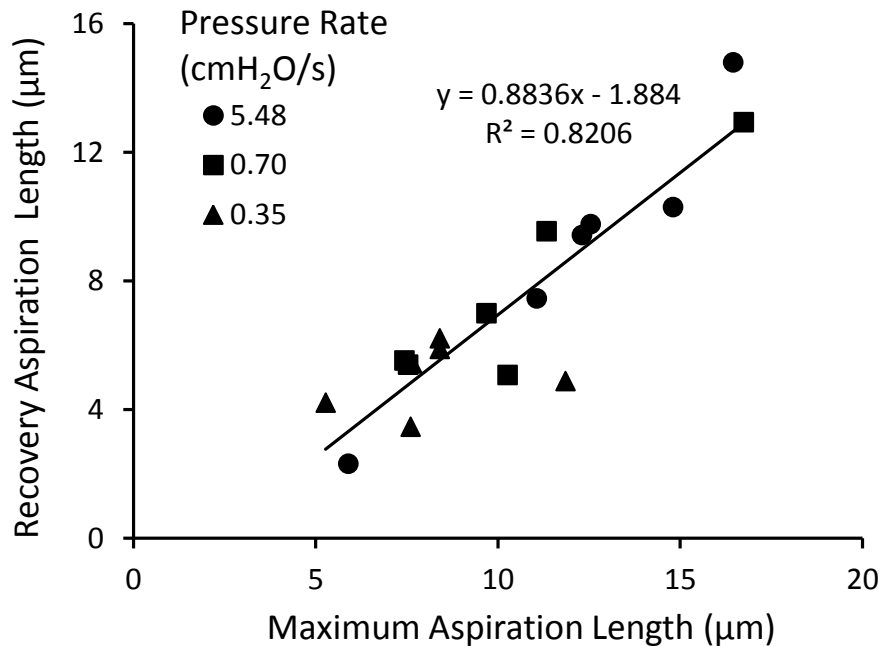
Figure 4.6. *A linear relationship existed between the maximum aspiration length at 7 cmH₂O and the recovery length at 0 cmH₂O.*

The surface area and volume of the chondrocytes were measured before and after aspiration at the three different pressure rates 0.35, 0.70 and 5.48 cmH$_2$O/s. This was further analysed to compute the percentage change in the surface area and volume of the chondrocytes. The process of aspiration was associated with a significant increase in the surface area of the chondrocytes after aspiration, at the three different pressure rates (Figure 4.7A). In absolute terms, the surface area of the chondrocytes increased by values of 16% and 20% at the slow and fast pressure rates, respectively. Furthermore, the cell deformation was also associated with significant changes in the volume of the chondrocyte at the pressure rate of 0.70 and 5.48 cmH$_2$O/s (Figure 4.7B). By contrast, at the slowest pressure rate the mean change in volume was approximately 2%, which was not statistically significant ($p > 0.05$). No significant changes in surface area and volume of the chondrocytes was observed between the three different pressure rates.
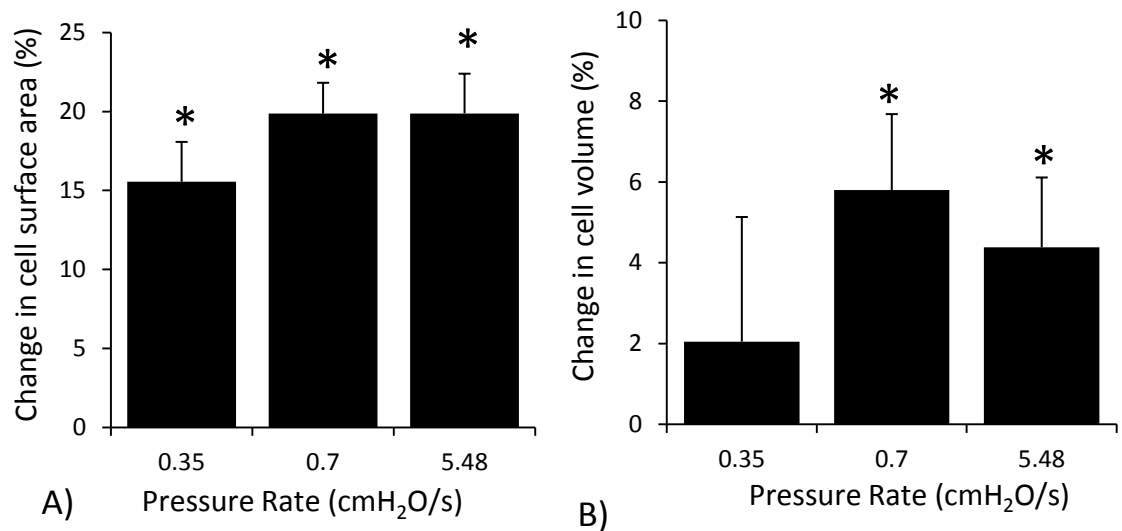
Figure 4.7. *The percentage changes in the A) surface area and B) volume of the chondrocytes after aspiration. Significant differences in surface area and volume of chondrocytes before and after aspiration is indicated by * (p < 0.05).*

The temporal changes in the aspiration length of the chondrocytes in the initial 180 s period were mathematically fitted using both the SLS and BSLS models. These models yielded the three viscoelastic parameters, namely, instantaneous modulus, equilibrium modulus and viscosity (Figure 4.8). The viscoelastic parameters generated using both SLS and BSLS model are approximately similar at pressure rate 5.48 cmH$_2$O/s. However discrepancy is introduced in the viscoelastic parameters between the SLS and BSLS model at pressure rates of 0.35 and 0.70 cmH$_2$O/s. The SLS model tended to over-estimate the instantaneous modulus as compared to that estimated using the BSLS model (Figure 4.8). As the pressure rate increased, the moduli and viscosity decreased correspondingly with differences being statistically significant (Figure 4.8). For example, the BSLS model analysis revealed that for the pressure rate of 5.48 cmH$_2$O/s, a 3.6 fold increase was observed in the instantaneous modulus along with a 4.1 and 3.8 fold increase in the equilibrium modulus and apparent viscosity respectively, as compared to the corresponding values at the slower pressure rate of 0.35 cmH$_2$O/s.
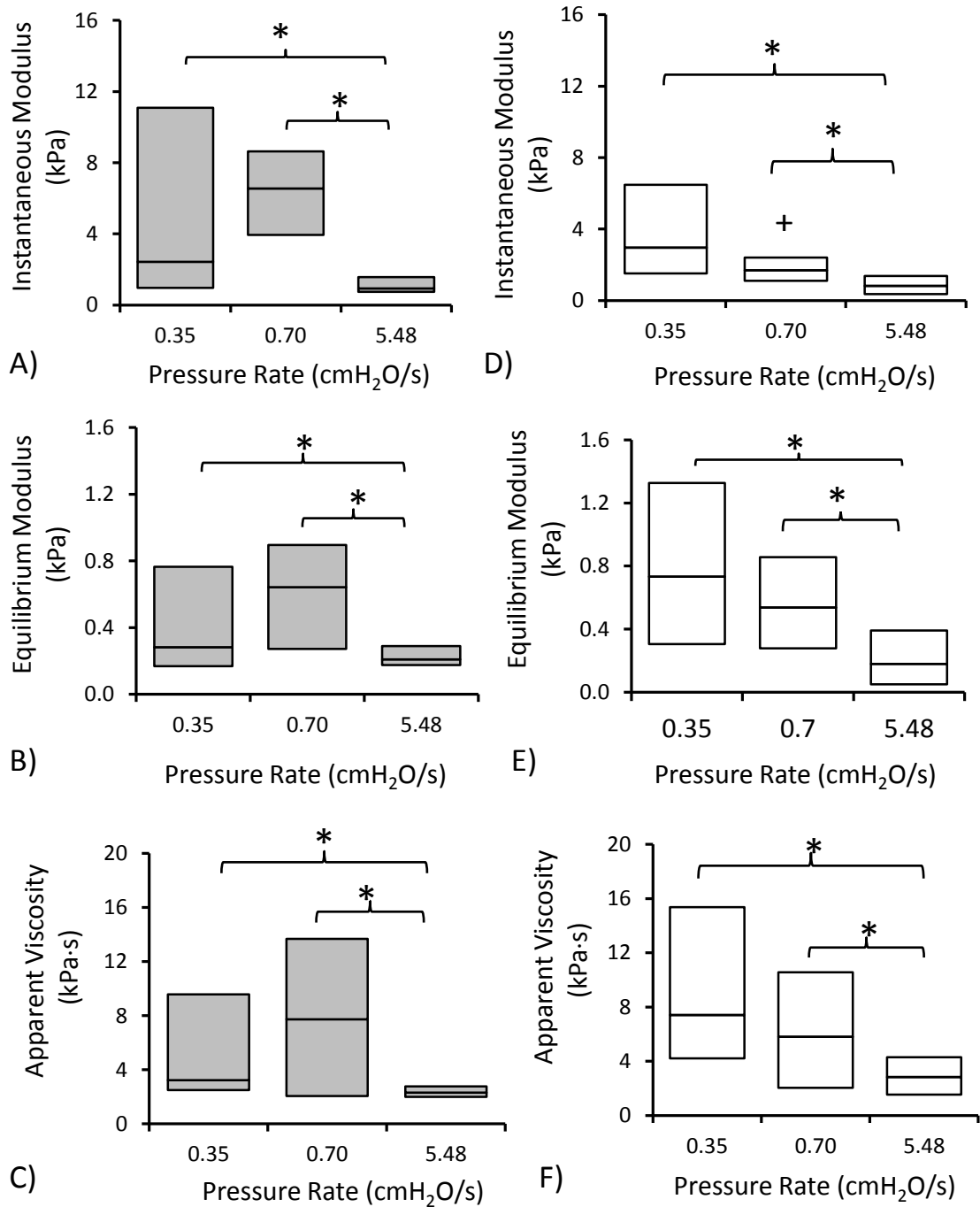
Figure 4.8. *The viscoelastic parameters for the primary chondrocytes obtained by applying the SLS model (A-C) and BSLS model (D-F) to the experimental data for micropipette aspiration at three different pressure rates 0.35, 070 and 5.48 cmH₂O/s. Significant differences are indicated by * (p < 0.05). Bar represents median and interquartile range.*

4.3.2 EFFECTS OF REPEAT ASPIRATION

Representative images of chondrocytes aspirated with the pre-conditioning pressure rate of 0.35 cmH$_2$O/s followed by either 0.35 cmH$_2$O/s or 5.48 cmH$_2$O/s are presented in Figures 4.9 and 4.10, respectively. The temporal changes in the aspiration length of the chondrocytes for the two rates are shown in Figure 4.11.
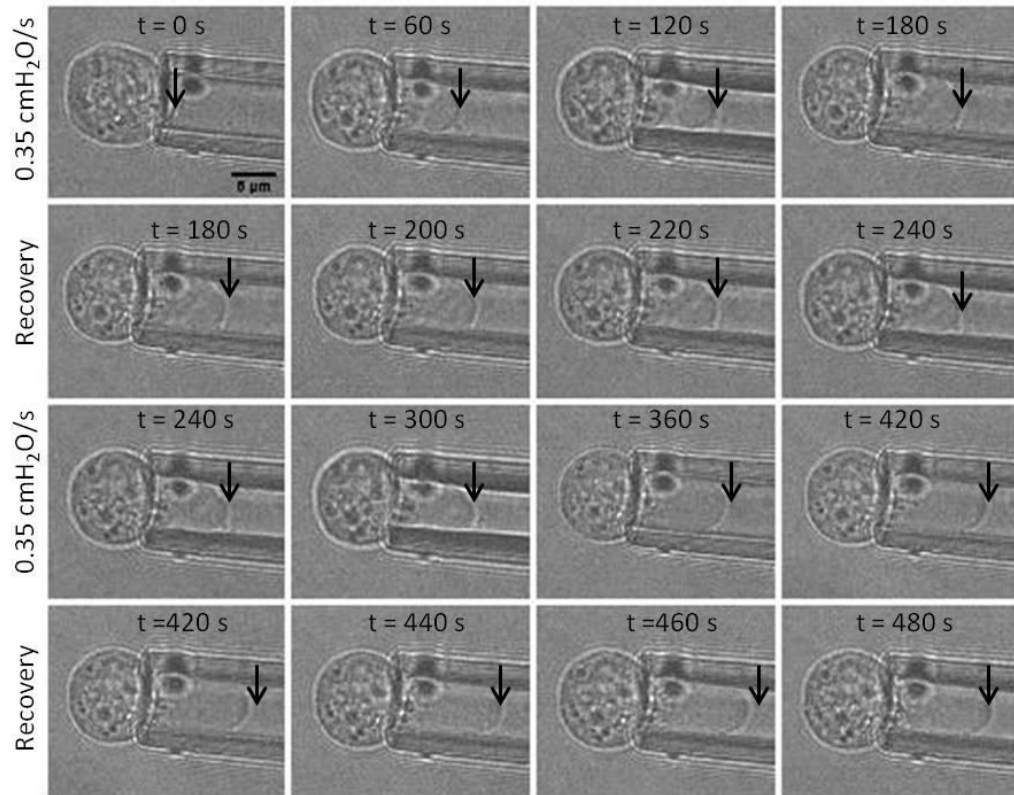
Figure 4.9. Sequential images of micropipette aspiration of chondrocytes (1st panel: first aspiration at 0.35 cmH$_2$O/s; 2nd panel: recovery for first aspiration; 3rd panel: second aspiration at 0.35 cmH$_2$O/s; 4th panel: recovery for second aspiration). The arrows indicate the extent of the aspiration length within the micropipette. Scale bar 5 µm.
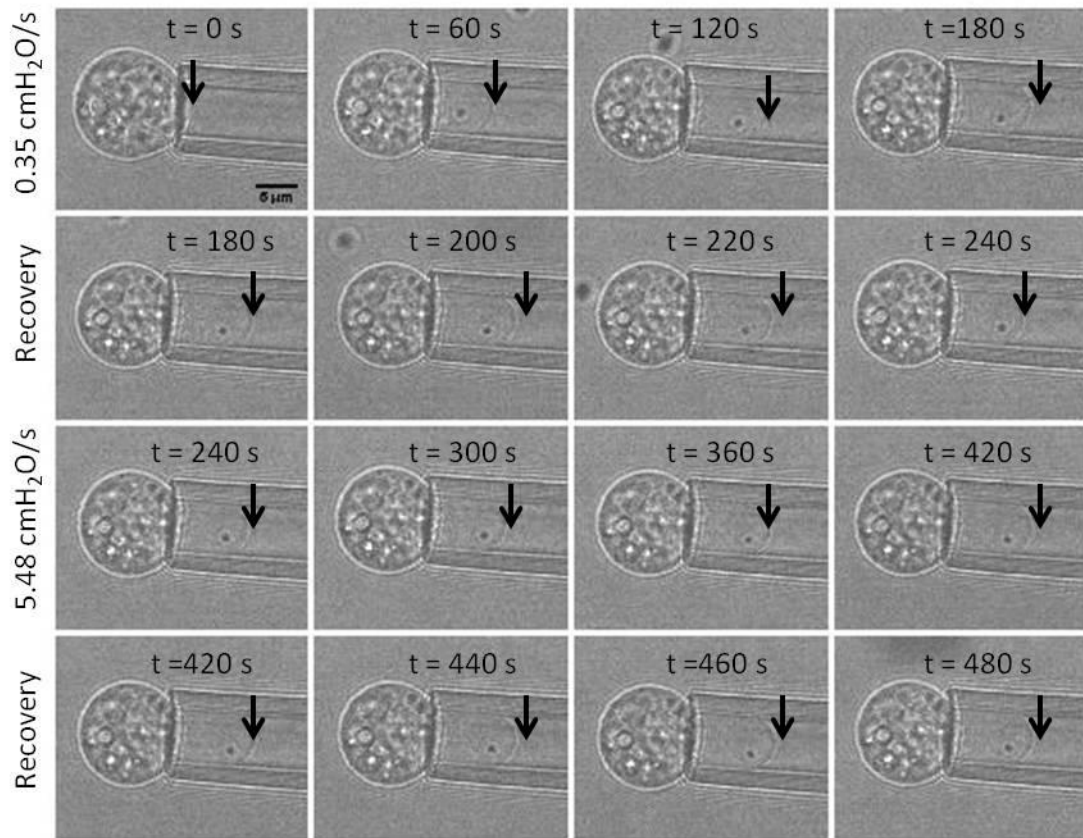
Figure 4.10. *Sequential images of micropipette aspiration of chondrocytes (1ˢᵗ panel: first aspiration at 0.35 cmH₂O/s; 2ⁿᵈ panel: recovery for first aspiration; 3ʳᵈ panel: second aspiration at 5.48 cmH₂O/s; 4ᵗʰ panel: recovery for second aspiration). The arrows indicate the extent of the aspiration length within the micropipette. Scale bar 5 μm.*

From the Figure 4.11 it can be noted that the response of the chondrocytes aspirated at two different pressure rates is different after the pre-conditioning. When the second aspiration was performed on the chondrocytes at pressure rate 0.35 cmH$_2$O/s, the aspiration length was reduced compare to the aspiration length of the chondrocytes aspirated at pressure rate of 5.48 cmH$_2$O/s. It is remarkable to note that the cells does not recover after removal of the pressure in the case of second aspiration performed using 0.35 cmH$_2$O/s. The preconditioning does have effect on the cellular behaviour of the chondrocytes that needs further investigation
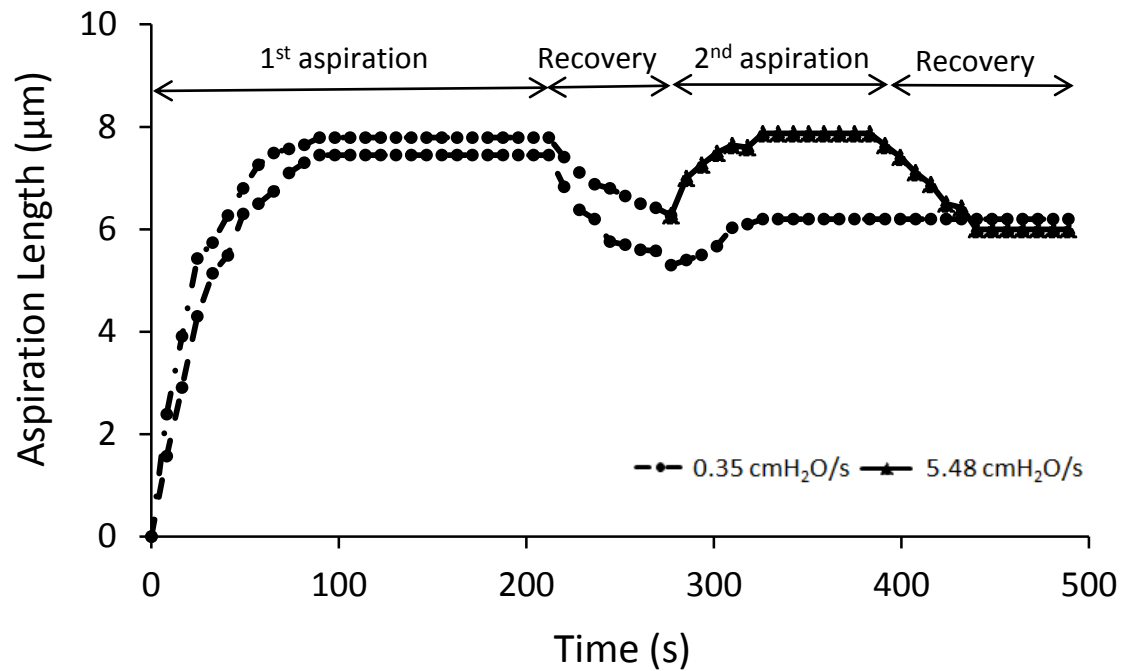
Figure 4.11. *Data from two representative cells in Figure 4.9 and Figure 4.10 showing the temporal changes in the aspiration length during the repeat aspiration protocol. For the initial aspiration, 7 cmH₂O/s was applied at a rate of 0.35cmH₂O/s. For the second aspiration pressures was applied at 0.35 or 5.48 cmH₂O/s.*

The surface area of the chondrocytes were measured before aspiration and after the second aspiration at the pressure rates of 0.35 cmH$_2$O/s and 5.48 cmH$_2$O/s. Figure 4.12A shows the significant changes in the surface areas of the chondrocytes after second aspiration. Similarly chondrocyte volumes were measured before aspiration and after second aspiration at pressure rates of 0.35 cmH$_2$O/s and 5.48 cmH$_2$O/s. Figure 4.12B shows the significant changes in the cell volume after the second aspiration at pressure rate 5.48 cmH$_2$O/s. A huge variability in changes in the surface area of the chondrocytes was observed in the case of the 0.35 - 0.35 cmH$_2$O/s pressure rate. This might be due to the differences in the response of the cell during the second aspiration at pressure rate 0.35 cmH$_2$O/s.
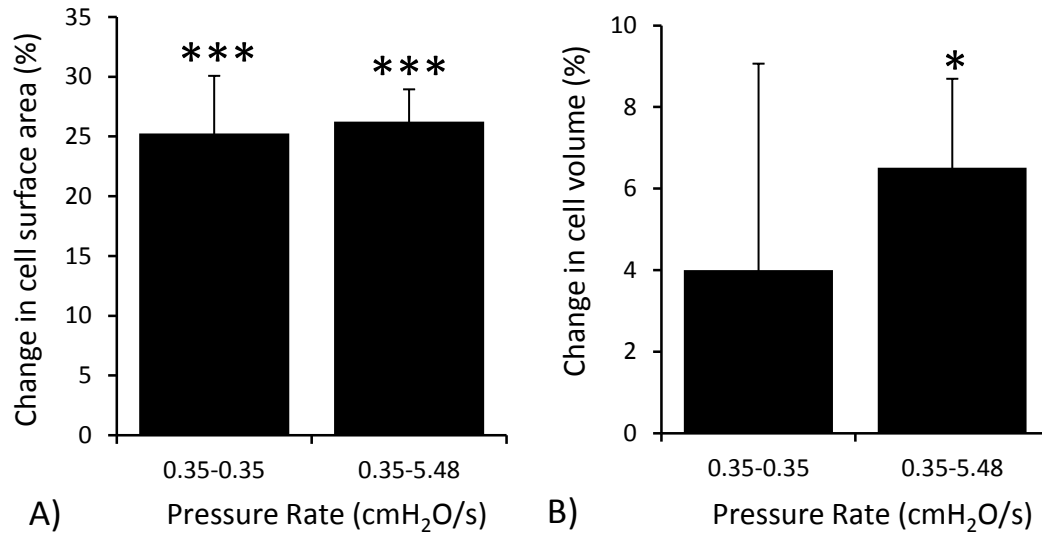
Figure 4.12. *The percentage changes in the A) surface area and B) volume of the chondrocytes after second aspiration. Significant differences in surface area and volume, before and after second aspiration is indicated by * (p < 0.05) and *** (p < 0.001).*

4.4 DISCUSSION

The present series of experiments demonstrated that a controlled micropipette aspiration system provided an accurate and efficient method for applying controlled pressure to single chondrocytes at three different pressure rates. The effects of varying aspiration pressure rates on the mechanics of chondrocytes were examined by using a micropipette aspiration system at pressure rates of 0.35, 0.70 and 5.48 cmH$_2$O/s. In response, the chondrocytes showed characteristic viscoelastic behaviour, with the application of step increase in pressure inducing a gradual increase in the aspiration length within the micropipette, reaching an equilibrium after approximately 90 s, as shown in Figure 4.4. The subsequent viscoelastic creep behaviour of the chondrocytes was consistent with the results of previous studies involving chondrocytes as well as other cell types (Hochmuth, 2000; Jones et al., 1999; Sato et al., 1990; Theret et al., 1988; Trickey et al., 2000).

141

4.4.1 EFFECTS OF APPLIED PRESSURE CHANGE RATE

Interestingly, a significant difference ($p < 0.05$) was observed in the aspiration lengths of the chondrocytes during the equilibrium and recovery phases (Figure 4.5). Approximately 30% of the aspiration length was recovered at all the three different pressure rates. Further, the permanent deformation level was proportional to the equilibrium aspiration length at 7 cmH_2O (Figure 4.5). Based on the linear model fitted to these data, permanent deformation was considered to occur when the aspirated length was approximately 2 µm or greater (Figure 4.6).

The cell surface area and volume were computed for the chondrocytes aspirated at three different pressure rates and subjected to repeat aspiration. Interestingly, the post-aspiration surface area of the chondrocytes was significantly different from the pre-aspiration at any of the three pressure rates (Figure 4.7A). Additionally the surface area was significantly increased after the second aspiration irrespective of the applied pressure rate possibly due to changes in the intracellular contents (Figure 4.12).

Additionally, the post-aspiration volume of the chondrocytes was significantly higher than the pre-aspiration volume (Figure 4.7B). These findings are consistent with those of previous studies reporting the changes in the cell volume using the technique of micropipette aspiration (Jones et al., 1999; Trickey et al., 2006). However it has been previously demonstrated that chondrocytes volume decreases in vivo joint loading in rabbits (Abusara et al., 2011). This is due to the compressive loading of the articular cartilage that led to reduction in the osmotic pressure within the tissue.

Moreover in case of the repeat aspiration, no significant changes were observed when cells were aspirated again with 0.35 cmH_2O/s (Figure 4.12B). Therefore the pre-conditioning at a lower pressure rate followed by repeat aspiration may have lead to lesser deformation. The results of the present study also indicated that the chondrocytes are not completely incompressible. It has been reported using micropipette aspiration technique that the chondrocytes are compressible with Possion's ratio found to be 0.38

(Trickey et al., 2006). During micropipette aspiration, the cell either undergoes deformation over time or due to mechanical stretching, wherein extracellular fluid flows into the portion of the cell within the micropipette (Bidhendi and Korhonen, 2012b). The hydrostatic pressure applied to the cell due to the aspiration pressure is then balanced by the inward flow of the fluid resulting from the osmotic swelling, leading to an equilibrium state. Therefore, in the equilibrium state, the hydrostatic pressure in the micropipette can be considered to be equal to the osmotic pressure of the cell; this phenomenon is also observed at the tissue level. For example, the osmotic pressure of the proteoglycans is balanced by the pressure resulting from the tensile stesses exerted in the collagen fibre network in the articular cartilage, as reviewed in section 1.3.1. The findings of the present study indicate that the osmotic gradient across the cell has a significant influence on the mechanical properties of the cells (Guilak et al., 2002). Although the solid viscoelasticity of a cell and its time-dependent deformation is attributed to the fluid flow, known to play a crucial role in cell deformation (Bidhendi and Korhonen, 2012b).

In the present study, the viscoelastic creep behaviour of chondrocytes was successfully determined by the SLS model, with the results being in agreement with those of previous studies (Trickey et al., 2000). Furthermore, the data was also modelled using the BSLS model, which is essentially a modification of the SLS model with the Boltzmann superposition incorporated to account for a finite pressure rate (Merryman et al., 2009) (see section 3.5). 88% of the cells successfully passed the analysis criteria using BSLS model compare to 62% of SLS model (see Table 4.1). The BSLS model thus improves the estimation of the cellular mechanical properties, particularly at slower aspiration pressure rates where in the time over which the pressure is applied is greater than 2 s (Zhao et al., 2009). Therefore only BSLS model was used to analyse the cell aspiration data in the subsequent chapters.

The SLS and BSLS model analyses both indicated that the rate at which pressure was applied influenced the cellular viscoelastic behaviour. In the case of the fastest aspiration

rate used in this experiment, i.e. 5.48 cmH$_2$O/s, the instantaneous and equilibrium moduli and viscosity were in agreement with previous estimates reported under similar conditions with an equilibrium modulus of 0.22 kPa (Bader et al., 2002; Zhao et al., 2009) However, at the slower aspiration rates, the extent of cell deformation within the micropipette decreased as the modulus and viscosity increased (Figure 4.8), which means at lower pressure rate cellular deformation decreases. This behaviour was in contrast to that expected from a viscoelastic material and so dynamic nature of the intracellular content, such as actin filaments plays a crucial role in the cellular response to the loading.

A relative high variability was observed in the viscoelastic parameters of the cells indicated by the interquartile ranges (Figure 4.8). This may be due to inhomogeneities in the structure and composition of the cell. The SLS and BSLS model used to compute these viscoelastic parameters assumes the cell behaviour to be homogenous half-space. The results of the present study demonstrated the effects of different loading (pressure) rates on the viscoelastic mechanical properties of chondrocytes. The cells became stiffer and deformed to a lesser extent when aspirated at lower pressure rates compared to the higher pressure rate. The mechanisms governing the behaviour of chondrocytes in response to varying pressure rates and the resultant permanent cell deformation remain unexplained. It has been reported that microfilaments and possibly intermediate filaments contribute to the mechanical properties of chondrocytes (Trickey et al., 2004). Actin and its structural remodelling have therefore been considered to be involved in these alterations in the mechanics of the chondrocytes. It is possible that when cells were aspirated at a low pressure rate, the actin filaments have sufficient time to undergo remodelling, which was not available at the higher pressure rate. To examine this hypothesis the following chapter analyses the role of actin filaments in the mechanisms governing the behaviour of chondrocytes aspirated at varying pressure rates.

Chapter 5

EFFECTS OF GFP-ACTIN AND EGTA ON THE MORPHOLOGY AND VISCOELASTIC PROPERTIES OF ISOLATED CHONDROCYTES

5.1 INTRODUCTION

5.2 METHODOLOGY

    5.2.1 GFP-Actin Transfection

    5.2.2 EGTA Treatment

    5.2.3 Chondrocyte Micropipette Aspiration

    5.2.4 Statistical Analysis

5.3 RESULTS

    5.3.1 Effects of GFP-actin Transfection on the Cell Aspiration

    5.3.2 Effects of EGTA on the Morphology on the Cell Aspiration

    5.3.3 Actin Breakdown and Remodelling

5.4 DISCUSSION

    5.4.1 Unstrained Cell Morphology

    5.4.2 Actin Breakdown and Remodelling During Micropipette Aspiration

    5.4.3 The Influence of Actin Dynamics on the Mechanical Properties of Cells

5. EFFECTS OF GFP-ACTIN AND EGTA ON THE MORPHOLOGY AND VISCOELASTIC PROPERTIES OF ISOLATED CHONDROCYTES

5.1 INTRODUCTION

Isolated chondrocytes were transfected with GFP-actin to investigate the distortion and remodelling of actin during micropipette aspiration. The cells were aspirated at two different pressure rates, 0.35 cmH$_2$O/s and 5.48 cmH$_2$O/s, and visualised using bright-field and confocal fluorescence microscopy. Temporal and spatial variation in actin organisation was quantified in terms of the fluorescence intensity of the GFP.

In addition, further studies were conducted to examine the mechanism leading to changes in actin organisation and the in particular the role of calcium signalling which is activated by cell deformation (Ohashi et al., 2006; Pingguan-Murphy et al., 2005; Roberts et al., 2001) and is known to regulate actin organisation (Lange and Gartzke, 2006). In deed, previous studies have described calcium mediated actin remodelling in chondrocytes subjected to hyperosmotic challenges (Erickson et al., 2003) and compression in 3D agarose (Campbell and Knight, 2007b) In order to investigate the dependence of the actin deformation during micropipette aspiration on the calcium signalling, chondrocytes were treated with ethylene glycol tetraacetic acid (EGTA) and subjected to the micropipette aspiration. EGTA is known to chelate the extracellular Ca^{2+} ions, blocking the Ca^{2+} pathways and is previously used in various studies (Erickson et al., 2003; Pritchard and Guilak, 2006; Roberts et al., 2001). The BSLS model was used to examine the effects of GFP-actin transfection and EGTA treatment on the mechanical properties of the chondrocytes.

5.2 Methodology

Bovine articular chondrocytes were isolated from adult bovine full-depth cartilage from the metacarpo-phalangeal joints, as described in section 3.6.2.

5.2.1 GFP-Actin Transfection

Primary chondrocytes were transfected with GFP-actin using BacMam reagent (CellLight® Reagent BacMam 2.0, Invitrogen). The reagent was directly added to a cell suspension at a cell density of 1×10^6 cells/mL at 1–10% vol/vol. 4 µl of GFP-actin reagent was used to transfect cell suspension of 100 µl. The cells were incubated for 2 h at room temperature on a rocker. Subsequently, the cells were plated at 0.5×10^6 cells/cm^2 in a 96-well plate and incubated at 37°C and 5% CO_2 for 16–19 h. The reagent was diluted by the addition of fresh DMEM + 10% FCS (100 µL/well) and incubated overnight at 37°C and 5% CO_2. Cells were trypsinised and used for the micropipette aspiration experiments. The GFP-actin structure was further examined using Alexa Phalloidin 555 staining. The monolayer cultures of the transfected cells were fixed with 0.4% formaldehyde for 10 min at room temperature. Then, they were washed 3 times with PBS and permeabilised with 0.5% Triton X-100 for 10 min at room temperature. For staining, 5 µL of Alexa Phalloidin with 200 µL of PBS was added to the transfected cell monolayer followed by a PBS wash 3 times. The GFP-actin intensity measurement on the single transfected chondrocytes were performed using confocal microscopy associated software named Leica LCS Lite.

5.2.2 EGTA Treatment

The GFP-actin transfected chondrocytes were treated with EGTA similar to the study conducted in the host laboratory (Roberts et al., 2001). Transfected chondrocytes (cell density 1×10^6/mL) were treated with 1 mL of 10 mM EGTA and incubated. The treated cells were aspirated after 1 h and were maintained in EGTA solution throughout the experiment.

5.2.3 CHONDROCYTE MICROPIPETTE ASPIRATION

GFP-actin transfected chondrocytes, either treated with EGTA or untreated, were aspirated at two pressure rates, i.e. 0.35 cmH_2O/s and 5.48 cmH_2O/s, as described in section 4.2.1. The cells were monitored and images were acquired over 180 s during aspiration and after the removal of the pressure for further 180 s. The aspiration length (L) of the cell within the micropipette was measured from the bright-field images for each pressure rate ($\Delta P/t$). Additionally the viscoelastic parameters were obtained by curve fitting the experimental data using the equation 3.4 for BSLS model (Merryman et al., 2009). The diameter of the cells was measured as shown in Figure 3.8. The cell morphological properties such as surface area and volume were computed using equations 3.10 and 3.11 respectively.

5.2.4 STATISTICAL ANALYSIS

The surface area and volume data of the chondrocytes were assumed to be normal distribution and values of mean and standard deviation was estimated. The paired Student's t-test was used to determine the significant difference in cell morphological properties before and after aspiration. The unpaired Student's t-test was used to determine the significant difference in the cell morphological properties between the two pressure rates.

Cell diameter, aspiration length of the chondrocytes and the mechanical property data of the cell were assumed to be non-normal distribution and was presented in terms of the median and interquartile range. Accordingly Mann-Whitney U tests (2-tailed) were used to determine the statistical significance of the differences in each of the three viscoelastic mechanical parameters. The level of statistical significance both the parametric and non-parametric analysis of the data was set at $p < 0.05$, unless otherwise mentioned.

5.3 Results

In order to clarify the role of actin in the changes observed in the mechanics of the chondrocytes, micropipette aspiration was performed on the GFP-actin transfected chondrocytes, either untreated or treated with EGTA. The number of chondrocytes tested for each experiment is presented in Table 5.1. The temporal changes in the aspiration length of chondrocytes in response to different pressure rates were modelled using the Boltzmann solid linear standard (BSLS) model, which yielded the three viscoelastic parameters, namely, instantaneous modulus, equilibrium modulus and apparent viscosity. Cells that were successfully aspirated were included in the analyses of cell morphology. However, cells were rejected from the cell mechanics analyses depending on the given conditions:

- the cells did not aspirate

- the analytical model did not converge or produce an accurate fit (R < 0.95)

- the estimated constants reached the pre-set limit $k_2 > 100$

It can be seen from the Table 5.1 that in case of the chondrocytes treated with EGTA and aspirated at pressure rate 0.35 cmH_2O/s, only a single cell successfully passed criteria for the analysis. Primary chondrocytes were successfully transfected with GFP-actin. The actin network observed was similar to that seen in the non-transfected cells stained with Alexa-Phalloidin 555 (Figure 5.1). In both cases, multiple thin stress fibres were observed in the chondrocytes in the monolayer culture. Representative images of GFP-actin transfected chondrocytes subjected to pressure rates of 0.35 cmH_2O/s and 5.48 cmH_2O/s are shown in Figures 5.2.

Table 5.1. *The number of cells accepted for each experimental conditions. Percentage values represent those cells of the total which were successively analysed using BSLS models.*

Pressure Rate (cmH$_2$O/s)	Total No. of Cells Tested	Cell Aspiration	Convergence	R $\geq$ 0.95	k$_2$ < 100
Transfected Chondrocytes					
5.48	12	11	11	11	10 (83%)
0.35	19	16	16	15	13 (68%)
Transfected Chondrocytes Treated With EGTA					
5.48	19	15	15	15	12 (64%)
0.35	10	8	6	6	1 (10%)
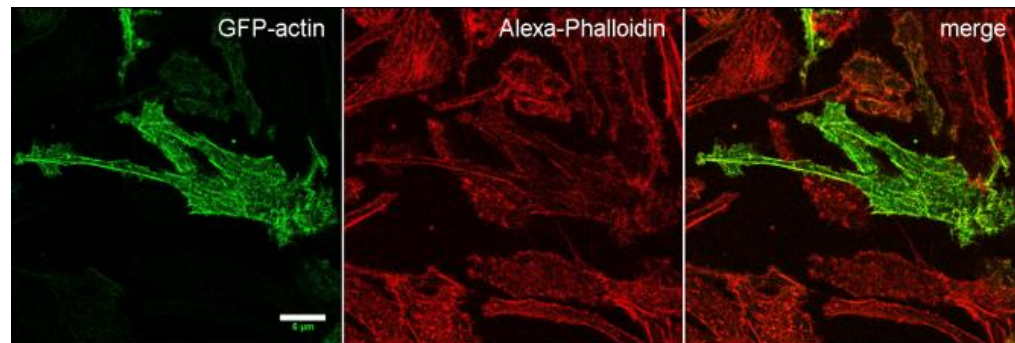
Figure 5.1.*Representative confocal images showing characteristic actin organisation in a chondrocyte transfected with GFP-actin (green). F-actin has been co-labelled with Alexa-Phalloidin (red). Scale bar 5µm.*
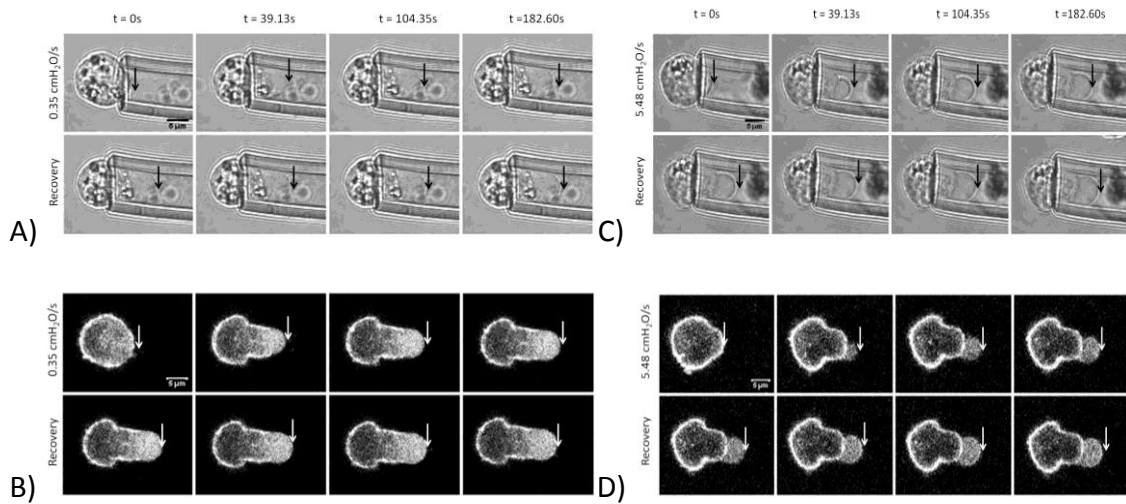
Figure 5.2. *Sequential images of micropipette aspiration of a transfected chondrocyte at 0.35 cmH$_2$O/s (A-B) and 5.48 cmH$_2$O/s (C-D). Bright field: upper panel and GFP-actin: lower panel. The arrows indicate the extent of the aspiration length into the micropipette. Scale bar is 5 μm.*

5.3.1 EFFECTS OF GFP-ACTIN TRANSFECTION ON CELL ASPIRATION

The diameter of the non-transfected and transfected chondrocytes were measured pre-aspiration. It is evident from the data in Figure 5.3 that no significant differences were found in the diameter between the non-transfected and transfected chondrocytes (p > 0.05). Interestingly, the aspiration length of the transfected chondrocytes aspirated at 0.35 cmH$_2$O/s significantly increased compare to the non-transfected chondrocytes (Figure 5.4). Although the median aspiration length of the transfected chondrocytes aspirated at 5.48 cmH$_2$O/s was lower compare to the non-transfected chondrocytes, no statistical significant difference was observed.
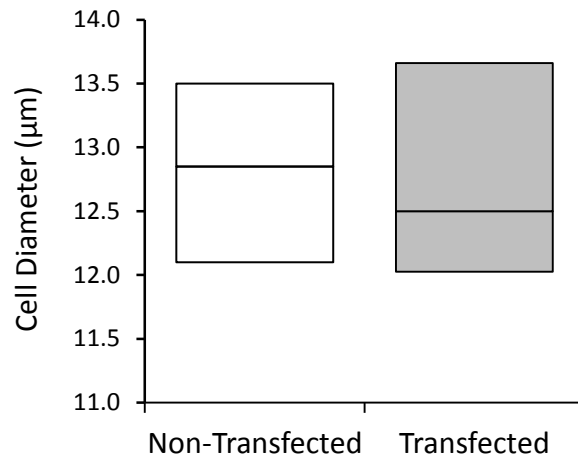
Figure 5.3. *Changes in the chondrocytes diameters with and without transfection.*
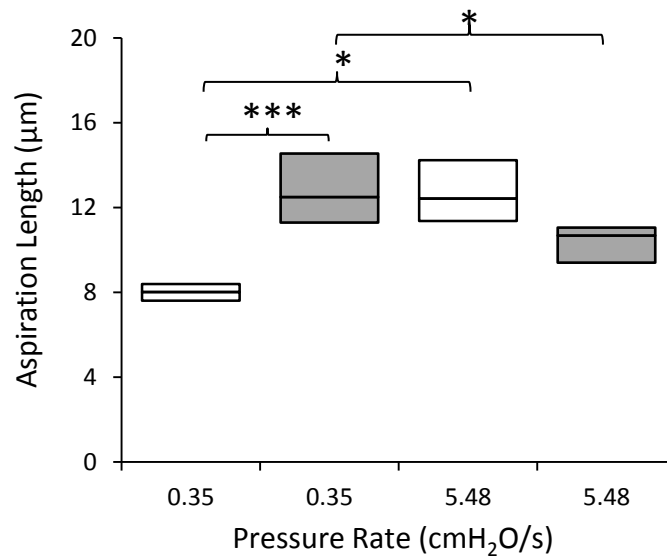
Figure 5.4. *The aspiration length of the GFP-actin non- transfected (☐) and transfected (▨) chondrocytes aspirated at two different pressure rate. Significant differences indicated by *(p < 0.05) and *** (p < 0.001).*

The surface area of the non-transfected and transfected chondrocytes were measured before and after aspiration at the two different pressure rates, i.e. 0.35 cmH_2O/s and 5.48 cmH_2O/s. These were further used to compute the percentage change in the surface

area of the cells after aspiration. The surface area of non-transfected and transfected chondrocytes significantly changed after aspiration for each pressure rate as shown in Figure 5.5A. The percentage change in the surface area of the transfected chondrocytes was higher compared to the non-transfected chondrocytes, with a significant difference noted at the pressure rate 0.35 cmH_2O/s. In a similar manner, the cell volume of the non-transfected and transfected chondrocytes was measured pre-aspiration and post-aspiration. When cells were aspirated at pressure rate 0.35 cmH_2O/s and 5.48 cmH_2O/s, the volume of the non-transfected and transfected chondrocytes increased by mean values of 2%, 5%, 6% and 9%, respectively (Figure 5.5B) differences being statistically significant for the non-transfected chondrocytes aspirated at 5.48 cmH_2O/s. A high variability was observed in the percentage change in the volume data of the transfected chondrocytes.
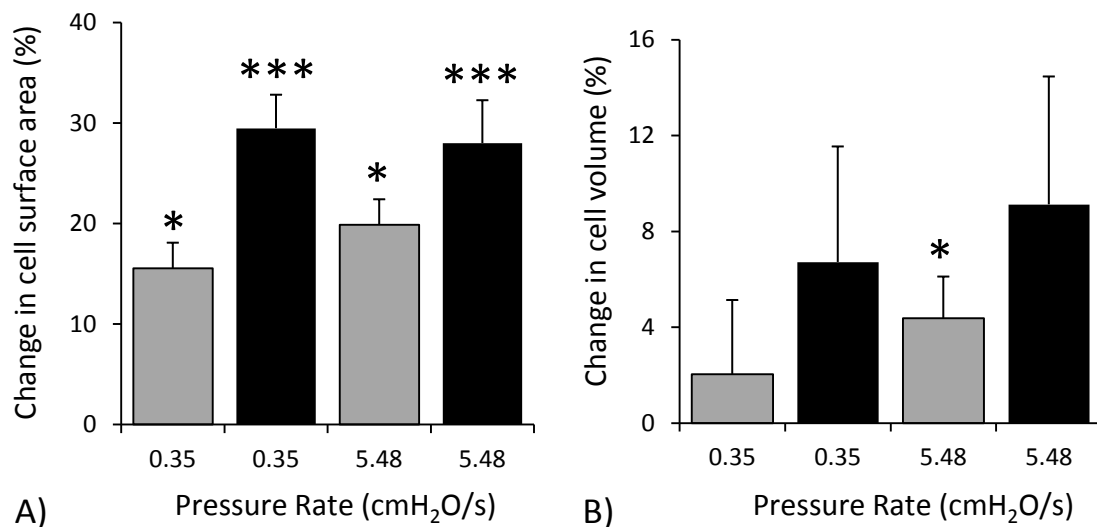
***Figure 5.5**. Changes in the A) surface area and B) volume of the GFP-actin non-transfected (▫) and transfected (■) chondrocytes aspirated at two different pressure rate. Significant differences indicated by * (p < 0.05) and *** (p < 0.001).*

The temporal changes in the aspiration lengths of the non-transfected and transfected chondrocytes aspirated at pressure rate 0.35 cmH$_2$O/s and 5.48 cmH$_2$O/s were analysed using the BSLS model generated three viscoelastic parameters, the results of which are presented in Figures 5.6. The chondrocytes expressing GFP-actin exhibited similar mechanical properties to the non-transfected cells at the pressure rate of 5.48 cmH$_2$O/s, by indicating no significant differences between the two groups for the three viscoelastic parameters (Figures 5.6). By contrast data at the lower pressure rate of 0.35 cmH$_2$O/s revealed higher values for all three parameters associated with the non-transfected cells (Figures 5.6). The differences were statistical significant between the two groups ($p < 0.05$ for each parameter).
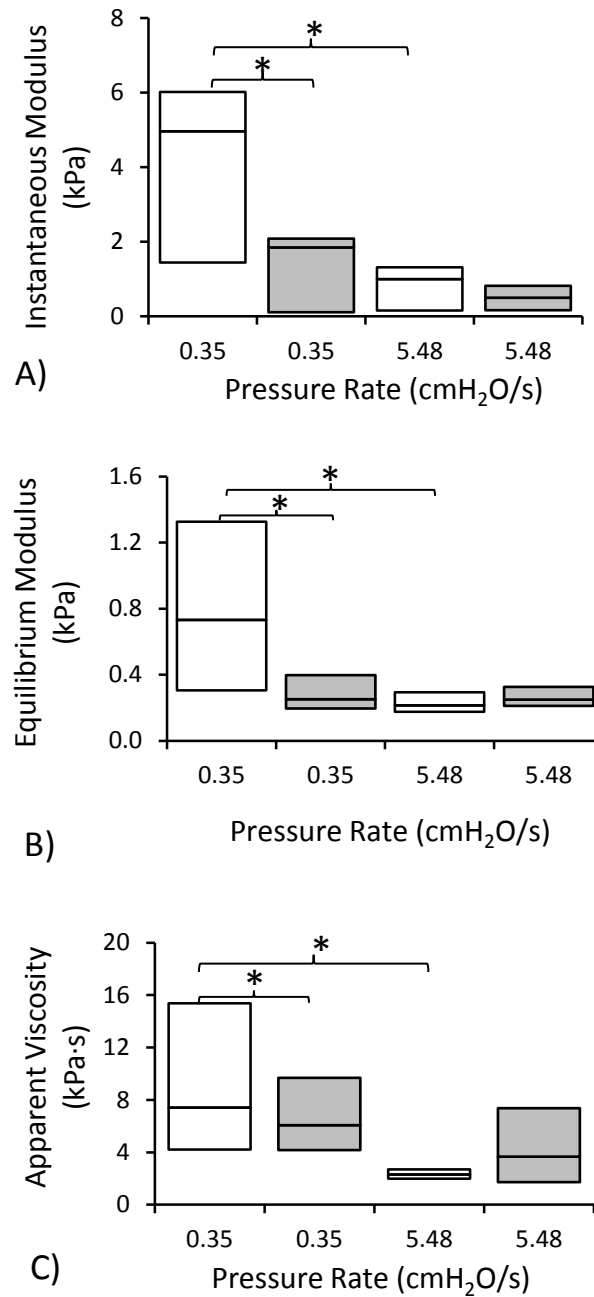
Figure 5.6. *The viscoelastic parameters namely A) instantaneous modulus, B) equilibrium modulus and C) apparent viscosity for non-transfected (▢) and transfected (▨) chondrocytes aspirated at two pressure rates 0.35 and 5.48 cmH_2O/s obtained by applying the experimental data for micropipette aspiration into the BSLS model. Significant differences between transfected and non-transfected cells are indicated by * (p < 0.05).*

5.3.2 Effects of EGTA on the Cell Aspiration

Representative images of untreated and treated chondrocytes subjected to pressure rates of 0.35 cmH$_2$O/s and 5.48 cmH$_2$O/s are shown in Figures 5.7.
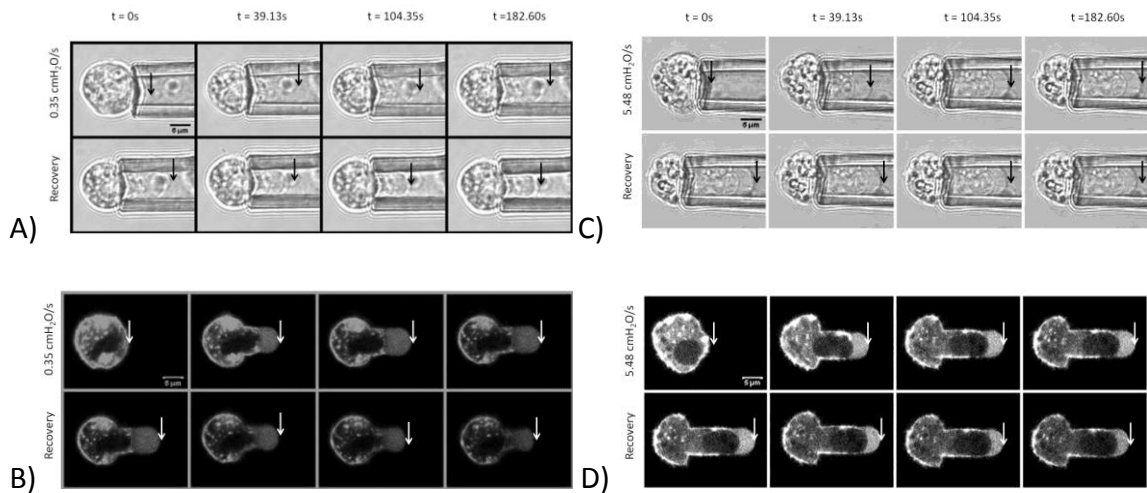
Figure 5.7. *Sequential images of micropipette aspiration of GFP-actin transfected chondrocytes treated with EGTA at 0.35 cmH$_2$O/s (A-B) and 5.48 cmH$_2$O/s (C-D). Bright field: upper panel and GFP-actin: lower panel. The arrows indicate the extent of the aspiration length into the micropipette. Scale bar is 5 µm.*

EGTA treatment of the chondrocytes did not alter the cell diameter (Figure 5.8). It can be noted from the Figure 5.9 that median aspiration length of the transfected chondrocytes treated with EGTA is smaller compare to the untreated cells. However no statistical significant difference exists in aspiration length of the untreated and treated cells. Significant differences (p < 0.001) were observed between the cell surface areas before and after aspiration for the EGTA-treated chondrocytes aspirated at both pressure rates, as illustrated in Figure 5.10A. The high variability is observed in the aspiration length of the EGTA-treated chondrocytes aspirated at both pressure rates indicated by higher values of the interquartile range.
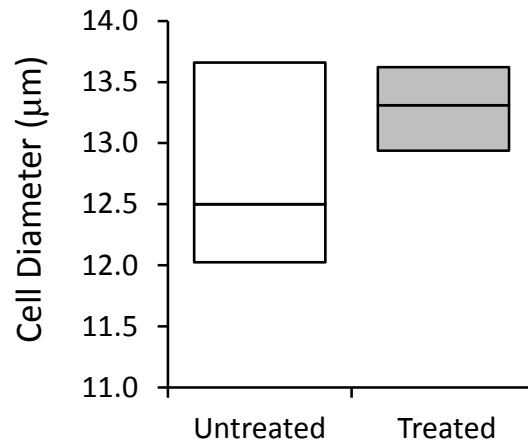
Figure 5.8. *Changes in the chondrocytes' diameters with and without treatment with EGTA.*
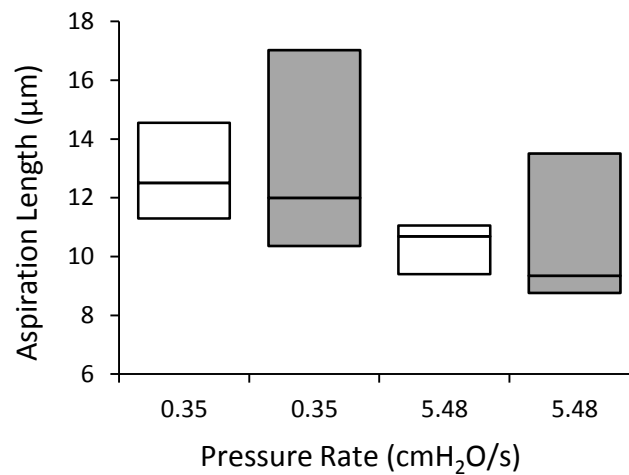
Figure 5.9. *The aspiration length of the GFP-actin transfected chondrocytes untreated (☐) and treated (▨) with EGTA and aspirated at two different pressure rate.*

A statistically significant difference ($p < 0.001$) was observed in the cell volumes before and after aspiration in the EGTA treated chondrocytes aspirated at the higher pressure rate (Figure 5.10B). By contrast when chondrocytes were aspirated at pressure rate 0.35 cmH_2O/s, the volume of cell was variable with a mean values of less than 2%. However no significant different was found in the percentage change in the volume of

the chondrocytes aspirated at 0.35 and 5.48 cmH$_2$O/s (p > 0.06). Relative high variability was observed in the percentage change in volume for cells.
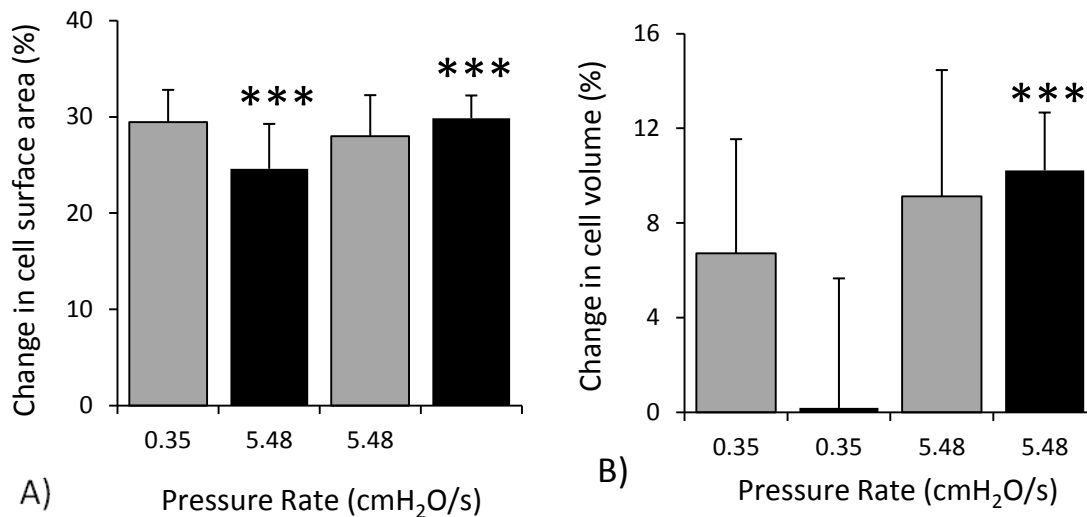
Figure 5.10. *Changes in the A) surface area and B) volume of the GFP-actin transfected (■) and transfected (■) chondrocytes treated with EGTA and where aspirated at two different pressure rate. Significant differences indicated by * (p < 0.05) and *** (p < 0.001).*

The aspirated chondrocytes demonstrated viscoelastic creep behaviour, as described in section 4.3.1, irrespective of transfection or EGTA treatment. The numbers of treated chondrocytes aspirated at different pressure rates are summarized in Table 5.1. However, the majority of the cells reached the pre-set limit (k$_2$ > 100) at the aspiration pressure rate of 0.35 cmH$_2$O/s. Therefore the viscoelastic parameters of cells aspirated at 5.48 cmH$_2$O/s were only computed. The median values of the moduli and apparent viscosity of the EGTA treated chondrocytes are higher compared to the untreated chondrocytes, although the difference is not statistically significant Figures 5.11.
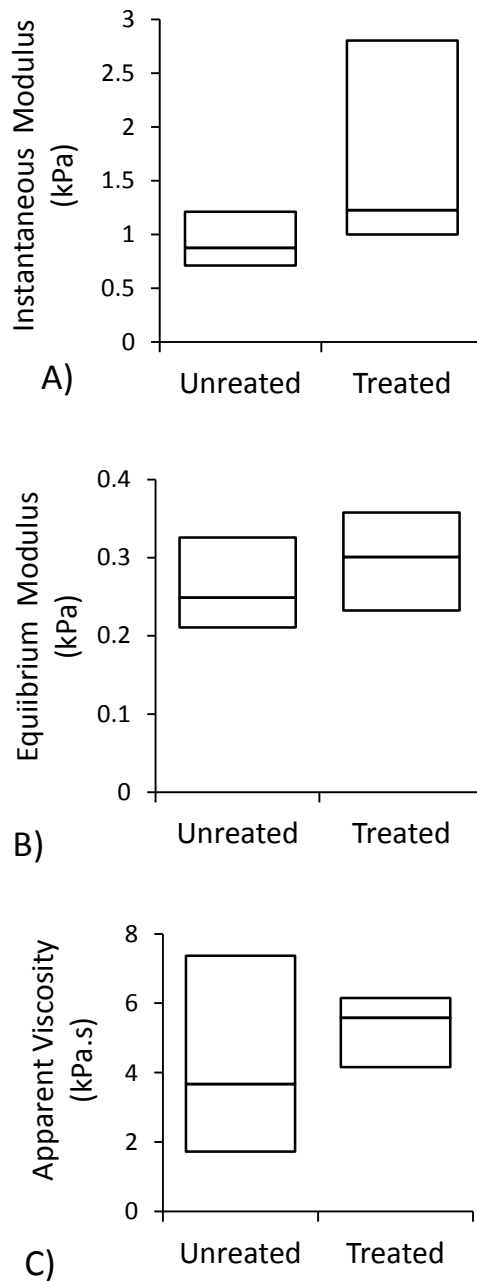
Figure 5.11. *The viscoelastic parameters namely A) instantaneous modulus, B) equilibrium modulus and C) apparent viscosity for untreated and EGTA-treated chondrocytes obtained by applying the experimental data for micropipette aspiration at pressure rate 5.48 cmH$_2$O/s into the BSLS model.*

5.3.3 ACTIN BREAKDOWN AND REMODELLING

Representative images of GFP-actin transfected chondrocytes subjected to the aspiration pressure rate of 0.35 and 5.48 cmH$_2$O/s are shown in Figure 5.12A and 5.13A, respectively. Similar to the non-transfected chondrocytes, the GFP-actin-transfected cells exhibited a viscoelastic response during micropipette aspiration. The temporal changes in the aspiration lengths measured from the GFP-actin images for both pressure rates matched those measured from the bright-field images obtained from the same cell.

A close examination of the GFP-actin images revealed that chondrocyte deformation during aspiration with pressure rate 0.35 cmH$_2$O/s and 5.48 cmH$_2$O/s, was associated with distortion and remodelling of the cortical actin into the micropipette, leading to a rapid breakdown of this cortex (Figure 5.12A-5.13A). This behaviour was quantified by measuring the changes in the GFP-actin intensity at the regions of interest, (ROI) positioned over the GFP-actin cortex of the aspirated cell in the micropipette (ROI 1 and ROI 2) and outside the micropipette (ROI 3) as indicated in the Figure 5.12B and Figure 5.13B. The majority of the cell aspirated at both pressure rates showed the breakdown of the actin cortex in the leading edge of the cell (ROI 1s) as the cell deform during the micropipette (Figure 5.12B and 5.13B). This was followed by the subsequent remodelling and reformation of the actin cortex over time into the micropipette. This behaviour for the representative cell aspirated at 0.35cmH$_2$O/s and 5.48cmH$_2$O/s is shown in the Figure 5.12C and Figure 5.13C respectively. However a membrane bleb is appeared when the cells were aspirated at 5.48cmH$_2$O/s, which is further aspirated into the micropipette (Figure 5.13C). In this case localised actin breakdown may have occurred during the formation of the membrane bleb. However, the GFP-actin intensity in those parts of the cell in contact with the walls of the micropipette did not exhibit any subsequent recovery (ROI 2, Figure 5.12C). On the other hand the GFP-actin intensity of the chondrocytes aspirated at 5.48cmH$_2$O/s slightly drop and did not

recover as seen from Figure 5.13C. The GFP-actin intensity in ROI 3, which represented the non-aspirated region of the cell outside of the micropipette, remained stable throughout the experiment for both pressure rates (Figure 5.12C and 5.13c). This indicates that the actin dynamics is spatially localised inside the cells.

(A)

(B)

(C)
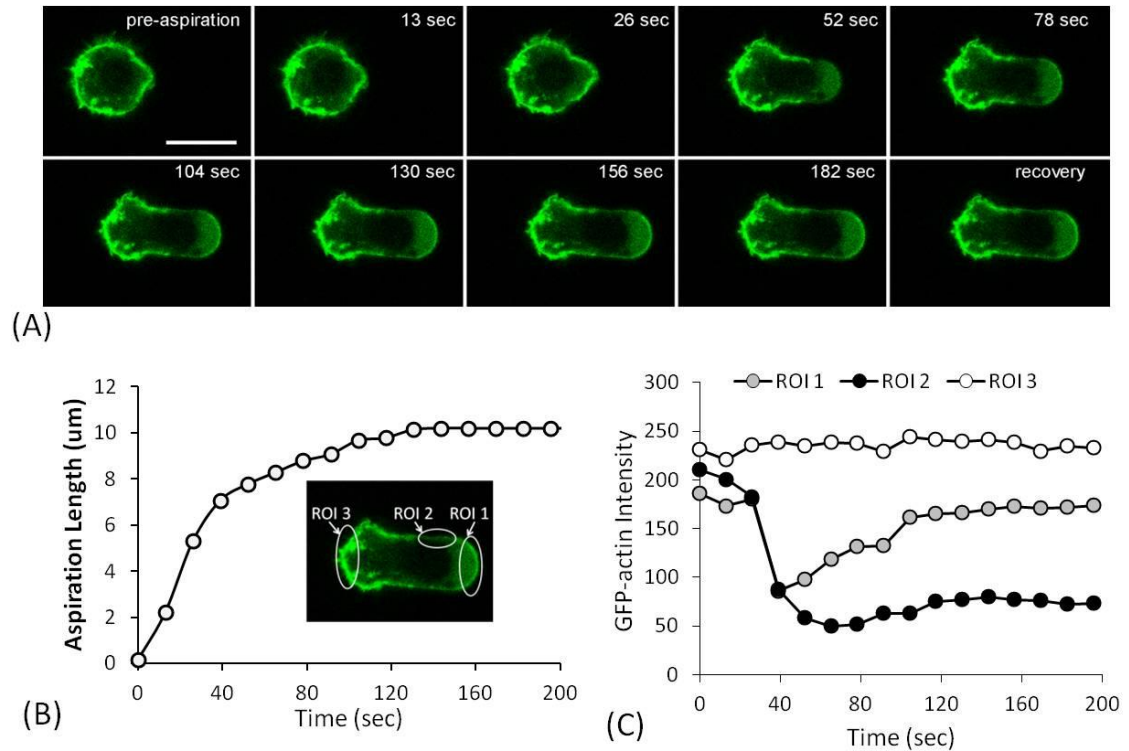
Figure 5.12. Confocal images of GFP-actin during aspiration where in the cell was aspirated at 0.35 cmH₂O/s (A). Corresponding temporal changes in the aspiration length (B) and cortical GFP-actin intensity (C). The GFP-actin intensity were measured at the regions of interest, (ROI) positioned over the GFP-actin cortex of the aspirated cell in the micropipette (ROI 1 and ROI 2) and outside the micropipette (ROI 3). Arrow indicates cortical actin breakdown during micropipette aspiration of the chondrocytes. Scale bar 10µm.

The analysis of the corresponding actin showed breakdown and/or bleb formation occurred between 25 and 50 s after the application of pressure and at a approximate aspiration length of 5 µm into the micropipette. The cortical actin rapidly disappeared

during the deformation in the micropipette and therefore no abrupt change in the aspiration length was observed in the case of the both pressure rates (Figure 5.12B and 5.13B).
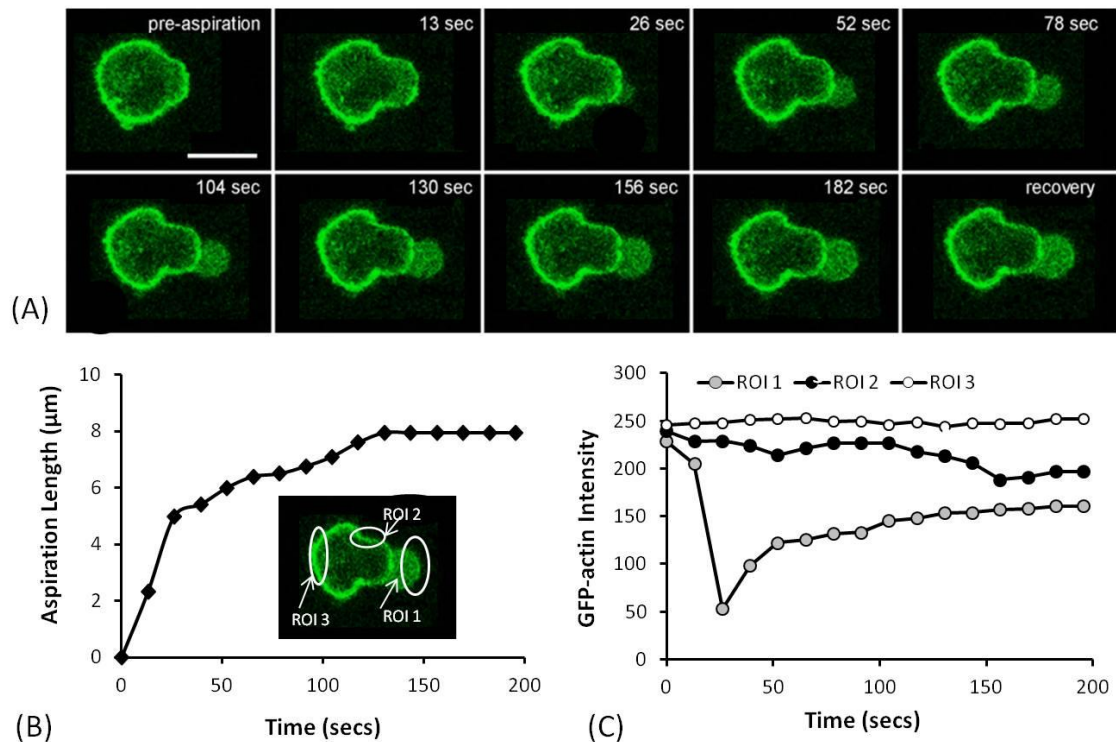
Figure 5.13. *Confocal images of GFP-actin during aspiration where in the cell was aspirated at 5.48 cmH$_2$O/s (A). Corresponding temporal changes in the aspiration length (B) and cortical GFP-actin intensity (C).Arrow indicates cortical actin breakdown during micropipette aspiration of the chondrocytes. Scale bar 10µm.*

The actin breakdown of the cells was quantified by the sudden drop in the GFP-actin intensity at the leading edge (ROI 1) (Figure 5.12B and Figure 5.13B). The aspiration lengths were measured at the time point where there was sudden drop in the corresponding GFP-actin intensity. No significant changes were observed in the actin breakdown lengths with different pressure rates or EGTA treatment (Figure 5.14).
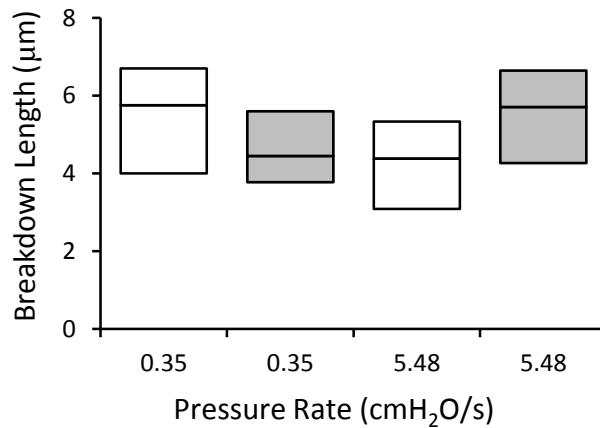
Figure 5.14. *Changes in the aspiration lengths at which actin breakdown in the untreated (▢) and EGTA-treated (▨) chondrocytes for two pressure rates 0.35 and 5.48 cmH₂O/s.*

The sudden drop and recovery in the GFP-actin intensity was quantified as the breakdown and recovery intensity respectively. There was a significant difference in the actin breakdown intensity between untreated and EGTA-treated chondrocytes aspirated at a pressure rate 5.48 cmH$_2$O/s (Figure 5.15A). Furthermore, the GFP-actin intensity in the recovery phase (Figure 5.15B) of the chondrocytes aspirated at the two pressure rates showed a significant difference between the untreated and EGTA-treated chondrocytes.
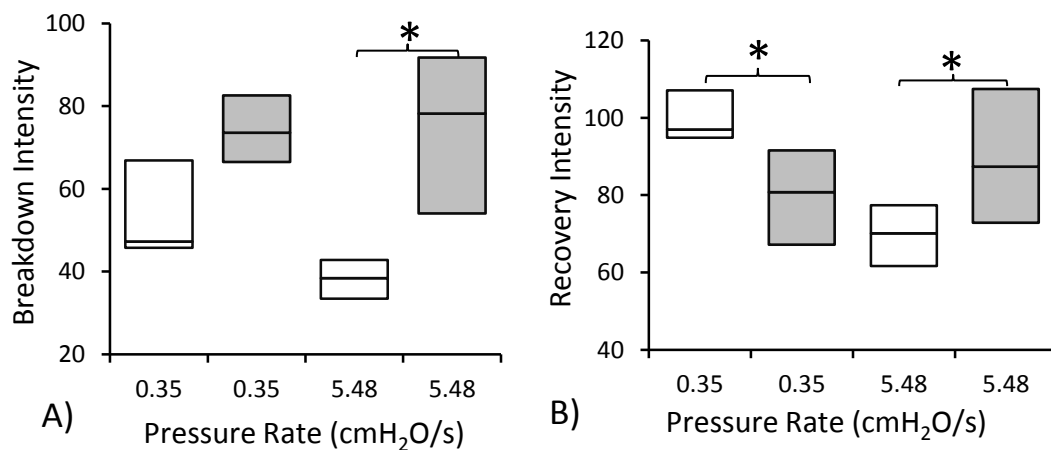
Figure 5.15. *Changes in the A) breakdown intensity and B) during recovery intensity of GFP-actin in the untreated (▢) and EGTA-treated (▨) chondrocytes at two pressure rates 0.35 and 5.48 cmH$_2$O/s. Significant differences are indicated by * (p < 0.05).*

At the slower aspiration rate of 0.35 cmH$_2$O/s, untreated cells showed greater levels of recovery. By contrast at 5.48 cmH$_2$O/s, cells treated with EGTA exhibited a higher recovery intensity.

5.4 DISCUSSION

5.4.1 UNSTRAINED CELL MORPHOLOGY

It is interesting to note that the GFP-transfection of chondrocytes did not have any influence on the cell diameter (Figure 5.3). This could be due the GFP-actin transfection having no effect on the actin organisation of the chondrocytes (Deibler et al., 2011). This is supported by no difference observed in the actin organisation of the chondrocytes co-labelled with GFP-actin and Alexa Phalloidin in monolayer (Figure 5.1). Furthermore the EGTA treatment also did not induce any changes in the cell diameter of the chondrocytes (Figures 5.8).

5.4.2 ACTIN BREAKDOWN AND REMODELLING DURING MICROPIPETTE ASPIRATION

It is well known that the actin cytoskeleton contributes significantly to the mechanical properties of living cells (Ingber et al., 1994; Ohashi et al., 2006; Trickey et al., 2004). In the GFP-actin transfected chondrocytes, cell deformation during micropipette aspiration was observed to be associated with distortion of cortical actin, leading to rapid breakdown of the actin cortex in the portion of the cell within the pipette. This was followed by the formation of a membrane bleb and a gradual remodelling of the cortical actin within the bleb (Figure 5.12-5.13). It can be suggested that loss of cortical tension attributed to the actin breakdown and bleb formation enables cellular osmotic swelling pressure to drive extracellular fluid into the cell. This results in the small increase in cell volume after aspiration as the cell membrane expands into the micropipette (Figure 5.5B and Figure 5.10B). The rapid disappearance of the cortical actin and/or formation of the

bleb into the micropipette was not associated with any step change in the aspiration length of the chondrocytes (Figure 5.12-5.13). This suggests that actin breakdown is not a determining factor in facilitating the aspiration of the cell into the pipette, but instead may be the result of detachment of the membrane from the actin cortex and loss of tensile forces as previously reported (Chen et al., 2010).

Distinct spatial variation in actin breakdown and remodelling was observed at both the pressure rate (Figure 5.12-5.13). This is consistent with the topological reorganisation of polymerised actin as reported previously (Horoyan et al., 1990). Over a period of 3 mins, the aspirated portion of the cell showed rapid actin fluidisation followed by slower reassembly. This timeline was in agreement with the findings of previous studies involving chondrocytes actin dynamics and response to compression in agarose (Campbell and Knight, 2007a; Chen et al., 2010). The results also agree with previous studies of the smooth muscle cells cultured on elastic substrates where rapid actin fluidisation was observed in response to substrate stretch (Chen et al., 2010). In the present study, actin fluidisation is believed to occur via the release of tensile forces associated with tethering to the cell membrane. This led to actin disassociation, rather than the activation of cellular signalling pathways (Chen et al., 2010). This may also explain why the breakdown of cortical actin observed in the present micropipette aspiration study was more pronounced than that previously reported in mechanical compression of the chondrocytes in agarose constructs (Campbell and Knight, 2007b) where the tensile forces on the cell membrane are likely to be significantly less, however, compression of chondrocytes in agarose does result in small bleb formation around the equator of the oblate ellipsoid morphology where any tensile forces would be greatest (Knight, 1997). This hypothesis is to some extent supported by the lack of changes in the mechanical parameters of EGTA-treated chondrocytes. However, the extent of actin breakdown and remodelling did appear to be influenced by treatment with EGTA and hence the presence of calcium.

The levels of actin remodelling represented by the GFP-actin intensity following the recovery phase, were significantly different at the two aspiration pressure rates (Figure 5.15B). This supports the hypothesis that the pressure rate influences the actin breakdown and remodelling however, there is relatively high variability in the GFP-actin intensity measurements possibly due to the cell to cell variation in the structure of GFP-actin. Additionally the aspirated chondrocytes represents the population of the cells obtained from the different zones of the cartilage. Distinct variation is seen in cytoskeletal structure of the chondrocytes obtained from different zones of the articular cartilage (Durrant et al., 1999) (Figure 1.12).

Actin remodelling behaviour has also been reported in a carcinoma cell line, wherein micropipette aspiration induced cortical actin breakdown followed by bleb formation and subsequent actin remodelling (Charras et al., 2005; Keller et al., 2002; Tinevez et al., 2009). While bleb formation is known to be physiologically important in cell locomotion (Keller, 2000), mitosis (Laster and Mackenzie, 1996; Schroeder, 1978) and apoptosis (Laster and Mackenzie, 1996), the present study associates this behaviour of actin with the viscoelastic parameters of chondrocytes and their biomechanics and the effects of varying pressure rates.

The data presented here indicate that cell deformation during micropipette aspiration results in the disassembly and subsequent reassembly of specific portions of cortical actin. Thus, the aspiration pressure rate appears to regulate the viscoelastic mechanical properties of living cells by altering the dynamics and remodelling of the actin cytoskeleton. These findings are expected to further clarify the regulation of cellular biomechanics and changes in the actin cytoskeleton in response to external and internal mechanical forces.

As seen in the previous chapter, the cell undergoes permanent deformation irrespective of the aspiration pressure rate. This permanent deformation appears to be linked to the reassembly of the cortical actin cytoskeleton. The reassembly of the cortical actin follows

the actin cortex fluidisation (Chen et al., 2010) and bleb formation, which is enhanced at faster aspiration rates.

5.4.3 The Influence of Actin Dynamics on the Mechanical Properties of Cells

The present investigation has revealed that the GFP-actin transfected chondrocytes did not exhibit the same pressure rate-sensitive behaviour as demonstrated by the non-transfected cells (Figure 5.6). Instead, the presence of GFP-actin prevented the increase in cell moduli values and viscosity at the lower aspiration rate of 0.35 cmH_2O/s, and when compared to the values at 5.48 cmH_2O/s, the difference was statistically significant. The aspiration of the transfected cells at 0.35 cmH_2O/s results in more deformation than that associated with non-transfected chondrocytes as seen from increase in the aspiration length of the chondrocytes (Figures 5.4). The finding of the present study suggests that the GFP-actin interferes with the viscoelastic response of the chondrocytes when aspirated at 0.35 cmH_2O/s. It has been reported previously that although GFP does not alter the actin organisation as shown in Figure 5.1, it can influence the actin dynamics (Deibler et al., 2011; Ketelaar et al., 2004). This could explain why GFP-actin transfected chondrocytes did not show the increase moduli and viscosity at slower aspiration pressure rate as observed in the non-transfected cells. This supports the hypothesis that this behaviour is regulated by actin dynamics although the precise mechanism remains unclear.

Furthermore the majority of the EGTA-treated chondrocytes aspirated at 0.35 cmH_2O/s, were rejected from analysis of the cell mechanics as they reach the pre-set limit of the k_2. This could be due to the inhomogeneities in the GFP-actin structure and its deformation during the micropipette aspiration. The relative high variability was observed in volume (Figure 5.5A and 5.10A) of the chondrocytes aspirated at 0.35 cmH_2O/s. This may be due to assumption made for the computation of these morphological properties (discussed in section 8.2.3).

The results presented here suggest that at the slower aspiration rate, sufficient time is available for mechanically-induced actin remodelling facilitating viscoelastic deformation in to the pipette, thereby preventing membrane detachment from the cortical actin, subsequent actin fluidisation and bleb formation. Thus the rate at which pressure is applied influences degree of deformation into the pipette and hence the mechanical properties of the cells. In the succeeding chapters the importance of these mechanical properties of the cells are further investigated in the context of the disease and passage.

Chapter 6

EFFECT OF CYTOKINE-INDUCED AND MECHANICALLY-INDUCED INJURY ON THE MORPHOLOGY AND VISCOELASTIC PROPERTIES OF ISOLATED CHONDROCYTES

6.1   INTRODUCTION

6.2   METHODOLOGY

6.2.1   IL-1β Treatment of Chondrocytes in Monolayer

6.2.2   IL-1β Treatment of Cartilage Explants

6.2.3   In vitro Mechanical Injury Model

6.2.4   Cell Viability

6.2.5   Micropipette Aspiration

6.2.6   Statistical Analysis

6.3   RESULTS

6.3.1   Effects of IL-1β Treatment on Chondrocytes in Monolayer

6.3.2   Effects of IL-1β Treatment on the Cartilage Explants

6.3.3   Effects of in vitro Mechanical Injury on the Cartilage Explants

6.4   DISCUSSION

6.4.1   Unstrained Cell Morphology

6.4.2   Effects of Cell Aspiration

6. EFFECT OF CYTOKINE-INDUCED AND MECHANICALLY-INDUCED INJURY ON THE MORPHOLOGY AND VISCOELASTIC PROPERTIES OF ISOLATED CHONDROCYTES

6.1 INTRODUCTION

This chapter describes a series of experiments investigating the effects of both interleukin-1β (IL-1β) treatment and mechanical injury on the mechanics of chondrocytes using the micropipette aspiration technique. The biochemical treament using IL-1β on both cartilage explants and the monolayer culture was executed similar to that previously described (Pritchard and Guilak, 2006; Wann et al., 2010). In addition a separate cartilage explants mechanical injury model was adopted. This model has previously been reported to stimulate catabolic signalling in chondrocytes (DiMicco et al., 2004). The behaviour of the cell during aspiration was characterised using the Boltzmann standard linear solid (BSLS) model. As established in previous chapters, this model permits the estimation of three mechanical parameters namely, instantaneous modulus, equilibrium modulus and apparent viscosity.

6.2 METHODOLOGY

6.2.1 IL-1B TREATMENT OF CHONDROCYTES IN MONOLAYER

Full-depth cartilage was harvested from the proximal articular surfaces of 3 adult bovine metacarpo-phalangeal joints, which were obtained from a local abattoir. The cartilage explants were immersed in culture medium (DMEM + 10% FBS). The chondrocytes were isolated as described in section 3.6.2. The isolated chondrocytes were seeded at a density of 60 000 cells/cm^2 in T75 flasks and incubated at 37°C and 5% CO_2 for 24 h. The cells were washed with PBS. The experimental groups were treated with 10 ng/mL of IL-1β for 1 h. The control group remained in DMEM + 10% FCS without IL-1β. The treated

and untreated (control) chondrocyte monolayers were washed with PBS before trypsinisation. The chondrocytes were detached from the culturing flasks using 10 mL of 0.05% trypsin/EGTA (Sigma) followed by incubation for 3 min. An equal amount of the culture media was added to neutralise the trypsin. The cell suspension was transferred to the centrifuge tube and mixed thoroughly, and centrifuged at 1400 rpm for 5 min to obtain the cell pellet. The cells were re-suspended in the culture media at a density of 0.5 × 10^6 cells/mL and then subjected to micropipette aspiration.

6.2.2 IL-1B TREATMENT OF CARTILAGE EXPLANTS

Explants of full-thickness cartilage, harvested from the 3 different metacarpo-phalangeal joints of adult steers, were immersed in culture media (DMEM + 10% FBS) and incubated at 37°C and 5% CO_2 for 24 h. One set of explants were treated with 10 ng/mL of IL-1β in DMEM + 10% FCS for 5 days. This culture media was replaced every 24 h along with fresh IL-1β. Controls were treated in an identical way but without the presence of IL-1β. Following the treatment, chondrocytes were isolated from the treated and untreated (control) explants, using the procedure described in section 3.6.2. The isolated cells were suspended in the culture media at a density of 0.5 × 10^6 cells/mL, and subjected to micropipette aspiration.

6.2.3 IN VITRO MECHANICAL INJURY MODEL

Full-thickness cartilage explants were pooled from 6 different metacarpo-phalangeal joints and divided into two equal groups as follows: Uninjured (control) and Injured. The explants from the uninjured and the injured groups were cultured for 24 h in media (DMEM + 10% FBS), and the explants for the freshly isolated group were sequentially digested to isolate cells, as previously described in section 3.6.2.
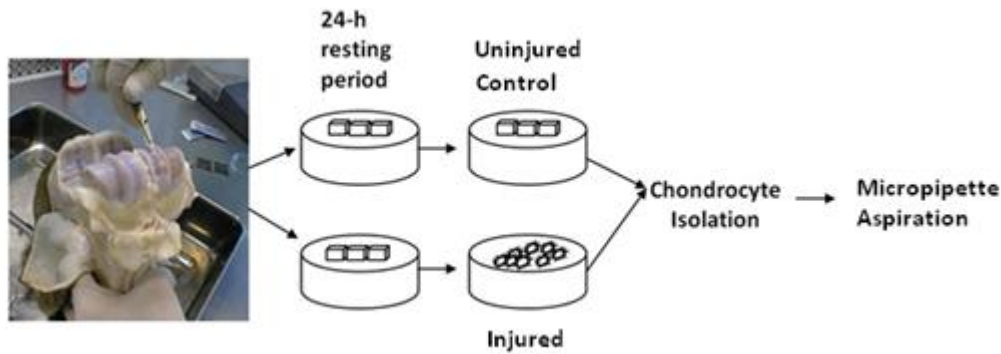
Figure 6.1. *Schematic diagram showing experiment protocol (see text for details).*

After 24 h, explants from the injured groups were finely diced using a scalpel and cultured for 5 days in culture media (DMEM + 10% FBS), as indicated in Figure 6.1. Cartilage explants from the uninjured group were maintained in identical culture condition for 5 days. For both groups, the culture media was changed every 2 days. The chondrocytes were isolated from each group and resuspended in the culture media at a density of 0.5×10^6 cells/mL. Cells from both groups were aspirated on the same day to avoid sample variations.

6.2.4 CELL VIABILITY

Representative cells from all the test conditions were suspended in 1 mL of culture media after isolation. The cell viability was determined using a trypan blue exclusion assay; values in excess of 95% were observed for the control groups. However, a lower cell viability of 85% was observed for the injured group.

6.2.5 MICROPIPETTE ASPIRATION

Cells from IL-1β treated chondrocytes monolayer and cartilage explants, and cells from mechanically injured cartilage were aspirated under similar conditions. An aspiration pressure rate of 5.48 cmH$_2$O/s was applied to a final aspiration pressure of 7 cmH$_2$O. This pressure was then kept constant for 180 s, and images were obtained during this period

at a rate of 1.54 s per frame. The temporal changes in aspiration length were imported into MatLab, and the data were curve-fitted using the Boltzmann standard linear solid (BSLS) model.

6.2.6 STATISTICAL ANALYSIS

The surface area and volume data of the cell was assumed to be normal distribution and values of mean and standard deviation was estimated. The paired Student's t-test was used to determine the significant difference before and after aspiration and unpaired Student's t-test was used to determine the significant difference between the untreated/treated and uninjured/injured.

The cell diameter, aspiration length of the chondrocytes and mechanical data of the cell was assumed to be non-normal distribution and was presented in terms of the median and interquartile range. Accordingly Mann-Whitney U tests (2-tailed) were used to determine the statistical significance of the differences in each of the three viscoelastic mechanical parameters. The level of statistical significance both the parametric and non-parametric analysis of the data was set at $p < 0.05$, unless otherwise mentioned

6.3 RESULTS

The numbers of the cells tested are presented in Table 6.1 for each of the experiments, namely, the chondrocytes in monolayer culture and explants culture either treated with IL-1β or injured mechanically. In all the experiments, more than 80% of the cells were successfully aspirated except for untreated monolayer, as shown in Table 6.1. The BSLS model yielded the three viscoelastic parameters namely, instantaneous modulus, equilibrium modulus and apparent viscosity. Cells that were successfully aspirated were included in the analyses of cell morphology.

However, cells were rejected from the cell mechanics analyses if:

- the cells did not aspirate

- the analytical model did not converge or produce an accurate fit (R < 0.95)

- the estimated constants reached the pre-set limit ($k_2 > 100$)

Table 6.1 shows the number of cells rejected under each of the above criteria along with the total number of cells successfully analysed for each separate experiment. The convergence was greater than 80% in all the cases accept for untreated monolayer.

Table 6.1. The number of cells accepted for each experimental conditions. Percentage values represent those cells of the total which were successively analysed using SLS and BSLS models. Treatment performed on the monolayer and explants using IL-1β.

Experiment	Total No. of Cells	Cell Aspiration	Convergence	R ≥ 0.95	$k_2 < 100$
Untreated Monolayer	18	15	14	14	12 (67%)
Treated Monolayer	16	14	14	14	14 (88%)
Untreated Explant	19	17	17	17	17 (89%)
Treated Explant	18	18	18	18	17 (94%)
Freshly Isolated	40	38	37	37	36 (90%)
Uninjured Explant	39	38	38	37	36 (95%)
Injured Explant	30	28	28	28	27 (90%)

6.3.1 EFFECTS OF IL-1B TREATMENT ON CHONDROCYTES IN MONOLAYER

The chondrocytes obtained from the untreated and IL-1β treated monolayer cultures were aspirated rapidly into the micropipette during the first 90 s. This was followed by a decrease in the rate of aspiration until equilibrium was reached, as shown in Figure 6.2. The trend observed for temporal changes in the aspiration length of the chondrocytes was similar to that described in Figure 4.4.
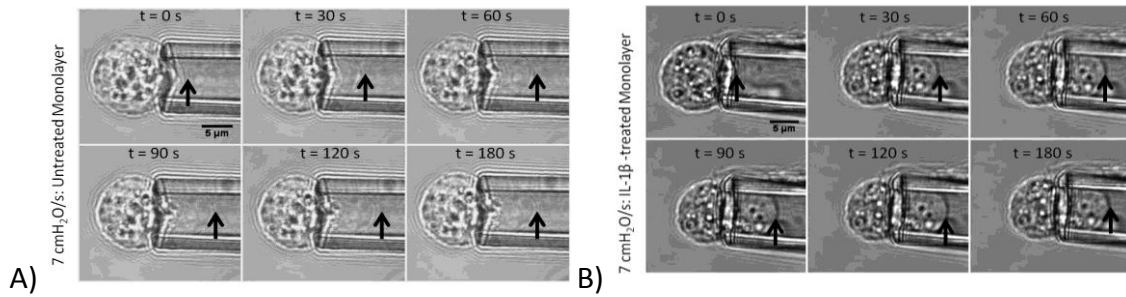
Figure 6.2. *Micropipette aspiration of the chondrocytes aspirated at 7 cmH$_2$O/s retrieved from the A) IL-1β untreated and B) treated monolayers. The arrow represents the extent of the cell membrane aspirated into the micropipette. Scale bar 5μm.*

UNSTRAINED CELL MORPHOLOGY

The measured cellular dimensions before and after aspiration were processed to compute the cell surface area and volume, as described in section 3.6.4. No significant difference was noted in the chondrocyte diameters between the untreated and treated groups, as indicated in Figure 6.3. Although the median diameters of the IL-1β untreated and treated chondrocytes were 13.2 μm and 12.8 μm respectively, the differences between the groups were not found to be statistically significant (p > 0.05) (Figure 6.3).
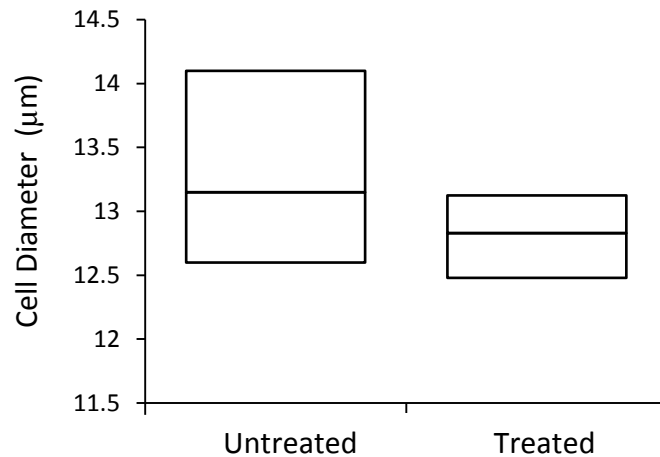
Figure 6.3. *The diameter of the chondrocytes obtained from IL-1β-treated (n = 14) and untreated (n = 15) monolayers prior to micropipette aspiration.*

175

CELL ASPIRATION

It can be noted from Figure 6.4 that the IL-1β treatment did not influence the aspiration length of chondrocytes obtained from untreated and treated monolayers. The surface area of the chondrocytes obtained from the untreated and treated monolayer was altered after the aspiration for both untreated and IL-1β treated groups. The percentage increase were 22% and 24%, respectively, as indicated in Figure 6.5A. Furthermore, it is interesting to note that for both untreated and treated groups, the cell volume increased after aspiration (Figure 6.5B). The three mechanical parameters estimated for the chondrocytes obtained from IL-1β-treated and untreated monolayers are presented in Figure 6.6A-C. For each parameter, a range of absolute values was noted, with no significant differences between values for each group.
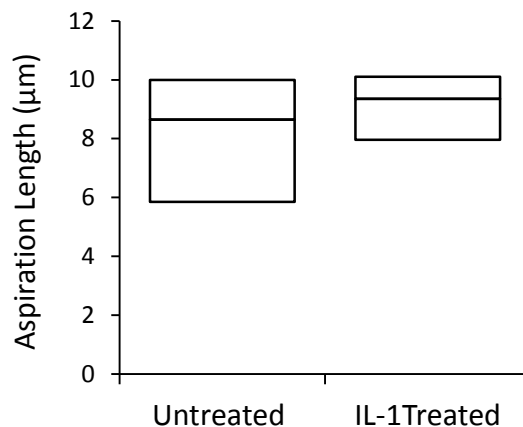
Figure 6.4.*The aspiration length of the chondrocytes obtained from IL-1β untreated (n = 14) and treated (n = 12) monolayers aspirated at pressure rate 5.48 cmH$_2$O/s.*
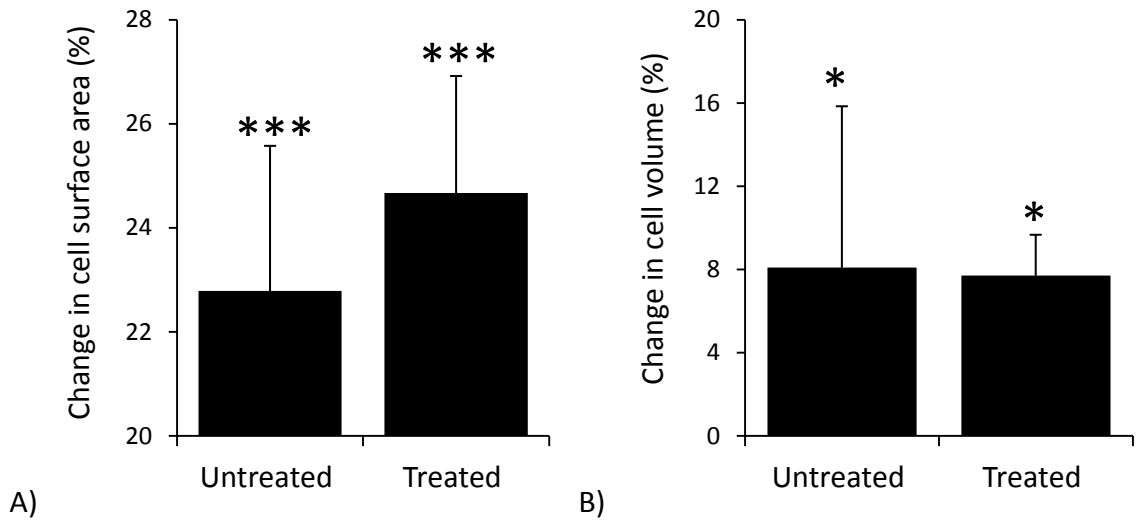
Figure 6.5. *Changes in the A) surface area and B) volume of the chondrocytes obtained from IL-1β-treated (n = 14) and untreated (n = 12) monolayers after micropipette aspiration at a pressure rate 5.48cmH$_2$O/s. Significant differences indicated by * (p < 0.05) and *** (p < 0.001).*
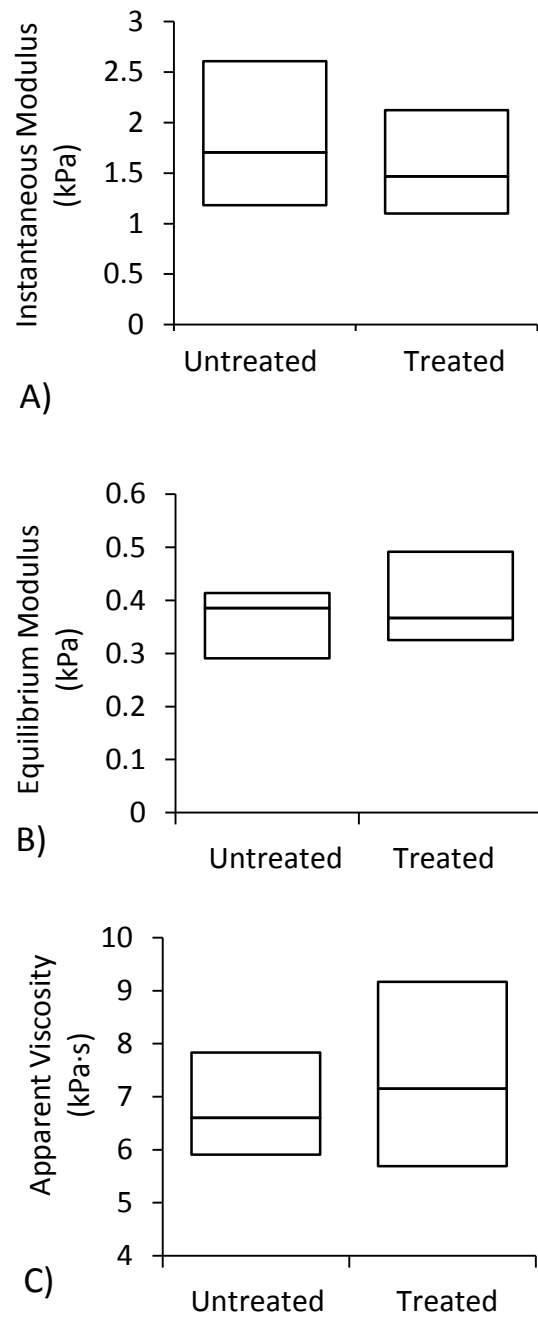
***Figure 6.6**. Three viscoelastic parameters namely A) instantaneous modulus B) equilibrium modulus and C) apparent viscosity of chondrocytes obtained from the IL-1β-treated (n = 14) and untreated (n = 12) monolayers determined using the BSLS model.*

6.3.2 EFFECTS OF IL-1β TREATMENT ON THE CARTILAGE EXPLANTS

Representative images obtained during micropipette aspiration of chondrocytes isolated from the explants in both the IL-1β-treated and untreated cultures are shown in Figure 6.7. It is evident that the temporal changes in the aspiration length mostly occurred during the first 90 s, beyond which minimal further changes in aspiration length were observed since an equilibrium state had been attained.
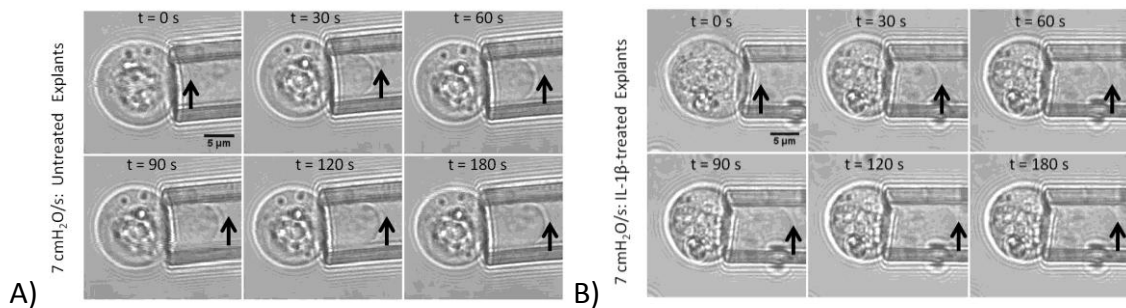
Figure 6.7. *Micropipette aspiration of the chondrocytes at 7 cmH$_2$O/s obtained from the A) IL-1β untreated and B) treated cartilage explants. Scale bar 5μm.*

UNSTRAINED CELL MORPHOLOGY

No significant differences were observed in the chondrocyte diameters between the untreated and treated groups, with median values of 14.1 μm and 14.0 μm, respectively, as presented in Figure 6.8.
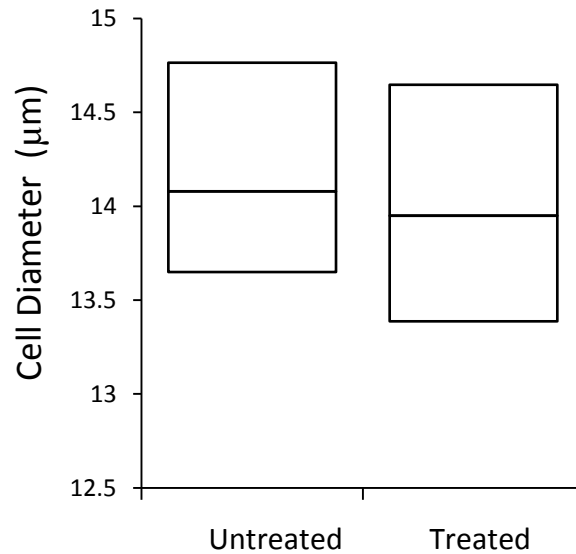
Figure 6.8. *The diameter of the chondrocytes obtained from the untreated (n = 17) and IL-1β-treated (n = 18) cartilage explants prior to micropipette aspiration*

CELL ASPIRATION

Although the median aspiration length of the chondrocytes obtained IL-1β-treated explants higher than untreated explants, no statistical difference was observed (Figure 6.9). A dramatic increase in cell surface was observed after aspiration for the untreated and treated groups (Figure 6.10A). Indeed in both groups, the surface area of the chondrocytes increased by more than 20%, the differences being statistically significant at the 1% level in both the groups. With regard to the cell volume, relatively small increases were observed after aspiration (Figure 6.10B). However no statistical difference was observed in the cell volume between pre and post aspiration for each control or experimental groups.
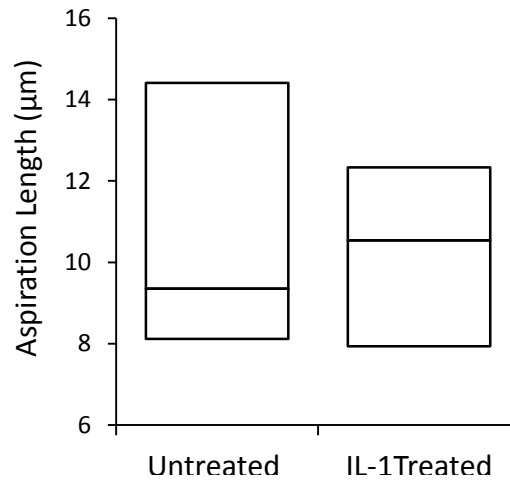
Figure 6.9. *The aspiration length of the chondrocytes obtained from IL-1β untreated (n = 17) and treated (n = 17) cartilage explants aspirated at pressure rate 5.48 cmH₂O/s.*
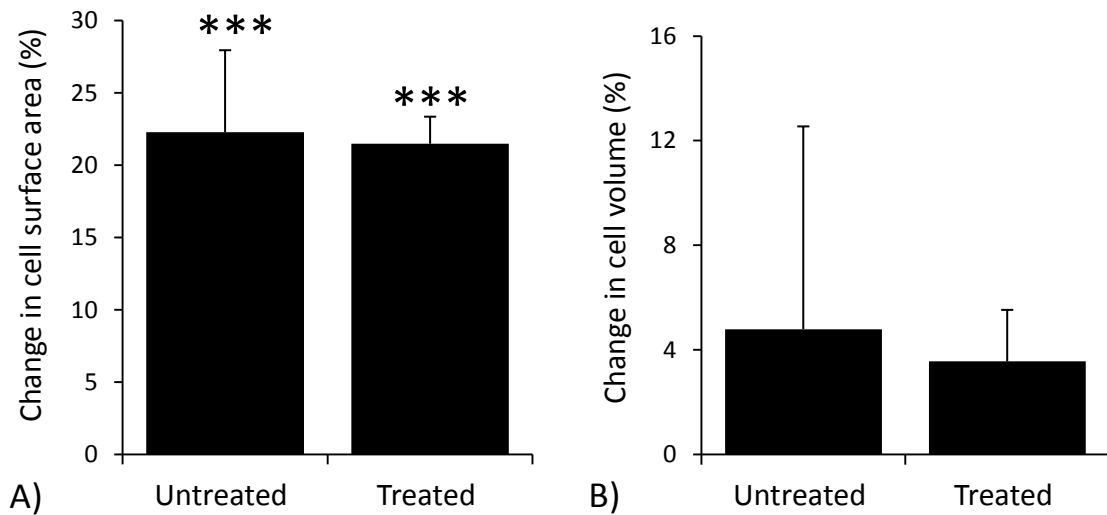
Figure 6.10. *Changes in the A) surface area and B) volume of the chondrocytes obtained from IL-1β-treated (n= 18) and untreated (n= 17) cartilage explants after micropipette aspiration at a pressure rate of 5.48cmH₂O/s. Significant differences indicated by *** (p < 0.001).*

Figure 6.11A indicates the increase in the instantaneous modulus of chondrocytes obtained from the explants treated with IL-1β as compared with the untreated groups. Although there was evident variability associated with the experimental group, its values were statistically significantly higher than the untreated values ($p < 0.05$). By contrast, the corresponding values of the equilibrium modulus for the chondrocytes from the untreated explants overlapped with those for the chondrocytes from the treated explants, as indicated in Figure 6.11B. The median value of the apparent viscosity of the chondrocytes from the treated explants was higher than that from the treated explants, as shown in Figure 6.11C, although the differences were not statistically significant ($p > 0.05$).
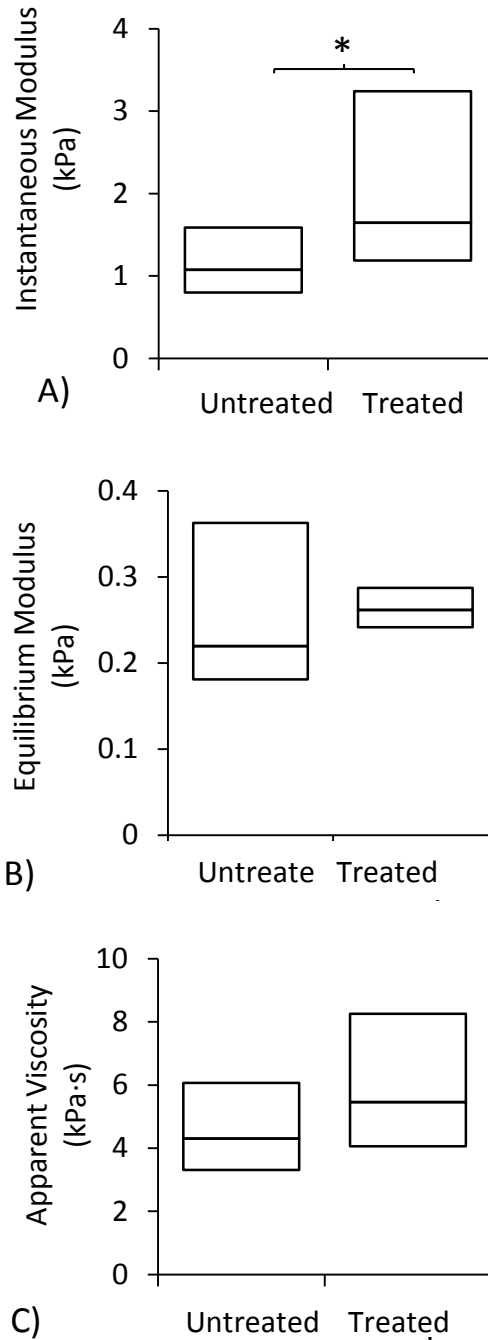
Figure 6.11. *Three viscoelastic parameters A) instantaneous modulus, B) equilibrium modulus and c) apparent viscosity of chondrocytes obtained from the untreated (n = 17) and IL-1β-treated (n = 17) cartilage explants determined using the BSLS model. A statistically significant difference was observed, indicated by * (p < 0.05).*

6.3.3 EFFECT OF IN VITRO MECHANICAL INJURY ON THE CARTILAGE EXPLANTS

Representative images of chondrocytes obtained from uninjured and injured cartilage explants are presented in Figure 6.12.
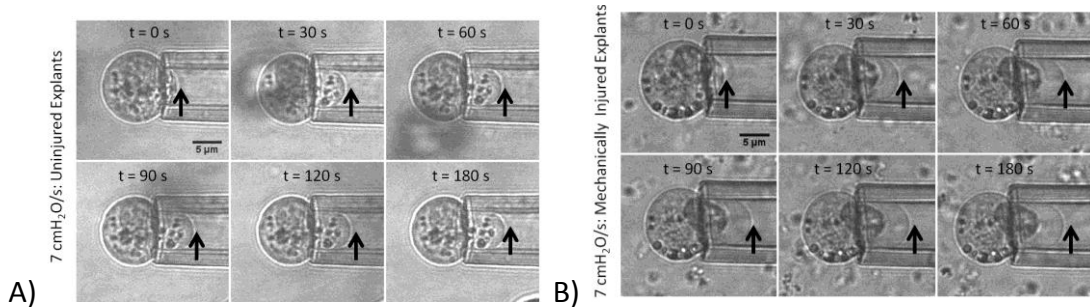
Figure 6.12. *Micropipette aspiration of chondrocytes obtained from mechanically A) uninjured and B) injured cartilage explants at 7 cmH₂O/s. The arrow represents the extent of the cell membrane into the micropipette. Scale bar 5μm.*

UNSTRAINED CELL MORPHOLOGY

The diameters of the chondrocytes obtained from the uninjured and mechanically injured cartilage explants before micropipette aspiration are presented in Figure 6.13. Differences in the diameters between groups were not statistically significant (p > 0.05).
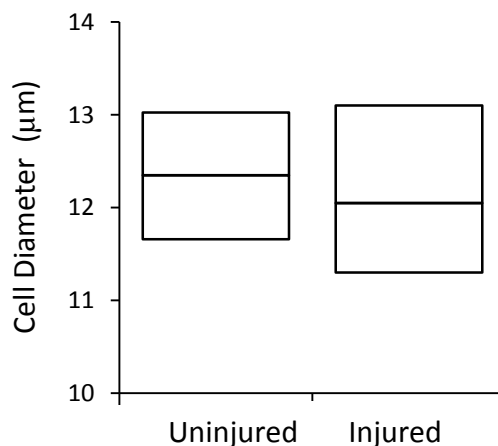
Figure 6.13. *The diameter of the chondrocytes obtained from the uninjured (n = 38) and mechanically injured (n = 28) cartilage explants prior to micropipette aspiration.*

CELL ASPIRATION

A statistically significant difference was observed in the aspiration length of the chondrocytes obtained from uninjured and injured cartilage explants (Figure 6.14). The cell surface area of the chondrocytes obtained from the uninjured and mechanically injured explants revealed highly statistical differences between before and after aspiration (Figure 6.15A). Indeed the surface area of the chondrocytes increased by approximately 16% for the chondrocytes obtained from the uninjured and injured explants, after aspiration. A smaller increase in the cell volume was also observed for both groups after aspiration (Figure 6.15B). These differences in cell volume were, however, only statistically significant for the uninjured group (p < 0.05).
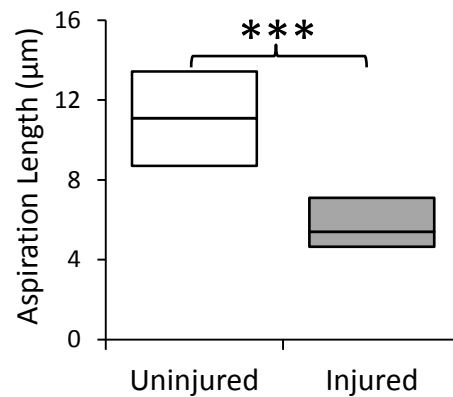
Figure 6.14. *The aspiration length of the chondrocytes obtained from uninjured (n = 36) and injured (n = 27) cartilage explants aspirated at pressure rate 5.48 cmH$_2$O/s. Significant differences indicated by *** (p < 0.001).*
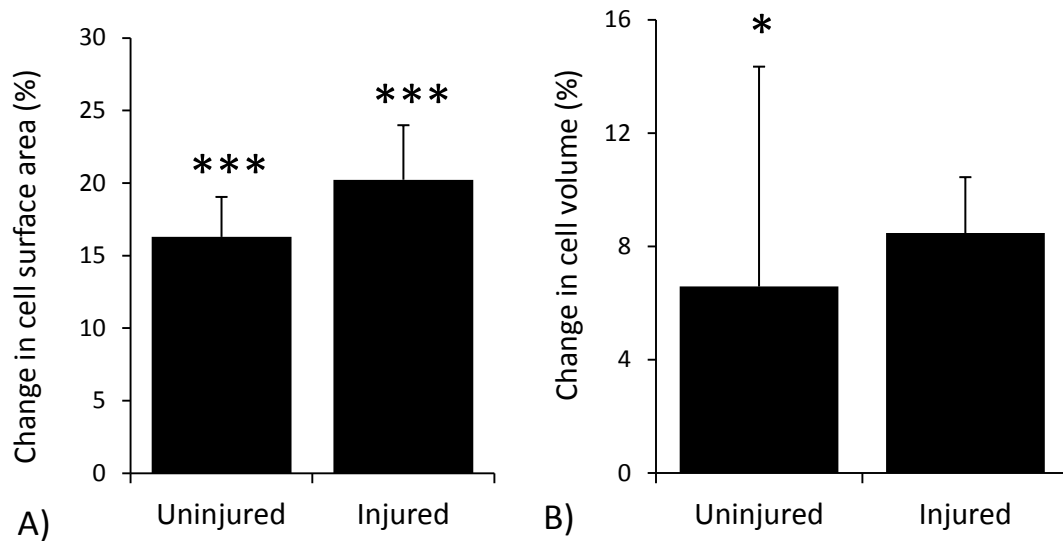
Figure 6.15. *Changes in the A) surface area and B) volume of the chondrocytes obtained from the uninjured (n = 36) and mechanically injured (n = 27) cartilage explants after micropipette aspiration at a pressure rate of 5.48cmH$_2$O/s. Significant differences indicated by* (p < 0.05) and *** (p < 0.001).*

A considerable difference was observed for all the three mechanical parameters between the uninjured and injured groups of cells (Figures 6.16A-C). For all three parameters, the median values for the former were significantly higher than for the uninjured cells (p < 0.001 in each case). It is interesting to compare the three viscoelastic parameters resulting from chondrocytes isolated from explants and subjected to either biochemical or mechanical treatment. The data, as summarised in Table 6.2, revealed significantly higher values for all the three parameters in chondrocytes exposed to the mechanical treatment.
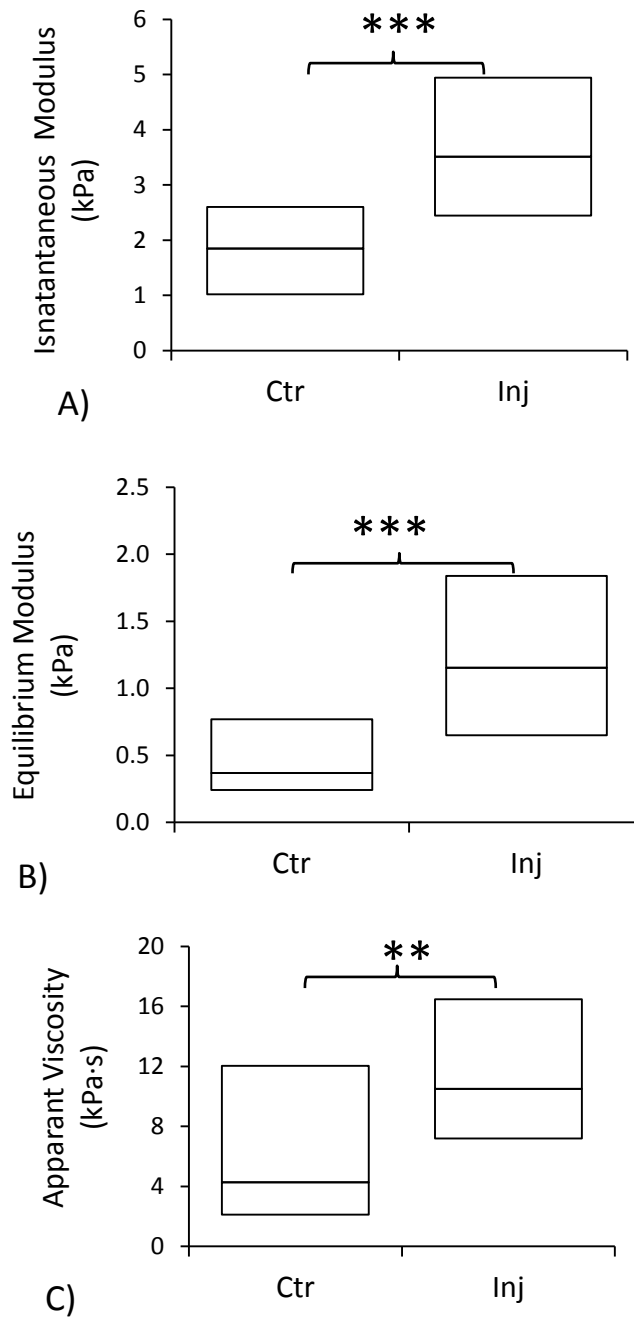
Figure 6.16. *The viscoelastic parameters namely A) instantaneous modulus, B) equilibrium modulus and C) apparent viscosity of chondrocytes obtained from uninjured (n = 36) and mechanically injured (n = 27) cartilage explants determined using the BSLS model. Statistically significant differences were observed, indicated by *** (p < 0.001) and ** (p < 0.01).*

Table 6.2. *Viscoelastic properties of the chondrocytes isolated from the explants exposed to mechanical injury and IL-1β treatment showing median values (and inter-quartile ranges)*

	Mechanical Injury		IL-1β treatment	
Parameters	**Uninjured**	**Injured**	**Untreated**	**Treated**
E_{in} (kPa)	1.9 (1–2.6)	3.5 (2.4–4.9)	1.1 (0.8–1.6)	1.7 (1.2–3.2)
E_{eq} (kPa)	0.4 (0.2–0.8)	1.2 (0.7–1.8)	0.2 (0.2–0.4)	0.3 (0.2–0.3)
μ (kPa·s)	4.3 (2.1–12)	10.5 (7.2–16.5)	4.3 (3.3–6.1)	5.4 (4.1–8.3)

E_{in} – instantaneous modulus E_{eq} – equilibrium modulus, μ - apparent viscosity

6.4 DISCUSSION

6.4.1 UNSTRAINED CELL MORPHOLOGY

The chondrocyte biology is investigated using invitro culture system namely, cartilage explant culture , chondrocyte 3D culture and monolayer culture (Stewart et al., 2000). However in the present study the chondrocytes monolayer and cartilage explants culture is investigated. Chondrocyte in monolayer flattens out and adopts fibroblast-like morphology. This is associated with down regulation of the collagen type-II and upregulation of collagen type I (Benya and Shaffer, 1982). Furthermore chondrocyte metabolism is altered during the expansion in the monolayer (Heywood and Lee, 2008). On the other hand in the cartilage explants chondrocytes maintains the some of the phenotypic expression (Asanbaeva et al., 2007). In the present study the chondrocyte monolayer and articular cartilage explants were treated with 10ng/ml of IL-1β. This concentration has been previously reported to induce the release of sGAG over a 5 day culture period (Arner et al., 1998). Approximately 15-30% of the proteoglycan was

released into the culture media at the end of the IL-1β treatment period (Wann et al., 2010).

The chondrocytes diameter obtained from IL-1β-untreated cartilage explants was greater than the monolayer. This could be due to the difference in culture period, as explants were cultured for 5 days whereas the chondrocyte in monolayer were cultured for 24 hours. Previous study have shown that the presence of foetal bovine serum in the media induces excessive cell proliferation (Strehl et al., 2002). Even though the control group of the IL-1β treatment cartilage explants and mechanically injured cartilage explants were cultured in similar conditions for 5 days, difference was observed in the cell diameter. This might be due to the inter-animal variation (further discussed in section 8.2.1). It might be hypothesised that the reduction in cell viability with the mechanical injury model occurred predominantly in the surface zone. This would be likely to produced a difference in cell size between the injured and control cells as deep cells are known to be larger (Lee et al., 1998). However no such difference in cell diameter was detected suggesting the loss of viability occurred uniformly across the cartilage thickness.

6.4.2 EFFECTS OF CELL ASPIRATION

In the present study, in vitro models were utilised to investigate the changes in the mechanics of the chondrocytes following biochemical treatment or mechanical injury. Chondrocytes obtained from monolayers and those isolated from explants were successfully aspirated using an optimised micropipette aspiration system for each of the treatment modalities. All chondrocytes demonstrated typical viscoelastic creep behaviour, similar to that observed in section 4.3.1. Neither the IL-1β treatment on monolayer and explants had any effect on the aspiration length of the chondrocytes (Figure 6.4, 6.9, 6.14). However there was a significant difference in the aspiration length of the chondrocytes obtained from uninjured and injured explants. Additionally, statistical difference was observed in the surface areas of the chondrocytes after aspiration for data from both control cells and cells subjected to IL-1β or mechanical

trauma (Figure 6.5A, 6.10A, 6.15A). Remarkably, in the present study, the chondrocyte volume also increased after aspiration, although the changes were not statistically significant in cells subjected to IL-1β treatment or mechanical injury of explants (Figure 6.5B, 6.10B, 6.15B). The increase in surface area and volume of chondrocytes after aspiration is discussed in section 4.4.1.

The chondrocytes behaviour in response to micropipette aspiration was modelled using the BSLS model. Individual cells were included in the statistical analyses based on the criteria stated in section 6.3. Variability was observed in the viscoelastic parameters of the cells indicated by the interquartile ranges for the chondrocytes obtained from IL-1β treated explants and monolayer, injured explants. This may be due to inhomogeneities in the structure and composition of the tissue. The SLS and BSLS model used to compute these viscoelastic parameters assumes the cell behaviour to be homogenous half-space. Furthermore this model assumes cells to be incompressible that is not the case in the experimental condition as evident by increase in the cell volume after aspiration (Figure 6.5B, 6.10B, 6.15B).

 The BSLS model provides an approximation of the cell elastic behaviour as estimated by the instantaneous modulus, and its viscoelastic behaviour reflected by values for the equilibrium modulus and apparent viscosity. Interestingly, a significant increase in the instantaneous modulus value was observed for chondrocytes derived from the IL-1β-treated cartilage explants when compared to the corresponding untreated control group (Figure 6.11A, 6.16A), as well as for the chondrocytes obtained from the mechanically injured explants. Interestingly no significant difference was observed for cells treated with IL-1β in monolayer (Figure 6.6). Previous studies have shown that IL-1β produces a small but statistically significant increase in the organisation of the cortical F-actin cytoskeleton both in situ and in isolated chondrocytes in suspension (Pritchard and Guilak, 2006). This change in actin organisation might be expected to influence cell mechanics (Qi et al., 2006). However the present study found no differences in the

mechanical properties of chondrocytes treated in monolayer with IL-1β compared to untreated controls (Fig. 6.6). This may indicate that IL-1β has no effect on actin organisation in monolayer or that any effect is lost once cells are trypsinised and tested in suspension. Further studies would be required to quantify actin organisation following exposure to IL-1β in monolayer and subsequent trypsinisation. The present data shows that there is a significant difference in instantaneous modulus between cells treated in explants and untreated controls (Fig. 6.11). This suggests that actin differences may be maintained following isolation from the cartilage.

Therefore an alternative hypothesis is that IL-1β influences cell mechanics in explants by modulating the pericellular mechanical environment associated with degradation of the tissue (Wann et al., 2010). Alterations in ECM stiffness are known to influence the micromechanical environment of the cells and this, in turn, may lead to reorganisation of the F-actin cytoskeleton with subsequent changes in the mechanical properties of the cells (Alexopoulos et al., 2005). Indeed Trickey and colleagues (2004) used a micropipette aspiration to demonstrate the role played by F-actin microfilaments and intermediate filaments in influencing the viscoelastic properties of chondrocytes. This may also explain the significant increase in instantaneous modulus for chondrocytes subjected to mechanical injury in explants since the model is also known to result in degeneration of the matrix (Dell'accio et al., 2006).

IL-1β treatment indicated a significant alteration in the elastic parameters of the chondrocytes, possibly due to changes in the micromechanical environment of chondrocytes regulating its mechanical properties. Thus the so-called mechanoniche, which comprises the mechanical properties of both the extracellular matrix and the chondrocytes per se along with external mechanical cues, could be disturbed by matrix degradation following either IL-1β treatment or injurious mechanical trauma. Indeed previous studies have demonstrated changes in the mechanical properties of the ECM by both enzymatic treatment of tissue explants (Bader et al., 1992) and mechanical injury to

191

explants either by impact loading (Henson and Vincent, 2008; Jeffrey et al., 1997) or via uniaxial confined compression (Lee et al., 2005; Quinn et al., 1998). The resultant injuries induced matrix damage, decreased matrix synthesis and decreased cell viability. Based on these previous reports and the present findings, it may be hypothesized that the micromechanical environment of a chondrocyte is altered following both IL-1β-induced chemical injury and mechanical injury.

The values for the viscoelastic properties i.e. the equilibrium modulus and apparent viscosity were not statistically different between the untreated and IL-1β-treated explants. However, when examining the effects of mechanical injury both the elastic and viscoelastic parameters were significantly enhanced when compared to the values associated with the IL-1β-treated explants (Table 6.2). The present findings support an earlier study which reported significant changes in both elastic and viscoelastic parameters in chondrocytes derived from mechanically injured explants (Alexopoulos et al., 2005). The exposure of cartilage explants to IL-1β treatment alone did not lead to significant changes in the equilibrium modulus of the chondrocytes. In contrast, the mechanical injury model appeared to replicate various mechanisms occurring in OA, including changes in cellular mechanical properties (Kornaat et al., 2006; Trickey et al., 2000).

The present findings suggest that the changes observed in the mechanical properties of the explants that were mechanically injured may more closely resemble those observed in OA chondrocytes (Trickey et al., 2000). The mechanical injury model presented here, which demonstrated changes in both the elastic and viscoelastic properties of the chondrocytes, may thus be a suitable model for investigating the micromechanical changes within chondrocytes. The model may also clarify relationship between the microenvironment and the mechanical behaviour of the cell, particularly for pathological conditions such as OA. Chondrocytes in a monolayer culture, are entirely isolated from their native mechanical environment. Thus this technique is unsuitable for replicating

the mechanical and associated physiochemical changes occurring in physiological or pathological conditions. Therefore the effects of mechanical injury were only observed in explants.

While the overall aetiology of OA remains unclear, biomechanical factors are known to play a crucial role in its onset and development (Clair et al., 2009). As reviewed in section 1.3.1, articular cartilage is consistently subjected to compressive loading in physiological conditions. During cartilage degeneration, mechanotransduction will be affected via various signalling pathways (Clouet et al., 2009), as described in section 1.5, wherein mechanical cues are transferred to cells via the extracellular matrix.

The findings of the present study revealed that exposure of the cartilage explants to chemical and mechanical injuries induced various alterations in the morphology and mechanics of the cultured chondrocytes. In particular, the mechanical injury model had significantly greater effects on the mechanical properties of the cells when compared to those induced by the IL-1β injury model. From these data, it is tempting to suggest that the changes occurring in chondrocytes as a result of mechanical injury accurately represent the changes evident in the mechanical properties of OA chondrocytes. However the precise cellular mechanism and signalling pathways responsible for such changes are unclear.

Chapter 7

EFFECTS OF CELL PASSAGE ON THE MECHANICS OF CHONDROCYTES

7.1   **INTRODUCTION**

7.2   **METHODOLOGY**

    7.2.1   Cell Passaging

    7.2.2   Chondrocyte Micropipette Aspiration

    7.2.3   Statistical Analysis

7.3   **RESULTS**

    7.3.1   Effect of Cell Passage on the Unstrained Cell Morphology

    7.3.2   Effect of Cell Passage on the Cell Aspiration

7.4   **DISCUSSION**

    7.4.1   Unstrained Cell Morphology

    7.4.2   Effects of Cell Passage on the Cell Aspiration

7. EFFECTS OF CELL PASSAGE ON THE MECHANICS OF CHONDROCYTES

7.1 INTRODUCTION

This chapter describes a series of experiments that examined the effects of cell passaging on the mechanics of chondrocytes measured using the micropipette aspiration technique. The cell diameter, surface area, and volume were computed using the measured aspiration length of the cell, pipette diameter, and the cell diameter before and after micropipette aspiration. Furthermore, temporal changes in the aspiration lengths were applied in the BSLS model through MatLab to compute the three viscoelastic parameters of the cells, i.e. instantaneous modulus, equilibrium modulus, and apparent viscosity. The micropipette aspiration data for the chondrocytes were analysed to test the hypothesis that chondrocyte expansion in the monolayer induced changes in the unstrained cell morphology and mechanical properties of the cells.

7.2 METHODOLOGY

Bovine articular chondrocytes were isolated from full-depth adult cartilage from the metacarpo-phalangeal joints, as described in section 3.6.2.

7.2.1 CELL PASSAGING

Freshly isolated chondrocytes (designated passage zero, P0), were plated in T-75 cm^2 culture flasks at an initial density of 60000/cm^2 and cultured for 5 days. The cells were allowed to proliferate at 37°C in 5% CO_2 to a visually estimated value of 90% confluence. Cells were incubated in 10 mL of DMEM + FCS (section 3.6.1) with media changed on day 3. The chondrocytes were detached from the culturing flask according to the standard trypsinisation technique as follows. Cells were washed three times with PBS and then treated with 10 mL of 0.05% trypsin/EDTA (Sigma, Poole, UK) followed by incubation for 3 min at 37°C and 5% CO_2. An equivalent amount of the culture medium was then added

to neutralise the trypsin. This cell suspension was transferred to the centrifuge tube and mixed thoroughly and subsequently centrifuged at 1400 rpm for 5 min to obtain a cell pellet which was re-suspended in 1 mL of fresh culture medium. A trypan blue assay was used to determine cell viability and cell count, revealing cell viability values of 95% and above. At this time point, passage 1 (P1), 60% of cells were removed for micropipette aspiration. The remaining chondrocytes were divided into two separate flasks at the same initial seeding density (60000 cells/cm^2) and allowed to grow for further expansion in monolayer until the required passage. Overall, 3 cell passages were conducted over a culture period of 14 days.

7.2.2 CHONDROCYTE MICROPIPETTE ASPIRATION

At four passage points (P0, P1, P2 and P3) cells were aspirated to 7 cmH$_2$O/s using a custom-built apparatus in accordance with the standard operating procedure (see section 3.6.3). Micropipettes with diameters ranging from 6.5 to 7.5 μm were used for all the experiments. The cell aspiration was monitored for 180 s, and the data was analysed using the Leica LCS Lite software. The diameter of the cells was measured as shown in Figure 3.8. The cell morphological properties such as surface area and volume were computed using equations 3.10 and 3.11 respectively (see section 3.6.4). The mechanical properties of the chondrocytes were computed using the BSLS model executed in MatLab.

7.2.3 STATISTICAL ANALYSIS

Cell surface area and volume data were assumed to have a normal distribution which was characterised by mean and standard deviation values was estimated. The paired Student's t-test was used to determine the significant difference in cell surface area and volume before and after aspiration. The unpaired Student's t-test was used to determine the significant difference in the cell morphological properties between the two pressure rates.

The diameter, aspiration length and mechanical property data of the cell was assumed to have a non-normal distribution and was presented in terms of the median and interquartile range. Accordingly Mann-Whitney U tests (2-tailed) were used to determine the statistical significance differences in each of the three derived viscoelastic mechanical parameters for each cell passage. The level of statistical significance for both the parametric and non-parametric analysis of the data was set at $p < 0.05$, unless otherwise mentioned.

7.3 RESULTS

The chondrocytes obtained from different passages were successfully aspirated as shown in Figure 7.1, showing sequential images of cells during micropipette aspiration. In all cases, the trend observed for the temporal changes in the aspiration length was similar to that described previously in section 4.3.1. The number of chondrocytes tested at each passage is summarized in Table 7.1. Cells that were successfully aspirated were included in the analysis of cell morphology. However, cells were rejected from the cell mechanics analyses depending on the given conditions:

- the cells did not aspirate
- the analytical model did not converge or produce an accurate fit (R < 0.95)
- the estimated constants reached the pre-set limit $k_2 > 100$

It should be noted that at later passages, particularly P1, a large number of successfully aspirated cells were rejected from analysis due to the estimated value of k_2 reaching the preset limit of 100 (Table 7.1).
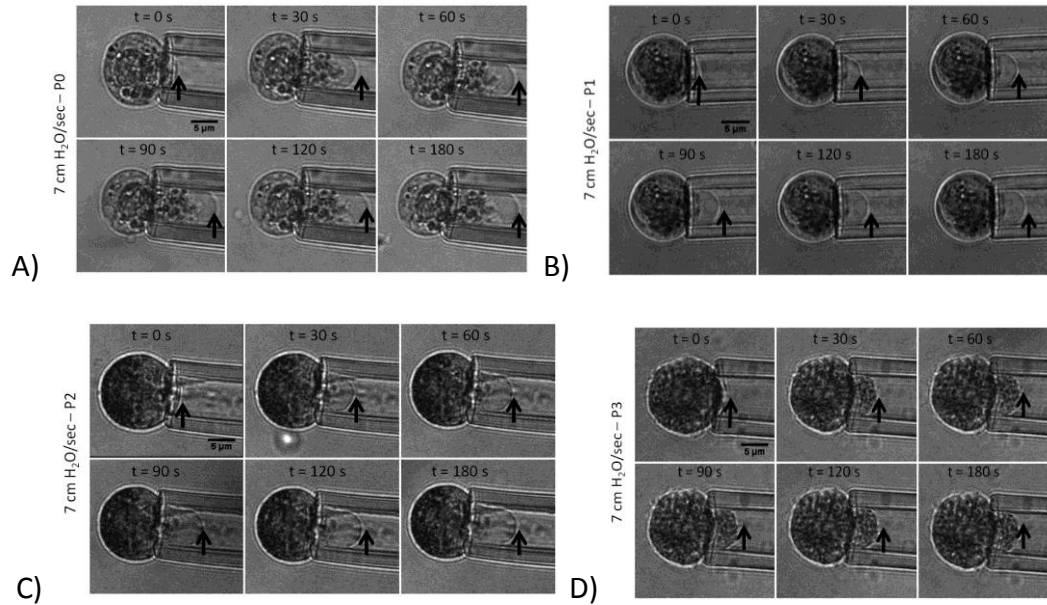
Figure 7.1. *Representative sequential images of micropipette aspiration of isolated chondrocyte at A) P0, B) P1, C) P2 and D) P3. The arrow represents the extent of the cell membrane into the micropipette. Scale bar 5µm.*

Table 7.1. *The number of cells accepted for each experimental conditions. Values in brackets represent percentage of the cells that were successively analysed using BSLS models.*

Passage	Total No. of Cells Tested	Cell Aspiration	Convergence	$R \geq 0.95$	$k_2 < 100$
P0	22	20	20	20	16 (72%)
P1	25	21	17	17	3 (12%)
P2	26	21	18	18	8 (38%)
P3	25	21	17	17	9 (36%)

7.3.1 EFFECTS OF CELL PASSAGE ON UNSTRAINED CELL MORPHOLOGY

Over time, the growth and expansion of the chondrocytes in the monolayer induced changes in the cell diameter, as shown in Figure 7.2. In particular, from P0 to P1 the diameter increased by approximate 20%, the difference being statistically significant ($p < 0.001$). Thereafter significant differences were noted between the cell diameters at P2 and P3 relative to P0. The median diameter of the freshly isolated chondrocytes was 12.4 µm, while those for the passaged chondrocytes at P1, P2 and P3 were 15.0, 15.8 and 16.3, respectively, thus over the entire culture period the median cell diameter increased by approximately 30%.
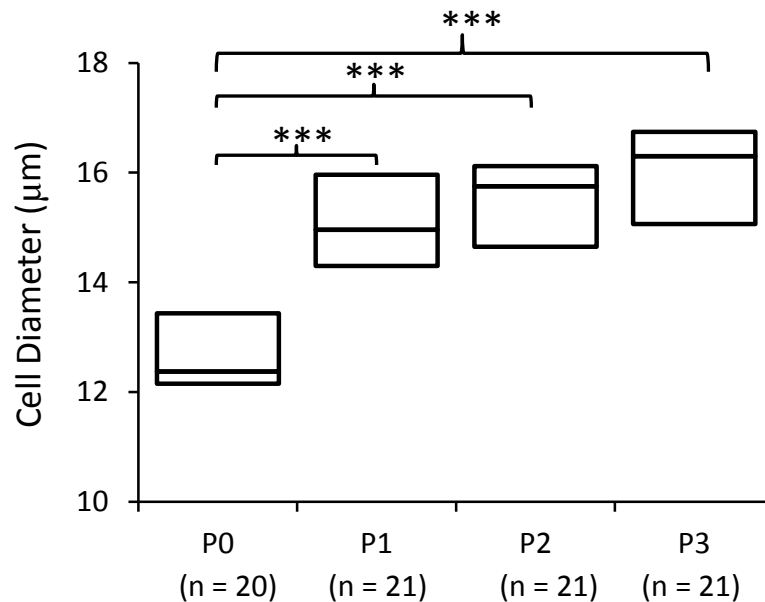
Figure 7.2. *The diameter of freshly isolated and passaged chondrocytes prior to aspiration. Significant difference indicated by *** relative to P0 by (p < 0.001).*

7.3.2 EFFECTS OF CELL PASSAGE ON CELL ASPIRATION

Figure 7.3 represents the changes in the aspiration length of the chondrocytes with passage. Statistically significant differences in aspiration length were observed between P0-P1 and P1-P3 as indicated. To further investigate the changes in the dimensions of the passaged chondrocytes, the surface area of the chondrocytes was measured before and

after aspiration. The surface area of the passaged chondrocytes significantly increased after aspiration for all the cases as indicated from the Figure 7.4A.
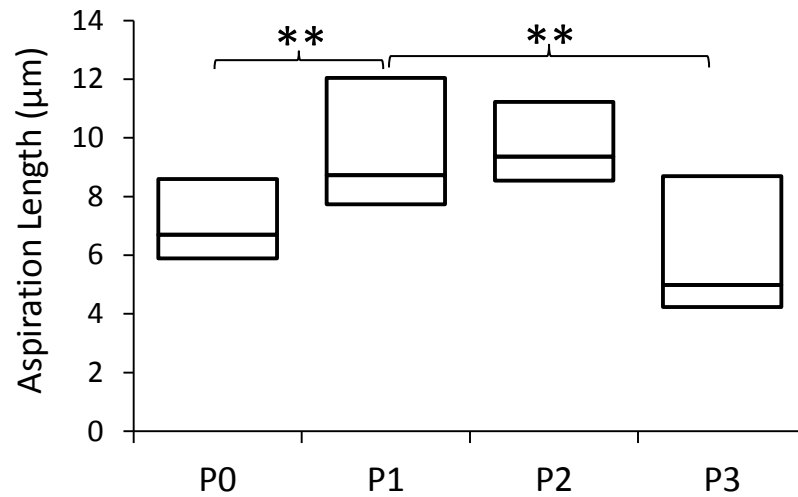
Figure 7.3. *The equilibrium aspiration length of freshly isolated and passaged chondrocytes. Significant difference indicated by ** (p < 0.01).*

The surface area increased by more than 10% of the initial surface area regardless of the passage time points. The volume of the chondrocytes was calculated at each cell passage, before and after aspiration. The percentage change in the chondrocytes volume is presented in Figure 7.4B. The volume of the chondrocytes increased after aspiration with difference being statistically significant (p < 0.001) at P1 and P2 with mean values changes of approximately 8% and 7% respectively.
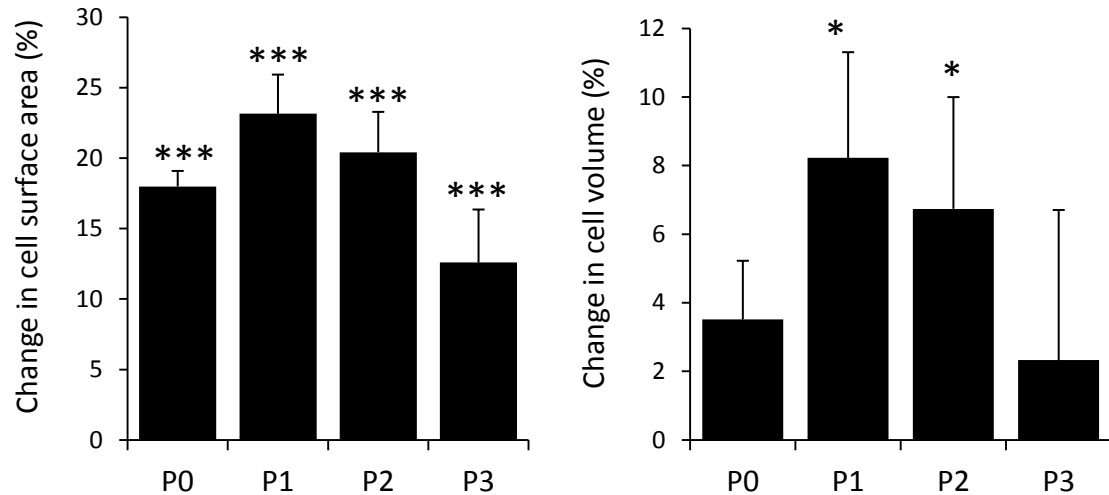
Figure 7.4. *The percentage changes in the A) surface area and B) the volume of the chondrocytes after aspiration. Significant relative to the pre-aspiration state are indicated by * (0 < 0.05) and *** (p < 0.001).*

The growth and expansion of the chondrocytes in the monolayer culture was associated with significant changes in the mechanical properties of the chondrocytes with an increase in instantaneous, equilibrium modulus and apparent viscosity as shown in Figure 7.5 respectively. However, no significant difference was observed between P0 and P1 in terms of instantaneous modulus (Figure 7.5A). This may be due to the fact that more than 75% of the cells from P1 generated $k_2 > 100$ and therefore were rejected from the analysis of the instantaneous modulus. However the instantaneous modulus values of the passaged chondrocytes increased significantly relative to P0. Figure 7.5B demonstrates that the equilibrium modulus increased significantly ($p < 0.001$) with increasing passage as compared to P0. For chondrocytes tested at P0–P3, the median equilibrium modulus values ranged from 0.21 to 0.60 kPa.
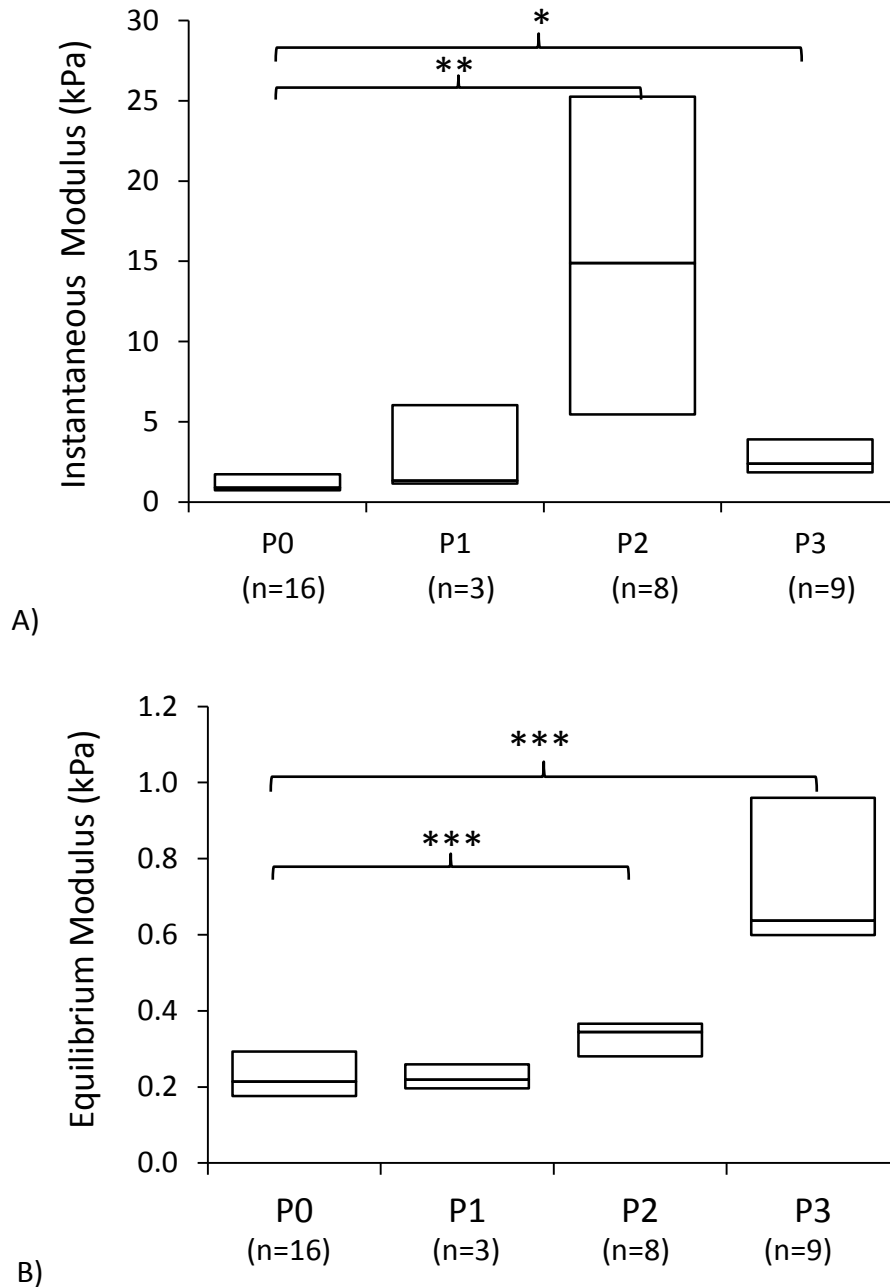
Figure 7.5. *The A) instantaneous modulus and B) the equilibrium modulus for the primary chondrocytes (P0) and the passaged chondrocytes (P1–P3) obtained by applying the experimental data for micropipette aspiration into the BSLS model. Significant differences relative to P0 are indicated by * (p < 0.05), ** (p < 0.01) and ** (p < 0.001).*

The equilibrium modulus increased significantly P1-P2 and P2-P3 (p < 0.05). Characteristic differences were noted in the apparent viscosity of the chondrocytes tested at different passages, as shown in Figure 7.6. The apparent viscosity of the chondrocytes increased significantly (p < 0.001) with the increasing passage number relative to P0 with median apparent viscosity values ranging from 2.31 to 4.86 kPa·s.
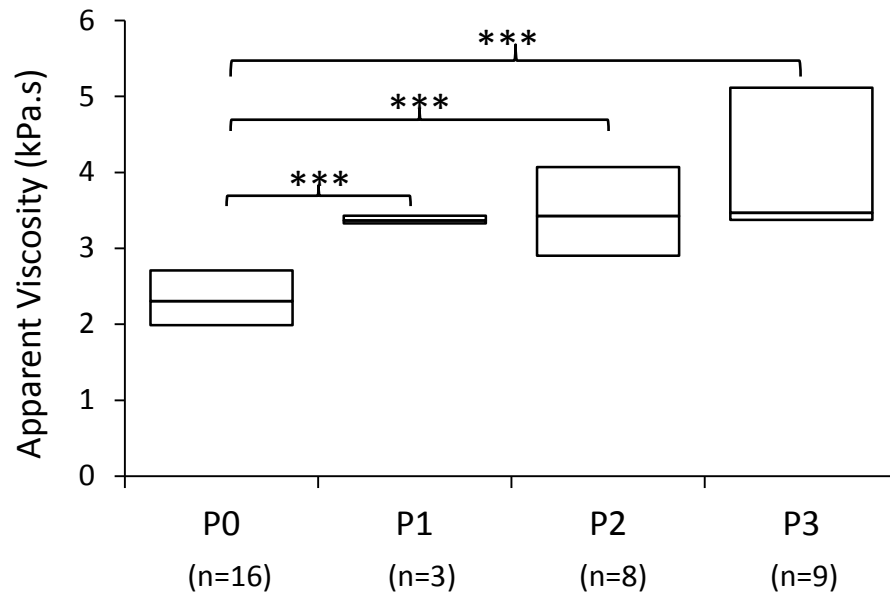
Figure 7.6. *The apparent viscosity of the primary chondrocytes (P0) and the passaged chondrocytes (P1–P3) obtained by applying the experimental data for micropipette aspiration into the BSLS model. Significant differences relative to P0 are indicated by *** (p < 0.001).*

7.4 DISCUSSION

7.4.1 UNSTRAINED CELL MORPHOLOGY

The diameters of chondrocytes were measured for freshly isolated chondrocytes (P0) and following the removal from monolayer culture at P1, P2 and P3. The cell diameter increased with passage number, with the major changes observed during the transition of the initial state of the chondrocytes (P0) to the first cell passage (P1). Similar observation was previously made whereby the diameters of the chondrocytes culture in monolayer

were greater than of chondrocytes either *in situ* or 3D culture (Sasazaki et al., 2008). In contrast, no significant changes were observed in the cell diameter from P1 to P3. These findings can be explained by the previously reported increased matabolitic activity and associated with increased cytoplasmic volume (Heywood and Lee, 2008). As in monolayer cultures, chondrocytes are attached to the culture surface and flattened out, thus adopting a more fibroblastic morphology which is accompanied by increased proliferation (Brodkin et al., 2004). The chondrocytes morphological changes are associated with changes in the extracellular matrix production, shifting from type II collagen to type I collagen and cytoskeleton assembly (Benya and Shaffer, 1982; Schulze-Tanzil et al., 2009; Zheng et al., 2004). This might be due to the chondrocytes synthetic activity changing as early as first passage (Schulze-Tanzil *et al.*, 2002).

The actin cytoskeleton in the cell monolayer is known to undergo various changes, transforming from a filament network located at the cortex into large cables running along the entire length of the cell, forming stress fibres (Malleingerin et al., 1991). It is possible that changes in the actin network were involved in the morphological changes observed in the present study. However these changes were not observed in situ or 3D culture (Sasazaki et al., 2008). It has been shown that the treatment of the chondrocytes monolayer with cytochalasin D leads to rounding of the de-differentiated chondrocytes (Loty et al.*,* 1995). While further subsequent changes may have occurred in the intracellular contents of the cell these could not be documented using the present experimental approach.

7.4.2 Effects of Cell Passage on the Cell Aspiration

When changes in the mechanics of the chondrocytes were investigated following cell passage, the findings demonstrated that the viscoelastic properties of the chondrocytes underwent changes. The viscoelastic creep behaviour of the chondrocytes was modelled using the BSLS model that provides an approximation of the chondrocytes elastic parameter i.e. the instantaneous modulus—as well as the viscoelastic parameters i.e., the equilibrium modulus and apparent viscosity.

The instantaneous modulus of the cells was computed using k_2 values. For a majority of the cells, these k_2 values were beyond the acceptable range; therefore, only 12% of the cell population could be included in the computation of the instantaneous modulus for P1 cells, as shown in Table 7.1. The small number of cells representing the whole population of the cell at specific time point was included in the presented results. Thus no significant difference was observed in the instantaneous modulus between P0 and P1.

The equilibrium modulus values of the cells increased with an increase in the number of cell passages. These findings were consistent with those of a previous study (Darling et al., 2009), wherein atomic force microscopy was employed to measure the mechanical properties of the cells. In addition to the equilibrium modulus, the apparent viscosity values also increased with subsequent passages relative to P0. Both the elastic and viscolastic properties of the chondrocytes thus underwent alterations with cell passage relative to P0.

Trickey et al. (2004) previously demonstrated similar changes in the elastic and viscoelastic properties of chondrocytes using a similar micropipette aspiration technique after treating cells with F-actin-disrupting agents. They treated chondrocytes with cytochalasin D and shown reduction in the moduli and apparent viscosity of the cells. Therefore the manipulation in the cytoskeleton on the cells was reflected in the viscoelastic properties of the cells. Further, Leipzig et al. (2006) also reported changes in the elastic and viscoelastic properties of chondrocytes using different techniques involving the use of F-actin-enhancing agents. The mechanisms regulating this feature—i.e. the alterations in the elastic and viscoelastic properties of chondrocytes following monolayer and 3D cultures—has not been fully elucidated thus far. However, it is suggested that the morphological properties of chondrocytes, including their shape and phenotype, are also linked to the actin cytoskeleton, in turn suggesting its relationship with the mechanical properties of chondrocytes (Malleingerin et al., 1991; Trickey et al., 2004).

A relative high variability was observed in the viscoelastic parameters of the cells indicated by the interquartile ranges. Additionally, the percentage of cells with limiting k_2

values decreased with subsequent cell passages, i.e. from P0 to P3, not allowing a larger proportion of the cells tested to be included in the results. This may be due to inhomogeneities in the structure and composition of the cell. The SLS and BSLS model used to compute these viscoelastic parameters assumes the cell behaviour to be homogenous half-space. Furthermore this model assumes cells to be incompressible that is not the case in the experimental condition as evident by increase in the cell volume after aspiration. The viscoelastic model is independent of changes in cell size providing that the ratio of cell to pipette is more than 3 (Baijens et al, 2005). In the present study the cell to pipette ratio changed from approximately 2 for freshly isolated cells to 2.5 for cells at P3 Therefore the increases in cell volume during passage (Figure 7.2) may be partly responsible for the increase in the viscoelastic parameters (Fig.ure 7.5 and 7.6). However the biggest change in cell diameter occurred from P0 to P1 whilst the the mechanical properties only increase at P3.

Moreover the ratio of the cell diameter to pipette diameter also vary with the passage which in turn will affect the ability of the model to curve fit the cellular response (see section 3.8.2).

Autologous chondrocyte transplantation (ACT), which is an increasingly popular technique for articular cartilage repair (Redman et al., 2005) as well as in joint replacement surgeries (Clouet et al., 2009), currently uses chondrocytes cultured in a monolayer to a minimum density of 10^7 (see section 1.6.3) (Brittberg et al., 1994). Previous *in vivo* studies have shown that implanted chondrocytes may form fibrous tissues that are inferior to native cartilage (Moriya et al., 2007). An alternate approach to the standard technique of chondrocyte growth in monolayer cultures has been developed, wherein chondrocytes are expanded in the monolayer prior to seeding in a 3D culture system (Kino-Oka et al., 2005). A return to the 3D environment restores the rounded morphology of the chondrocytes; however, protein synthesis is not completely restored (Zaucke et al., 2001). These findings indicate that the ability of the transplanted monolayer-culture chondrocytes to regenerate damaged tissue may be impaired. The findings of the present experiment demonstrated various changes in the cellular dimensions and mechanical

properties of chondrocytes grown in monolayer cultures, including an increased stiffness of chondrocytes with increasing cell passages. Such changes are likely to be linked to alterations in the actin cytoskeleton and hence the dedifferentiation of the cells towards a more fibroblastic phenotype leading to the ultimate production of inferior repair cartilage.

Chapter 8

DISCUSSION AND FUTURE DIRECTIONS

8. DISCUSSION AND FUTURE DIRECTIONS

8.1 INTRODUCTION

This chapter begins with a critical assessment of the micropipette aspiration technique employed in the experimental work of this thesis, which enabled the measurement of cell mechanics under various experimental conditions.

The next section discusses the present findings to clarify our understanding of chondrocyte mechanics in healthy and diseased states, with a particular emphasis on actin remodelling. This chapter of the thesis describes two additional experimental works. The first collaborative experiment examines the influence of the 3D microenvironment on cell mechanics and actin organisation. This is of particular interest when considering data obtained using micropipette aspiration, which requires cells to be isolated from their normal tissue environment. The following section describes, the influence of a specific actin dysfunction associated with the Bardet Biedel syndrome and how this influences cell mechanics. Subsequently, the implications of micropipette aspiration technique for early diagnosis and treatments are discussed. An analysis of the possible future directions of research is then presented, by aiming at more sophisticated experimental techniques for the measurement of cellular viscoelastic parameters along with the incorporation of finite element analysis, which would enable a better understanding of similar experimental data.The chapter concludes with a summary of the key findings of the thesis in the context of the overall aims and objectives.

8.2 CRITIQUE OF THE DEVELOPED TECHNIQUES

8.2.1 MICROPIPETTE ASPIRATION TECHNIQUE

The micropipette aspiration technique has been used for more than a decade to examine the viscoelastic behaviour of biological cells as reviewed in section 2.3 (Hochmuth, 2000; Jones et al., 1999; Trickey et al., 2000). In the present study, an automated micropipette

aspiration system was successfully developed and optimised to ensure precise temporal control over pressure applied to single cells in conjunction with confocal microscopy. This system enabled the application of a range of pressure rates to chondrocytes to investigate different aspects of their mechanical behaviour. Bovine chondrocytes were selected to be used in the experiments due to the availability of metacarpophalangeal joints from the local abattoir. Additionally they are regularly used to examine many aspects of chondrocyte behaviour in both the host and other laboratories worldwide.

This population of primary chondrocytes isolated from full-depth cartilage tissue represented a combination of cells from different zones of the cartilage. However, it is recognised that this represents a heterogeneous source of chondrocytes, as many aspects of the cell morphology and function vary with the cartilage zone (section 1.4.2). It has been reported that cell of the superficial zone are smaller than cells from deep zone. However approximately 40% of the total cell yield is obtained from superficial tissue and 60% of the total cell yield obtained from deep tissue after isolation (Lee et al., 1998). The median value of the diameter of freshly isolated chondrocytes is 12.4 μm with lower and upper quartile being 13.8 μm and 11.0 μm respectively.

The ratio of the cell diameter to pipette diameter is crucial for modelling temporal changes in the aspiration lengths of the cell when using the SLS and BSLS models, as discussed in section 3.8.2. The micropipettes used in this study were fabricated in-house to an inner diameter ranging from 6.5 to 7.5 μm. For a chondrocytes with diameter ranging from 11.0 to 13.8 μm, this produces a cell:pipette ratio of 1.7 to 2.1. Clearly, this is below minimum of 3 suggested by Baijens et al (2005). However other pipette aspiration studies on chondrocytes have used similar sized pipettes (Trickey et al., 2000). Furthermore initial experiments showed that approximately 80 % of cells did not aspirate when pipette smaller diameters were used (Figure 3.14). It is possible that the poor aspiration with smaller diameter pipettes is due to friction between the cell and the pipette wall, despite the use of Sigma coating. Friction may also explain why the SLS and BSLS models were unable to model the cellular response in some cases, resulting in very high k_2 values (further discussed in section 8.2.4). The friction between the pipette wall

and the cell invalidates the assumption of zero friction associated with the wall parameter used in the SLS and BSLS models (section 2.3.2). Therefore future experiments might look to improve the applications of the Sigma coating which would enable the use of pipettes with smaller diameters thereby satisfying the requirement of the SLS and BSLS model. However even with an optimised Sigma coating, it is likely that the friction component may not be constant and that future analytical models need to incorporate the possibility of static and dynamic friction at the cell-pipette interface.

The chondrocyte cell membrane is known to exhibit a ruffled morphology (Guilak et al. 2002). Consequently the bending rigidity associated with the unravelling of these membrane folds may contribute to the mechanical properties of the cell. The present studies utilised a tare pressure of 1 cm of water to ensure that the cell was attached to the micropipette forming a complete seal necessary for the aspiration protocol. The tare pressure resulting in small degree of cell aspiration is likely to reduce the subsequent impact of membrane bending rigidity on the aspiration length and the calculation of cell moduli and viscosity.

Using the aspiration technique described in this study, only single chondrocytes in suspension can be tested. However, chondrocytes are located within the pericellular matrix which is in turn surrounded by the territorial and inter-territorial matrix (see section 1.2). Recent studies from colleagues Chen et al. (2012) described in detail in section 8.4, suggested that the mechanical properties of the 3D microenvironment influence chondrocytes mechanics. Thus moduli of chondrocytes in situ within articular cartilage may be larger than that estimated for isolated chondrocytes in suspension using micropipette aspiration.
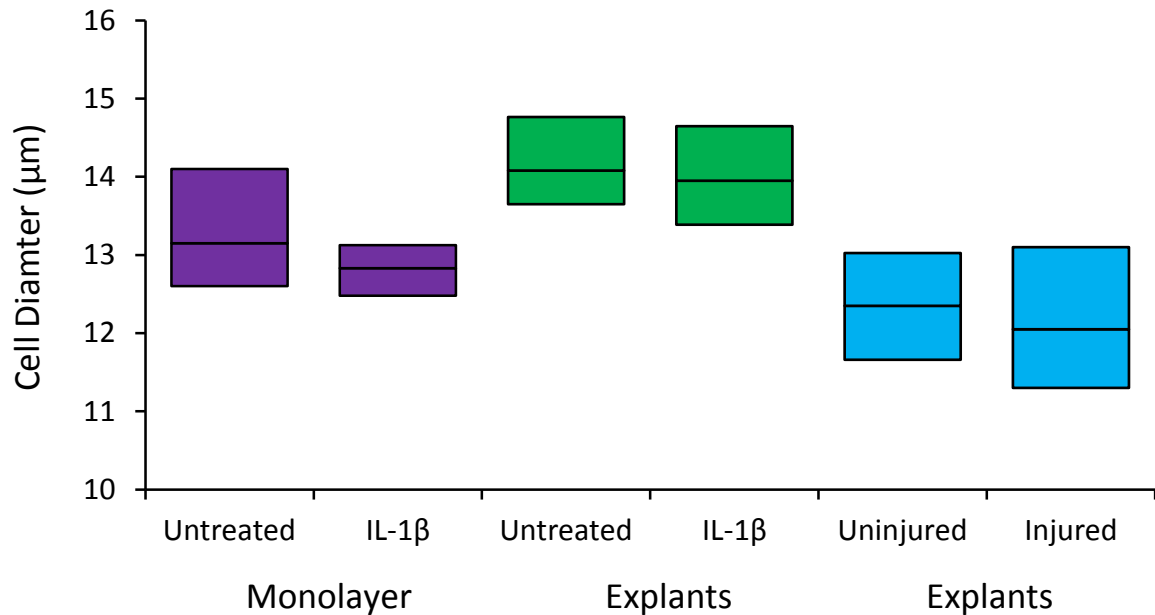
Figure 8.1. *The diameter of the chondrocytes obtained from different test conditions.*

Figure 8.1 presents the median and interquartile values of the chondrocytes diameter obtained from primary cells and those cultured in monolayer cartilage explants with or without cytokine treatment or mechanical trauma. The diameters of the chondrocytes obtained from the untreated IL-1β and mechanically uninjured articular cartilage explants were significant different ($p < 0.05$) possibly due to animal to animal variation and differences in the relative amount of surface and deep tissue. Furthermore previous studies have reported differences in the moduli of chondrocytes isolated from the superficial and deep zones (Shieh and Athanasiou, 2006). The mean value of instantaneous modulus for the superficial cell is greater than the deep zone cells (see section 2.4.2). These differences may be partly caused by the differences in the moduli of surrounding pericellular matrix as previously reported (Guilak et al., 2005). However no correlation was observed between the cell diameters and mechanical properties of the P0 obtained at pressure rate 5.48 cmH_2O/s (Figure 8.2).
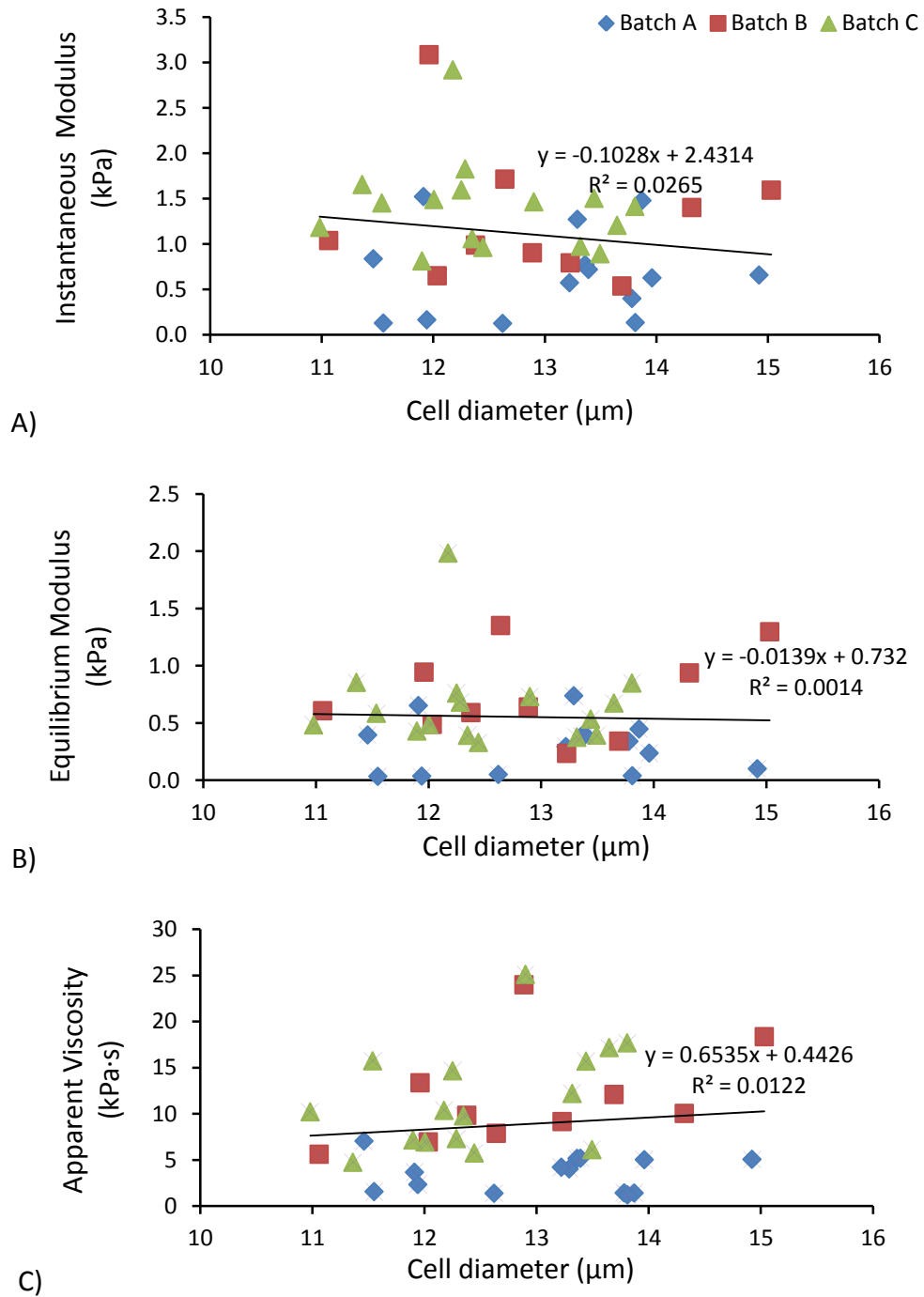
***Figure 8.2**. The relation between the viscoselastic parameters, A) instantaneous modulus, B) equilibrium modulus and C) apparent viscosity and cell diameters of P0 cells aspirated as pressure rate 5.48 cmH$_2$O/s.*

8.2.2 GFP-ACTIN TRANSFECTION

In chapter 5, primary chondrocytes were transfected using GFP-actin. As shown in Figure 5.6 responses of transfected and non-transfected chondrocytes differed at an aspiration pressure rate of 0.35 cmH$_2$O/s. Although it has been demonstrated that the organization of actin is not affected by GFP-actin transfection (Deibler et al., 2011), the dynamics of actin were observed to be altered in the present study (Figures 5.12 and 5.13). By contrast Riedl et al. (2008) demonstrated that actin dynamics did not alter when cells were transfected using LifeAct. However LifeAct was not employed in the present study because of its unavailability during time of the experiments. But future studies should consider using this method for GFP-actin transfection and visualisation as LifeAct is made recently economically available.

8.2.3 COMPUTATION OF CELL SURFACE AREA AND VOLUME

In the present study, the surface area and volume of the chondrocytes were computed before and after aspiration. This enabled the calculation of the percentage changes in both the surface area and volume of the cell after aspiration. These measurements provide insights into the morphological changes in chondrocytes following aspiration as well as an improved understanding of chondrocyte behaviour following the application of external mechanical stimuli.

The morphological properties were computed using the formulae detailed in the section 3.6.4. The cell is initially assumed to be completely outside the pipette and therefore to be spherical. However, to ensure contact between cell and the micropipette, a tare pressure of 1 cmH$_2$O was applied, which resulted in a small aspiration into the micropipette. The equations for surface area and volume were based on the assumption that the cell is spherical in the pre-aspiration stage and that the leading edge of the aspirated cell is hemispherical in form with a diameter equivalent to that of the inner diameter of the micropipette. However during aspiration, some cells showed irregular blebbing as the cell membrane detaches from the cortical actin (Figure 5.13). Thus, the leading edge of the cell was not equivalent to a half-hemisphere. These variations may

214

have potentially resulted in an overestimation of the morphological properties of the cell and the corresponding post-aspiration changes therein.
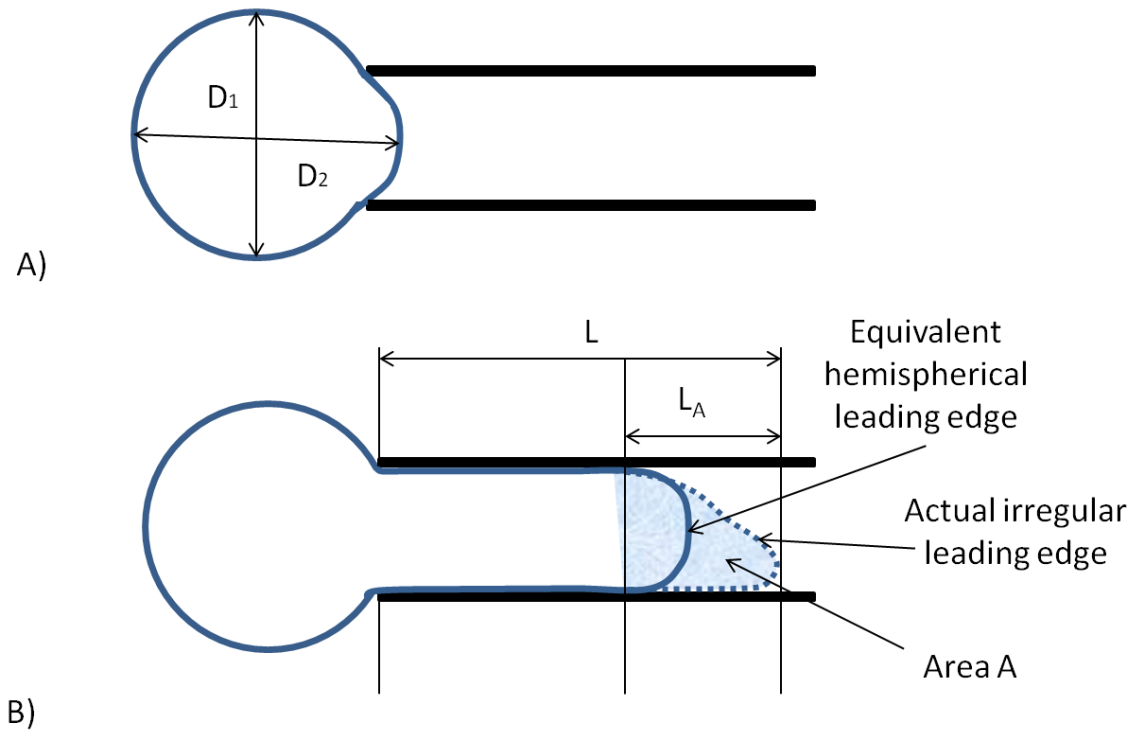
Figure 8.3. Schematic of cell being aspirated into the micropipette. A) pre-aspiration with tare pressure and B) post aspiration.

These inaccuracies in surface area and volume could be reduced by calculating an equivalent hemispherical radius by measuring the cross-sectional area A (Figure 8.3B). In addition, the volume and surface area measurements could also be improved by obtaining two orthogonal measurements for the cell diameter outside the pipette (D_1 and D_2) Figure 8.3A.

$$Cell\ Surface\ Area = \left(D_1 + D_2\right)^2 \pi + \pi D_p \left(L - L_A\right) + \left(\frac{\pi r_A^2}{2}\right) \qquad Equation\ 8.1$$

$$Cell\ Volume = \frac{4\pi}{3}\left(\frac{D_1 + D_2}{3}\right)^3 + \frac{\pi D_p^2}{4}\left(L - L_A\right) + \frac{4}{6}\pi r_A^3 \qquad Equation\ 8.2$$

$$Where\ r_A = \sqrt{\frac{2A}{\pi}}$$

8.2.4 VISCOELASTIC MODELS

The viscoelastic models SLS and BSLS have been traditionally used to compute the mechanical properties of the cells. As evident from the results presented in Figures 4.8, the BSLS model was determined to be more appropriate for the computation of the mechanical properties of the cell when aspirating at lower pressure rates. Indeed modelling of the temporal changes in the aspiration lengths in MatLab resulted in the generation of three parameters, namely k_1, k_2 and μ. These parameters were then used to compute the instantaneous modulus, equilibrium modulus and apparent viscosity of the cell (equations 2.5, 2.6 and 2.7), respectively. The k_2 represents the elastic component, whereas k_1 and μ represent the viscous component of the model. Figure 8.4 represents the changes in the k_2 values with the preset limit for four representative cells. It can be noted that for cells 1-3, the generated value of k_2 is substantially greater than 100, while for cell 4, k_2 is less than 100, and remains constant even at increased values of the preset limit. k_2 was thus suggested to be very sensitive to the initial deformation response of the cell.

In the present study, the limit for k_2 was set at 1×10^{12}, where the computed values of the k_2 did not change as shown for the 4 representative cells in figure 8.4. The cells for which the value of k_2 reached this preset limit were rejected from the analysis of subsequent mechanical parameters. In most cases this limit was not reached. However, as shown in Table 7.1, a relatively high proportion of cells were rejected from the analysis particularly for P0 aspirated at 5.48 cmH$_2$O/s, as well as for the chondrocytes obtained from EGTA-treated explants aspirated at 0.35 cmH$_2$O/s (also see Table 5.1). One of the reasons for the k_2 value reaching the preset limit is that the SLS and BSLS models assume that each cell represents an infinite, homogenous and incompressible half-space under a pressure gradient (Figure 2.10). This assumption is only valid if the ratio of the cell-to-micropipette radii is greater than 3. Moreover, following aspiration, a significant increase in the cell volume was also observed. The SLS and BSLS models could not incorporate the finite size of the cell, the changes in the cellular response, particularly those related to volume, and therefore were unable to accurately model the data without exceeding the preset limit. It

216

is also possible that the poor fit and inability to calculate k_2 may be due to the friction at the cell-pipette interface which invalidates the use of the simple wall parameter in the SLS and BSLS models as discussed in section 2.3.2. This problem with estimation of k_2 remains a problematic feature of the combined experimental and computational approach.
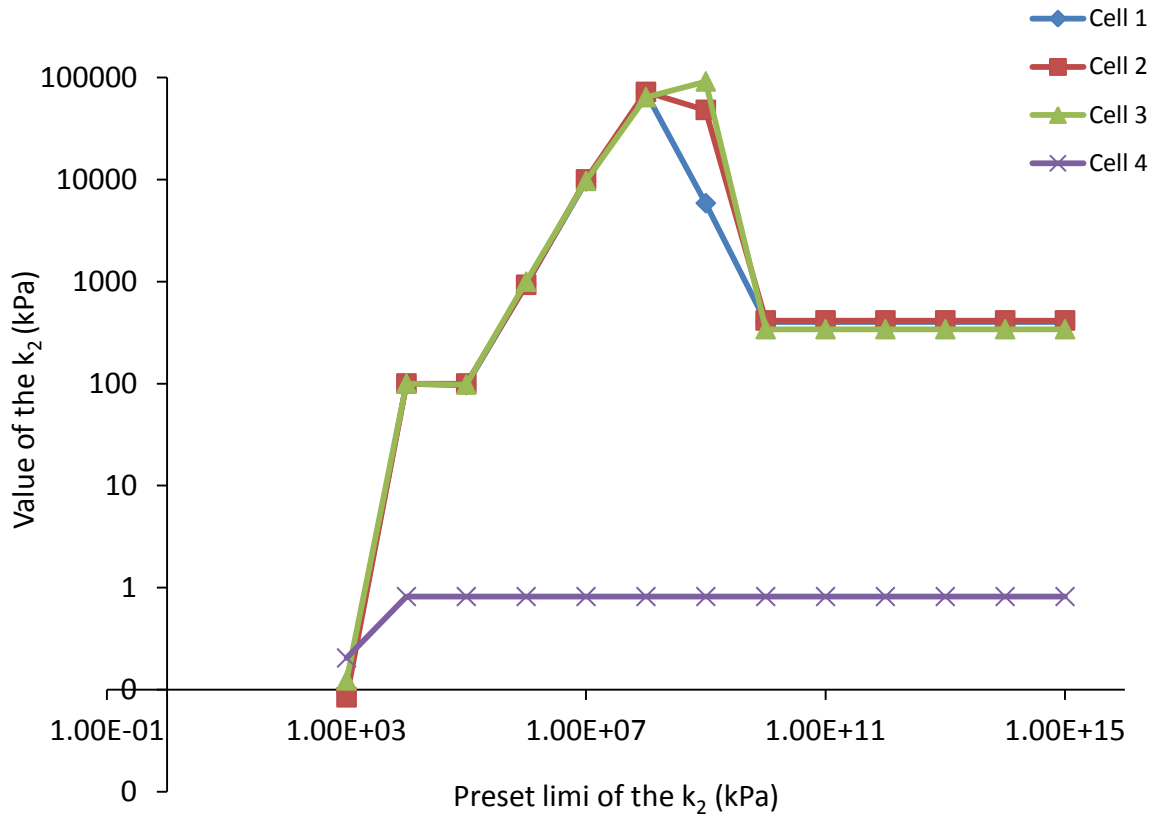
Figure 8.4. *Changes in the k_2 value in relation to the predicted limit of k_2 for four individual cells*

8.3 T<small>HE</small> B<small>IOMECHANICS AND</small> M<small>ORPHOLOGY OF</small> C<small>HONDROCYTES</small> S<small>UBJECTED</small> <small>TO</small> P<small>IPETTE</small> A<small>SPIRATION</small>

The viscoelastic parameters of the chondrocytes decreased with an increase in the pressure, regardless of the model used to compute these parameters, i.e. SLS or BSLS. This reduction in the moduli was associated with cortical actin remodelling, as described in sections 5.3.3. The cortical actin of the chondrocytes showed characteristic viscoelastic behaviour (Figures 5.12 and 5.13). At slow pressure rates, the cell is gradually drawn into

the pipette (Figure 5.12), and cortical actin deforms with time (Figure 8.5A-B), eventually reaching an equilibrium state. However, at faster aspiration rates, the membrane detaches from the cortical actin (Figure 8.5C), leading to cell swelling due to the osmotic pressure, since the restraining force on the actin has been eliminated (Figure 8.5D). This is evident by the increase in the cell volume (Figure 5.5A) and the results of previous studies that report increases in chondrocyte volume following disruption of actin with cytochalasin D (Orek et al., 2009).

The loss of actin tension also cause actin breakdown and subsequent remodelling, as seen in Figure 5.13 also in Figure 8.5E-F. The subsequent cell swelling results in an increased aspiration length and an apparent softening of the cell. In contrast, at a slower aspiration rate, adequate time is available for actin remodelling, thereby preventing both detachment of the membrane and bleb formation. Therefore, for an improved insight into cell mechanics, micropipette aspiration should be performed using a slow aspiration rate, in contrast to the majority of previous chondrocytes based studies (Jones et al., 1999; Trickey et al., 2000) which have been performed using faster aspiration rates as required by the SLS model.

A) Before aspiration swelling of the cell due to the existing osmotic gradient across the cell membrane is restrained by the cortical actin and linkage with cell membrane.

D) A membrane bleb forms due to osmotic pressure as the swelling pressure is no longer restrained by attachment to the cortical actin. Thus the cell volume increases with increasing aspiration length leading to a apparent softening of the cell.

B) The cell is aspirated into the pipette involving cortical actin deformation and/or remodelling.

E) The cortical actin breakdowns and depolymerises at the original leading edge due to loss of tension.

C) The membrane is physically detached from the cortical actin particularly at fast aspiration rates.

F) The cortical actin repolymerises at the new leading edge formed by the membrane bleb. Thus the cell does not return to its original spherical morphology once pressure is removed.

Figure 8.5. Schematic diagram showing suggested mechanisms regulating cell deformation and structural reorganisation during pipette aspiration.

8.4 EFFECT OF MICROENVIRONMENT ON CELL MECHANICS

The micropipette aspiration technique provides an estimate of the mechanical properties of isolated cells in suspension. However, *in vivo*, the majority of cell types, including articular chondrocytes, exist within a 3D extracellular matrix microenvironment. A series of studies have therefore been conducted to test the hypothesis that cells within 3D

culture exhibit different mechanical properties to those reported for cells in suspension and these properties are modulated by the modulus of the microenvironment (Chen et al., 2012) This work, conducted in the host laboratory, used computational modelling to estimate cell mechanics based on measurements of cell deformation in compressed 3D hydrogels of different moduli. Linear elastic and hyper-elastic models suggested that chondrocytes in low-modulus alginate or 1% agarose gels exhibited equilibrium or Young's modulus of approximately 5.3 kPa. This represents a notably increased value for modulus of isolated chondrocytes in suspension to that reported in previous papers (Bader et al., 2002; Ohashi et al., 2006; Trickey et al., 2004). Furthermore, in the stiffer 3% agarose gels, the estimated cell modulus was significantly enhanced with a predicted value of at approximately 20 kPa.

Additional studies were conducted to determine whether these differences in cell mechanics were associated with differences in cortical actin cytoskeletal organisation, which is known to influence cell mechanics. These studies also examined the timescales over which changes in actin organization occurred following seeding of isolated chondrocytes into 3D agarose constructs. Bovine articular chondrocytes were isolated, as previously described in section 3.6.2, and seeded either in 1% or 3% agarose (w/v, type IX, Sigma). After 1, 5, 18 and 24 h in culture, the agarose-cell constructs were fixed in 4% formaldehyde (15 min at 37°C) and stained with Alexa 564-Phalloidin. The constructs were then washed in PBS and visualised using confocal microscopy (Leica SP2). Single chondrocyte images were obtained by bisecting the centre of individual cells in 1% and 3% agarose specimens using the same imaging settings throughout.

The mean intensity of the cortical actin was quantified by measuring the cortical intensity, within a beigel region of interest (ROI) incorporating two concentric circles—the outer circle around the periphery of the cell and the inner circle at a distance of 1 μm from the outer circle. The mean Alexa-Phalloidin intensity within the ROI represented the level of the cortical actin staining. The cortical actin ratio was obtained by normalising the cortical actin intensity to the mean cytoplasmic intensity within the inner circle in an identical manner to that previously reported (Erickson et al., 2003).

Chondrocytes in both 1% and 3% agarose exhibited cortical actin staining, as previously observed, in situ within articular cartilage explants (Blain, 2009). Although in the first 5 h of culture, only minimal changes in cortical actin intensity were observed, by 18 h, significant changes were evident in the agarose concentrations (p < 0.001, Figure 8.6B). Close examination of the images revealed a greater cortical actin staining intensity associated with the 3% agarose constructs, with a punctuated cortical actin ring clearly evident (Figure 8.6A). Thus, changes in the surroundings of the chondrocytes, as simulated with the varying agarose concentrations, appeared to be directly or indirectly translated to the intracellular structures that modulate cell mechanics.
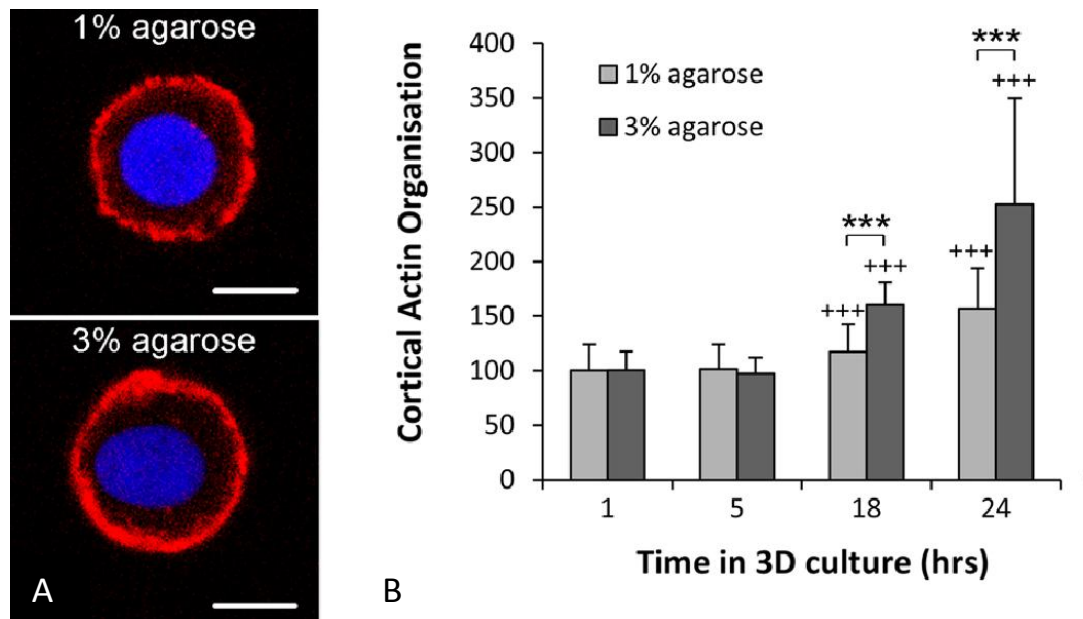
Figure 8.6. *(a) Confocal section image of the chondrocytes after 24 h in 1% and 3% agarose. Nuclei are labelled with Hoescht (blue); and F-actin, with Alexa 564-Phalloidin (red). Scale bar represents 5 μm. (b) The increase in the cortical actin ratio with time in culture. At 18 and 24 h, the intensity for the cells in 3% agarose was greater than that in 1% agarose (p < 0.001, ***). The intensity values are presented as the mean with error bars indicating SEM (n = 40–80).*

8.5 INFLUENCE OF ACTIN GENETIC MUTATION ON CELL MECHANICS

8.5.1 INTRODUCTION

The Bardet-Biedll syndrome (BBS) is a genetic disorder associated with obesity, cognitive impairment and kidney dysplasia (Slavotinek et al., 2000). This is associated with mutations in at least 15 BBS genes (Harville et al., 2010). It has been shown previously that the associated BBS proteins are required for primary cilia formation and cell motility (Kim et al., 2004; Tobin et al., 2008). Studies by Prof. Beales' group at the Institute of Child Health, London, have revealed that the organisation of the actin stress fibres is disrupted in Bbs4-/- renal medullary cells (Hernandez-Hernandez et al., 2012) (Figure 8.7A). The present study examined whether differences in actin organisation between wild-type (WT) and Bbs4-/- cells in monolayer were associated with changes in cellular mechanical properties. The micropipette aspiration technique described in section 4.2.1 was used to examine the mechanical properties of cells in suspension. Subsequently, studies were conducted to examine whether differences in actin organisation in the monolayer persisted when cells were trypsinised.

8.5.2 METHODS

To visualise actin distortion during aspiration, the WT and Bbs4-/- cells were transfected with GFP-actin following methods similar to those described in section 5.2.1. The cells were aspirated at a pressure rate of 5.48 cmH$_2$O/s up to a maximum pressure of 7 cmH$_2$O. Additionally, Bbs4-/- cells were treated with the RhoA inhibitor, Y27632, prior to micropipette aspiration. The temporal changes in the aspiration length were modelled using the BSLS model to derive three viscoelastic parameters, namely, instantaneous modulus, equilibrium modulus and viscosity.

8.5.3 RESULTS

In the WT cells, regularly organised stress fibres were observed (Figure 8.7A). In contrast, in the Bbs4-/- cells, the actin was disorganised, especially in the apical region. However, in suspension, there was no difference in the actin organisation between the WT and Bbs4-/-

cells, which both showed cortical punctuate actin organisation (Figure 8.7B). The WT and Bbs4-/- cells treated with Y-27632 both exhibited a reduction in the actin aggregate formation in the monolayer culture, as shown in Figure 8.8. This inhibitor prevents actin polymerisation. However it was also observed that the actin organisation (Figure 8.8) and primary cilia length (data not shown) in Bbs4-/- cells were restored. Pipette aspiration successfully determined the mechanical properties of the WT cells and Bbs4-/- cells with and without treatment with Y27632. Representative plots showing the temporal changes in the aspiration length are shown in Figure 8.9, which reveal the characteristic viscoelastic response demonstrated by chondrocytes throughout this thesis.
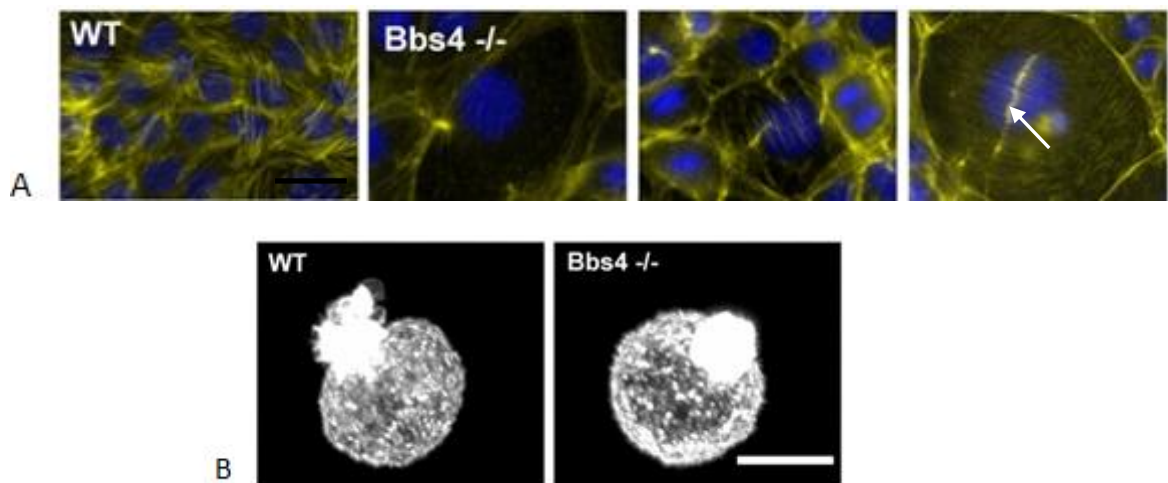
Figure 8.7. *Actin organisation in WT and Bbs4-deficient cells in (A) monolayer, an arrow showing the formation of the actin scare in the apical region of the cell and (B) suspension. Cells in monolayer show actin labelled with GFP whilst those in suspension have been stained with rhodamine-Phalloidin. Black scale bar in A, 50 μm; white scale bar in B, 20 μm.*
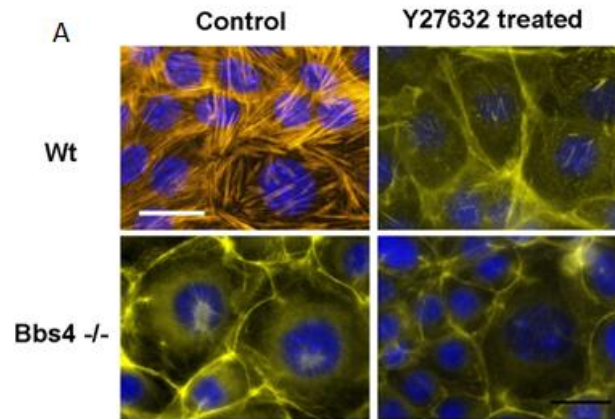
Figure 8.8. *Reduction in the stress fibres aggregate formation in Bbs4-/- cells following treatment with the RhoA inhibitor, Y27632. Scale bar, 30 μm.*
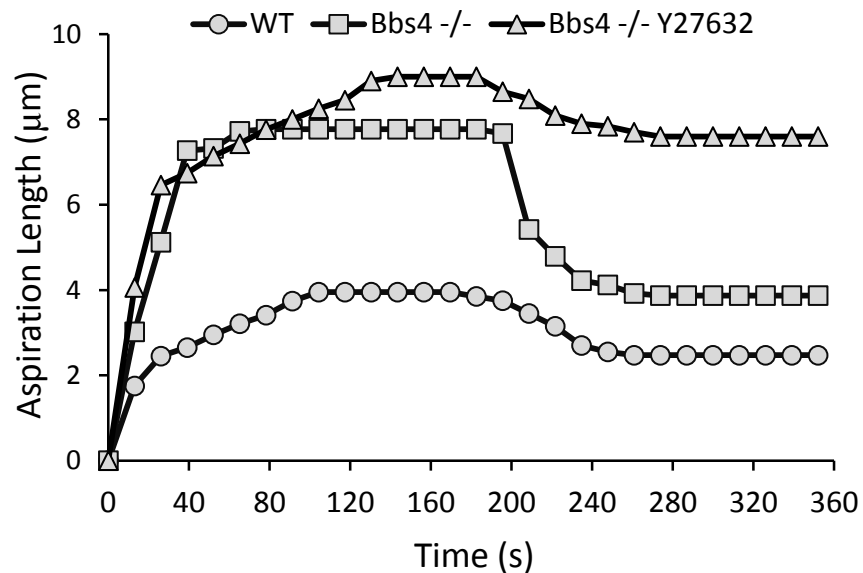
Figure 8.9. *Temporal changes in the aspiration length with recovery of the wild-type (WT) cells, Bbs4-deficient cells and Bbs4-deficient cells treated with the Y27632 RhoA inhibitor.*

The maximum and recovery aspiration lengths for the samples of cells tested from the three experimental groups are illustrated in Figure 8.10. It is evident that cells from all three groups showed a reduction in the aspiration length once the pressure was removed,

224

as reflected by statistically significant differences between the recovery and maximum aspiration lengths (p < 0.05 in all three cases) (Figure 8.10).
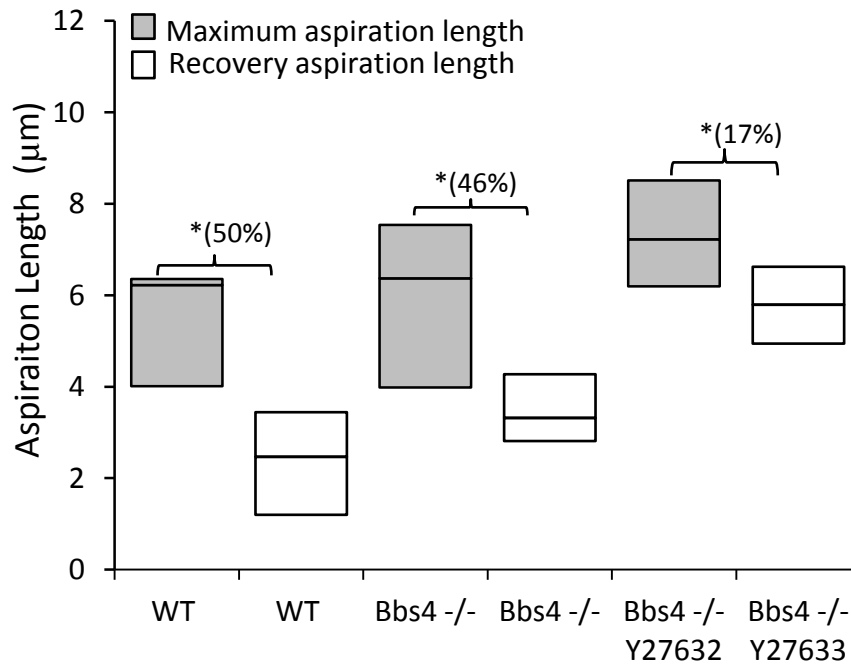
Figure 8.10. *Median and quartile values for cells subjected to the aspiration pressure of 7 cmH$_2$O applied at 5.48 cmH$_2$O/s. A statistically significant decrease in the aspiration length was observed for all the cells during the recovery period (*, p < 0.05). The median percentage recovery of the aspiration length is given in parentheses.*

For analysis of micropipette aspiration data using the BSLS model, exclusion criteria were applied as described in section 4.3. The resulting numbers of cells are shown in Table 8.1. It can be noted that very small percentage of the cells were aspirated in the case of wild type as well as Bbs 4 -/- Y27632 cells. Native renal medullary cells had an instantaneous modulus of approximately 4 kPa, an equilibrium modulus of approximately 0.5 kPa, and a viscosity of 15 kPa (Figure 8.11). These values are broadly similar to those found for articular chondrocytes as reported in this thesis and in previous studies. No statistically significant differences were found between WT and the Bbs4-deficient cells for any of the

viscoelastic parameters. Similarly, there were no differences between the Bbs4-deficient cells with and without treatment with Y27632 (Figure 8.11).

Table 8.1. *The number of cells accepted for each experimental condition. Percentage values represent the number of cells successively analysed using BSLS models.*

Experiment	Total No. of Cells	Cell Aspiration	Convergence	R ≥ 0.95	$k_2 < 100$
Wild Type	14	11	7	6	4 (29%)
Bbs 4 -/-	13	12	11	11	9 (69%)
Bbs 4 -/- Y27632	14	9	7	7	5 (36%)
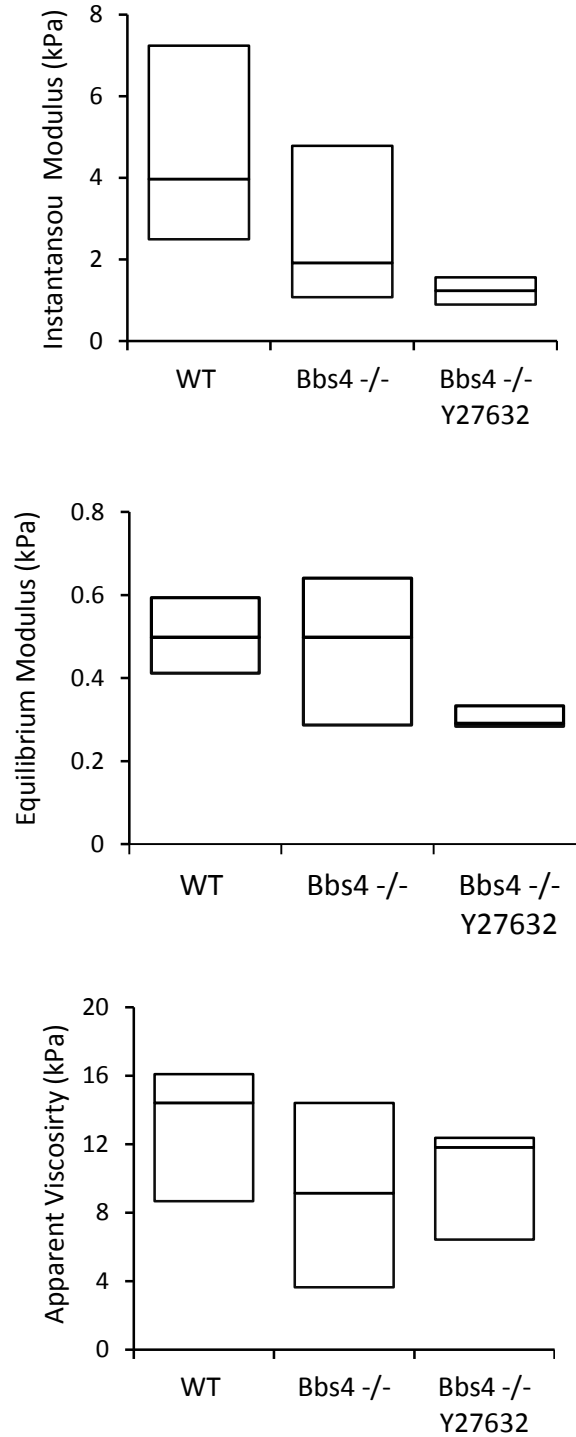
Figure 8.11. *No significant difference (p > 0.05) was observed in instantaneous modulus, equilibrium modulus and apparent viscosity between wild-type (WT) and the Bbs4-deficient cells or between the Bbs4-deficient cells and Bbs4-deficient cells treated with the Y27632 RhoA inhibitor.*

8.5.4 DISCUSSION

Bbs4 appears to regulate actin stress fibre organisation in monolayer culture leading to alterations in cell function. However, the present biomechanical findings studies suggest that the cortical actin organisation, and hence the mechanical properties of the cells, are unaffected by the loss of Bbs4. However the mechanical properties of the cells were based on small percentage of cells particularly in case of wild type and Bbs 4-/- Y27632 (Table 8.1). It has been assumed that cell mechanics may be used as a diagnostic indicator to reveal changes in cell structure and function associated with disease or injury. In particular, cellular mechanical properties are sensitive to changes in actin dynamics as demonstrated in chapter 5. Additionally the mechanical properties of the chondrocytes changes with expansion the chondrocytes in monolayer with time as discussed in chapter 7. The changes in the actin cytoskeleton with formation of stress fibers are reflected in the mechanical properties of the passaged chondrocytes.

 However, the present results with Bbs4-/- cells indicate that although cell mechanics are heavily dependent on actin organisation and dynamics, this is specific to cortical actin rather than the stress fibres or other forms of actin structures. Hence, the mechanical properties of cells provide a more selective indicator of actin behaviour and cellular structure-function. It would be interesting to examine whether cells in monolayer show differences in the mechanical properties associated with the differences in actin stress fibre organisation. However, mechanical testing of cells in the monolayer is not possible with the pipette aspiration and BSLS modelling approach.

8.6 IMPLICATIONS FOR EARLY DIAGNOSIS AND TREATMENT OF OSTEOARTHRITIS

The deviation of stem cells from the 'mechano niche' causes differentiation and alterations in the cellular function (Lee et al., 2011), which may be regulated by the mechanical parameters of cells. This basic principle could also be applied to chondrocytes,

whereby cellular behaviour may be considered to be governed by biochemical parameters such as external mechanical stimuli, mechanics of the extracellular matrix and the mechanical properties of the cell. These parameters are interrelated and regulate the normal functioning of the cell (Lee et al., 2011). Therefore, physiological loading of articular cartilage is essential for the normal functioning of the chondrocytes. As seen from Figures 4.8, the rate at which chondrocytes are subjected to loading affects the mechanical properties of the cells.

In the present study, it has been demonstrated that IL-1β treatment and mechanical injury to cartilage explants causes changes in the mechanical properties of the chondrocytes isolated from these explants. This is possibly due to a disruption in the 'mechano niche' of the chondrocytes, caused by changes in the micromechanical environment by either IL-1β treatment or mechanical injury. It should be noted that significant differences have been reported in the mechanical properties of non-OA and OA cells (Trickey et al., 2000), using techniques similar to those used in the present study. These findings indicate that the mechanical properties of chondrocytes are critical for their normal functioning. The micropipette aspiration and analysis technique developed here could provide the means for early detection of osteoarthritis by testing the mechanical properties of the cells obtained from tissue biopsy. Such a test could also provide information regarding the progression of the disease as well as its response to therapy.

The present study analysed the effects of the pressure rate, biochemical and mechanical trauma, and cell passage on the chondrocytes' mechanics. In each case, the mechanical properties of the cells were observed to be altered. The changes in the mechanical properties of the cells can be attributed to the changes in the F-actin of the cell (section 5.4.2). Actin organisation in the normal and diseased cells is known to be different (Capin-Gutierrez et al., 2004). It is possible that the above mentioned factors induce changes in the actin cytoskeleton through a specific target molecule. If this target molecule is identified, it can be manipulated pharmacologically in order to reverse the pathological changes in the actin cytoskeleton. Recently, this has been achieved by magnetic manipulation of actin orientation and polymerization *in vitro* (Chen et al., 2011). This

technique could be the first step towards the development of a truly effective treatment for OA whereby the changes in the diseased cell are reversed, and the disease progression is halted at the cellular level.

One of the techniques currently used to the treat osteoarthritis is autologous chondrocytes transplantation, which involves the expansion of cells in monolayer followed by their subsequent implantation in the patient, as described in section 1.6.3. However, it is evident from the findings presented in chapter 7 that serial expansion of the chondrocytes in monolayer leads to alterations in the mechanical properties of the cells. As discussed in section 7.4.2, the chondrocytes in a monolayer adopt a more fibroblastic morphology accompanied with increased proliferation (Brodkin et al., 2004). Therefore, the implanted cells would not exhibit mechanical properties similar to those of primary native chondrocytes. However, diseased OA cells could be altered to normal healthy cells by actin manipulation, as mentioned above, and transplanted into a scaffold for tissue regeneration and transplantation. Additionally, actin manipulation could also take into account the zonal variations in chondrocyte morphology, possibly enabling tissue regeneration that potentially resembles the heterogeneous structure of native tissue structure. This implication is not only important for autologous chondrocytes transplantation, but also for the other cell-based strategies associated with tissue engineering/regenerative medicine.

8.7 Future Directions

8.7.1 Microfluidics

Although the micropipette aspiration technique is a powerful and versatile tool (see section 2.2.7), it has two major drawbacks. First, specific skills are required in the manufacture and polishing of individual micropipettes. Additionally, the aspiration of a single cell one of a time represents a time-consuming process, particularly when a large group of cells are to be aspirated. To address these drawbacks, the microfluidic system

(Abdelgawad, 2010; Kim, 2010) has been developed through which multiple cells can be deformed simultaneously, with single-cell resolution. This system does not require the usage of the micropipette, thereby eliminating the need of expertise in the manufacturing of the micropipettes. In this device, micro-aspiration channels are created on a chip that is composed of several cell traps. Once all the traps are filled with cells, the negative pressure is applied simultaneously. Similar to the traditional analysis of micropipette aspiration data, the SLS model (Sato et al., 1990) has been used in this technique.

The use of the microfluidic system would certainly increase the output of cellular data from a significant cell population. One of the limitations of this technique is the square channels for the aspiration of the cells as this could for poor seal. Additionally if higher pressure is used to trap the cell, it could undergo lysis (Abdelgawad, 2010). However various research groups have come up with the ways to produce circular channels including back side UV exposure (Futai et al., 2004) and casting polydimethylsiloxane on wire (Jia et al., 2008). Although these techniques produce semicircular channels, it requires the bonding of two micro channels to form circular channel. These are impractical solutions to form a complex microfluidic system and expensive manufacturing process. Furthermore these micro channels will be required to coat with Sigma coating to prevent cell adhesion. Additionally due to the scale of this device, the aspiration images obtained using this technique could result in low-resolution images. Therefore, this technique requires further development to be used successfully in the experimental conditions.

8.7.2 SURFACE AND DEEP ZONE CELLS

The morphology of the chondrocytes obtained from the surface and deep zones of the cartilage is different. Accordingly, mixed population of cells this may have greater proportion of the deep zone chondrocytes. The mean value of instantaneous modulus for the superficial cell is greater than the deep zone cells (Shieh and Athanasiou, 2006) (see section 2.4.2). Additionally variation in the actin structure is also seen in the chondrocytes from different zones. Therefore it will be interesting to the investigate the zonal effect on

the mechanical properties of the chondrocytes obtained from explants treated with the IL-1β and mechanically injury. The isolation of the chondrocytes from superficial zone and deep zone of the cartilage has been previously performed (Heywood et al., 2010).

8.7.3 AUTOMATED MEASUREMENT OF THE ASPIRATION LENGTH

In each individual experiment, the aspiration lengths of the cell into the micropipette were analysed, and their temporal changes were estimated using LCS Leica software. Although this is a simple technique, the manual measurement of the aspiration lengths was fairly time consuming. In the future, it would be ideal to develop a protocol using MatLab, or an alternative software package, for the analysis of temporal changes in the aspiration lengths of cells into the micropipette. This would eventually allow the development of a completely automated technique for analysing micropipette aspiration data.

8.7.4 FINITE ELEMENT MODELLING

To estimate the mechanical properties of the chondrocytes from the micropipette aspiration data, the SLS model (Sato et al., 1990) has been traditionally used for analysing the deformation history of the cell. In this model, a cell is considered to be an infinitely large half-space that is incompressible. However, the cell volume increases during aspiration, particularly at faster aspiration rates (Figure 4.7). In the present study, the ramp timing was incorporated into the cell mechanics analyses by using the BSLS model. However, to further address the limitations of the SLS and BSLS models such as those pertaining to cell size, deformation and compressibility, a finite element model for the single cell has been developed (Baaijens et al., 2005; Bidhendi and Korhonen, 2012a; Zhao et al., 2009).Furthermore, in host laboratory Chen et al. (2012) developed a the finite element model to investigate the micromechanical environment of the single cell. Finite element models account for geometric constraints and nonlinearities, boundary conditions and material nonlinearities; therefore, these models are recommended for future studies. As seen in Section 8.3, the pressure rate response of the cell is regulated by the remodelling of the actin cortex. It is evident from Figure 5.13 that the detachment of

the membrane from cortical actin plays a crucial role in governing the cell mechanics (Brugues et al., 2010). Therefore, the finite element model would need to incorporate the actin cortex, the bond between the cortex and the membrane as well as the swelling pressure of the cell to yield more accurate and realistic results.

8.7.5 REPEAT ASPIRATION MODELLING

In the present study cells appeared stiffer when aspirated at 0.35 cmH$_2$O/s compared to 5.48 cmH$_2$O/s. In order to test whether this effect was due to a stiffening of the cell caused by the slower aspiration rate, further studies tested cells after slow aspiration by performing a second aspiration (see section 4.3.2). The first aspiration was performed at a pressure rate of 0.35 cmH$_2$O/s and the second aspiration was performed at either 0.35 cmH$_2$O/s or 5.48 cmH$_2$O/s. However, it was not possible to use the SLS and BSLS models to compute the mechanical properties of the cells from the second aspiration. This was because the cells did not fully recover after first aspiration and therefore stated in deformed state such that at t = 0 the aspiration length was greater than zero. A finite element model therefore incorporates this protocol and accurately models the experimental data needs to be developed. Such analyses are expected to provide further insight with regard to the mechanisms underlying actin remodelling.

8.8 GENERAL SUMMARY

This thesis presents the optimization and development of the micropipette aspiration technique for applying precise and controlled pressure on single chondrocytes. A series of experiments were constructed using this technique to further investigate the effect of pressure rate, cytokine-induced injury, mechanical injury, and cell passage on the mechanical parameters reflecting the viscoelastic behaviour of chondrocytes. The main findings of the present study are summarised below.

- Morphological properties of chondrocytes undergo alterations following micropipette aspiration.

- The BSLS model is a versatile tool and should be used for analysis when a lower pressure rate is employed.

- With a decrease in the pressure rate, the viscoelastic parameters of the chondrocytes increase irrespective of the models used to compute the parameters (Figures 4.8).

- Distinct variations in the cortical actin with deformation during micropipette aspiration of the GFP-actin transfected chondrocytes were observed, with cortical actin remodelling over time.

- GFP-actin affects the viscoelastic parameters of chondrocytes at lower aspiration pressure rates (Figures 5.6).

- GFP-actin inhibits the pressure-sensitive effect on chondrocytes viscoelastic parameters. This is associated with actin remodelling within the chondrocytes

- Exposure of the cartilage explants to chemical and mechanical injuries induced various alterations in the mechanics of the cultured chondrocytes.

- The mechanical injury model of the cartilage explants is a reasonable representation of the OA tissue rather than the IL-1β treatment of cartilage. Changes in the chondrocytes mechanics due to mechanical injury resemble and represent the changes occurring in OA chondrocytes.

- Morphological and mechanical properties of the chondrocytes undergo alterations with cell passage.

In conclusion, the viscoelastic mechanics of chondrocytes are governed by the rate of mechanical loading of the cells. These changes are associated with actin remodelling.

APPENDIX A – MECHANICAL PROPERTIES OF CHONDROCYTES

Table A.1. Summary of the mechanical properties of the chondrocytes obtained using various techniques.

Cell Type	Method	Model	Material Properties	Reference
Human Chodrocytes				
Non-OA	Micropipette Aspiration	Elastic half-space Standard linear solid	E = 0.65kPa E_{int} = 0.41kPa; E_{eqi} = 0.24kPa; μ = 3.0 kPa.s	Jones et al. 1999 Trickey et al. 2000
OA	Micropipette Aspiration	Elastic half-space Standard linear solid	E = 0.67kPa E_{int} = 0.63 kPa; E_{eqi} = 0.33 kPa; μ = 5.8 kPa.s	Jones et al. 1999 Trickey et al. 2000
Bovine Chodrocytes				
Adult (metacarphalangeal joint)	Micropipette Aspiration	Elastic half-space	E = 0.81 kPa	Bader et al. 2002
	AFM	Elastic half-space	E = 0.97 kPa E_{int} = 0.29 kPa; E_{eqi} = 0.17 kPa; μ = 0.61 kPa.s	Darling et al. 2006
	3D scaffold-cell system	Relaxation in 1% agarose	E = 2.7 kPa	Bader et al. 2002
	3D scaffold-cell	Relaxation in	E = 3.22 kPa	Knight et al.

Cell Type	Method	Model	Material Properties	Reference
system	2% agarose			2002
Distal surface of first metatarsal	Cytoindentation	Elastic half-space Standard linear solid	$E = 1.11$ kPa $E_{int} = 8.00$ kPa; $E_{eqi} = 1.09$kPa; $\mu = 1.5$kPa.s	Koay et al. (2003)
	Cytocompression	Elastic half-space Standard linear solid	$E = 2.55$ kPa $E_{int} = 2.47$ kPa; $E_{eqi} = 1.48$kPa; $\mu = 1.92$kPa.s	Leipzing and Athanasiou. (2005)

E = Youngs modulus E_{int} = Instantaneous modulus; E_{eqi} = Equilibrium modulus; μ = Apparent viscosity

APPENDIX B – MICROPIPETTE FABRICATION

B1   PULLING

The model P-97 Flaming/Brown Micropipette Puller (Sutter Instruments) was used to fabricate micropipettes from glass capillaries (GD-1, Narishinge, UK) as shown in Figure B-1. The system allows programmable control of the pulling parameters which in turn allows fabrication of pipettes of specific dimensions. A program consists of one or more cycles and a cycle consist of four programmable parameters namely: Heat, Pull, Velocity and either Time or Delay.

Figure B.1. Micropipette puller P97 (Oesterle, 2011).

A typical pull cycle in a program could be depicted in diagram as shown in Figure B.2. Once the program is activated by pressing the ' PULL ' switch the heat is turned on. The glass is heated up and the weak pull draws the glass out until it reached the programmed velocity.
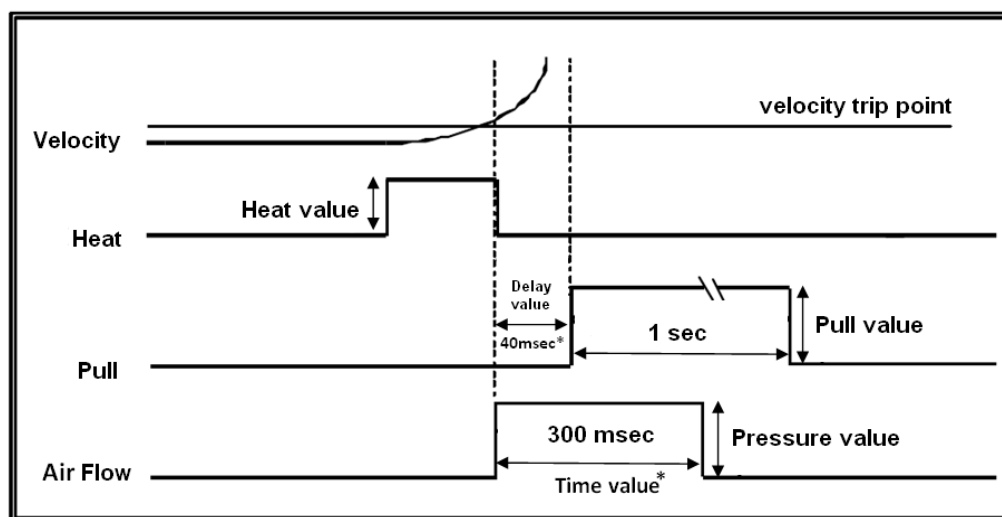
Figure B.2. *Pull cycle when DELAY > 0 and *pull cycle when TIME>0. (Oesterle, 2011)*

The heat is turned off and the air is turned on when the programmed velocity has been reached which is sensed by the velocity transducer. If TIME is > 0 the hard pull (if any) is executed after the delay of 40 msec and the air is activated for the specified TIME, If the DELAY is > 0 the air is activated for 300 msec and the hard pull is activated after specific DELAY (Oesterle, 2011). The description of various parameter is given below.

Heat (Range 0-999):- The level of electric current applied to the filament controls the Heat which is required to melt the glass capillary. The precise level of heating required is verified by ramp test and depends upon the nature of the electric filament and the types of glass capillary employed. The Heat values must be set relative to Ramp test value. The Ramp test allows establishing Heat values as a function of the filament/glass combination.

Pull (Range 0-255):- Higher the pull, the smaller the diameters of the pipette tip and longer the taper.

Velocity (Range 0-255):- When the glass softens and begins to pull apart, the velocity of the glass carriage system is measured under constant load. However, velocity is a function of the glass temperature. A lower value of the velocity is being used for the patch and injection pipettes and higher values for micropipettes.

238

Time (Range 0-255):- Time is one of two available modes of cooling and controls the length of time the cooling air is active. If the velocity is greater than zero then one unit of the TIME represents 1/2ms. If the velocity is zero then one unit of the TIME represents 10ms.

Delay (Range 0-255):- This parameter controls the delay time between when the heat turns off and when the hard pull is activated. The gas is automatically turned on for 300ms. The higher the DELAY values, the cooler the glass will be when the hard pull is applied. Therefore increasing the DELAY results with the decreased taper length and increased tip diameter. If the VEL > 0 then one unit of DELAY represents ½ ms. If the VEL=0 then one unit represents 10ms.

B2   PULL CYCLE

To generate reproducible program to pull pipettes, pipette must be pulled with stable velocity. Therefore to find the stable velocity settings, the entire range of the velocity was investigated for which the program looped the number of times indicated in the general program tables (Oesterle, 2011). The loop was defined as one cycle of the pulling event. To find stable velocity settings for the program looping 4 times, a series of the capillary was pulled while increasing the velocity setting in 2-3 increments until the puller begins to loop 3 times. Similarly, velocity setting was reduced until the puller loops 5 times. Then by using the mid-point of the velocity range, the most stable and reproducible program was created. For the program 61 and box filament 3mm x 3mm the velocity chart is shown below.

Table B.1. Velocity chart

Velocity	20	22	24	26	28	30	32	34	36	38	40
Loop	5	5	4	4	4	4	4	4	3	3	3

The stable velocity for the Program 61 was 30. The example of a program used to pull pipette is shown below:

Table B.2. *Example of values used for different parameter for pulling capillaries.*

Heat	Pull	Velocity	Time	Pressure	Loops
608	0	30	250	500	4

Once the program has been set a glass capillary was loaded into the V-groove in the puller bar (Figure B.3A), and the capillary was slid about 2 cm beyond clamp and the knob was tightened. The string stop (Figure B.3B) was depressed on each puller bar to release them from their catch position and the knob was slightly loosened to centre it (Figure B.3C).The thumb and index finger (Figure B.3D) are used to pull both the bars towards each other. Carefully slided the glass capillary through holes in the side of the heater chambers and into V grove of the opposite puller bar. Once the capillary was aligned horizontally in the chamber, the clamping knob was tightened (Figure B.3E). Once the pipettes have been pulled the clamping knobs and the pipette removed from the puller bars (Figure B.3F). The RESET can then be pressed to exit current program and start new program.
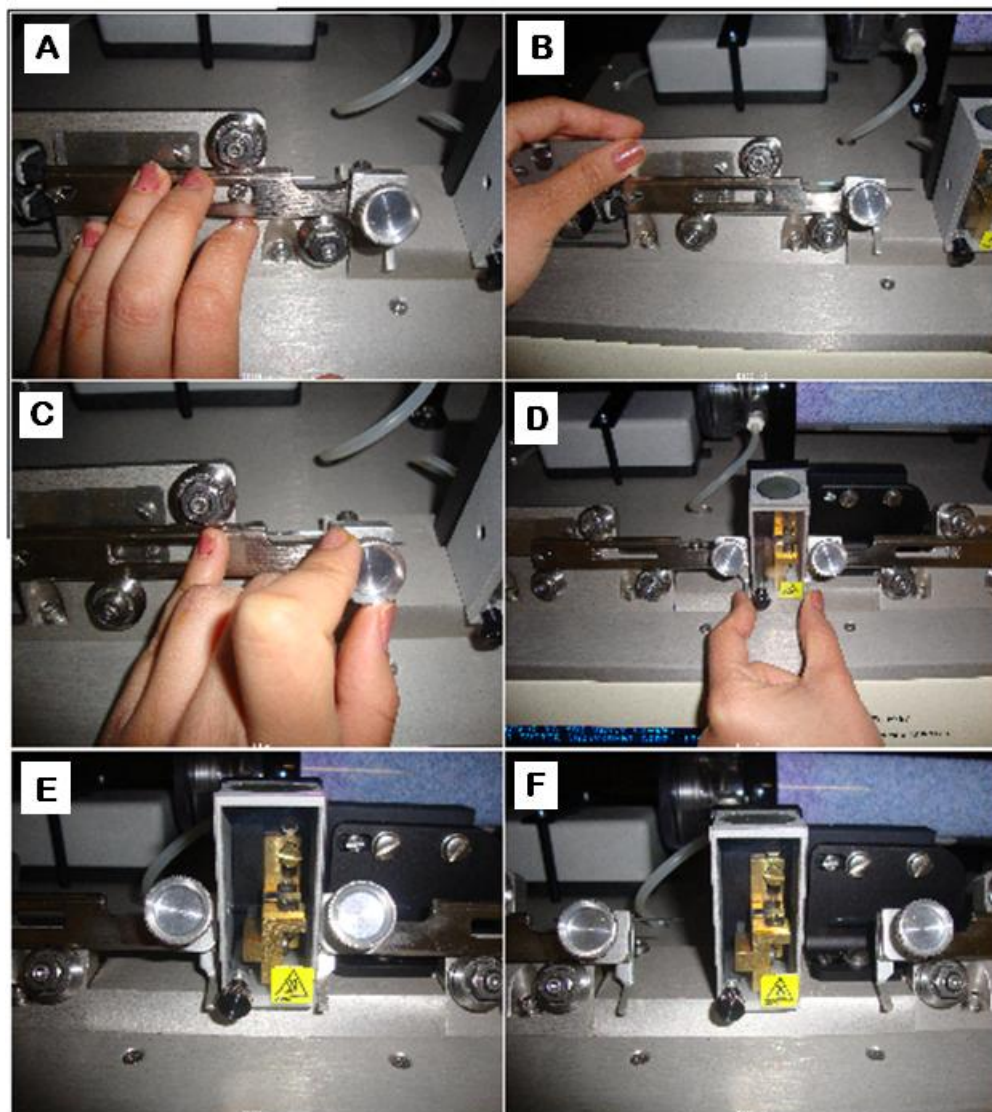
Figure B.3.*The procedure for pulling a micropipette using the P-97 puller, A – Loading of the glass pipette in the v-groove, B – Depressing the spring stop to release the puller bar from its catch position, C – Loosen the knob slightly to centre it. D – Using finger bars, both bars are pulled, E – Using the thumb and index finger to hold in this position making sure the pipette is in the centre of heating filament,. F – After pull is applied, two pipettes are generated.*

B3   POLISHING

The micropipiette aspiration of the cell is sensitive to the diameter of the pipette used.

The micropipette with certain diameter is required to maintain consistency in the results

and reduce variability. The raw micropipettes were made from the puller that can be cut at intended diameter using the microforge (Mf-900). The pulled pipettes are polished using the microforge (Figure B.4).
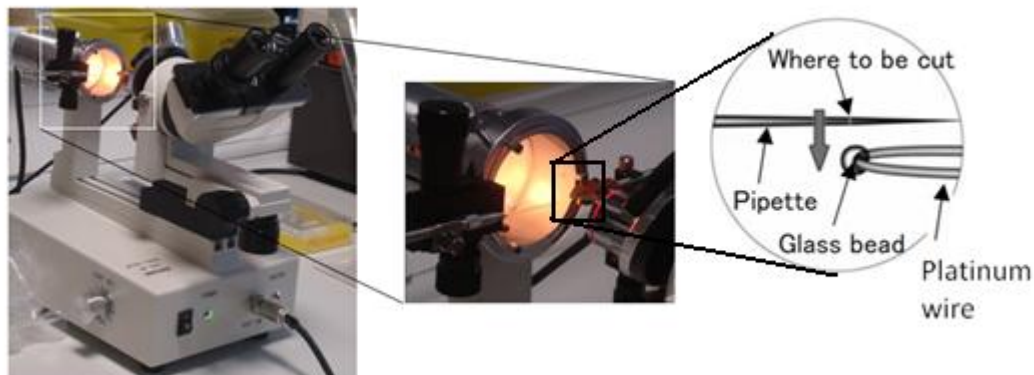
Figure B.4. *Pipettes polished by microforge.*

The polishing procedure involves using glass bead to make a cut on the pipette by heated platinum wire. The polished pipettes are shown in Figure B.5.
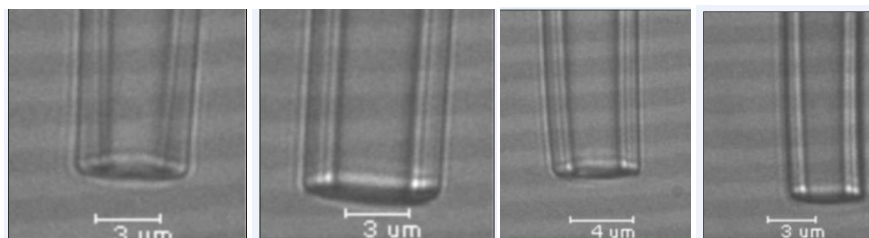
Figure B.5. Pipettes fabricated with inner diameter ranging from 3.5 - 4.5 μm.

B4   COATING

The micropipettes were coated using Sigmacoate to prevent cell adhesion. The micropipettes should be allowed to dry for 24 hrs before using it for the cell aspiration. As the remaining residual affects damages the cell membrane leading to blebbing off of the membrane. Additionally, pipette is surrounded with small particles obstructing cell to be aspirated.

APPENDIX C – ELASTIC PROPERTIES

This section provides the description of the protocol to estimate the elastic properties of the cells.

C1   EXPERIMENTAL METHOD

Chondrocytes were aspirated following protocol presented in Table C.1. Isolated chondrocytes were suspended in cell culture media with density of 1×10^6 cells/mL. The cell suspension was placed in the chamber mounted on the stage of the confocal microscope. Four steps of 2 cmH$_2$O pressure were applied to the cell with 60 seconds between each increment. Brightfield images were obtained 60 seconds after the application of each pressure increment. For each pressure, aspiration length was measured from bright field image using ImageJ.

Table C.1. Parameters for the elastic protocol.

Protocol	Elastic
Tare Pressure : P_T (cmH$_2$O)	1
Initial Time: T_0 (secs)	2
Step pressure: ΔP (cmH$_2$O)	5
No of steps:	4
Time interval: T_1 (secs)	60
Step time : T_2	15
Hold time: T_{hold} (secs)	60

Aspiration length was normalized to the inner radius of the micropipette and plotted against pressure. A linear regression was fitted to the experimental data and the

gradient was used to estimate apparent Young's modulus of the cell based on the model described Theret at al (1998). The governing relation between the aspiration length and Young's modulus is given in equation 2.2.

C2   RESULTS

The representative images obtained during the micropipette aspiration is presented in Figure C.1. The aspiration length of the cell increased with each pressure increment. It can be noted that when cell was ejected from the micropipette the deformed shape of the cell did not fully recover back to the spherical morphology.
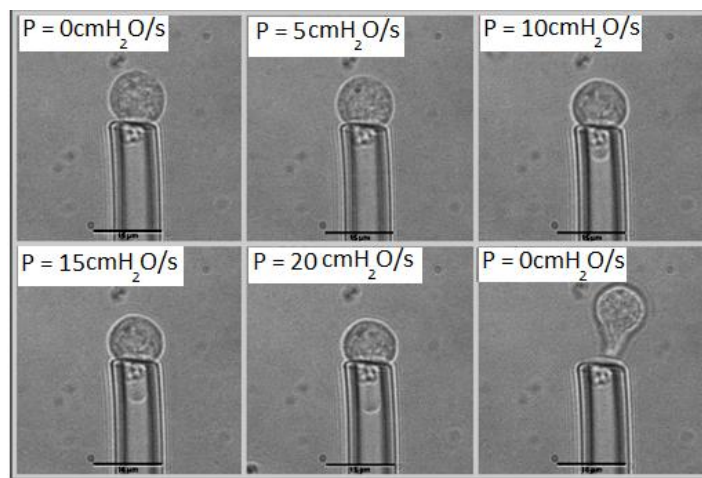
Figure C.1. Brightfield images showing aspiration of a single chondrocyte subjected 5, 10, 15 and 20 cmH₂O with 60 seconds interval between each step. The images were taken 60 seconds after each step pressure. Scale bar = 15μm.

The aspiration length of the chondrocytes was normalised with inner radius of the micropipette and plotted against the pressure (Figure C.2). The modulus computed for the chondrocytes was 2.58 ± 1.39 kPa. However the modulus computed by the (Jones et al., 1999)   is 0.65 kPa for human chondrocytes using similar technique to the present study. Other reported values are 0.81kPa (Bader et al., 2002) and 0.97 (Darling et al., 2006b) for bovine chondrocytes using different techniques. The variation in the elastic properties of the cells might be due to difference in the pressure used in the experiment.
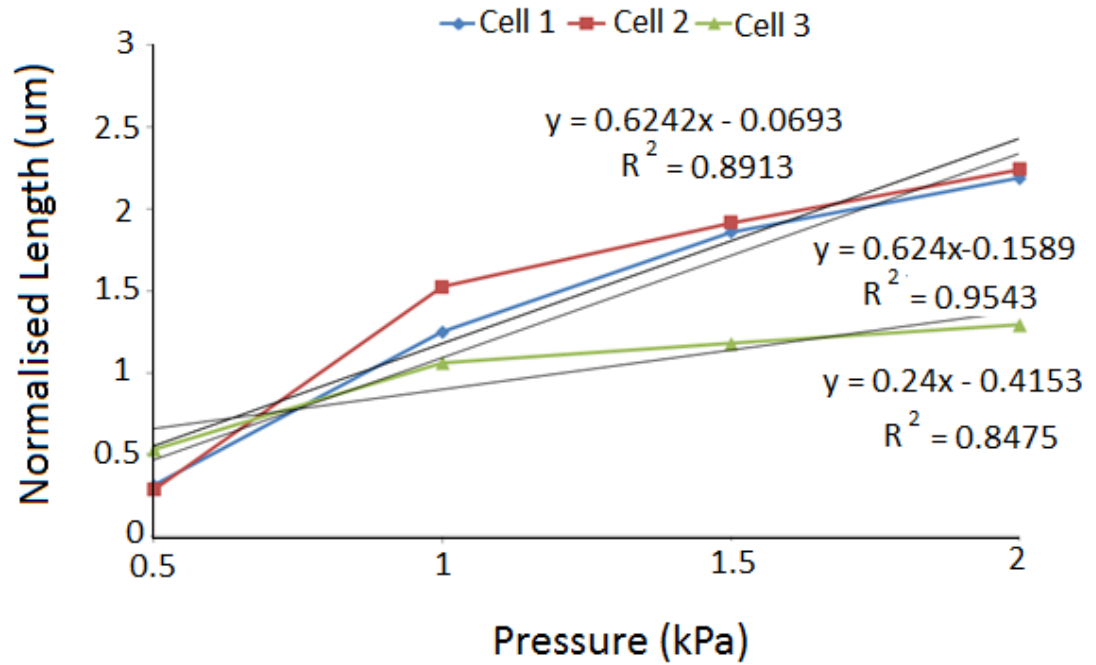
Figure C.2. *The plot of normalized length versus the applied pressure of an single chondrocyte.*

APPENDIX D – MATLAB PROGRAMMING

D1 STANDARD LINEAR SOLID MODEL

```matlab
Data=load('data.txt');
Parameters=load('arguments.txt');
t=Data(:,1);
L=Data(:,2);
phi=Parameters(1);
a=Parameters(2);
tforce=Parameters(3);
Dp=Parameters(4);
 x0=[100.1;100.1;1000.1];
% x = fsolve(@Lfun,x0)
 x = lsqnonlin(@Lfun,x0)
 k1=x(1);
k2=x(2);
mu=x(3);
 tau=mu*(k1+k2)/(k1*k2);
Lp=phi*a*Dp/(pi*k1)*(1-k2/(k1+k2)*exp(-t/tau));
 Lmean=mean(L);
Serr=sum((L-Lp).^2)
Stot=sum((L-Lmean).^2)
R2=1-Serr./Stot
figure(1)
plot(t,L,'b*')
hold on
plot(t,Lp,'r')
```

D2 BOLTZMANN STANDARD LINEAR SOLID MODEL

```
clear
% clc
% clear global
global Data Parameter
Data= load('data.txt');
%Data=load('data.txt');
Parameter=load('arguments.txt');
t=Data(:,1);
L=Data(:,2);
phi=Parameter(1);
a=Parameter(2);
tforce=Parameter(3);
Dp=Parameter(4);
lb=[0 0 0];
ub=[1000000000000000 1000000000000000 1000000000000000];
x0=[100.1;100.1;1000.1];
Q=(Dp/tforce);


for i=1:length(t)
    if t(i)<=tforce
        P(i,1)=Q*t(i);
    else
        P(i,1)=Q*tforce;
    end
end

% Constrained minimization
% x=fmincon(@Lfun,x0,[],[],[],[],lb,ub)

% Multivariable zero solver
%x = fsolve(@Lfun,x0)
```

```matlab
% Solve nonlinear least-squares (nonlinear data-fitting)
problems
x = lsqnonlin(@bsls,x0,lb,ub)


k1=x(1);
k2=x(2);
mu=x(3);
tau=mu*(k1+k2)/(k1*k2);
b=phi*a/(pi*k1);
c=k2/(k1+k2);


% Analytical solution of the integral
for i=1:length(t)
    if t(i)<=tforce
        Lp1(i,1)=t(i)*tau-tau^2+tau^2*exp(-t(i)/tau);
    else
        Lp1(i,1)=exp(-(t(i)-tforce)/tau)*(tforce*tau-
tau^2)+...
            tau^2*exp(-t(i)/tau)+tforce*(tau-tau*exp(-(t(i)-
tforce)/tau));
    end
end


Lp=b*P*(1-c)+((b*c)/(tau))*Q*Lp1;
Lmean=mean(L);
Serr=sum((L-Lp).^2)
Stot=sum((L-Lmean).^2)
R2=1-Serr./Stot
figure(2)
plot(t,L,'b*')
hold on
plot(t,Lp,'m')
```

REFERENCES

Abdelgawad, M., Chien,Wei-Yin, Liang, Ting-Kai and Sun, Yu. 2010. Microfluidic Platform with Circular Microchannels for Facile Cell Trapping and Single Cell Analysis. *In* 14th International Conference on Miniaturized Systems for Chemistry and Life Sciences, Groningen, The Netherlands.

Abusara, Z., R. Seerattan, A. Leumann, R. Thompson, and W. Herzog. 2011. A Novel Method for Determining Articular Cartilage Chondrocyte Mechanics in Vivo. *J Biomech*. 44:930-934.

Aigner, T., A. Sachse, P.M. Gebhard, and H.I. Roach. 2006. Osteoarthritis: Pathobiology-Targets and Ways for Therapeutic Intervention. *Adv Drug Deliv Rev*. 58:128-149.

Alexopoulos, L.G., G.M. Williams, M.L. Upton, L.A. Setton, and F. Guilak. 2005. Osteoarthritic Changes in the Biphasic Mechanical Properties of the Chondrocyte Pericellular Matrix in Articular Cartilage. *J Biomech*. 38:509-517.

Alonso, J.L., and W.H. Goldmann. 2003. Feeling the Forces: Atomic Force Microscopy in Cell Biology. *Life Sci*. 72:2553-2560.

Arkill, K.P., and C.P. Winlove. 2006. Fatty Acid Transport in Articular Cartilage. *Arch Biochem Biophys*. 456:71-78.

Armstrong, C.G., W.M. Lai, and V.C. Mow. 1984. An Analysis of the Unconfined Compression of Articular Cartilage. *J Biomech Eng*. 106:165-173.

Arner, E.C., C.E. Hughes, C.P. Decicco, B. Caterson, and M.D. Tortorella. 1998. Cytokine-Induced Cartilage Proteoglycan Degradation Is Mediated by Aggrecanase. *Osteoarthr Cartilage*. 6:214-228.

Asanbaeva, A., K. Masuda, E.J.M.A. Thonar, S.M. Klisch, and R.L. Sah. 2007. Mechanisms of Cartilage Growth - Modulation of Balance between Proteoglycan and Collagen in Vitro Using Chondroitinase Abc. *Arthritis and Rheumatism*. 56:188-198.

Athanasiou, K.A., A. Agarwal, and F.J. Dzida. 1994. Comparative-Study of the Intrinsic Mechanical-Properties of the Human Acetabular and Femoral-Head Cartilage. *J Orthopaed Res*. 12:340-349.

Athanasiou, K.A., A. Agarwal, A. Muffoletto, F.J. Dzida, G. Constantinides, and M. Clem. 1995. Biomechanical Properties of Hip Cartilage in Experimental Animal Models. *Clin Orthop Relat Res*:254-266.

Athanasiou, K.A., M.P. Rosenwasser, J.A. Buckwalter, T.I. Malinin, and V.C. Mow. 1991. Interspecies Comparisons of in Situ Intrinsic Mechanical Properties of Distal Femoral Cartilage. *J Orthop Res*. 9:330-340.

Athanasiou, K.A., and A.C. Shieh. 2002. Biomechanics of Single Chondrocytes and Osteoarthritis. 30:307-343.

Baaijens, F.P., W.R. Trickey, T.A. Laursen, and F. Guilak. 2005. Large Deformation Finite Element Analysis of Micropipette Aspiration to Determine the Mechanical Properties of the Chondrocyte. *Ann Biomed Eng*. 33:494-501.

Bader, D., and M. Knight. 2008. Biomechanical Analysis of Structural Deformation in Living Cells. *Medical and Biological Engineering and Computing*. 46:951-963.

Bader, D., Lee, D:. 2000. Structure-Properties Ofsoft Tissues. Articular Cartilage. *In* Structural Biological Materials Design Structure-Property Relationships. E. M, editor.

Bader, D.L., G.E. Kempson, J. Egan, W. Gilbey, and A.J. Barrett. 1992. The Effects of Selective Matrix Degradation on the Short-Term Compressive Properties of Adult Human Articular Cartilage. *Biochim Biophys Acta*. 1116:147-154.

Bader, D.L., T. Ohashi, M.M. Knight, D.A. Lee, and M. Sato. 2002. Deformation Properties of Articular Chondrocytes: A Critique of Three Separate Techniques. *Biorheology*. 39:69-78.

Ballestrem, C., B. Wehrle-Haller, and B.A. Imhof. 1998. Actin Dynamics in Living Mammalian Cells. *J Cell Sci*. 111 (Pt 12):1649-1658.

Bamac, B., S. Ozdemir, H.T. Sarisoy, T. Colak, A. Ozbek, and G. Akansel. 2006. Evaluation of Medial and Lateral Meniscus Thicknesses in Early Osteoarthritis of the Knee with Magnetic Resonance Imaging. *Saudi Med J*. 27:854-857.

Bao, G., and S. Suresh. 2003. Cell and Molecular Mechanics of Biological Materials. *Nat Mater*. 2:715-725.

Bartlett, W., C.R. Gooding, R.W.J. Carrington, J.A. Skinner, T.W.R. Briggs, and G. Bentley. 2005. Autologous Chondrocyte Implantation at the Knee Using a Bilayer Collagen Membrane with Bone Graft - a Preliminary Report. *Journal of Bone and Joint Surgery-British Volume*. 87B:330-332.

Baum, T., G.B. Joseph, A. Arulanandan, L. Nardo, W. Virayavanich, J. Carballido-Gamio, M.C. Nevitt, J. Lynch, C.E. McCulloch, and T.M. Link. 2012. Association of Magnetic Resonance Imaging-Based Knee Cartilage T2 Measurements and Focal Knee Lesions with Knee Pain: Data from the Osteoarthritis Initiative. *Arthritis Care Res (Hoboken)*. 64:248-255.

Bausch, A.R., W. Moller, and E. Sackmann. 1999. Measurement of Local Viscoelasticity and Forces in Living Cells by Magnetic Tweezers. *Biophys J*. 76:573-579.

Behrens, F., E.L. Kraft, and T.R. Oegema, Jr. 1989. Biochemical Changes in Articular Cartilage after Joint Immobilization by Casting or External Fixation. *J Orthop Res*. 7:335-343.

Beiser, I.H., and I.O. Kanat. 1990. Subchondral Bone Drilling: A Treatment for Cartilage Defects. *J Foot Surg*. 29:595-601.

Benya, P.D., and J.D. Shaffer. 1982. Dedifferentiated Chondrocytes Reexpress the Differentiated Collagen Phenotype When Cultured in Agarose Gels. *Cell*. 30:215-224.

Bidhendi, A.J., and R.K. Korhonen. 2012a. A Finite Element Study of Micropipette Aspiration of Single Cells: Effect of Compressibility. *Comput Math Method M*.

Bidhendi, A.J., and R.K. Korhonen. 2012b. A Finite Element Study of Micropipette Aspiration of Single Cells: Effect of Compressibility. *Comput Math Methods Med*. 2012:192618.

Binnig, G., C.F. Quate, and C. Gerber. 1986. Atomic Force Microscope. *Phys Rev Lett*. 56:930-933.

Blain, E.J. 2009. Involvement of the Cytoskeletal Elements in Articular Cartilage Homeostasis and Pathology. *Int J Exp Pathol*. 90:1-15.

Blain, E.J., S.J. Gilbert, A.J. Hayes, and V.C. Duance. 2006. Disassembly of the Vimentin Cytoskeleton Disrupts Articular Cartilage Chondrocyte Homeostasis. *Matrix Biol*. 25:398-408.

Blaschke, U.K., E.F. Eikenberry, D.J. Hulmes, H.J. Galla, and P. Bruckner. 2000. Collagen Xi Nucleates Self-Assembly and Limits Lateral Growth of Cartilage Fibrils. *J Biol Chem*. 275:10370-10378.

Bobick, B.E., F.H. Chen, A.M. Le, and R.S. Tuan. 2009. Regulation of the Chondrogenic Phenotype in Culture. *Birth Defects Res C Embryo Today*. 87:351-371.

Brittberg, M., A. Lindahl, A. Nilsson, C. Ohlsson, O. Isaksson, and L. Peterson. 1994. Treatment of Deep Cartilage Defects in the Knee with Autologous Chondrocyte Transplantation. *N Engl J Med*. 331:889-895.

Brodkin, K.R., A.J. Garcia, and M.E. Levenston. 2004. Chondrocyte Phenotypes on Different Extracellular Matrix Monolayers. *Biomaterials*. 25:5929-5938.

Brugues, J., B. Maugis, J. Casademunt, P. Nassoy, F. Amblard, and P. Sens. 2010. Dynamical Organization of the Cytoskeletal Cortex Probed by Micropipette Aspiration. *Proc Natl Acad Sci U S A*. 107:15415-15420.

Bubb, M.R., I. Spector, B.B. Beyer, and K.M. Fosen. 2000. Effects of Jasplakinolide on the Kinetics of Actin Polymerization - an Explanation for Certain in Vivo Observations. *Journal of Biological Chemistry*. 275:5163-5170.

Buckwalter, J.A., and H.J. Mankin. 1998a. Articular Cartilage: Degeneration and Osteoarthritis, Repair, Regeneration, and Transplantation. *Instr Course Lect*. 47:487-504.

Buckwalter, J.A., and H.J. Mankin. 1998b. Articular Cartilage: Tissue Design and Chondrocyte-Matrix Interactions. *Aaos Instr Cours Lec*. 47:477-486.

Buckwalter, J.A., H.J. Mankin, and A.J. Grodzinsky. 2005. Articular Cartilage and Osteoarthritis. *Instr Course Lect*. 54:465-480.

Buckwalter, J.A., J. Martin, and H.J. Mankin. 2000. Synovial Joint Degeneration and the Syndrome of Osteoarthritis. *Instr Course Lect*. 49:481-489.

Buckwalter, J.A., Mow, A.C.;. 1992. Cartilage Repair in Osteoarthritis. *In* Osteoarthritis: Diagnosis and Managment. H.D. Moskowitz RW, Goldberg VM, Mankin HJ, editor. WB Saunders, Philadelphia. 71-107.

Buckwalter, J.A., and L. Rosenberg. 1983. Structural Changes During Development in Bovine Fetal Epiphyseal Cartilage. *Coll Relat Res*. 3:489-504.

Buckwalter, J.A., P.J. Roughley, and L.C. Rosenberg. 1994. Age-Related Changes in Cartilage Proteoglycans: Quantitative Electron Microscopic Studies. *Microsc Res Tech*. 28:398-408.

Buckwalter, J.A., S.L. Woo, V.M. Goldberg, E.C. Hadley, F. Booth, T.R. Oegema, and D.R. Eyre. 1993. Soft-Tissue Aging and Musculoskeletal Function. *J Bone Joint Surg Am*. 75:1533-1548.

Burstein, D., A. Bashir, and M.L. Gray. 2000. Mri Techniques in Early Stages of Cartilage Disease. *Invest Radiol*. 35:622-638.

Buschmann, M.D., Y.A. Gluzband, A.J. Grodzinsky, and E.B. Hunziker. 1995. Mechanical Compression Modulates Matrix Biosynthesis in Chondrocyte/Agarose Culture. *J Cell Sci*. 108 (Pt 4):1497-1508.

Campbell, J.J., E.J. Blain, T.T. Chowdhury, and M.M. Knight. 2007. Loading Alters Actin Dynamics and up-Regulates Cofilin Gene Expression in Chondrocytes. *Biochem Biophys Res Commun*. 361:329-334.

Campbell, J.J., and M.M. Knight. 2007a. An Improved Confocal Frap Technique for the Measurement of Long-Term Actin Dynamics in Individual Stress Fibers. *Microsc Res Tech*. 70:1034-1040.

Campbell, J.J., and M.M. Knight. 2007b. Mechanical Loading Triggers Cortical Actin Disassembly in Articular Chondrocytes. *Tissue Eng*. 13:1723-1723.

Capin-Gutierrez, N., P. Talamas-Rohana, A. Gonzalez-Robles, C. Lavalle-Montalvo, and J.B. Kouri. 2004. Cytoskeleton Disruption in Chondrocytes from a Rat Osteoarthrosic (Oa)-Induced Model: Its Potential Role in Oa Pathogenesis. *Histology and Histopathology*. 19:1125-1132.

Chalut, K.J., A.E. Ekpenyong, W.L. Clegg, I.C. Melhuish, and J. Guck. 2012. Quantifying Cellular Differentiation by Physical Phenotype Using Digital Holographic Microscopy. *Integr Biol (Camb)*. 4:280-284.

Charras, G.T., J.C. Yarrow, M.A. Horton, L. Mahadevan, and T.J. Mitchison. 2005. Non-Equilibration of Hydrostatic Pressure in Blebbing Cells. *Nature*. 435:365-369.

Chen, C., R. Krishnan, E. Zhou, A. Ramachandran, D. Tambe, K. Rajendran, R.M. Adam, L. Deng, and J.J. Fredberg. 2010. Fluidization and Resolidification of the Human Bladder Smooth Muscle Cell in Response to Transient Stretch. *PLoS One*. 5:e12035.

Chen, J., J. Irianto, S. Inamdar, P. Pravincumar, D.A. Lee, D.L. Bader, and M.M. Knight. 2012. Cell Mechanics, Structure, and Function Are Regulated by the Stiffness of the Three-Dimensional Microenvironment *Biophysical Journal* 103:1188-1197.

Chen, Y., S. Guzik, J.P. Sumner, J. Moreland, and A.P. Koretsky. 2011. Magnetic Manipulation of Actin Orientation, Polymerization, and Gliding on Myosin Using Superparamagnetic Iron Oxide Particles. *Nanotechnology*. 22:065101.

Chowdhury, T.T., and M.M. Knight. 2006. Purinergic Pathway Suppresses the Release Of .No and Stimulates Proteoglycan Synthesis in Chondrocyte/Agarose Constructs Subjected to Dynamic Compression. *J Cell Physiol*. 209:845-853.

Chowdhury, T.T., D.M. Salter, D.L. Bader, and D.A. Lee. 2004. Integrin-Mediated Mechanotransduction Processes in Tgfbeta-Stimulated Monolayer-Expanded Chondrocytes. *Biochem Biophys Res Commun*. 318:873-881.

Clair, B.L., A.R. Johnson, and T. Howard. 2009. Cartilage Repair: Current and Emerging Options in Treatment. *Foot Ankle Spec*. 2:179-188.

Clouet, J., C. Vinatier, C. Merceron, M. Pot-vaucel, Y. Maugars, P. Weiss, G. Grimandi, and J. Guicheux. 2009. From Osteoarthritis Treatments to Future Regenerative Therapies for Cartilage. *Drug Discov Today*. 14:913-925.

Clutterbuck, A.L., K.E. Asplin, P. Harris, D. Allaway, and A. Mobasheri. 2009. Targeting Matrix Metalloproteinases in Inflammatory Conditions. *Curr Drug Targets*. 10:1245-1254.

Cohen, N.P., R.J. Foster, and V.C. Mow. 1998. Composition and Dynamics of Articular Cartilage: Structure, Function, and Maintaining Healthy State. *J Orthop Sport Phys*. 28:203-215.

Colombelli, J., A. Besser, H. Kress, E.G. Reynaud, P. Girard, E. Caussinus, U. Haselmann, J.V. Small, U.S. Schwarz, and E.H.K. Stelzer. 2009. Mechanosensing in Actin Stress Fibers Revealed by a Close Correlation between Force and Protein Localization. *J Cell Sci*. 122:1665-1679.

Conaghan, P.G., A. Tennant, C.G. Peterfy, T. Woodworth, R. Stevens, A. Guermazi, H. Genant, D.T. Felson, and D. Hunter. 2006. Examining a Whole-Organ Magnetic Resonance Imaging Scoring System for Osteoarthritis of the Knee Using Rasch Analysis. *Osteoarthritis Cartilage*. 14 Suppl A:A116-121.

Cooper, J.A. 1987. Effects of Cytochalasin and Phalloidin on Actin. *J Cell Biol*. 105:1473-1478.

Darling, E.M., and K.A. Athanasiou. 2005. Rapid Phenotypic Changes in Passaged Articular Chondrocyte Subpopulations. *J Orthop Res*. 23:425-432.

Darling, E.M., P.E. Pritchett, B.A. Evans, R. Superfine, S. Zauscher, and F. Guilak. 2009. Mechanical Properties and Gene Expression of Chondrocytes on Micropatterned Substrates Following Dedifferentiation in Monolayer. *Cell Mol Bioeng*. 2:395-404.

Darling, E.M., S. Zauscher, and F. Guilak. 2006a. Viscoelastic Properties of Zonal Articular Chondrocytes Measured by Atomic Force Microscopy. *Osteoarthr Cartilage*. 14:571-579.

Darling, E.M., S. Zauscher, and F. Guilak. 2006b. Viscoelastic Properties of Zonal Articular Chondrocytes Measured by Atomic Force Microscopy. *Osteoarthritis Cartilage*. 14:571-579.

Deibler, M., J.P. Spatz, and R. Kemkemer. 2011. Actin Fusion Proteins Alter the Dynamics of Mechanically Induced Cytoskeleton Rearrangement. *PLoS One*. 6.

Dell'Accio, F., C. De Bari, N.M. El Tawil, F. Barone, T.A. Mitsiadis, J. O'Dowd, and C. Pitzalis. 2006. Activation of Wnt and Bmp Signaling in Adult Human Articular Cartilage Following Mechanical Injury. *Arthritis Res Ther*. 8:R139.

Deng, L.H., N.J. Fairbank, B. Fabry, P.G. Smith, and G.N. Maksym. 2004. Localized Mechanical Stress Induces Time-Dependent Actin Cytoskeletal Remodeling and Stiffening in Cultured Airway Smooth Muscle Cells. *Am J Physiol-Cell Ph*. 287:C440-C448.

DiPaolo, B.C., G. Lenormand, J.J. Fredberg, and S.S. Margulies. 2010. Stretch Magnitude and Frequency-Dependent Actin Cytoskeleton Remodeling in Alveolar Epithelia. *Am J Physiol Cell Physiol*. 299:C345-353.

Doege, K.J., M. Sasaki, T. Kimura, and Y. Yamada. 1991. Complete Coding Sequence and Deduced Primary Structure of the Human Cartilage Large Aggregating Proteoglycan, Aggrecan. Human-Specific Repeats, and Additional Alternatively Spliced Forms. *J Biol Chem*. 266:894-902.

Durrant, L.A., C.W. Archer, M. Benjamin, and J.R. Ralphs. 1999. Organisation of the Chondrocyte Cytoskeleton and Its Response to Changing Mechanical Conditions in Organ Culture. *J Anat*. 194 (Pt 3):343-353.

Eckstein, F., F. Cicuttini, J.P. Raynauld, J.C. Waterton, and C. Peterfy. 2006. Magnetic Resonance Imaging (Mri) of Articular Cartilage in Knee Osteoarthritis (Oa): Morphological Assessment. *Osteoarthritis Cartilage*. 14 Suppl A:A46-75.

Eckstein, F., and W. Wirth. 2011. Quantitative Cartilage Imaging in Knee Osteoarthritis. *Arthritis*. 2011:475684.

Eitzen, G. 2003. Actin Remodeling to Facilitate Membrane Fusion. *Biochim Biophys Acta*. 1641:175-181.

Erickson, G.R., D.L. Northrup, and F. Guilak. 2003. Hypo-Osmotic Stress Induces Calcium-Dependent Actin Reorganization in Articular Chondrocytes. *Osteoarthr Cartilage*. 11:187-197.

Evans, E., and A. Yeung. 1989. Apparent Viscosity and Cortical Tension of Blood Granulocytes Determined by Micropipet Aspiration. *Biophysical Journal*. 56:151-160.

Ferry, J.J.D. 1970. Viscoelastic Properties of Polymers. Wiley.

Fitzgerald, J.B., M. Jin, D. Dean, D.J. Wood, M.H. Zheng, and A.J. Grodzinsky. 2004. Mechanical Compression of Cartilage Explants Induces Multiple Time-Dependent Gene Expression Patterns and Involves Intracellular Calcium and Cyclic Amp. *J Biol Chem*. 279:19502-19511.

Flik, e.a. 2007. Articular Cartilage Structure, Biology and Function. *In* Cartilage Repair Strategies. Human press, New York. 1-13.

Futai, N., W. Gu, and S. Takayama. 2004. Rapid Prototyping of Microstructures with Bell-Shaped Cross-Sections and Its Application to Deformation-Based Microfluidic Valves. *Advanced Materials*. 16:1320-+.

Gardel, M.L., J.H. Shin, F.C. MacKintosh, L. Mahadevan, P. Matsudaira, and D.A. Weitz. 2004. Elastic Behavior of Cross-Linked and Bundled Actin Networks. *Science*. 304:1301-1305.

Gelber, A.C., M.C. Hochberg, L.A. Mead, N.Y. Wang, F.M. Wigley, and M.J. Klag. 2000. Joint Injury in Young Adults and Risk for Subsequent Knee and Hip Osteoarthritis. *Ann Intern Med*. 133:321-328.

Godin, L.M., J. Vergen, Y.S. Prakash, R.E. Pagano, and R.D. Hubmayr. 2011. Spatiotemporal Dynamics of Actin Remodeling and Endomembrane Trafficking in Alveolar Epithelial Type I Cell Wound Healing. *Am J Physiol Lung Cell Mol Physiol*. 300:L615-623.

Goldman, R.D., A.E. Goldman, K.J. Green, J.C. Jones, S.M. Jones, and H.Y. Yang. 1986. Intermediate Filament Networks: Organization and Possible Functions of a Diverse Group of Cytoskeletal Elements. *J Cell Sci Suppl*. 5:69-97.

Goldring, M.B. 2000. Osteoarthritis and Cartilage: The Role of Cytokines. *Curr Rheumatol Rep*. 2:459-465.

Goldring, S.R., and M.B. Goldring. 2004. The Role of Cytokines in Cartilage Matrix Degeneration in Osteoarthritis. *Clin Orthop Relat R*:S27-S36.

Grodzinsky, A.J., M.E. Levenston, M. Jin, and E.H. Frank. 2000. Cartilage Tissue Remodeling in Response to Mechanical Forces. *Annu Rev Biomed Eng*. 2:691-+.

Guilak, F. 2000. The Deformation Behavior and Viscoelastic Properties of Chondrocytes in Articular Cartilage. *Biorheology*. 37:27-44.

Guilak, F., L.G. Alexopoulos, M.A. Haider, H.P. Ting-Beall, and L.A. Setton. 2005. Zonal Uniformity in Mechanical Properties of the Chondrocyte Pericellular Matrix: Micropipette Aspiration of Canine Chondrons Isolated by Cartilage Homogenization. *Ann Biomed Eng*. 33:1312-1318.

Guilak, F., G.R. Erickson, and H.P. Ting-Beall. 2002. The Effects of Osmotic Stress on the Viscoelastic and Physical Properties of Articular Chondrocytes. *Biophys J*. 82:720-727.

Guilak, F., W.R. Jones, H.P. Ting-Beall, and G.M. Lee. 1999. The Deformation Behavior and Mechanical Properties of Chondrocytes in Articular Cartilage. *Osteoarthritis Cartilage*. 7:59-70.

Hangody, L., G. Kish, Z. Karpati, I. Szerb, and I. Udvarhelyi. 1997. Arthroscopic Autogenous Osteochondral Mosaicplasty for the Treatment of Femoral Condylar Articular Defects. A Preliminary Report. *Knee Surg Sports Traumatol Arthrosc*. 5:262-267.

Harville, H.M., S. Held, A. Diaz-Font, E.E. Davis, B.H. Diplas, R.A. Lewis, Z.U. Borochowitz, W. Zhou, M. Chaki, J. MacDonald, H. Kayserili, P.L. Beales, N. Katsanis, E. Otto, and F. Hildebrandt. 2010. Identification of 11 Novel Mutations in Eight Bbs Genes by High-Resolution Homozygosity Mapping. *J Med Genet*. 47:262-267.

Haudenschild, D.R., J. Chen, N. Steklov, M.K. Lotz, and D.D. D'Lima. 2009. Characterization of the Chondrocyte Actin Cytoskeleton in Living Three-Dimensional Culture: Response to Anabolic and Catabolic Stimuli. *Mol Cell Biomech*. 6:135-144.

Head, D.A., A.J. Levine, and F.C. MacKintosh. 2003a. Deformation of Cross-Linked Semiflexible Polymer Networks. *Physical Review Letters*. 91.

Head, D.A., A.J. Levine, and F.C. MacKintosh. 2003b. Distinct Regimes of Elastic Response and Deformation Modes of Cross-Linked Cytoskeletal and Semiflexible Polymer Networks. *Phys Rev E*. 68.

Heinegard, D., Lorenzo P, Sommarin Y:. 1992. Cartilage Matrix Protein. *In* Articular Cartilage and Osteoarthritis. K.E. Kuettner, editor. Raven Press. 95-111.

Henson, F.M., and T.A. Vincent. 2008. Alterations in the Vimentin Cytoskeleton in Response to Single Impact Load in an in Vitro Model of Cartilage Damage in the Rat. *BMC Musculoskelet Disord*. 9:94.

Hernandez-Hernandez, V., Pravincumar, A. Diaz-Font, H. May-Simera, D. Jenkins, M.M. Knight, and B.P. L. 2012. Bardet-Biedl Syndrome Proteins Control Cilia Length through Regulation of Actin Polymerisation. Molecular Medicine Unit, UCL Institute of Child Health London.

Heywood, H.K., M.M. Knight, and D.A. Lee. 2010. Both Superficial and Deep Zone Articular Chondrocyte Subpopulations Exhibit the Crabtree Effect but Have Different Basal Oxygen Consumption Rates. *J Cell Physiol*. 223:630-639.

Heywood, H.K., and D.A. Lee. 2008. Monolayer Expansion Induces an Oxidative Metabolism and Ros in Chondrocytes. *Biochem Biophys Res Commun*. 373:224-229.

Hill, C.L., D.J. Hunter, J. Niu, M. Clancy, A. Guermazi, H. Genant, D. Gale, A. Grainger, P. Conaghan, and D.T. Felson. 2007. Synovitis Detected on Magnetic Resonance Imaging and Its Relation to Pain and Cartilage Loss in Knee Osteoarthritis. *Ann Rheum Dis*. 66:1599-1603.

Hochmuth, R.M. 2000. Micropipette Aspiration of Living Cells. *Journal of Biomechanics*. 33:15-22.

Horoyan, M., A.M. Benoliel, C. Capo, and P. Bongrand. 1990. Localization of Calcium and Microfilament Changes in Mechanically Stressed Cells. *Cell Biophys*. 17:243-256.

Huang, W., B. Anvari, J.H. Torres, R.G. LeBaron, and K.A. Athanasiou. 2003. Temporal Effects of Cell Adhesion on Mechanical Characteristics of the Single Chondrocyte. *J Orthop Res*. 21:88-95.

Hui, J.H., F. Chen, A. Thambyah, and E.H. Lee. 2004. Treatment of Chondral Lesions in Advanced Osteochondritis Dissecans: A Comparative Study of the Efficacy of Chondrocytes, Mesenchymal Stem Cells, Periosteal Graft, and Mosaicplasty (Osteochondral Autograft) in Animal Models. *J Pediatr Orthop*. 24:427-433.

Humphrey, D., C. Duggan, D. Saha, D. Smith, and J. Kas. 2002. Active Fluidization of Polymer Networks through Molecular Motors. *Nature*. 416:413-416.

Hunter, D.J., J. Li, M. LaValley, D.C. Bauer, M. Nevitt, J. DeGroot, R. Poole, D. Eyre, A. Guermazi, D. Gale, and D.T. Felson. 2007. Cartilage Markers and Their Association with Cartilage Loss on Magnetic Resonance Imaging in Knee Osteoarthritis: The Boston Osteoarthritis Knee Study. *Arthritis Res Ther*. 9:R108.

Idowu, B.D., M.M. Knight, D.L. Bader, and D.A. Lee. 2000. Confocal Analysis of Cytoskeletal Organisation within Isolated Chondrocyte Sub-Populations Cultured in Agarose. *Histochem J*. 32:165-174.

Ingber, D.E., L. Dike, L. Hansen, S. Karp, H. Liley, A. Maniotis, H. Mcnamee, D. Mooney, G. Plopper, J. Sims, and N. Wang. 1994. Cellular Tensegrity - Exploring How Mechanical Changes in the Cytoskeleton Regulate Cell-Growth, Migration, and Tissue Pattern During Morphogenesis. *Int Rev Cytol*. 150:173-224.

Issa, S.N., D. Dunlop, A. Chang, J. Song, P.V. Prasad, A. Guermazi, C. Peterfy, S. Cahue, M. Marshall, D. Kapoor, K. Hayes, and L. Sharma. 2007. Full-Limb and Knee Radiography Assessments of Varus-Valgus Alignment and Their Relationship to Osteoarthritis Disease Features by Magnetic Resonance Imaging. *Arthritis Rheum*. 57:398-406.

Janson, L.W., J. Kolega, and D.L. Taylor. 1991. Modulation of Contraction by Gelation Solation in a Reconstituted Motile Model. *Journal of Cell Biology*. 114:1005-1015.

Jeffrey, J.E., L.A. Thomson, and R.M. Aspden. 1997. Matrix Loss and Synthesis Following a Single Impact Load on Articular Cartilage in Vitro. *Biochim Biophys Acta*. 1334:223-232.

Jerry, H.K., Athanasiou;. 2003. Structure and Function of Articular Cartilage. *In* Handbook of Histology Methods for Bone and Cartilage. A.K. Yuehue, Martin, editor. Humana Press, Totowa. 73-95.

Jia, Y.F., J.H. Jiang, X.D. Ma, Y. Li, H.M. Huang, K.B. Cai, S.X. Cai, and Y.P. Wu. 2008. Pdms Microchannel Fabrication Technique Based on Microwire-Molding. *Chinese Sci Bull*. 53:3928-3936.

Jones, W.R., H.P. Ting-Beall, G.M. Lee, S.S. Kelley, R.M. Hochmuth, and F. Guilak. 1999. Alterations in the Young's Modulus and Volumetric Properties of Chondrocytes Isolated from Normal and Osteoarthritic Human Cartilage. *J Biomech*. 32:119-127.

Kalichman, L., Y. Zhang, J. Niu, J. Goggins, D. Gale, Y. Zhu, D.T. Felson, and D.J. Hunter. 2007. The Association between Patellar Alignment on Magnetic Resonance Imaging and Radiographic Manifestations of Knee Osteoarthritis. *Arthritis Res Ther*. 9:R26.

Keller, H., P. Rentsch, and J. Hagmann. 2002. Differences in Cortical Actin Structure and Dynamics Document That Different Types of Blebs Are Formed by Distinct Mechanisms. *Exp Cell Res*. 277:161-172.

Keller, H.U. 2000. Redundancy of Lamellipodia in Locomoting Walker Carcinosarcoma Cells. *Cell Motil Cytoskeleton*. 46:247-256.

Kempson, G.E., M.A. Tuke, J.T. Dingle, A.J. Barrett, and P.H. Horsfield. 1976. The Effects of Proteolytic Enzymes on the Mechanical Properties of Adult Human Articular Cartilage. *Biochim Biophys Acta*. 428:741-760.

Ketelaar, T., R.G. Anthony, and P.J. Hussey. 2004. Green Fluorescent Protein-Mtalin Causes Defects in Actin Organization and Cell Expansion in Arabidopsis and Inhibits Actin Depolymerizing Factor's Actin Depolymerizing Activity in Vitro. *Plant Physiology*. 136:3990-3998.

Kim, H.A., and F.J. Blanco. 2007. Cell Death and Apoptosis in Osteoarthritic Cartilage. *Curr Drug Targets*. 8:333-345.

Kim, J.C., J.L. Badano, S. Sibold, M.A. Esmail, J. Hill, B.E. Hoskins, C.C. Leitch, K. Venner, S.J. Ansley, A.J. Ross, M.R. Leroux, N. Katsanis, and P.L. Beales. 2004. The Bardet-Biedl Protein Bbs4 Targets Cargo to the Pericentriolar Region and Is Required for Microtubule Anchoring and Cell Cycle Progression. *Nat Genet*. 36:462-470.

Kim, W.H., A. 2010. A Micro-Aspirator Chip Using Vacuum Expanded Microchannels for High-Throughput Mechanical Characterization of Biological Cells. *In* 14th International Conference on Miniaturized Systems for Chemistry and Life Sciences, Groningen, The Netherlands.

Kim, Y.J., R.L. Sah, A.J. Grodzinsky, A.H. Plaas, and J.D. Sandy. 1994. Mechanical Regulation of Cartilage Biosynthetic Behavior: Physical Stimuli. *Arch Biochem Biophys*. 311:1-12.

Kino-oka, M., Y. Maeda, Y. Ota, S. Yashiki, K. Sugawara, T. Yamamoto, and M. Taya. 2005. Process Design of Chondrocyte Cultures with Monolayer Growth for Cell Expansion and Subsequent Three-Dimensional Growth for Production of Cultured Cartilage. *J Biosci Bioeng*. 100:67-76.

Kiviranta, I., J. Jurvelin, M. Tammi, A.M. Saamanen, and H.J. Helminen. 1987. Weight Bearing Controls Glycosaminoglycan Concentration and Articular Cartilage Thickness in the Knee Joints of Young Beagle Dogs. *Arthritis Rheum*. 30:801-809.

Knight, M.M. 1997. Deformation of Isolated Articular Chondrocytes Cultured in Agarose Constructs. Vol. PhD. Queen Mary, University of London, London.

Knight, M.M., J.V.D.B. Bravenboer, D.A. Lee, G.J.V.M. van Osch, H. Weinans, and D.L. Bader. 2002. Cell and Nucleus Deformation in Compressed Chondrocyte-Alginate Constructs: Temporal Changes and Calculation of Cell Modulus. *Bba-Gen Subjects*. 1570:1-8.

Ko, C.H., K.K. Chan, and H.L. Peng. 2007. Sonographic Imaging of Meniscal Subluxation in Patients with Radiographic Knee Osteoarthritis. *J Formos Med Assoc*. 106:700-707.

Koay, E.J., A.C. Shieh, and K.A. Athanasiou. 2003. Creep Indentation of Single Cells. *J Biomech Eng*. 125:334-341.

Kornaat, P.R., J.L. Bloem, R.Y. Ceulemans, N. Riyazi, F.R. Rosendaal, R.G. Nelissen, W.O. Carter, M.P. Hellio Le Graverand, and M. Kloppenburg. 2006. Osteoarthritis of the Knee: Association between Clinical Features and Mr Imaging Findings. *Radiology*. 239:811-817.

Kumar, S., I.Z. Maxwell, A. Heisterkamp, T.R. Polte, T.P. Lele, M. Salanga, E. Mazur, and D.E. Ingber. 2006. Viscoelastic Retraction of Single Living Stress Fibers and Its Impact on Cell Shape, Cytoskeletal Organization, and Extracellular Matrix Mechanics. *Biophysical Journal*. 90:3762-3773.

Kurz, B., A.K. Lemke, J. Fay, T. Pufe, A.J. Grodzinsky, and M. Schunke. 2005. Pathomechanisms of Cartilage Destruction by Mechanical Injury. *Ann Anat*. 187:473-485.

Lange, K., and J. Gartzke. 2006. F-Actin-Based Ca Signaling-a Critical Comparison with the Current Concept of Ca Signaling. *J Cell Physiol*. 209:270-287.

Langelier, E., R. Suetterlin, C.D. Hoemann, U. Aebi, and M.D. Buschmann. 2000. The Chondrocyte Cytoskeleton in Mature Articular Cartilage: Structure and Distribution of Actin, Tubulin, and Vimentin Filaments. *J Histochem Cytochem*. 48:1307-1320.

Laster, S.M., and J.M. Mackenzie, Jr. 1996. Bleb Formation and F-Actin Distribution During Mitosis and Tumor Necrosis Factor-Induced Apoptosis. *Microsc Res Tech*. 34:272-280.

Lee, C.S., Grad, M. W, Alini, M. . 2006. The Influence of Mechanical Stimuli on Articular Cartilage Tissue Engineering. *In* Topics in Tissue Engineering,. Vol. 2. 32.

Lee, D.A., M.M. Knight, J.F. Bolton, B.D. Idowu, M.V. Kayser, and D.L. Bader. 2000a. Chondrocyte Deformation within Compressed Agarose Constructs at the Cellular and Sub-Cellular Levels. *J Biomech*. 33:81-95.

Lee, D.A., M.M. Knight, J.J. Campbell, and D.L. Bader. 2011. Stem Cell Mechanobiology. *J Cell Biochem*. 112:1-9.

Lee, D.A., T. Noguchi, S.P. Frean, P. Lees, and D.L. Bader. 2000b. The Influence of Mechanical Loading on Isolated Chondrocytes Seeded in Agarose Constructs. *Biorheology*. 37:149-161.

Lee, D.A., T. Noguchi, M.M. Knight, L. O'Donnell, G. Bentley, and D.L. Bader. 1998. Response of Chondrocyte Subpopulations Cultured within Unloaded and Loaded Agarose. *J Orthop Res*. 16:726-733.

Lee, J.H., J.B. Fitzgerald, M.A. Dimicco, and A.J. Grodzinsky. 2005. Mechanical Injury of Cartilage Explants Causes Specific Time-Dependent Changes in Chondrocyte Gene Expression. *Arthritis Rheum*. 52:2386-2395.

Leipzig, N.D., and K.A. Athanasiou. 2005. Unconfined Creep Compression of Chondrocytes. *J Biomech*. 38:77-85.

Lele, T.P., J.E. Sero, B.D. Matthews, S. Kumar, S. Xia, M. Montoya-Zavala, T. Polte, D. Overby, N. Wang, and D.E. Ingber. 2007. Tools to Study Cell Mechanics and Mechanotransduction. *Methods Cell Biol*. 83:443-472.

Lieleg, O., M.M.A.E. Claessens, Y. Luan, and A.R. Bausch. 2008. Transient Binding and Dissipation in Cross-Linked Actin Networks. *Physical Review Letters*. 101.

Lim, C.T., E.H. Zhou, and S.T. Quek. 2006. Mechanical Models for Living Cells--a Review. *J Biomech*. 39:195-216.

Liverpool, T.B., A.C. Maggs, and A. Ajdari. 2001. Viscoelasticity of Solutions of Motile Polymers. *Physical Review Letters*. 86:4171-4174.

Loening, A.M., I.E. James, M.E. Levenston, A.M. Badger, E.H. Frank, B. Kurz, M.E. Nuttall, H.H. Hung, S.M. Blake, A.J. Grodzinsky, and M.W. Lark. 2000. Injurious Mechanical Compression of Bovine Articular Cartilage Induces Chondrocyte Apoptosis. *Arch Biochem Biophys*. 381:205-212.

Loeser, R.F. 2000. Chondrocyte Integrin Expression and Function. *Biorheology*. 37:109-116.

Loty, S., N. Forest, H. Boulekbache, and J.M. Sautier. 1995. Cytochalasin D Induces Changes in Cell Shape and Promotes in Vitro Chondrogenesis: A Morphological Study. *Biol Cell*. 83:149-161.

Lu, L., S.J. Oswald, H. Ngu, and F.C. Yin. 2008. Mechanical Properties of Actin Stress Fibers in Living Cells. *Biophys J*. 95:6060-6071.

Lu, X.L., and V.C. Mow. 2008. Biomechanics of Articular Cartilage and Determination of Material Properties. *Med Sci Sports Exerc*. 40:193-199.

M.D., E.D.G.W. 2006. The Arp2／3 Complex: An Actin Nucleator Comes of Age. *Nat. Rev. Mol. Cell Biol*. 7:713–726.

Malleingerin, F., R. Garrone, and M. Vanderrest. 1991. Proteoglycan and Collagen-Synthesis Are Correlated with Actin Organization in Dedifferentiating Chondrocytes. *European Journal of Cell Biology*. 56:364-373.

Mansour, J.M. 2009. Biomechanics of Cartilage. *In* Kinesiology: The Mechanics and Pathomechanics of Human Movement. Vol. 2. C.A. Oatis, editor. Lippincott Williams & Wilkins. 68-77.

Maroudas, A., and P. Bullough. 1968. Permeability of Articular Cartilage. *Nature*. 219:1260-1261.

Martin, I., G. Vunjak-Novakovic, J. Yang, R. Langer, and L.E. Freed. 1999. Mammalian Chondrocytes Expanded in the Presence of Fibroblast Growth Factor 2 Maintain the Ability to Differentiate and Regenerate Three-Dimensional Cartilaginous Tissue. *Exp Cell Res*. 253:681-688.

Martin, J.A., and J.A. Buckwalter. 2002. Aging, Articular Cartilage Chondrocyte Senescence and Osteoarthritis. *Biogerontology*. 3:257-264.

Merryman, W.D., P.D. Bieniek, F. Guilak, and M.S. Sacks. 2009. Viscoelastic Properties of the Aortic Valve Interstitial Cell. *J Biomech Eng*. 131:041005.

Millward-Sadler, S.J.W., M.O.;Flatman, P.W.;Salter, D.M. 2004. Atp in the Mechanotransduction Pathway of Normal Human Chondrocyte. *Biorheology*. 41:567-575.

Moriya, T., Y. Wada, A. Watanabe, T. Sasho, K. Nakagawa, P. Mainil-Varlet, and H. Moriya. 2007. Evaluation of Reparative Cartilage after Autologous Chondrocyte Implantation for Osteochondritis Dissecans: Histology, Biochemistry, and Mr Imaging. *J Orthop Sci*. 12:265-273.

Mow, V.C., M.H. Holmes, and W.M. Lai. 1984. Fluid Transport and Mechanical Properties of Articular Cartilage: A Review. *J Biomech*. 17:377-394.

Mow, V.C., Proctor, Cristopher S., Kelly, Michael A. 1980. Biomechanics of Articlar Cartilage. *In* Basic Biomechanics of the Skeletal System. V.H. Frankel, editor. Lea & Febiger.

Murphy, S.B., R. Ganz, and M.E. Muller. 1995. The Prognosis in Untreated Dysplasia of the Hip - a Study of Radiographic Factors That Predict the Outcome. *Journal of Bone and Joint Surgery-American Volume*. 77A:985-989.

Nizegorodcew, T., G. Gasparini, G. Maccauro, A. Todesca, and E. De Santis. 1997. Massive Osteolysis Induced by High Molecular Weight Polyethylene Wear Debris. *Int Orthop*. 21:14-18.

Oesterle, A. 2011. P-97 Pipette Cookbook.

Ohashi, T., M. Hagiwara, D.L. Bader, and M.M. Knight. 2006. Intracellular Mechanics and Mechanotransduction Associated with Chondrocyte Deformation During Pipette Aspiration. *Biorheology*. 43:201-214.

Ono, S. 2007. Mechanism of Depolymerization and Severing of Actin Filaments and Its Significance in Cytoskeletal Dynamics. *International Review of Cytology - a Survey of Cell Biology, Vol 258*. 258:1-82.

Pender, N., and C.A. McCulloch. 1991. Quantitation of Actin Polymerization in Two Human Fibroblast Sub-Types Responding to Mechanical Stretching. *J Cell Sci*. 100 (Pt 1):187-193.

Pingguan-Murphy, B., D.A. Lee, D.L. Bader, and M.M. Knight. 2005. Activation of Chondrocytes Calcium Signalling by Dynamic Compression Is Independent of Number of Cycles. *Arch Biochem Biophys*. 444:45-51.

Poole, C.A., M.H. Flint, and B.W. Beaumont. 1987. Chondrons in Cartilage: Ultrastructural Analysis of the Pericellular Microenvironment in Adult Human Articular Cartilages. *J Orthop Res*. 5:509-522.

Pritchard, S., and F. Guilak. 2006. Effects of Interleukin-1 on Calcium Signaling and the Increase of Filamentous Actin in Isolated and in Situ Articular Chondrocytes. *Arthritis Rheum*. 54:2164-2174.

Qi, J., A.M. Fox, L.G. Alexopoulos, L. Chi, D. Bynum, F. Guilak, and A.J. Banes. 2006. Il-1beta Decreases the Elastic Modulus of Human Tenocytes. *J Appl Physiol*. 101:189-195.

Quinn, T.M., A.J. Grodzinsky, M.D. Buschmann, Y.J. Kim, and E.B. Hunziker. 1998. Mechanical Compression Alters Proteoglycan Deposition and Matrix Deformation around Individual Cells in Cartilage Explants. *J Cell Sci*. 111 (Pt 5):573-583.

Ragan, P.M., A.M. Badger, M. Cook, V.I. Chin, M. Gowen, A.J. Grodzinsky, and M.W. Lark. 1999. Down-Regulation of Chondrocyte Aggrecan and Type-Ii Collagen Gene Expression Correlates with Increases in Static Compression Magnitude and Duration. *J Orthopaed Res*. 17:836-842.

Ramage, L., G. Nuki, and D.M. Salter. 2009. Signalling Cascades in Mechanotransduction: Cell-Matrix Interactions and Mechanical Loading. *Scand J Med Sci Sports*. 19:457-469.

Raynauld, J.P., J. Martel-Pelletier, M.J. Berthiaume, F. Abram, D. Choquette, B. Haraoui, J.F. Beary, G.A. Cline, J.M. Meyer, and J.P. Pelletier. 2008. Correlation between Bone Lesion Changes and Cartilage Volume Loss in Patients with Osteoarthritis of the Knee as Assessed by Quantitative Magnetic Resonance Imaging over a 24-Month Period. *Ann Rheum Dis*. 67:683-688.

Redman, S.N., S.F. Oldfield, and C.W. Archer. 2005. Current Strategies for Articular Cartilage Repair. *Eur Cell Mater*. 9:23-32; discussion 23-32.

Reginato, A.M., and B.R. Olsen. 2002. The Role of Structural Genes in the Pathogenesis of Osteoarthritic Disorders. *Arthritis Res*. 4:337-345.

Roberts, S.R., M.M. Knight, D.A. Lee, and D.L. Bader. 2001. Mechanical Compression Influences Intracellular Ca2+ Signaling in Chondrocytes Seeded in Agarose Constructs. *J Appl Physiol*. 90:1385-1391.

Roemer, F.W., A. Guermazi, J. Niu, Y. Zhang, A. Mohr, and D.T. Felson. 2012. Prevalence of Magnetic Resonance Imaging-Defined Atrophic and Hypertrophic Phenotypes of Knee Osteoarthritis in a Population-Based Cohort. *Arthritis Rheum*. 64:429-437.

Rotsch, C., and M. Radmacher. 2000. Drug-Induced Changes of Cytoskeletal Structure and Mechanics in Fibroblasts: An Atomic Force Microscopy Study. *Biophysical Journal*. 78:520-535.

Roughley, P.J. 2006. The Structure and Function of Cartilage Proteoglycans. *Eur Cell Mater*. 12:92-101.

Roughley, P.J., and E.R. Lee. 1994. Cartilage Proteoglycans: Structure and Potential Functions. *Microsc Res Tech*. 28:385-397.

Sasazaki, Y., B.B. Seedhom, and R. Shore. 2008. Morphology of the Bovine Chondrocyte and of Its Cytoskeleton in Isolation and in Situ: Are Chondrocytes Ubiquitously Paired through the Entire Layer of Articular Cartilage? *Rheumatology (Oxford)*. 47:1641-1646.

Sato, M., D.P. Theret, L.T. Wheeler, N. Ohshima, and R.M. Nerem. 1990. Application of the Micropipette Technique to the Measurement of Cultured Porcine Aortic Endothelial-Cell Viscoelastic Properties. *J Biomech Eng-T Asme*. 112:263-268.

Schinagl, R.M., D. Gurskis, A.C. Chen, and R.L. Sah. 1997. Depth-Dependent Confined Compression Modulus of Full-Thickness Bovine Articular Cartilage. *J Orthop Res*. 15:499-506.

Schroeder, T.E. 1978. Microvilli on Sea Urchin Eggs: A Second Burst of Elongation. *Dev Biol*. 64:342-346.

Schulze-Tanzil, G., P. de Souza, H. Villegas Castrejon, T. John, H.J. Merker, A. Scheid, and M. Shakibaei. 2002. Redifferentiation of Dedifferentiated Human Chondrocytes in High-Density Cultures. *Cell Tissue Res*. 308:371-379.

Schulze-Tanzil, G., R.D. Muller, B. Kohl, N. Schneider, W. Ertel, K. Ipaktchi, H. Hunigen, O. Gemeinhardt, R. Stark, and T. John. 2009. Differing in Vitro Biology of Equine, Ovine, Porcine and Human Articular Chondrocytes Derived from the Knee Joint: An Immunomorphological Study. *Histochem Cell Biol*. 131:219-229.

Sen, S., and S. Kumar. 2010. Combining Mechanical and Optical Approaches to Dissect Cellular Mechanobiology. *Journal of Biomechanics*. 43:45-54.

Setton, L.A., H. Tohyama, and V.C. Mow. 1998. Swelling and Curling Behaviors of Articular Cartilage. *J Biomech Eng*. 120:355-361.

Shelton, J.C., D.L. Bader, and D.A. Lee. 2003. Mechanical Conditioning Influences the Metabolic Response of Cell-Seeded Constructs. *Cells Tissues Organs*. 175:140-150.

Shieh, A.C., and K.A. Athanasiou. 2006. Biomechanics of Single Zonal Chondrocytes. *J Biomech*. 39:1595-1602.

Siczkowski, M., and F.M. Watt. 1990. Subpopulations of Chondrocytes from Different Zones of Pig Articular Cartilage. Isolation, Growth and Proteoglycan Synthesis in Culture. *J Cell Sci*. 97 (Pt 2):349-360.

Singh, S., C.C. Lee, and B.K. Tay. 1991. Results of Arthroscopic Abrasion Arthroplasty in Osteoarthritis of the Knee Joint. *Singapore Med J*. 32:34-37.

Slavotinek, A.M., E.M. Stone, K. Mykytyn, J.R. Heckenlively, J.S. Green, E. Heon, M.A. Musarella, P.S. Parfrey, V.C. Sheffield, and L.G. Biesecker. 2000. Mutations in Mkks Cause Bardet-Biedl Syndrome. *Nat Genet*. 26:15-16.

Sledge, S.L. 2001. Microfracture Techniques in the Treatment of Osteochondral Injuries. *Clin Sports Med*. 20:365-377.

Sokolova, A.V., L. Kreplak, T. Wedig, N. Mucke, D.I. Svergun, H. Herrmann, U. Aebi, and S.V. Strelkov. 2006. Monitoring Intermediate Filament Assembly by Small-Angle X-Ray Scattering Reveals the Molecular Architecture of Assembly Intermediates. *Proc Natl Acad Sci U S A*. 103:16206-16211.

Spector, I., F. Braet, N.R. Shochet, and M.R. Bubb. 1999. New Anti-Actin Drugs in the Study of the Organization and Function of the Actin Cytoskeleton. *Microsc Res Techniq*. 47:18-37.

Starodubtseva, M.N. 2011. Mechanical Properties of Cells and Ageing. *Ageing Res Rev*. 10:16-25.

Steinmeyer, J., B. Ackermann, and R.X. Raiss. 1997. Intermittent Cyclic Loading of Cartilage Explants Modulates Fibronectin Metabolism. *Osteoarthritis Cartilage*. 5:331-341.

Steklov, N., A. Srivastava, K.L. Sung, P.C. Chen, M.K. Lotz, and D.D. D'Lima. 2009. Aging-Related Differences in Chondrocyte Viscoelastic Properties. *Mol Cell Biomech*. 6:113-119.

Stewart, M.C., K.M. Saunders, N. Burton-Wurster, and J.N. Macleod. 2000. Phenotypic Stability of Articular Chondrocytes in Vitro: The Effects of Culture Models, Bone Morphogenetic Protein 2, and Serum Supplementation. *J Bone Miner Res*. 15:166-174.

Strehl, R., K. Schumacher, U. de Vries, and W.W. Minuth. 2002. Proliferating Cells Versus Differentiated Cells in Tissue Engineering. *Tissue Eng*. 8:37-42.

Suh, J.K., Z. Li, and S.L. Woo. 1995. Dynamic Behavior of a Biphasic Cartilage Model under Cyclic Compressive Loading. *J Biomech*. 28:357-364.

Sun, H.Q., K. Kwiatkowska, and H.L. Yin. 1995. Actin Monomer Binding-Proteins. *Current Opinion in Cell Biology*. 7:102-110.

Teichtahl, A.J., A.E. Wluka, M.L. Davies-Tuck, and F.M. Cicuttini. 2008. Imaging of Knee Osteoarthritis. *Best Pract Res Clin Rheumatol*. 22:1061-1074.

Tharmann, R., M.M.A.E. Claessens, and A.R. Bausch. 2007. Viscoelasticity of Isotropically Cross-Linked Actin Networks. *Physical Review Letters*. 98.

Theret, D.P., M.J. Levesque, M. Sato, R.M. Nerem, and L.T. Wheeler. 1988. The Application of a Homogeneous Half-Space Model in the Analysis of Endothelial Cell Micropipette Measurements. *J Biomech Eng*. 110:190-199.

Tinevez, J.Y., U. Schulze, G. Salbreux, J. Roensch, J.F. Joanny, and E. Paluch. 2009. Role of Cortical Tension in Bleb Growth. *P Natl Acad Sci USA*. 106:18581-18586.

Tobin, J.L., M. Di Franco, E. Eichers, H. May-Simera, M. Garcia, J. Yan, R. Quinlan, M.J. Justice, R.C. Hennekam, J. Briscoe, M. Tada, R. Mayor, A.J. Burns, J.R. Lupski, P. Hammond, and P.L. Beales. 2008. Inhibition of Neural Crest Migration Underlies Craniofacial Dysmorphology and Hirschsprung's Disease in Bardet-Biedl Syndrome. *Proc Natl Acad Sci U S A*. 105:6714-6719.

Trickey, W.R., F.P. Baaijens, T.A. Laursen, L.G. Alexopoulos, and F. Guilak. 2006. Determination of the Poisson's Ratio of the Cell: Recovery Properties of Chondrocytes after Release from Complete Micropipette Aspiration. *J Biomech*. 39:78-87.

Trickey, W.R., G.M. Lee, and F. Guilak. 2000. Viscoelastic Properties of Chondrocytes from Normal and Osteoarthritic Human Cartilage. *J Orthop Res*. 18:891-898.

Trickey, W.R., T.P. Vail, and F. Guilak. 2004. The Role of the Cytoskeleton in the Viscoelastic Properties of Human Articular Chondrocytes. *J Orthop Res*. 22:131-139.

Urban, J.P. 1994. The Chondrocyte: A Cell under Pressure. *Br J Rheumatol*. 33:901-908.

Urban, J.P. 2000. Present Perspectives on Cartilage and Chondrocyte Mechanobiology. *Biorheology*. 37:185-190.

Valiron, O., N. Caudron, and D. Job. 2001. Microtubule Dynamics. *Cell Mol Life Sci*. 58:2069-2084.

Wakatsuki, T., B. Schwab, N.C. Thompson, and E.L. Elson. 2001. Effects of Cytochalasin D and Latrunculin B on Mechanical Properties of Cells. *J Cell Sci*. 114:1025-1036.

Wann, A.K., J. Mistry, E.J. Blain, A.T. Michael-Titus, and M.M. Knight. 2010. Eicosapentaenoic Acid and Docosahexaenoic Acid Reduce Interleukin-1beta-Mediated Cartilage Degradation. *Arthritis Res Ther*. 12:R207.

Williams, R.J. 2007. *In* Cartilage Repair Strategies. Humanpress, New York. 1-12.

Williams, R.J., J.C. Dreese, and C.T. Chen. 2004. Chondrocyte Survival and Material Properties of Hypothermically Stored Cartilage - an Evaluation of Tissue Used for Osteochondral Allograft Transplantation. *Am J Sport Med*. 32:132-139.

Wu, H., C. Webber, C.O. Fuentes, R. Bensen, K. Beattie, J.D. Adachi, X. Xie, F. Jabbari, and D.R. Levy. 2007. Prevalence of Knee Abnormalities in Patients with Osteoarthritis and Anterior Cruciate Ligament Injury Identified with Peripheral Magnetic Resonance Imaging: A Pilot Study. *Can Assoc Radiol J*. 58:167-175.

Wu, Q.Q., and Q. Chen. 2000. Mechanoregulation of Chondrocyte Proliferation, Maturation, and Hypertrophy: Ion-Channel Dependent Transduction of Matrix Deformation Signals. *Exp Cell Res*. 256:383-391.

Xu, J., Y. Tseng, and D. Wirtz. 2000. Strain Hardening of Actin Filament Networks. Regulation by the Dynamic Cross-Linking Protein Alpha-Actinin. *J Biol Chem*. 275:35886-35892.

Yarmola, E.G., and M.R. Bubb. 2004. Effects of Profilin and Thymosin Beta4 on the Critical Concentration of Actin Demonstrated in Vitro and in Cell Extracts with a Novel Direct Assay. *J Biol Chem*. 279:33519-33527.

Yellowley, C.E., C.R. Jacobs, Z. Li, Z. Zhou, and H.J. Donahue. 1997. Effects of Fluid Flow on Intracellular Calcium in Bovine Articular Chondrocytes. *Am J Physiol*. 273:C30-36.

Zaucke, F., R. Dinser, P. Maurer, and M. Paulsson. 2001. Cartilage Oligomeric Matrix Protein (Comp) and Collagen Ix Are Sensitive Markers for the Differentiation State of Articular Primary Chondrocytes. *Biochem J*. 358:17-24.

Zhang, Q.Y., and W.Y. Chen. 2009. Age-Related Changes in Viscoelasticity of Rabbit Knee Articular Chondrocytes. *2009 3rd International Conference on Bioinformatics and Biomedical Engineering, Vols 1-11*:2735-2737.

Zhao, R., K. Wyss, and C.A. Simmons. 2009. Comparison of Analytical and Inverse Finite Element Approaches to Estimate Cell Viscoelastic Properties by Micropipette Aspiration. *J Biomech*. 42:2768-2773.

Zheng, M.H., E. King, Y. Kirilak, L. Huang, J.M. Papadimitriou, D.J. Wood, and J. Xu. 2004. Molecular Characterisation of Chondrocytes in Autologous Chondrocyte Implantation. *Int J Mol Med*. 13:623-628.

PUBLICATIONS

P. Pravincumar, D. L Bader and M. M. Knight. (2012) Viscoelastic cell mechanics and actin remodelling are dependent on the rate of applied pressure. *PLoS One, 7, (9).*

J. Chen, J. Irianto, S. Inamdar, P. Pravincumar, D.A. Lee, D.L. Bader, M.M. Knight. (2012) Cell mechanics, structure and function are regulated by the stiffness of the 3D microenvironment.*Biophys J, 103, (6) 1188-1197.*

V. Hernandez-Hernandez, P. Pravincumar, A.Diaz-Font, H. May-Simera, D. Jenkins, M M Knight, P. L. Beales. (2012) Bardet-Biedl syndrome proteins control cilia length through regulation of actin polymerisation. *Journal of Cell Biology (in press).*

CONFERENCES

P Pravincumar, D. L. Bader, M. M. Knight. Pressure rate dependent remodelling governs chondrocyte viscoelastic behaviour.

Bioengineering Conference, 12th – 13th Sept 2011, London, UK. and

Advances in Biomechanics and Mechanobiological Modelling, 21st April 2011, University of Oxford, UK.

P Pravincumar, D. L. Bader, M. M. Knight Pressure rate sensitive viscoelastic cell deformation involves actin remodelling.

European Society of Biomechanics, 1st – 4th July 2012, Lisboa-Portugal.